marine drugs

Special Issue Reprint

Diversity of Marine Fungi as a Source of Bioactive Natural Products, 2nd Edition

Edited by
Dehai Li

mdpi.com/journal/marinedrugs

MDPI

Diversity of Marine Fungi as a Source of Bioactive Natural Products, 2nd Edition

Diversity of Marine Fungi as a Source of Bioactive Natural Products, 2nd Edition

Guest Editor

Dehai Li

MDPI

Basel • Beijing • Wuhan • Barcelona • Belgrade • Novi Sad • Cluj • Manchester

Guest Editor
Dehai Li
Key Laboratory of Marine
Drugs
Ocean University of China
Qingdao
China

Editorial Office
MDPI AG
Grosspeteranlage 5
4052 Basel, Switzerland

This is a reprint of the Special Issue, published open access by the journal *Marine Drugs* (ISSN 1660-3397), freely accessible at: https://www.mdpi.com/journal/marinedrugs/special_issues/O57DK1CSOP.

For citation purposes, cite each article independently as indicated on the article page online and as indicated below:

Lastname, A.A.; Lastname, B.B. Article Title. *Journal Name* **Year**, *Volume Number*, Page Range.

ISBN 978-3-7258-4947-5 (Hbk)
ISBN 978-3-7258-4948-2 (PDF)
https://doi.org/10.3390/books978-3-7258-4948-2

© 2025 by the authors. Articles in this book are Open Access and distributed under the Creative Commons Attribution (CC BY) license. The book as a whole is distributed by MDPI under the terms and conditions of the Creative Commons Attribution-NonCommercial-NoDerivs (CC BY-NC-ND) license (https://creativecommons.org/licenses/by-nc-nd/4.0/).

Contents

About the Editor

Dehai Li

Dehai Li is a professor at the School of Medicine and Pharmacy, Ocean University of China. He received his bachelor's degree in Pharmacy from Shandong University in 2002 and obtained his Doctor of Medicine in 2007 from Ocean University of China. Thereafter, he completed his postdoctoral research with Professor Raymond J. Andersen at the University of British Columbia from 2007 to 2009. From 2014 to 2015, he moved to Professor Yi Tang's lab at the University of California, Los Angeles, as a visiting scientist. At present, his research is focused on marine natural products, including: (1) isolation and identification of fungi and actinomycete strains from various marine samples; (2) searching for novel bioactive secondary metabolites from marine-derived microorganisms; and (3) chemical synthesis and biosynthesis of natural products. In the past 15 years, his group has isolated over 5000 microorganism strains from marine environments and discovered more than 1000 new structures. He has published more than 160 papers and has had 10 patents authorized.

marine drugs

MDPI

Article

Discovery of Secondary Metabolites from the Sponge-Derived Fungus *Aspergillus templicola*

Kai Li [1,2], Yue Zhang [1,2], Lei Li [1,2], Sen Wang [1,2], Cili Wang [1,2,3,*] and Pinglin Li [1,2,*]

[1] Key Laboratory of Marine Drugs, Chinese Ministry of Education, School of Medicine and Pharmacy, Ocean University of China, Qingdao 266003, China; 17854232177@163.com (K.L.); zhangyue_00803@163.com (Y.Z.); ll1061602375@163.com (L.L.); wangsen19972021@163.com (S.W.)
[2] Laboratory for Marine Drugs and Bioproducts, Qingdao Marine Science and Technology Center, Qingdao 266237, China
[3] Key Laboratory of Marine Food Processing & Safety Control, College of Food Science and Engineering, Ocean University of China, Qingdao 266003, China
* Correspondence: wangcili881@163.com (C.W.); lipinglin@ouc.edu.cn (P.L.); Tel.: +86-532-8203-3054 (P.L.)

Abstract

Combining biosynthetic gene cluster analysis with the OSMAC strategy, fractionation of the fermentation extract of *Aspergillus templicola* from the sponge *Agelas* sp. led to the isolation of four novel cytochalasins, colachalasins J–M (**1**–**4**), a novel cyclic pentapeptide, avellanin P (**5**), together with five known compounds (**6**–**10**). The structures of **1**–**9** were elucidated using spectroscopic data, single crystal X-ray diffraction, and Marfey's analysis. Compound **2** exhibited potent anti-inflammatory activity in zebrafish assays. Additionally, Compounds **4** and **6** showed modest cytotoxicity against several human cancer cell lines with IC_{50} values ranging from 2.6 to 11.2 μm.

Keywords: *Aspergillus templicola*; cytochalasins; cyclic pentapeptides; anti-inflammatory activity; cytotoxic activity

1. Introduction

Marine-derived fungi are prominent producers of novel bioactive compounds and drug lead compounds [1]. With the advances in sequencing technologies, genomic data have emerged as a valuable resource containing unique biosynthetic gene clusters (BGCs), enabling the prediction of compound types, and facilitating the discovery of novel natural products (NPs) [2]. However, under traditional laboratory conditions, fungi transcribe only a small fraction of their biological genetic clusters, while most genes remain silent [3]. Consequently, traditional cultivation methods can access only a limited portion of the potential chemical diversity of fungal natural products [4]. Numerous strategies aim to activate these biosynthetic gene clusters to broaden metabolite diversity. One such approach is the One Strain Many Compounds (OSMAC) method, which diversifies culture media and growth conditions to generate environmental cues, induce silent biosynthetic clusters, and accumulate cryptic metabolites [5]. Co-cultivation and epigenetic modification represent other important components of the OSMAC approach [6,7].

During the early stages of our research, a partial gene cluster (*cck*) was discovered in *Aspergillus templicola*, isolated from the sponge *Agelas* sp. [8]. This *cck* gene cluster exhibits similarity to the previously reported *ccs* gene cluster [9], suggesting its potential for synthesizing cytochalasins. Our recent chemical investigations of the sponge-derived fungus

A. templicola cultured in liquid medium successfully yielded 13 cytochalasins, including 9 novel cytochalasins, colachalasins (A–I), and 4 known cytochalasins [8]. Furthermore, genomic analysis revealed another *par* gene cluster homologous to the previously reported *hcpA* cluster (Figure 1) [10], indicating its potential role in cyclic peptide biosynthesis. Cyclic peptides have attracted significant attention due to their unique biological activities, such as cytotoxicity [11], antimalarial activity [12], and antibacterial activity [13]. However, cyclic peptides were not found in our previous research. To activate cryptic biosynthetic pathways for cyclic peptides, an OSMAC strategy was employed by switching to a rice-based solid medium. Ultimately, this process led to the isolation of four novel cytochalasins, colachalasins J–M (**1**–**4**), a novel cyclic pentapeptide, avellanin P (**5**), along with five known compounds, cytochalasin Z_{16} (**6**) [14], 7-Deoxy-cytochalasin Z_7 (**7**) [15], aspochalasin I (**8**) [16], aspochalasin A_1 (**9**) [17], and cyclo-(*S*-Pro-*R*-Leu) (**10**) [18] (Figure 2). Herein, we report the isolation, structural elucidation, and biological activities of the new isolates.

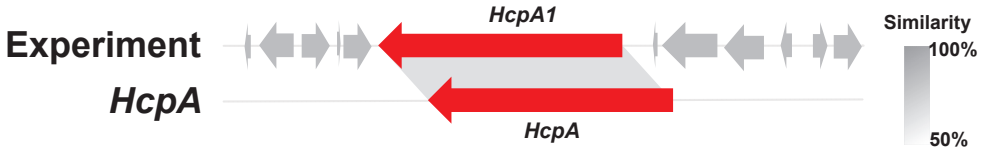

Figure 1. The *HcpA1* gene cluster in comparison to *HcpA*.

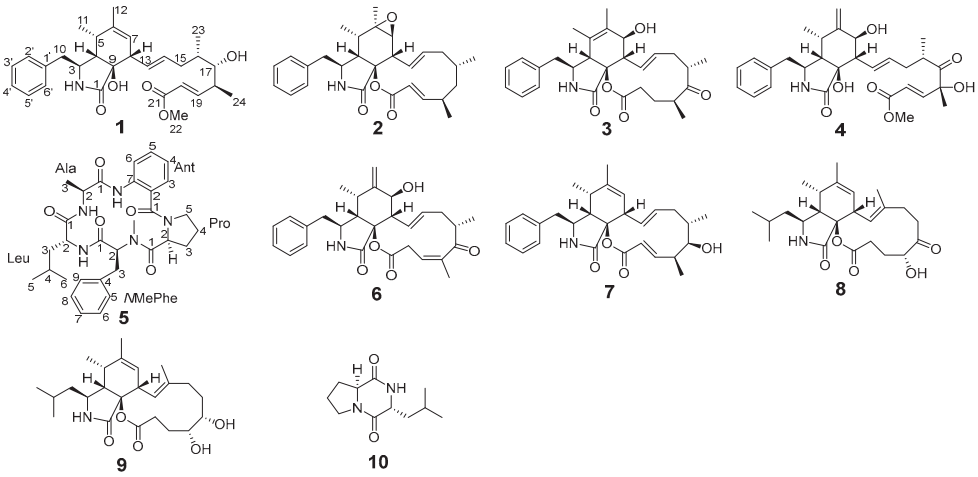

Figure 2. Structures of compounds **1**–**10**.

2. Results

Colachalasin J (**1**) was obtained as colorless crystals. The molecular formula was determined to be $C_{29}H_{39}NO_5$ based on the $[M + H]^+$ ion peak at m/z 482.2892 $[M + H]^+$ (calcd for 482.2901) in HRESIMS, requiring eleven degrees of unsaturation. The ^1H NMR data (Table S2) indicated the presence of four methyl groups, a methoxy group, three double bonds, and a monosubstituted phenyl group. The ^{13}C NMR data (Table S2) and the HSQC spectrum revealed 29 carbon signals, which were categorized into five methyl groups, two methylene groups, seventeen methine carbons (ten olefinic), and five non-hydrogenated carbons (two of which were carbonyls). These NMR data indicated that compound **1** is a cytochalasin [8].

Analysis of the 1D and 2D NMR data (Table S2 and Figure 3) revealed that the structure of compound **1** is similar to that of compound **7** (Figure 2), a cytochalasin previously isolated from a marine-derived fungus *Spicaria elegans* [15], with the main difference being the ester bond between C-9 and C-21 of **7** is cleaved in **1**, to give the open methyl ester. Compared

with **7**, the variation is that of an additional hydroxy group at C-9, and a methoxy group at C-22 in **1**. These structural differences are further confirmed by the HMBC correlations from H-19, H-20, and H_3-22 to C-21 (Figure 3), and from H-4 to C-9 (δ_C 80.2), which is consistent with the molecular formula.

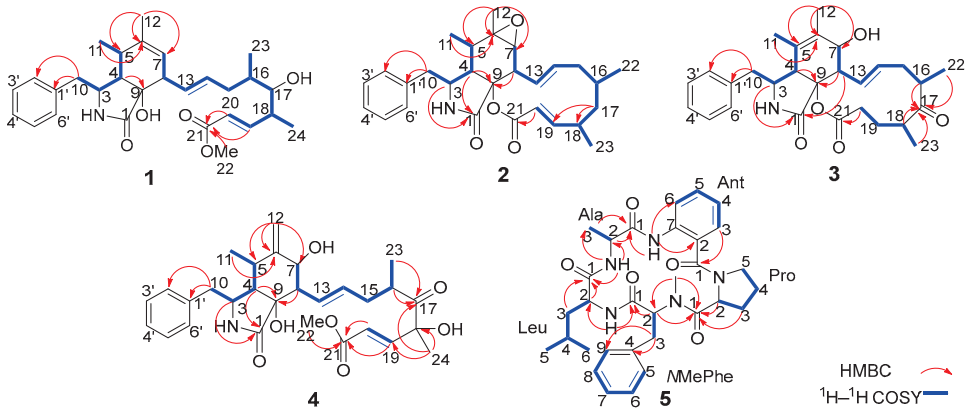

Figure 3. The Key ^{1}H–^{1}H COSY, HMBC correlations of compounds **1**–**5**.

In the NOESY spectrum of compound **1** (Figure 4), the correlation between H-3 and H_3-11 indicated their co-facial orientation, which was assigned as α-orientation. The correlations of H_2-10/H-4 confirmed the β-orientation of these protons. The large coupling constants ($J_{13,14}$ = 15.2 Hz; $J_{19,20}$ = 15.8 Hz) indicated that the Δ^{13} and Δ^{19} double bonds were both *trans* configured. The determination of the relative configuration at C-8, C-9, C-16, C-17, and C-18 was challenging on account of the absence of effective NOESY correlations. Fortunately, suitable single crystals were acquired and subjected to a Bruker APEX-II CCD diffractometer with Cu Kα radiation, determining the absolute configuration of compound **1** as 3*S*, 4*S*, 5*S*, 8*S*, 9*R*, 16*S*, 17*S*,18*S*, with a Flack parameter of 0.03 (11) (Figure 5).

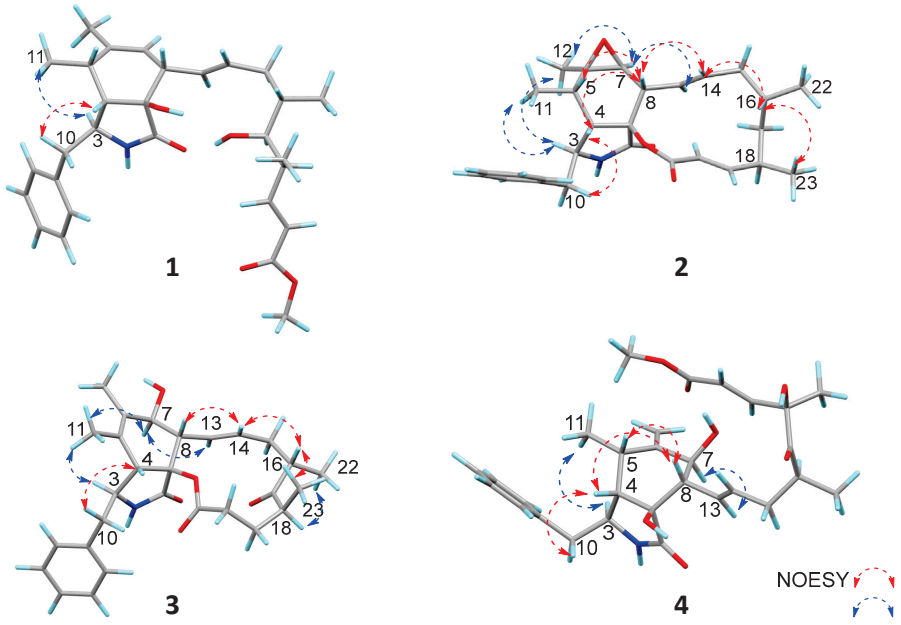

Figure 4. The Key NOESY correlations of compounds **1**–**4**.

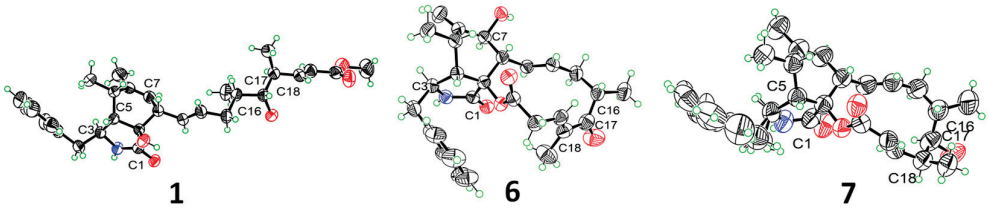

Figure 5. X-ray crystal structures of **1**, **6**, **7**. The ellipsoids of non-hydrogen atoms of **1**, **6**, **7** are shown at 50% probability levels.

Colachalasin K (**2**) was obtained as a colorless powder. The molecular formula was determined to be $C_{28}H_{35}NO_4$ based on the $[M + H]^+$ ion peak at m/z 450.2631 (calcd for 450.2639) in HRESIMS. The 1D NMR data (Table S2) indicated that the structure of compound **2** were similar to those of colachalasin D (Figure S1), a cytochalasin previously isolated from the fungus *A. templicola* [8]. The key difference between them were the absence of a 17-carbonyl group and the an additional Δ^{19} double bond in compound **2**, as confirmed by the ^1H–^1H COSY correlations of H-16/H-17/H-18 (Figure 3), the HMBC correlations of H-17/C-18, H-17/C-19, H-20/C-21 (Figure 3), and the chemical shifts of C-17 (δ_C 44.8), C-19 (δ_C 161.9), and C-20 (δ_C 118.9). Thus, the planar structure of compound **2** was established.

The relative configuration of compound **2** was determined by the analysis of the NOESY spectrum (Figure 4). The correlations of H-3/H_3-11, H-3/H_3-12, H_3-12/H-7, H-7/H-13 suggested the α-orientation of H-3, H_3-11, H_3-12, H-7. Additionally, the NOESY correlation of H-5/H-8, and H-4/H_2-10, H-4/H-8, H-8/H-14, H-14/H-16, H-16/H_3-23, suggested the β-orientation of H-4, H-5, H-8, H-16, H_3-23. Previous studies have suggested that the core structural elements of cytochalasins mostly share a conserved stereochemical configuration, and that is the 5/6 ring junction and the trans-stereochemistry of the macrocyclic ring [19]. This stereochemical assignment is further corroborated by X-ray crystallographic data of cytochalasins [8]. Consequently, the oxygen atom at C-9 is β-oriented. The large coupling constants ($J_{13,\,14}$ = 15.5 Hz; $J_{19,\,20}$ = 15.9 Hz) indicated that the Δ^{13} and Δ^{19} double bonds were both *trans* configured. The absolute configurations of compound **2** were assigned as 3*S*, 4*S*, 5*S*, 6*R*, 7*S*, 8*S*, 9*S*, 16*S*, 18*R* by comparison of their similar ECD spectra between **2** and colachalasin D (Figure 6).

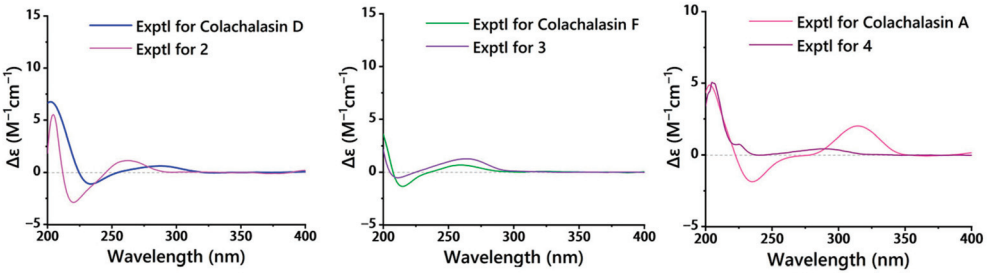

Figure 6. ECD spectra of **2** and colachalasin D, **3** and colachalasin F, **4** and colachalasin A.

Colachalasin L (**3**), obtained as colorless powder, was determined to have the molecular formula $C_{28}H_{35}NO_5$ based on the HRESIMS ion at m/z 464.2430 (calcd for 464.2442) $[M - H]^-$. The ^1H and ^{13}C NMR data (Table S3) indicated that the structure of compound **3** was similar to colachalasin F (Figure S1), a cytochalasin previously isolated from the fungus *A. templicola* [8], with the exception of an additional 17-carbonyl group and the absence of the Δ^{19} double bond in compound **3** compared to colachalasin F. This was further confirmed by the HMBC correlations of H-16, H-18, H_3-22, H_3-23/C-17 (δ_C 216.8) (Figure 3) and the chemical shifts of C-19 (δ_C 29.3) and C-20 (δ_C 33.2).

The relative configuration of the stereocenters and the configuration of the double bond in compound **3** were determined by analysis of NOESY data and coupling constants (Figure 4 and Table S3). In the NOESY spectrum, correlations of H-3/H_3-11, H_3-11/H-7, H-7/H-13 suggested the α-orientation of H-3, H-7. The correlations of H-4/H_2-10, H-8/H-14, H-14/H-16, H-16/H_3-23 suggested the β-orientation of H-4, H-8, H-16, H_3-23. The large coupling constants ($J_{13,14}$ = 15.4 Hz) indicated that the Δ^{13} double bond was *trans* configured. Based on a comparison of ECD spectra (Figure 6) between **3** and colachalasin F, which showed similar structures, the absolute configuration of compound **3** was assigned as 3*S*, 4*S*, 7*S*, 8*S*, 9*S*, 16*S*, 18*S*.

Colachalasin M (**4**) was isolated as a colorless oil. The molecular formula was determined to be $C_{29}H_{37}NO_7$ based on the HRESIMS data (*m*/*z* 512.2653 $[M + H]^+$, calcd for 512.2643). The 1D NMR data (Table S3) of compound **4** were similar to those of colachalasin A (Figure S1), a cytochalasin previously isolated from the fungus *A. templicola* [8]. The only notable difference was that of the presence of a disubstituted terminal double bond at C-6 in **4**, which was replaced by the 6, 7-epoxide ring in colachalasin A. These differences are further supported by the HMBC correlations of H_2-12/C-5 (δ_C 31.6), H_2-12/C-6 (δ_C 148.9), and H_2-12/C-7 (δ_C 70.2) (Figure 3).

The relative configuration of compound **4** was determined based on NOESY correlations (Figure 4). In the NOESY spectrum, correlations between H-3/H_3-11, H-7/H-13, and H-4/H_2-10, H-4/H-8, H-5/H-8 suggested the α-orientation of H-3, H_3-11, H-7, and the β-orientation of H-4, H-5, H-8. The large coupling constants ($J_{13,14}$ = 15.3 Hz; $J_{19,20}$ = 15.8 Hz) indicated that the Δ^{13} and Δ^{19} double bonds were both *trans* configured. The stereochemical configuration of the long carbon chain in compound **4** was deduced from the NMR data. The nearly identical NMR data for the chiral centers of the side chain in compounds **4** and colachalasin A suggest that the relative configuration of the side chain in compound **4** is the same as in colachalasin A. A comparison of ECD spectra between **4** and colachalasin A (Figure 6) determined the absolute configuration of compound **4** as 3*S*, 4*S*, 5*S*, 7*S*, 8*S*, 9*S*, 16*S*, 18*R*.

Compound **5** was obtained as a yellow oil. The molecular formula, $C_{31}H_{39}N_5O_5$, was determined based on HRESIMS data (*m*/*z* 562.3037 $[M + H]^+$, calcd for 562.3024), implying fifteen degrees of unsaturation. The ^{1}H NMR data (Table S4) and HSQC spectrum indicated the presence of three amide protons (δ_H 9.30, δ_H 7.01, and δ_H 7.54) and one *N*-methyl group (δ_H 2.01). The ^{13}C NMR data (Table S4) and HSQC spectrum revealed the presence of 31 carbons, including 8 non-protonated carbons (2 olefinic and 5 carbonyl), 14 methines (5 sp^3 hybridized and 9 olefinic), 5 methylenes (all sp^3 hybridized), and 4 methyls (all sp^3 hybridized).

Further analysis of 2D NMR spectra (Figures S38–S40) led to the identification of five amino-acid components. Alanine (Ala) was confirmed by the ^{1}H−^{1}H COSY correlations for H-2 (δ_H 5.19)/H_3-3 (δ_H 1.52), together with the HMBC correlations for H-2, H_3-3/C-1 (δ_C 171.2), NH (δ_H 7.54)/C-2, and NH (δ_H 7.54)/C-3 (Figure 3). The anthranilic acid unit (Ant) was confirmed by the ^{1}H−^{1}H COSY correlations for a spin system consisting of four adjacent aromatic protons (δ_H 6.85, 6.76, 7.03, and 8.57), together with the HMBC correlations for H-3/C-1(δ_C 169.0) and NH (δ_H 9.30)/C-2, NH (δ_H 9.30)/C-6. Another aliphatic amino acid, proline (Pro), was deduced from sequential ^{1}H−^{1}H COSY correlations for H-2 (δ_H 3.97)/H_2-3 (δ_H 1.17)/H_2-4 (δ_H 1.43/1.03)/H_2-5 (δ_H 2.70) and the HMBC correlations for H-2, H_3-3/C-1(δ_C 172.2). An *N*Me-phenylalanine unit (*N*Me-Phe) was confirmed by the HMBC correlations of an *N*Me (δ_H 2.01)/C-2 (δ_C 69.4), the ^{1}H−^{1}H COSY correlations of H-2 (δ_H 3.47)/H_2-3 (δ_H 3.67/3.87), and a phenyl ring assigned at C-3 by sequential ^{1}H−^{1}H COSY correlations of five CH (δ_H 6.91, 7.02) protons and the HMBC correlations of H-3/C-4, H-3/C-9. The last unit was assigned as leucine (Leu) by the ^{1}H−^{1}H COSY correlations for

H-2 (δ_H 5.10)/H_2-3 (δ_H 2.41/2.01)/H-4 (δ_H 1.89)/H_3-5 (δ_H 0.93), and H-4/H-6 (δ_H 0.97), together with the HMBC correlations for H-2, H_2-3/C-1 (δ_C 171.7), and NH (δ_H 7.01)/C-2.

The connectivity among the five amino acid residues was determined by the HMBC correlations from Ant-NH to Ala-C1, AlaNH to Leu-C1, Leu-NH to *N*Me-Phe-C1, and *N*Me-Phe-CH_3 to Pro-C1 (Figure 3). The correlations between Ant to Pro was established based on HRESIMS data (*m/z* 562.3037 $[M + H]^+$, calcd for 562.3024), implying fifteen degrees of unsaturation. Finally, the Marfey's analysis confirmed the absolute configurations of each amino acid (Figure S51). Thus, compound **5** was determined as *cyclo* (Ant^1-$_L$-Pro^2-*N*Me-$_L$-Phe^3-$_D$-Leu^4-$_L$-Ala^5).

Furthermore, the known compounds **6** and **7** were crystallized from a mixed solvent of ethanol and H_2O, and their single-crystal X-ray diffraction analysis is shown in Figure 5.

Considering the remaining amount of these compounds, compounds **1**, **2**, **4**, **5** were selected for evaluation of anti-inflammatory activity in $CuSO_4$-induced transgenic fluorescent zebrafish. The extent of inflammation was assessed by monitoring the migration of macrophages along the lateral line. As shown in Figure 7A, compounds **2**, **4**, and **5** reduced inflammatory, as evidenced by a higher accumulation of macrophages at the lateral line compared to controls. Furthermore, as shown in Figure 7B, compound **2** at 20 μm demonstrated superior anti-inflammatory activity compared to the positive control indomethacin at 20 μm.

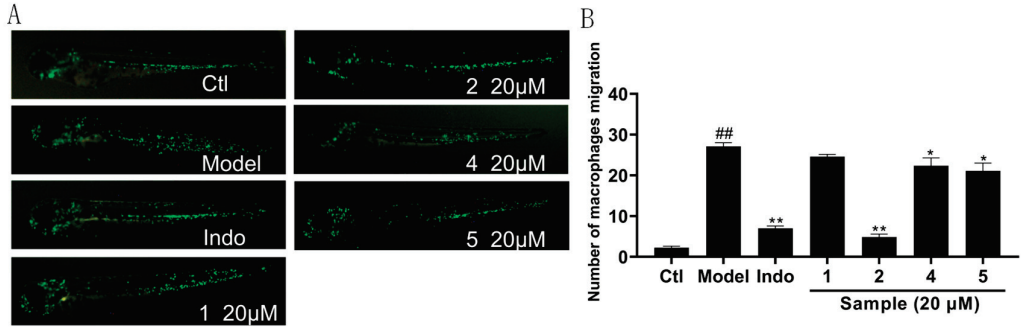

Figure 7. Anti-inflammatory effect of compounds **1, 2, 4, 5.** (**A**) Inflammatory areas in transgenic fluorescent zebrafish (Tg: *zlyz-EGFP*) generated by $CuSO_4$ that express enhanced green fluorescent protein after being treated with compounds **1, 2**, **4**, **5.** (**B**) Quantitative evaluation of fluorescent macrophage counts in the vicinity of inflammatory sites in zebrafish treated with compounds **1, 2**, **4**, **5**. The results were subjected to analysis using one-way analysis of variance followed by Dunnett's post hoc *t*-test. $^{\#\#}$ $p \leq 0.01$ vs. Ctl, * $p \leq 0.05$ vs. model, ** $p \leq 0.01$ vs. Model.

The cytotoxicity of the isolated compounds **1**–**2** and **4**–**7** was evaluated against human leukemia K562, human pancreatic cancer ASPC-1, human breast cancer MDA-MB-231, and human small cell lung cancer NCI-H446/NCI-H446/EP cell lines. As shown in Table 1, compounds **4** and **6** exhibited moderate cytotoxicity against NCI-H446 cell lines with IC_{50} values of 4.2 and 2.6 μm, respectively, as well as against NCI-H446/EP cell lines with IC_{50} values of 6.5 and 11.2 μm, respectively. The IC_{50} value of compound **4** against MDA-MB-231 cells was 9.0 μm. Other compounds were weakly active or totally inactive against the human cancer cell lines.

Table 1. Cytotoxic activities of compounds **1**–**2** and **4**–**7**.

Compound	IC_{50} (μm)				
	K562	ASPC-1	NCI-H446	MDA-MB-231	NCI-H446/EP
1	>30	>30	>30	>30	>30
2	>30	>30	29.2	>30	>30
4	>30	>30	4.2	9.0	6.5
5	>30	>30	>30	>30	>30
6	>30	>30	2.6	>30	11.2
7	>30	>30	>30	>30	>30
DOX [a]	<1	<1	<1	<1	<1

[a] DOX (Doxorubicin) was used as positive control.

3. Materials and Methods

3.1. General Experimental Procedures

Optical rotations were measured using a Jasco P-1020 digital polarimeter (Jasco, Tokyo, Japan). Ultraviolet (UV) spectra were recorded on a Beckman DU640 spectrophotometer (Brea, CA, USA). Electronic circular dichroism (ECD) spectra were acquired using a Jasco J-810 spectropolarimeter (Jasco, Tokyo, Japan). NMR spectra were obtained on an Agilent DD2-500 (^{1}H, 500 MHz; ^{13}C, 125 MHz; Agilent, Beijing, China). For NMR spectra in $CDCl_3$, the residual $CHCl_3$ resonance (δ_H 7.26 ppm) and the $CDCl_3$ resonance (δ_C 77.16 ppm) served as internal references for ^{1}H and ^{13}C NMR, respectively. Similarly, in CD_3OD, the residual CH_3OH resonance (δ_H 3.31 ppm) and the CD_3OD resonance (δ_C 49.00 ppm) were used as internal standards. For NMR spectra in C_6D_6, the residual C_6D_6 resonance (δ_H 7.16 ppm) and the C_6D_6 resonance (δ_C 128.1 ppm) were used as internal standards. High-resolution electrospray ionization mass spectrometry (HRESIMS) data were collected on a Micromass Q-Tof Ultima GLOBAL GAA076LC mass spectrometer (Autospec-Ultima-TOF, Waters, Shanghai, China). Semi-preparative HPLC was performed using a Waters 1525 pump equipped with a 2998 photodiode array detector and a YMC C18 column (10 × 250 mm, 5 μm). Column chromatography was carried out using silica gel (200–300 mesh, 300–400 mesh, or H grade). Melting points were determined on a ZGX-5 Plus microscopic melting point apparatus (Shanghai Zhuoguang Instrument Technology Co., Ltd., Shanghai, China).

3.2. Fungus Material

The fungal strain 18XS-01-ZM-05, isolated in July 2018 from the South China Sea sponge *Agelas* sp. (Xisha Island [Yagong Island]; 16°34′N, 111°41′E), was identified as *A. templicola* through ITS sequence analysis (GenBank PQ685989), which showed 99% identity to the corresponding sequence of *A. templicola* (GenBank OL711823.1). The strain was deposited at the Key Laboratory of Marine Drugs, Chinese Ministry of Education, Ocean University of China.

3.3. Fermentation, Extraction, and Isolation

Solid-state fermentation was conducted in 100 flasks, each containing a sterile medium of rice (100 g), glucose (2 g), NaCl (1 g), and distilled water (100 mL). *A. templicola* was aseptically inoculated into each flask. After 56 days of fermentation, the fermentations were all combined and the supernatant was extracted three times with EtOAc.

The ethyl acetate extract (96.2 g) was fractionated by a silica gel column chromatography (CC) eluted with sequential gradient elution petroleum ether/acetone (from 100:1 to 1:1, *v*/*v*), then eluted with a gradient of CH_2Cl_2/CH_3OH (from 20:1 to 1:1, *v*/*v*) to obtain eight fractions.

Fr.4 (2.8 g) was subjected to silica gel CC (petroleum ether/acetone, from 30:1 to 1:1, *v*/*v*), yielding six subfractions (Fr.4.1–Fr.4.6). Fr.4.5 was further purified by silica gel CC (petroleum

ether/acetone, from 20:1 to 1:1, *v/v*), resulting in six subfractions (Fr.4.5.1–Fr.4.5.6). Fr.4.5.3 was purified using semi-preparative HPLC (ODS, 5 μm, 250 × 10 mm; CH_3OH/H_2O, 75:25, *v/v*; 2 mL·min^{-1}) to yield **1** (2.2 mg).

Fr.5 (3.1 g) was subjected to silica gel CC (petroleum ether/acetone, from 25:1 to 1:1, *v/v*) and divided into nine subfractions (Fr.5.1–Fr.5.9). Fr.5.2 was purified by silica gel CC (petroleum ether/acetone, from 25:1 to 1:1, *v/v*), resulting in six subfractions (Fr.5.2.1–Fr.5.2.6). Fr.5.2.4 was purified using semi-preparative HPLC (ODS, 5 μm, 250 × 10 mm; CH_3OH/H_2O, 70:30, *v/v*; 2 mL·min^{-1}) to yield **8** (21.6 mg), **9** (22.2 mg). Fr.5.6 was separated by silica gel CC (petroleum/acetone, from 15:1 to 1:1, *v/v*) into five subfractions (Fr.5.6.1–Fr.5.6.5). Fr.5.6.2 was purified by semi-preparative HPLC (ODS, 5 μm, 250 × 10 mm; CH_3OH/H_2O, 68:32, *v/v*; 2 mL·min^{-1}) to afford **5** (2.2 mg).

Fr.6 (2.5 g) was separated by silica gel CC (petroleum/acetone, from 20:1 to 1:1, *v/v*) into eight subfractions (Fr.6.1–Fr. 6.8). Fr.6.2 was subjected to silica gel CC (petroleum/acetone, from 20:1 to 1:1, *v/v*), yielding nine fractions (Fr.6.2.1–Fr.6.2.9). Fr.6.2.2 was purified using semi-preparative HPLC (ODS, 5 μm, 250 × 10 mm; CH_3OH/H_2O, 65:35, *v/v*; 2 mL·min^{-1}) to yield **7** (14.5 mg). Fr.6.8 was separated by silica gel CC (petroleum/acetone, from 15:1 to 1:1, *v/v*) into five fractions (Fr.6.8.1–Fr.6.8.5). Fr.6.8.5 was purified by semi-preparative HPLC (ODS, 5 μm, 250 × 10 mm; CH_3CN/H_2O, 45:55, *v/v*; 2 mL·min^{-1}) to afford **4** (3.8 mg).

Fr.7 (5.1 g) was separated by silica gel CC (petroleum/acetone, from 15:1 to 1:1, *v/v*) into nine subfractions (Fr.7.1–Fr. 7.9). Fr.7.2 was subjected to silica gel CC (petroleum/acetone, from 15:1 to 1:1, *v/v*), yielding five fractions (Fr.7.2.1–Fr.7.2.5). Fr.7.2.3 was purified using semi-preparative HPLC (ODS, 5 μm, 250 × 10 mm; CH_3OH/H_2O, 65:35, *v/v*; 2 mL·min^{-1}) to yield **2** (2.6 mg). Fr.7.7 was separated by silica gel CC (petroleum/acetone, from 10:1 to 1:1, *v/v*) into six fractions (Fr.7.7.1–Fr.7.7.6). Fr.7.7.4 was purified by semi-preparative HPLC (ODS, 5 μm, 250 × 10 mm; CH_3CN/H_2O, 40:60, *v/v*; 2 mL·min^{-1}) to afford **3** (4.4 mg) and **6** (6.5 mg).

Fr.8 (8.3 g) was subjected to silica gel CC (petroleum ether/acetone, from 10:1 to 1:1, *v/v*), yielding nine subfractions (Fr.8.1–Fr.8.9). Fr.8.5 was further purified by silica gel CC (petroleum ether/acetone, from 10:1 to 1:1, *v/v*), resulting in six subfractions (Fr.8.5.1–Fr.8.5.6). Fr.8.5.2 was purified using semi-preparative HPLC (ODS, 5 μm, 250 × 10 mm; CH_3OH/H_2O, 50:50, *v/v*; 2 mL·min^{-1}) to yield **10** (86.3 mg).

Colachalasin J (**1**)

Colorless crystal; mp 160.1–164.2 °C; $[\alpha]_D^{25}$ + 30.2 (*c* 0.2, CH_3OH); UV (CH_3OH) λ_{max} (log ε) 196 (1.67), 214 (0.75), 250 (0.09) nm; ECD (0.25 mm, CH_3OH) λ_{max} ($\Delta\varepsilon$) 206 (4.73), 229 (–1.16), 258 (0.07) nm; IR (KBr) ν_{max} 2969, 2361, 2335, 1699, 1540, 1454, 1268, 1100 cm^{-1}; ^{1}H and ^{13}C NMR data see Table S2; HRESIMS *m/z* 482.2892 $[M + H]^+$ (calcd for $C_{29}H_{40}NO_5$, 482.2901).

Colachalasin K (**2**)

Colorless powder; $[\alpha]_D^{25}$ + 40.2 (*c* 0.2, CH_3OH); UV (CH_3OH) λ_{max} (log ε) 196 (1.23), 215, (0.52), 250 (0.06) nm; ECD (0.25 mm, CH_3OH) λ_{max} ($\Delta\varepsilon$) 204.5 (5.53), 220 (−2.88), 262.5 (1.14) nm; IR (KBr) ν_{max} 2361, 2339, 1702, 1650, 1540, 1457, 1271, 1098 cm^{-1}; ^{1}H and ^{13}C NMR data see Table S2; HRESIMS *m/z* 450.2631 $[M + H]^+$ (calcd for $C_{28}H_{36}NO_4$, 450.2639).

Colachalasin L (**3**)

Colorless powder; $[\alpha]_D^{25}$ + 25.5 (*c* 0.2, CH_3OH); UV (CH_3OH) λ_{max} (log ε) 195 (1.21), 210 (2.71), 250 (0.26) nm; ECD (0.25 mm, CH_3OH) λ_{max} ($\Delta\varepsilon$) 211 (−0.53), 263 (1.27) nm; IR (KBr) ν_{max} 2807, 2730, 2354, 1660, 1582, 1386, 1350, 1083 cm^{-1}; ^{1}H and ^{13}C NMR data see Table S3; HRESIMS *m/z* 464.2430 $[M - H]^-$ (calcd for $C_{28}H_{34}NO_5$, 464.2442).

Colachalasin M (**4**)

Colorless oil; $[\alpha]_D^{25}$ + 33.1 (*c* 0.2, CH_3OH); UV (CH_3OH) λ_{max} (log ε) 199 (2.80), 210 (1.63), 220 (0.53) nm; ECD (0.25 mm, CH_3OH) λ_{max} ($\Delta\varepsilon$) 205 (5.06), 242 (−0.01), 293 (0.43) nm; IR (KBr) ν_{max} 2808, 2730, 2354, 2338, 1660, 1386, 1350, 1083 cm^{-1}; ^1H and ^{13}C NMR data see Table S3; HRESIMS *m*/*z* 512.2653 $[M + H]^+$ (calcd for $C_{29}H_{38}NO_7$, 512.2643).

Avellanin P (**5**)

Yellow oil; $[\alpha]_D^{25}$ + 23.3 (*c* 0.2, CH_3OH); UV (CH_3OH) λ_{max} (log ε) 196 (2.83), 209 (2.73), 245 (0.95) nm; ECD (0.25 mm, CH_3OH) λ_{max} ($\Delta\varepsilon$) 211 (−7.14), 233 (4.18) nm; IR (KBr) ν_{max} 2829, 2708, 1660, 1591, 1381, 1350 cm^{-1}; ^1H and ^{13}C NMR data see Table S4; HRESIMS *m*/*z* 562.3037 $[M + H]^+$ (calcd for $C_{31}H_{40}N_5O_5$, 562.3024).

3.4. X-Ray Crystallographic Analysis

Colorless crystals of compounds **1**, **6**, **7** were obtained from a mixed solvent of ethanol and H_2O at room temperature. X-ray crystallographic data were collected using a Bruker APEX-II CCD diffractometer. The crystal structures were solved with the ShelXT structure solution program using Intrinsic Phasing and refined with the ShelXL refinement package through Least Squares minimization. The crystallographic data are provided in Tables S5–S7. The crystallographic data in CIF format have been deposited at the Cambridge Crystallographic Data Centre (deposition number: CCDC 2423674, 2464770, 2464771).

3.5. HPLC Analysis of Marfey's Derivatives

Compound 5 (0.5 mg) was dissolved in 6 N HCl (1 mL) in a sealed glass bottle and incubated at 70 °C for 12h. After cooling, the resultant hydrolysate was dried to remove the remaining HCl, then it was dissolved in 100 μL of H_2O. Subsequently, 1 M $NaHCO_3$ (20 μL) and 1% FDAA (Marfey's reagent, 100 μL) were added and the mixture, which was then incubated at 40 °C for 1 h. The reaction was quenched by adding 2 N HCl (10 μL). The mixture was dissolved in MeOH (500 μL) and analyzed by HPLC (SilGreen C-18 column, 250 × 4.6 mm) with gradient elution CH_3CN/H_2O with 0.1% HCOOH (from 15% to 45% acetonitrile during 55 min, flow rate 1.0 mL/min, detector at 340 nm). The standard amino acids L-Pro, D-Pro, L-*N*MePhe, D-*N*MePhe, L-Ala, D-Ala, L-Leu, D-Leu were treated as the above process. Retention times for the FDAA-derivative amino-acid standards were 28.5 min for L-Pro, 30.5 min for D-Pro, 43.8 min for L-*N*MePhe, 48.8 min for D-*N*MePhe, 43.5 min for L-Ala, 49.0 min for D-Ala, 26.5 min for L-Leu, and 31.5 min for D-Leu. Acid hydrolysate of **5** contained L-Pro (28.5 min), L-*N*MePhe (43.8 min), D-Leu (49.0 min), and L-Ala (26.5 min).

4. Conclusions

In conclusion, four new cytochalasins (**1**–**4**), a new cyclic pentapeptides (**5**), and five known compounds (**6**–**10**) were isolated from the endophytic fungus *A. templicola* guided by the analysis of biosynthetic gene clusters and the OSMAC strategy. Their structures were elucidated through extensive spectroscopic, X-ray diffraction analyses, and Marfey's analysis. In bioactivity assays, compound **2** demonstrated potent anti-inflammatory activity in zebrafish. Compounds **4** and **6** showed cytotoxicity against selected cell lines. These findings provide valuable insights for the development of anti-inflammatory and antitumor agents derived from cytochalasins. These results demonstrate that integrating biosynthetic gene cluster analysis with the OSMAC strategy effectively promotes the production of bioactive secondary metabolites.

Supplementary Materials: The following supporting information can be downloaded at: https://www.mdpi.com/article/10.3390/md23070285/s1, *HcpA1* Amino acid sequence; crystallographic data of **1**, **6**, and **7**; spectroscopic data including 1D and 2D NMR of **1**–**5**; spectroscopic data including

1D NMR of **6**–**10**; HRESIMS and IR spectra of **1**–**5**; experimental ECD spectra of **1** and **5**; HPLC analysis of Marfey's derivatives of avellanin P (**5**); Anti-inflammatory Assays [20]; Cytotoxicity Assays [21]. (PDF). CIF file for **1**, **6**, and **7**. (CIF).

Author Contributions: P.L. designed the experiments, supervised, and acquired funding; K.L. performed the experiments, isolated the compounds, and analyzed the spectral data; K.L., Y.Z., L.L., and S.W. prepared the Supplementary Materials; S.W. and Y.Z. recorded data.; K.L. and C.W. analyzed the spectral data and wrote the paper. All authors have read and agreed to the published version of the manuscript.

Funding: This research was funded by the National Natural Science Foundation of China (Grant No. 42276088 and 81991522), Foundation of State Key Laboratory of Component-based Chinese Medicine (Grant No. CBCM2024203).

Institutional Review Board Statement: Not applicable.

Data Availability Statement: Data are contained within the article or Supplementary Materials; further inquiries can be directed to the corresponding author.

Conflicts of Interest: The authors declare no conflicts of interest.

References

1. Jiang, M.; Wu, Z.; Guo, H.; Liu, L.; Chen, S. A Review of Terpenes from Marine-Derived Fungi: 2015–2019. *Mar. Drugs.* **2020**, *18*, 321. [CrossRef] [PubMed]
2. Scherlach, K.; Hertweck, C. Mining and unearthing hidden biosynthetic potential. *Nat. Commun.* **2021**, *12*, 3864. [CrossRef] [PubMed]
3. Frank, M.; Hartmann, R.; Plenker, M.; Mandi, A.; Kurtan, T.; Ozkaya, F.C.; Muller, W.E.G.; Kassack, M.U.; Hamacher, A.; Lin, W.; et al. Brominated Azaphilones from the Sponge-Associated Fungus *Penicillium canescens* Strain 4.14.6a. *J. Nat. Prod.* **2019**, *82*, 2159–2166. [CrossRef] [PubMed]
4. Wei, Q.; Bai, J.; Yan, D.; Bao, X.; Li, W.; Liu, B.; Zhang, D.; Qi, X.; Yu, D.; Hu, Y. Genome mining combined metabolic shunting and OSMAC strategy of an endophytic fungus leads to the production of diverse natural products. *Acta Pharm Sin B.* **2021**, *11*, 572–587. [CrossRef]
5. Hewage, R.T.; Aree, T.; Mahidol, C.; Ruchirawat, S.; Kittakoop, P. One strain-many compounds (OSMAC) method for production of polyketides, azaphilones, and an isochromanone using the endophytic fungus *Dothideomycete* sp. *Phytochemistry* **2014**, *108*, 87–94. [CrossRef]
6. Yu, G.; Sun, Z.; Peng, J.; Zhu, M.; Che, Q.; Zhang, G.; Zhu, T.; Gu, Q.; Li, D. Secondary Metabolites Produced by Combined Culture of *Penicillium crustosum* and a *Xylaria* sp. *J. Nat. Prod.* **2019**, *82*, 2013–2017. [CrossRef]
7. Wang, M.-H.; Jiang, T.; Ding, G.; Niu, S.-B.; Wang, X.-W.; Yu, M.; Gu, Y.-C.; Zhang, Q.-B.; Chen, J.-H.; Jia, H.-M.; et al. Molecular epigenetic approach activates silent gene cluster producing dimeric bis-spiro-azaphilones in *Chaetomium globosum* CBS148.51. *J. Antibiot.* **2017**, *70*, 801–804. [CrossRef]
8. Li, K.; Zhang, Y.; Jin, T.; Li, L.; Yang, J.; Wang, S.; Wang, C.; Li, P. Cytochalasins from the Sponge-Derived Fungus *Aspergillus templicola* and Their Biological Activities. *J. Nat. Prod.* **2025**, *88*, 1309–1318. [CrossRef]
9. Qiao, K.; Chooi, Y.-H.; Tang, Y. Identification and engineering of the cytochalasin gene cluster from *Aspergillus clavatus* NRRL 1. *Metab. Eng.* **2011**, *13*, 723–732. [CrossRef]
10. Andersen, M.R.; Ali, H.; Ries, M.I.; Lankhorst, P.P.; van der Hoeven, R.A.M.; Schouten, O.L.; Noga, M.; Hankemeier, T.; van Peij, N.N.M.E.; Bovenberg, R.A.L.; et al. A Non-Canonical NRPS Is Involved in the Synthesis of Fungisporin and Related Hydrophobic Cyclic Tetrapeptides in *Penicillium chrysogenum*. *PLoS ONE* **2014**, *9*, e98212.
11. Weber, M.; Dékány, M.; Nagyné, A.N.; Felegyi-Tóth, C.A.; Suratno, S.; Krámos, B.; Bodó, E.; Béni, Z.; Ványolós, A. Gymnopeptides C and D, Highly N-Methylated Fungal Cyclopeptides. *J. Nat. Prod.* **2025**, *88*, 644–649. [CrossRef] [PubMed]
12. Li, H.; Chen, Y.; Tang, B.; Liu, Z.; Peng, B.; Li, J.; Gao, H.; Wang, S.; Li, Z. Cyclopeptide Avellanins D–O with Antimalarial Activity from the Mariana Trench Anemone-Derived *Hamigera ingelheimensis* MSC5. *J. Nat. Prod.* **2024**, *87*, 2695–2708. [CrossRef] [PubMed]
13. Igarashi, Y.; Gohda, F.; Kadoshima, T.; Fukuda, T.; Hanafusa, T.; Shojima, A.; Nakayama, J.; Bills, G.F.; Peterson, S. Avellanin C, an inhibitor of quorum-sensing signaling in Staphylococcus aureus, from *Hamigera ingelheimensis*. *J. Antibiot.* **2015**, *68*, 707–710. [CrossRef] [PubMed]
14. Zhang, H.-W.; Zhang, J.; Hu, S.; Zhang, Z.-J.; Zhu, C.-J.; Ng, S.; Tan, R.-X. Ardeemins and Cytochalasins from *Aspergillus terreus* Residing in *Artemisia annua*. *Planta Medica* **2010**, *76*, 1616–1621. [CrossRef]

15. Lin, Z.-J.; Zhu, T.-J.; Zhang, G.-J.; Wei, H.-J.; Gu, Q.-Q. Deoxy-cytochalasins from a marine-derived fungus *Spicaria elegans*. *Can. J. Chem.* **2009**, *87*, 486–489. [CrossRef]
16. Zhou, G.-X.; Wijeratne, E.M.K.; Bigelow, D.; Pierson, L.S.; VanEtten, H.D.; Gunatilaka, A.A.L. Aspochalasins I, J, and K: Three New Cytotoxic Cytochalasans of *Aspergillus flavipes* from the Rhizosphere of *Ericameria laricifolia* of the Sonoran Desert. *J. Nat. Prod.* **2004**, *67*, 328–332. [CrossRef]
17. Zheng, C.-J.; Shao, C.-L.; Wu, L.-Y.; Chen, M.; Wang, K.-L.; Zhao, D.-L.; Sun, X.-P.; Chen, G.-Y.; Wang, C.-Y. Bioactive Phenylalanine Derivatives and Cytochalasins from the Soft Coral-Derived Fungus, *Aspergillus elegans*. *Mar. Drugs.* **2013**, *11*, 2054–2068. [CrossRef]
18. Huang, R.-M.; Ma, W.; Dong, J.-D.; Zhou, X.-F.; Xu, T.; Lee, K.J.; Yang, X.; Xu, S.-H.; Liu, Y. A New 1,4-Diazepine from South China Sea Marine Sponge *Callyspongia Species*. *Molecules* **2010**, *15*, 871–877. [CrossRef]
19. Liu, R.; Lin, Z.; Zhu, T.; Fang, Y.; Gu., Q.; Zhu, W. Novel Open-Chain Cytochalsins from the Marine-Derived Fungus *Spicaria elegans*. *J. Nat. Prod.* **2008**, *71*, 1127–1132. [CrossRef]
20. Nguyen, T.H.; Le, H.D.; Nguyen Thi Kim, T.; Pham The, H.; Nguyen, T.M.; Cornet, V.; Lambert, J.; Kestemont, P. Anti–Inflammatory and Antioxidant Properties of the Ethanol Extract of *Clerodendrum Cyrtophyllum* Turcz in Copper Sulfate-Induced Inflammation in Zebrafish. *Antioxidants.* **2020**, *9*, 192. [CrossRef]
21. Zhang, G.; Yin, R.; Dai, X.; Wu, G.; Qi, X.; Yu, R.; Li, J.; Jiang, T. Design, synthesis, and biological evaluation of novel 7-substituted 10,11-methylenedioxy-camptothecin derivatives against drug-resistant small-cell lung cancer in *vitro* and in *vivo*. *Eur. J. Med. Chem.* **2022**, *241*, 114610. [CrossRef]

Disclaimer/Publisher's Note: The statements, opinions and data contained in all publications are solely those of the individual author(s) and contributor(s) and not of MDPI and/or the editor(s). MDPI and/or the editor(s) disclaim responsibility for any injury to people or property resulting from any ideas, methods, instructions or products referred to in the content.

marine drugs

MDPI

Article

Structural and Functional Insights into a Novel *Aspergillus ochraceus* Polysaccharide from the Weddell Sea: Implications for Melanoma Immunotherapy In Vitro

Jiale Hao [1,†], Kouame kra Wilfred Armel [1,†], Pengcheng Gao [1], Jinglei Wang [1], Weibin Zhang [1], Kexin Du [1], Qi Li [1], Huishu Gao [1], Guangli Yu [1,2,*] and Guoyun Li [1,2,*]

[1] Key Laboratory of Marine Drugs, Shandong Key Laboratory of Glycoscience and Glycotherapeutics, Ministry of Education, School of Medicine and Pharmacy, Ocean University of China, Qingdao 266003, China; hjl9700@163.com (J.H.); kouamewfu@gmail.com (K.k.W.A.); gaopengchengsir@163.com (P.G.); wjinglei920@163.com (J.W.); zwb19960327@163.com (W.Z.); 15206566923@163.com (K.D.); 15166013795@163.com (Q.L.); gaohuishu0628@163.com (H.G.)

[2] Laboratory for Marine Drugs and Bioproducts, Qingdao Marine Science and Technology Center, Qingdao 266237, China

* Correspondence: liguoyun@ouc.edu.cn (G.Y.); glyu@ouc.edu.cn (G.L.)

† These authors contributed equally to this work.

Abstract: Immunotherapy is a transformative strategy in oncology, yet the development of novel immunomodulatory agents remains essential. This study explores the anti-tumor potential of a structurally unique polysaccharide isolated from an *Aspergillus ochraceus* (AOP), sourced from the Antarctic Weddell Sea. Using alkaline-assisted extraction and chromatographic purification, we obtained a homogeneous polysaccharide predominantly composed of galactose and mannose, with an average molecular weight of 39.67 kDa. The structure was characterized by an integrated nuclear magnetic resonance spectroscopy and mass spectrometry analysis, revealing that the AOP is composed of β (1→5)-linked galactofuranose units, with a minor substitution by α-D-mannopyranose residues via (1→2) glycosidic bonds at the C2 of the galactofuranose. Functional assays, including CCK8 and wound-healing tests, demonstrated that this polysaccharide, referred to as AOP, inhibited melanoma cell proliferation and migration in a dose-dependent manner. Additionally, the AOP activated RAW264.7 and bone marrow-derived macrophage (BMDM) cells without exhibiting significant cytotoxicity, leading to the release of inflammatory factors such as TNF-α, IL-1β, and IL-6. Mechanistically, the AOP was found to upregulate the expression of CD86 and IFN-γ, while downregulating genes like IL-4 and Arg1. These findings position the AOP as the first documented Antarctic fungal polysaccharide with macrophage-reprogramming capabilities against melanoma, offering novel molecular insights for marine-derived immunotherapeutics.

Keywords: *Aspergillus ochraceus*; melanoma; immunotherapy; macrophages; anti-tumor; polysaccharide

1. Introduction

In recent years, the advent of immunotherapy has revolutionized traditional melanoma treatment approaches [1]. Increasing evidence highlights the critical role of macrophages in tumors, with their primary functions encompassing immune defense [2], immune regulation [3], and immune secretion [4]. Macrophages are adept at recognizing pathogen-associated molecular patterns (PAMPs) and damage-associated molecular patterns (DAMPs) [5]. Traditionally, activated macrophages are classified into two polarization

states within the tumor microenvironment (TME), collectively known as tumor-associated macrophages (TAMs): M1-TAMs, or classically activated macrophages, and M2-TAMs, or alternatively activated macrophages [6]. M1 macrophages play a pivotal anti-tumor role by mediating phagocytosis and antibody-dependent cell cytotoxicity, while releasing pro-inflammatory cytokines such as tumor necrosis factor alpha (TNF-α), interleukin-1β (IL-1β), and interleukin-6 (IL-6) [7]. In contrast, M2-TAMs contribute to tumor development and metastasis by promoting anti-inflammatory processes, enhancing tumor angiogenesis, and facilitating tumor progression [8] through mechanisms such as the epithelial-to-mesenchymal transition (EMT) process [9]. Melanoma, known for its aggressive metastatic behavior, is significantly influenced by EMT; this process is characterized by the transition from E-cadherin to N-cadherin, along with the upregulation of genes like vimentin, slug, and snail, which enables melanoma cells to form N-cadherin-mediated adhesion with stromal fibroblasts [10]. Therefore, encouraging the conversion of M2-TAMs to M1-TAMs represents a promising therapeutic strategy, with the potential to regulate macrophage activity and overall tumor progression.

Marine ecosystems represent an underexplored resource for pharmacological compounds, with 68% of novel natural products in clinical trials derived from marine organisms, particularly deep-sea fungi that thrive under extreme conditions and have developed unique biosynthetic pathways to produce stress-adapted metabolites [11]. Genomic analyses show that deep-sea fungi contain a higher abundance of carbohydrate-active enzymes (CAZymes) compared to their terrestrial counterparts, enabling the synthesis of structurally novel glycans with distinctive sulfation patterns and branching architectures, which are inaccessible via land-based synthesis [12]. Structural diversity fosters a plethora of biological activity. The *Aspergillus ochraceus* has complex biotechnological potential. Zou found that the strain *Aspergillus ochraceus* MCCC 3A00521 isolated from the Northeastern Pacific has strong inhibitory activity against ferroptosis by downregulating HMOX-1 expression [13]; Nasr et al. discovered that a protease activator (PAPC) secreted by *Aspergillus ochraceus* can disrupt the biofilm of Staphylococcus aureus, thereby exerting antibacterial activity [14]; Guo et al. identified a galactomannan with a novel structure produced by the coral endophytic fungus *Aspergillus ochraceus*, although its biological activity remains untested [15]. Despite these findings, there is still limited research on the structure and bioactivity of cell wall polysaccharides derived from *Aspergillus ochraceus*.

In recent years, we have been focusing on exploring the anti-tumor activity of marine-derived polysaccharides. This study aims to extract and purify cell wall polysaccharides from *Aspergillus ochraceus* captured in the Weddell Sea of Antarctica, further characterize its chemical structure, and preliminarily evaluate the anti-melanoma activity in vitro. Thus, the AOP (*Aspergillus ochraceus* polysaccharide) might become a novel leading compound for melanoma treatment due to its multiple potential effects.

2. Results

2.1. Yield and Purification

The AOP (300 mg, yielding 18.2% of the crude polysaccharide) was eluted with 0.2 M NaCl from the DEAE Sepharose Fast Flow column. The polysaccharide was further purified using a Sephacryl S-200 HR column, resulting in the isolation of a polysaccharide designated AOP (200 mg, yielding 47% of *Aspergillus ochraceus* biomass).

2.2. Molecular Weight and Monosaccharide Composition

The HPGPC analysis displayed a single symmetrical peak at approximately 27.46 min, confirming the homogeneity of the AOP, as shown in Figure 1A. Understanding the monosaccharide composition is crucial for characterizing polysaccharides, as monosaccha-

rides play a significant role in determining both the structure and biological activity of polysaccharides [16]. The HPLC analysis revealed that the AOP is a neutral polysaccharide (Figure 1B), primarily composed of mannose (Man) and galactose (Gal), with a molar ratio of 20.93:79.07. Notably, galactose was the predominant component in the AOP, comprising over 80% of the total polysaccharide content. This composition contrasts with findings from another study, which reported a different structure for the galactomannan produced by the coral endophytic fungus *Aspergillus ochraceus* [15]. The variations in monosaccharide composition may be attributed to differences in the extraction and purification methods employed in the studies.

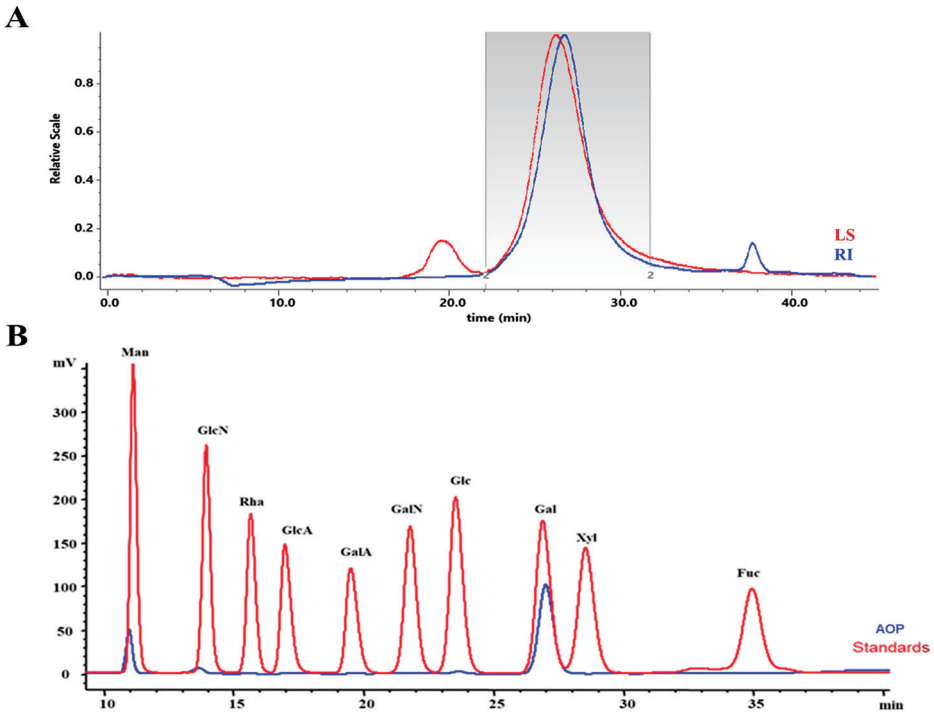

Figure 1. Characterization of polysaccharides. (**A**) The homogeneity of AOP using HPGPC. Peak with the molecular weight at 39.67 kDa was examined in the standard curve. (**B**) Monosaccharide composition analysis of AOP.

2.3. NMR Spectroscopy Analysis

The structural characterization of the polysaccharide was conducted through a comprehensive nuclear magnetic resonance (NMR) analysis. As shown in the ^{1}H-NMR spectrum (Figure 2A), two distinct anomeric proton signals were observed, at 5.21 ppm (G, unsubstituted β-D-galactofuranose backbone) and 5.05 ppm (M, α-D-mannopyranose). Non-anomeric protons (H2-H6) resonated between 3.60 and 4.20 ppm. The analysis of the ^{13}C-NMR spectrum (Figure 2B) revealed two characteristic anomeric carbon signals in the 90–110 ppm region: the G unit displayed an unusual C1 chemical shift at 108.48 ppm, significantly upfield-shifted compared to typical β-pyranose configurations (97–105 ppm). Our observed chemical shift data for C1 (≈108–110 ppm) corroborate prior characterizations of β-D-galactofuranose residues in *Aspergillus ochraceus* galactomannan [15,17–19], collectively confirming the β-furanose configuration. The corresponding anomeric proton signal (5.21 ppm) aligned with established β-Gal$_f$ H1 chemical shifts (5.0–5.5 ppm). The M unit exhibited a C1 signal at δ 102.01 ppm, within the conventional β-pyranose range. However, its associated H1 proton resonance at 5.21 ppm displayed an unusual downfield shift compared to typical β-pyranoses (4.5–5.0 ppm), suggesting α-mannopyranose configuration (5.2–5.4 ppm for α-anomers). Additional carbon signals (60.94–85.8 ppm) included a

characteristic unsubstituted C6 resonance at 62.66 ppm. The ^{1}H-^{13}C HSQC correlation spectrum (Figure 2C) confirmed the G unit assignment through direct correlation between H1 (5.21 ppm) and C1 (108.38 ppm). The exceptional C1 chemical shift deviation from standard β-pyranoses further supported the β-Gal$_f$ assignment, suggesting potential →5)-β-Gal$_f$-(1→ linkages through furanose ring formation. Structural connectivity was elucidated through HMBC analysis (Figure 2D). Key cross-peaks included GC5/GH1 (76.93/5.21 ppm), indicating →5)-β-Gal$_f$-(1→ glycosidic linkages; GC1/GH5 (108.38/3.97 ppm), confirming consecutive (1→5)-linked galactofuranose residues; and GC2/MH1 (83.96/5.05 ppm), suggesting mannopyranose attachment to the C2 of galactofuranose. The quantitative analysis of ^{1}H-NMR integrals revealed a G: M ratio of 14.0:1.0. This apparent discrepancy from the monosaccharide composition may arise from differential acid hydrolysis stability, as furanosidic bonds (G units) are more prone to degradation than pyranosidic linkages (M units) during acidic hydrolysis, leading to the relative enrichment of mannopyranose residues [20].

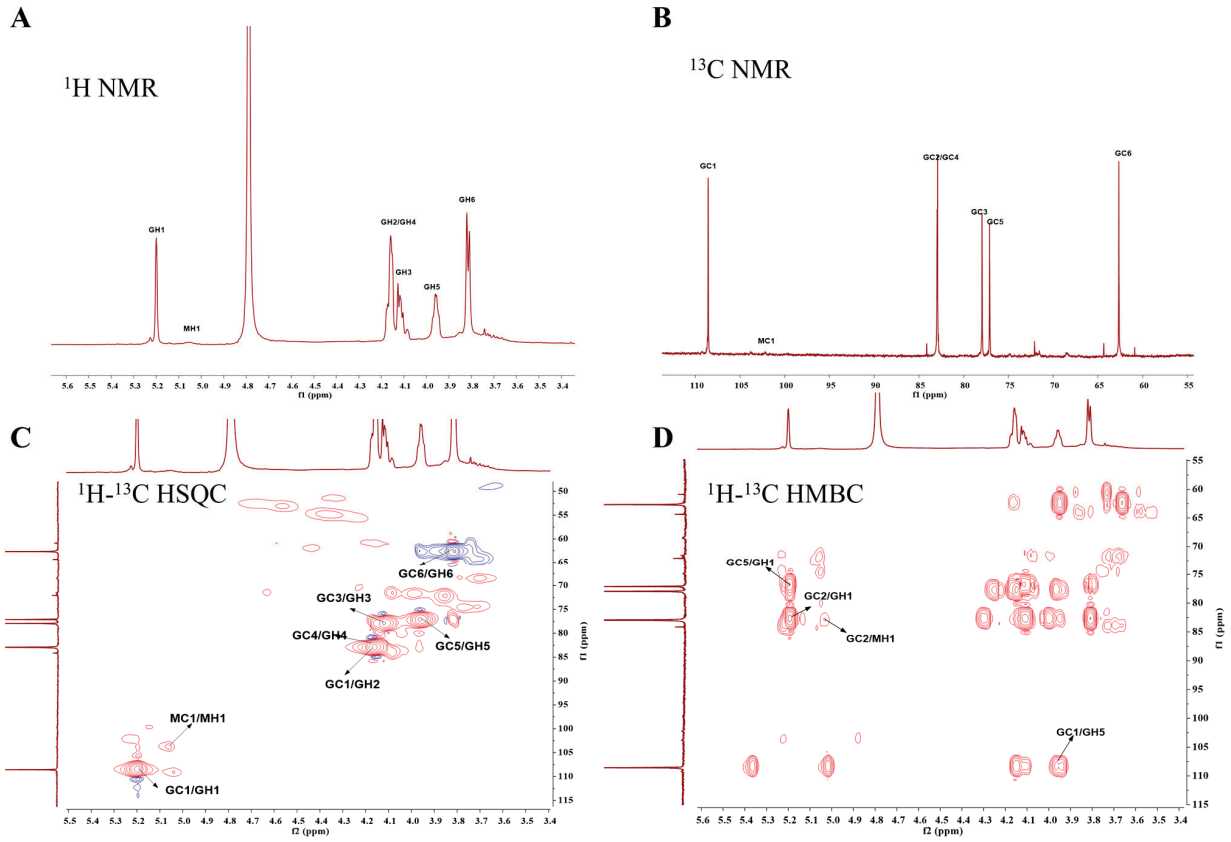

Figure 2. 1D and 2D spectra of AOP. (**A**) ^{1}H NMR spectrum; (**B**) ^{13}C NMR spectrum; (**C**) ^{1}H-^{13}C HSQC spectrum; and (**D**) ^{1}H-^{13}C HMBC spectrum. Chemical shifts are expressed in ppm using acetone as an internal standard at 2.225 ppm for ^{1}H and 31.07 ppm for ^{13}C. G or M correspond to → 5)-β-D-Gal$_f$ (1→and Man$_p$ α (1→2)-linked to the C2 position of Gal$_f$, respectively. Gal$_f$: galactofuranose, Man$_p$: mannopyranose.

2.4. Mass Spectrometric Fragment Ion Analysis of AOP Oligosaccharides

The oligosaccharide fragments generated by the controlled acid hydrolysis of the AOP were characterized by ESI-CID-MS^{2}. Given the structural homology with the galactomannan system reported in prior studies [15], we adopted their nomenclature system for fragment ion assignment. A typical cleavage was designated as W-series ions (W1, W2) representing C4-C5 bond cleavage at consecutive reducing-end glycosyl units, with A-type cross-ring fragments (A2, A3) assigned to non-reducing-end cleavages. A mass

spectrometry analysis was conducted in negative ion mode, revealing that the controlled acid degradation products predominantly comprised dp2–dp4 oligomers. The interpretation of the oligosaccharides' secondary fragment ions and their structural schematic diagram are illustrated in Figure 3. Characteristic C/Y-type glycosidic cleavages produced prominent ions at m/z 503.03 (Δ−162 Da) and 340.94 (Δ−324 Da), accompanied by B/Z-type fragments at m/z 323.03, 485.15, and 647.17. Cross-ring dissociation patterns included ^{3,4}A-series ions (m/z 232.93, 394.87, 557.10) and ^{0,3}A-type fragments (m/z 412.88, 574.96), while the W-series progression (m/z 280.91→442.98→605.03) showed sequential mass decreases of 162 Da, consistent with the loss of galactofuranose units. These spectral features were consistent with the →5)-β-Gal$_f$-(1→ linkage pattern identified by NMR, with W-type ions confirming terminal β-Gal$_f$ positioning and ^{3,4}A cleavages supporting a furanose ring geometry. The structural assignments derived from the tandem mass spectrometric analysis of MS^2 fragment ions were systematically corroborated through a comparative evaluation with NMR spectroscopic data, demonstrating a complementary agreement in the elucidation of glycosidic linkage patterns and monosaccharide configurations. The comprehensive structural analysis reveals that the *Aspergillus ochraceus* polysaccharide (AOP) possesses a backbone composed of β-(1→5)-linked galactofuranosyl residues. This predominant furanogalactan framework is partially substituted at the C2 position of galactofuranose residues by α-D-mannopyranose units via (1→2)-glycosidic bonds. The quantitative analysis of the repeating unit demonstrates an exact stoichiometric ratio of 15 monosaccharide constituents per structural repeat unit, comprising 14 galactofuranose moieties in the main chain and 1 mannopyranose residue as the pendant group. This architectural configuration results in a distinctive polysaccharide structure characterized by periodic mannan substitutions along the galactose backbone at defined intervals.

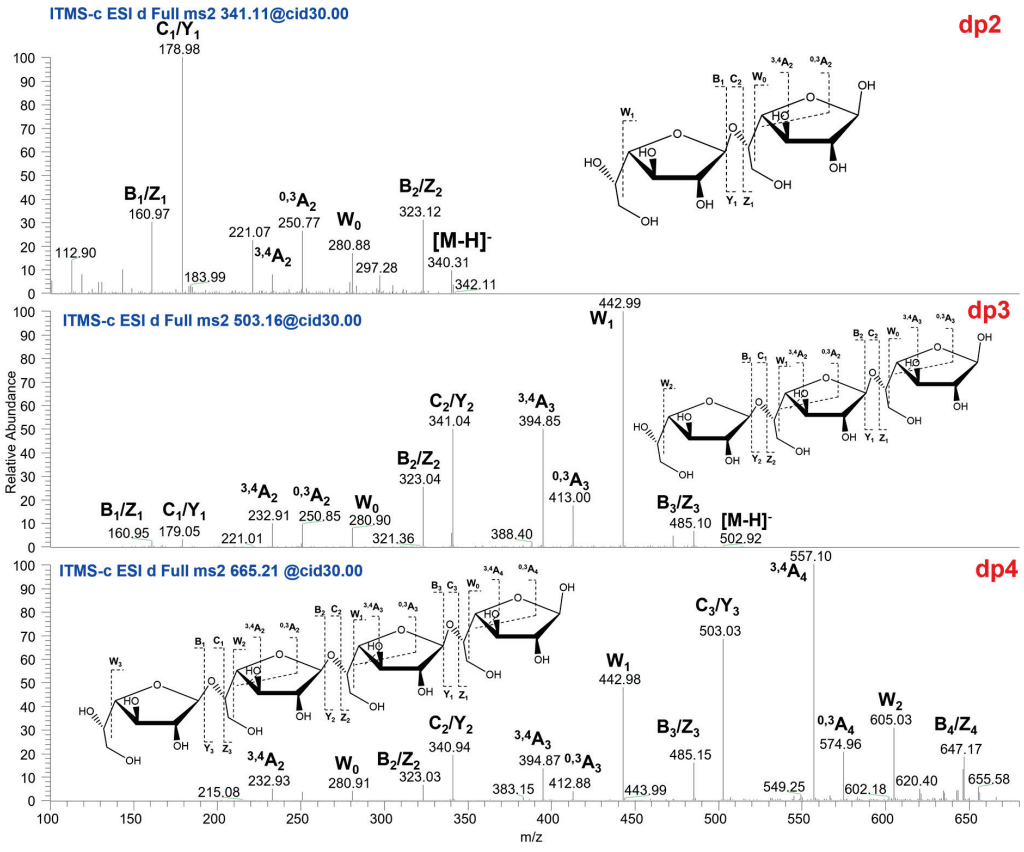

Figure 3. ESI-CID-MS^2 product ion spectrum and assignments of the ions of dp2-dp4. The sequence is shown to indicate the proposed fragmentations.

2.5. Cell Proliferation Analysis

Melanoma is one of the most aggressive forms of skin cancer and one of the most common cancers in humans [21]. Consequently, the development of effective therapeutic drugs is urgently needed. To explore the impact of the AOP on melanoma cell proliferation, we first treated B16-F10 cells with varying concentrations of AOP. As shown in Figure 4A, the AOP treatment at 24 h exhibited no significant toxicity to B16-F10 cells. However, when the incubation time was extended to 48 and 72 h, AOP at a concentration of 50 μM significantly inhibited cell proliferation. To assess the apoptosis rate induced by the AOP, flow cytometry was employed. As illustrated in Figure 4B,C, nearly no apoptosis was observed in the control group of B16-F10 cells. After treating with the AOP at 100 and 200 μM for 48 h, apoptosis rates increased to approximately 13.16% and 17.95%, respectively. The simultaneous evaluation of AOP activity on A375 cells was performed. However, A375 cells appeared to be more sensitive to AOP treatment after 72 h, with proliferation being inhibited at lower concentrations (Figure 4D). Flow cytometry results indicated apoptosis rates of 23.02% and 42.76% at 100 and 200 μM, respectively (Figure 4E). This differential sensitivity may stem from the genetic variations between these two tumor types. Overall, it is suggested that the AOP's primary action is to inhibit the proliferation of melanoma cells rather than to induce apoptosis.

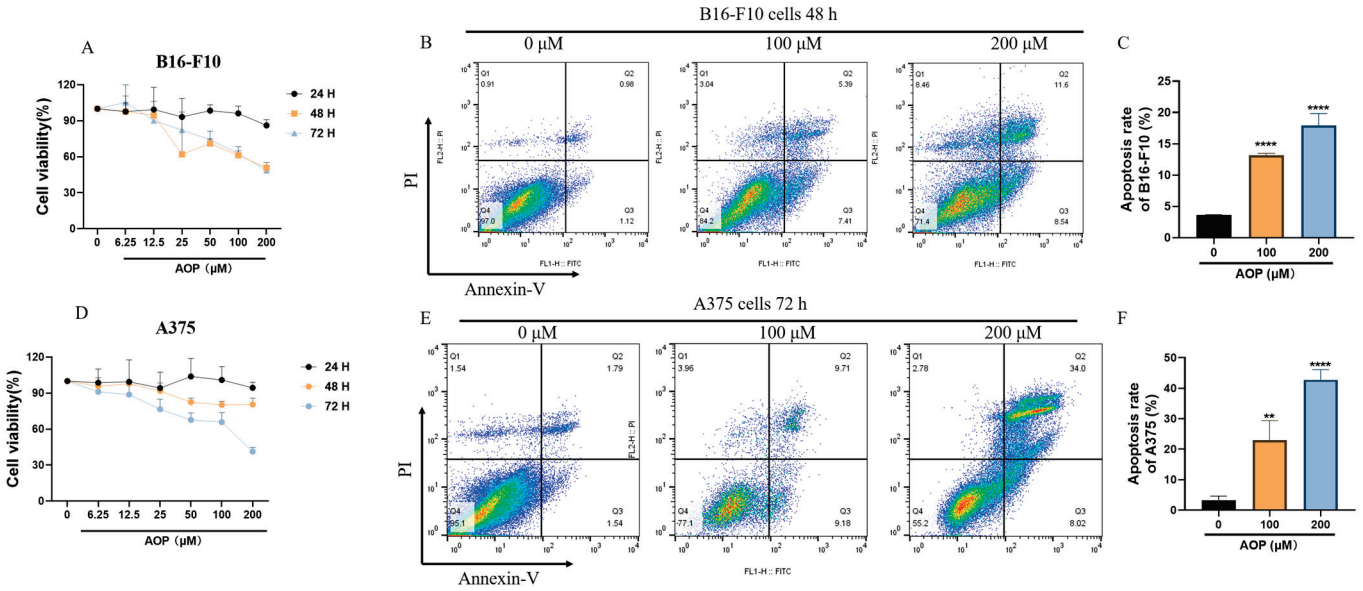

Figure 4. AOP could directly promote apoptosis of B16-F10 and A375 cells at high doses. B16-F10 cells (**A**) and A375 cells (**D**) were treated with different concentrations of AOP for 24, 48, and 72 h, followed by measuring cell viability by CCK8. Then, the amounts of apoptosis cells of B16-F10 cells (**B**) and A375 cells (**E**) were analyzed by flow cytometry, respectively. The statistical graph of three independent repeated experiments of (**C**,**F**). All data were obtained from three independent experiments and were presented as mean ± S.D., **, $p < 0.01$, ****, $p < 0.0001$, $n = 3$.

2.6. AOP Might Inhibit the Migration of Melanoma Cells by Suppressing the EMT Process

Melanoma is recognized as one of the most metastatic cancers, presenting significant challenges for clinical treatment [22]. To investigate the effects of the AOP on the migration of B16-F10 and A375 cells, we conducted wound-healing assays, transwell migration assays, and colony formation experiments. Initially, as demonstrated in Figure 5A,B, at the 0 h mark in B16-F10 cells, the scratch widths in both the control and AOP-treated groups were comparable. However, after further incubation for 5 and 12 h, the AOP significantly inhibited wound healing; the migration rates were 56.42% and 28.21%, respectively. By

24 h, the control group had nearly completed healing, while the 200 μM AOP treatment group showed incomplete wound closure with the migration rates of 85.68%, indicating that the AOP effectively inhibits the migration of B16-F10 cells, particularly within the first 12 h.

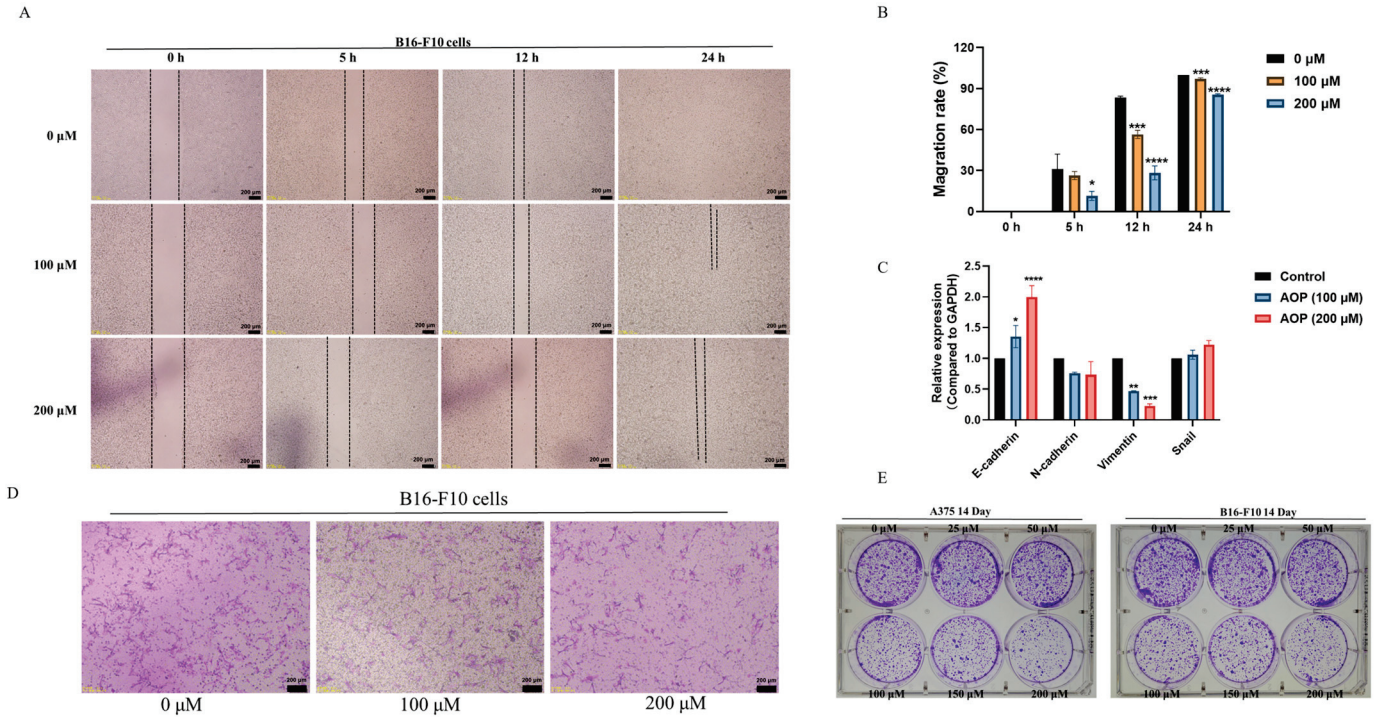

Figure 5. AOP could inhibit the migration of B16-F10 cells by inhibiting the EMT process. (**A**) B16-F10 cells were incubated with 100 μM or 200 μM AOP; subsequently, the wound healing of B16-F10 cells was observed at 5, 12, and 24 h, and the migration rates are shown in (**B**). Following the treatment with AOP for 12 h, total RNA was extracted and reversed transcription to cDNA, and the expression of E-cadherin, N-cadherin, snail, and vimentin were tested by qPCR assay (**C**). Furthermore, the effect of AOP on the migration ability of B16-F10 cells using transwell experiments is shown (**D**). Finally, after incubating B16-F10 cells or A375 cells with AOP or not, cultivation was continued for 14 days and the formation of clones was observed (**E**). The cell morphology was observed with Olympus CKX41 under bright field; the scale bar = 200 μm.; *, $p < 0.05$, **, $p < 0.01$, ***, $p < 0.001$, ****, $p < 0.0001$, $n = 3$.

Subsequently, as shown in Figure 5D, the AOP notably reduced the number of B16-F10 cells migrating from the upper chamber to the lower chamber of the transwell assay at concentrations of 100 and 200 μM. In the colony formation experiment, we observed a significant decrease in the number of clones formed by both B16-F10 (right) and A375 (left) cells following AOP incubation (Figure 5E). The epithelial-to-mesenchymal transition (EMT) is a critical process in cancer metastasis, during which epithelial cells acquire mesenchymal characteristics, enhancing their motility and migratory abilities [16]. Therefore, we next evaluated the expression of genes associated with the EMT process [23]. As illustrated in Figure 5C, the AOP treatment resulted in the downregulation of N-cadherin and vimentin, both of which promote EMT, while simultaneously upregulating the expression of E-cadherin. Based on these observations, we hypothesize that the AOP may inhibit the migration of B16-F10 and A375 cells by suppressing the EMT process.

2.7. AOP Could Exert Immune Anti-Tumor Activity In Vitro by Activating M1 Macrophages

Recent advancements in tumor immunotherapy have led to the approval of multiple immunotherapeutic drugs by the U.S. Food and Drug Administration (FDA) [24].

Macrophages play a pivotal role in anti-tumor immunity, regulating immune responses and eliminating tumor cells. However, the tumor microenvironment may "reprogram" macrophages, leading to tumor growth promotion [25]. Thus, we evaluated the effect of the AOP on macrophage activation. Our findings indicate that the AOP demonstrated no cytotoxic effects on raw264.7 cells while promoting the secretion of nitric oxide (NO), TNF-α, IL-1β, and IL-6 in a dose-dependent manner (Figure 6A). To validate these results further, we isolated primary bone marrow-derived macrophages (BMDMs), which similarly showed an enhanced release of inflammatory cytokines and NO in response to the AOP, without any signs of cytotoxicity (Figure 6B). Given the heterogeneity of macrophages in tumor settings, we hypothesize that the AOP may facilitate the reprogramming of macrophages from the M2 phenotype to the M1 phenotype. As depicted in Figure 6C,D, the AOP can downregulate M2-related genes such as IL-4, Arg1, and TGF-β1, while simultaneously upregulating M1-related genes like CD86, iNOS, IFN-γ, and COX2, supporting our hypothesis. It is worth noting that although the protein level of CD206 showed a trend of low-level increase, its expression did not exceed the baseline level of the control group. This phenomenon can be interpreted as the existence of a transitional activation state in macrophages.

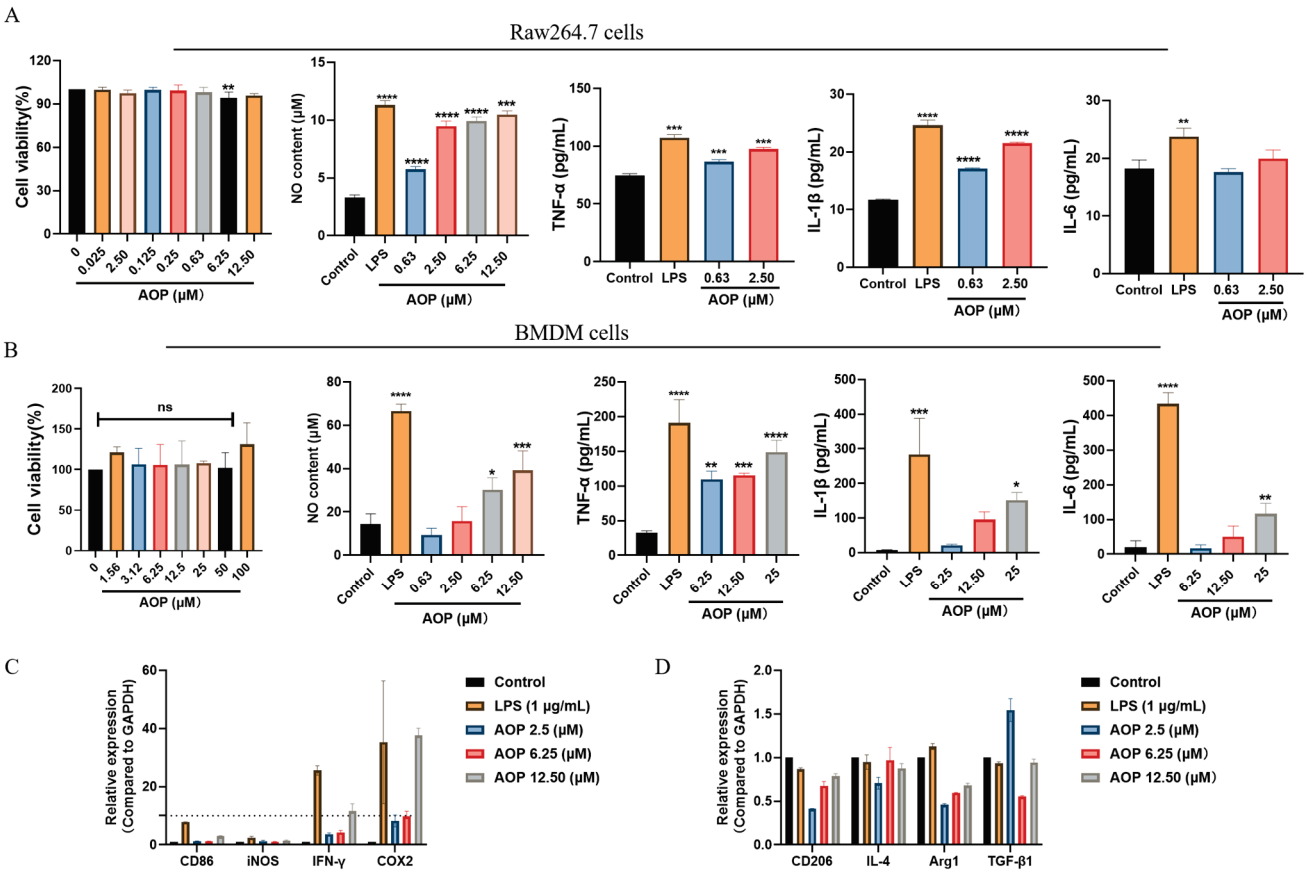

Figure 6. AOP could activate macrophages and promote their transformation to the M1 type at low concentrations. Raw264.7 cells (**A**) or BMDM cells (**B**) were treated with different concentrations of AOP for 24 h; then, the cell supernatant was collected, and the content of nitric oxide, TNF-α, IL-1β, and IL-6 in the supernatant was detected using ELISA assay. Total RNA of BMDM cells was extracted and reversed transcribed to cDNA, and the expression of CD86, iNOS, IFN-γ, and COX2 (**C**), and CD206, IL-4, Arg1, and TGF-β1 (**D**) was detected by qPCR assay. LPS was used as the positive control. Significance levels by two-tailed t-test: * $p < 0.05$, ** $p < 0.01$, *** $p < 0.001$, **** $p < 0.0001$.

To investigate whether macrophage activation by the AOP translates into anti-tumor efficacy, we established a luciferase-expressing B16-F10 model (B16-F10-luc) for the real-

time monitoring of tumor cell viability. The comparison of the transfection group to the control group revealed a strong green fluorescence, indicating successful plasmid incorporation (Figure 7A). Importantly, we noted no significant difference in proliferation between transfected B16-F10-luc cells and normal B16-F10 cells (Figure 7B). We then assessed the anti-tumor efficacy of AOP using a co-culture system through two approaches: direct contact and transwell indirect contact. In the direct contact assay, BMDM cells co-cultured with B16-F10-luc cells showed a 34.82% decrease in luminescence compared to the non-co-culture (NC) group, indicating a baseline cytotoxic effect of BMDMs. Furthermore, the AOP treatment resulted in additional reductions in luminescence, with decreases of 41.02% at 2.5 μM, 57.93% at 6.25 μM, and 64.64% compared to the NC group (Figure 7C). In contrast, when we employed the transwell indirect contact method, the anti-tumor activity of the AOP was not evident (Figure 7D). These findings suggest that the AOP can exert immune anti-tumor activity by promoting the activation of M1 macrophages, with this effect being dependent on direct cell-to-cell contact.

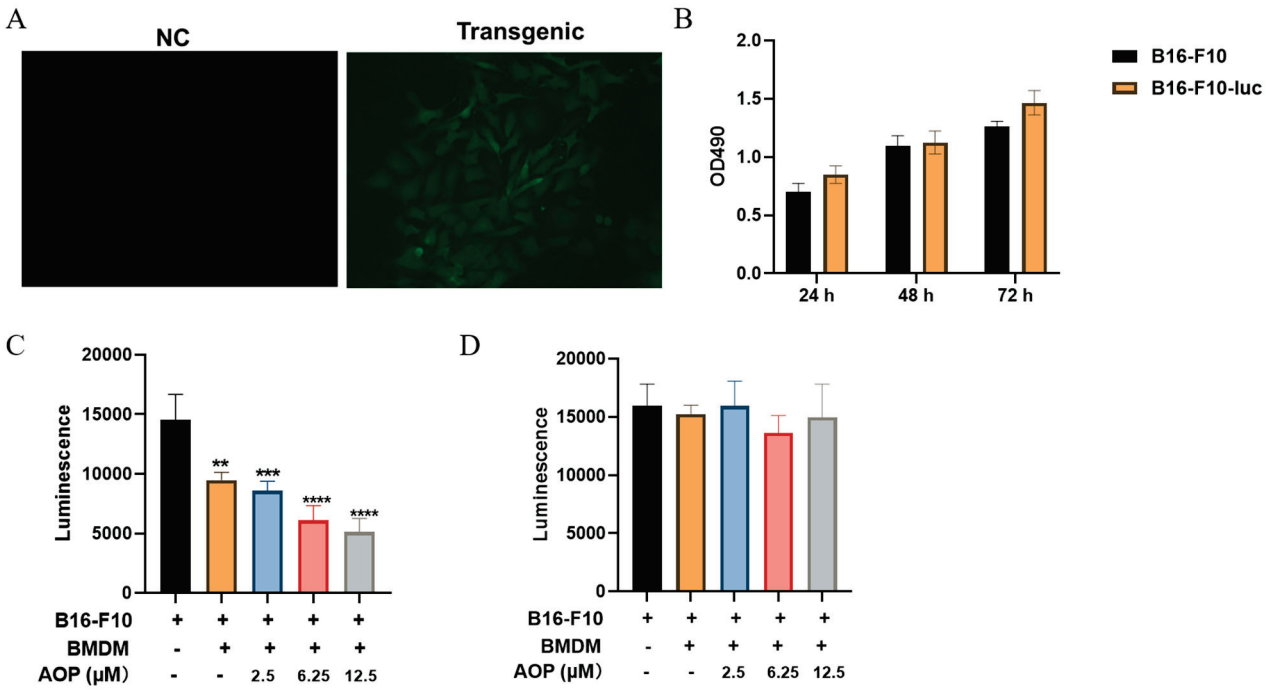

Figure 7. AOP could promote apoptosis of B16-F10 cells by activating BMDM at low concentrations. Briefly, plasmids containing the luc-EGFP sequence were transfected into cells to construct the B16-F10-luc stable transgenic cell line (**A**), and the difference in proliferation ability between B16-F10 and B16-F10-luc cells was evaluated (**B**). B16-F10 cells are incubated separately or together with AOP or BMDM cells for 24 hl subsequently, the proliferative ability of B16-F10 cells was evaluated using the luminescence value (**C**). The killing effect of AOP and BMDM on tumor cells without direct contact with B16-F10 was evaluated through transwell experiments (**D**). **, $p < 0.01$, ***, $p < 0.001$, ****, $p < 0.0001$, $n = 3$.

3. Discussion

The abyssal biome exerts unique evolutionary pressures that drive marine fungi to develop specialized chemobiosynthetic compensatory mechanisms [26]. While previous research on marine natural products has primarily concentrated on small-molecule secondary metabolites, the therapeutic potential of fungal structural polysaccharides remains significantly underexplored. *Aspergillus ochraceus*, a member of the *Aspergillus* genus, has been the subject of limited research regarding its polysaccharide content, particularly its cell wall polysaccharides [27]. Bardalaye et al. extracted a galactomannan peptide from the

Aspergillus niger hyphal wall, which contains 89% of carbohydrates and 11% of proteins [28]; Gomez-Miranda, B et al. isolated alkaline soluble α-glucan and insoluble β-glucan-chitin complexes from the cell wall of *Aspergillus alliaceus* sclerotia and analyzed an α-linked extracellular polysaccharide containing *D*-galactosamine (70%), *D*-galactose (10.5%), *D*-glucose (10.5%), and acetate ions (2.6%) [29]. Guo et al. analyzed an extracellular polysaccharide, isolated from the fermented broth of the fungus *Aspergillus ochraceus* derived from coral *Dichotella gemmacea*, called AW1, which is a galactomannan containing a mannan core [15].

Contrasting with these previous investigations, which have largely focused on structural analyses, our study primarily highlights the biological activities of the cell wall polysaccharides extracted from *Aspergillus ochraceus*. We have uncovered that these polysaccharides can inhibit the proliferation of melanoma cells and activate M1 macrophages in vitro. A clear distinction emerges between the current ratio of the monosaccharide composition of the AOP and the composition of galactomannans reported. Variations in monosaccharide composition are likely to influence the structural differences, subsequently leading to diverse bioactivities related to the anti-tumor effects observed. Currently, we have conducted only in vitro activity tests. In future work, we aim to further investigate the pharmacological activities and underlying mechanisms of these polysaccharides against melanoma.

4. Materials and Methods

4.1. Chemicals and Reagents

DEAE Sepharose Fast Flow and Sephacryl S-200 HR were purchased from GE Healthcare (Danderyd, Sweden). Monosaccharide standards (galacturonic acid (GalA), glucose (Glc), galactose (Gal), xylose (Xyl), arabinose (Ara), mannose (Man), and fucose (Fuc)) were purchased from Aladdin Bio-Chem Technology Co., Ltd. (Shanghai, China). The medium potatoe dextrose water (PDA) was purchased from Hope Bio-Technology Co., Ltd. (Qingdao, China). D_2O (99.9%) was purchased from Cambridge Isotope Laboratories, Inc. (Tewksbury, MA, USA). Puromycin (puro) and CCK8 were from Yeasen Biotechnology (Shanghai, China). Lipopolysaccharide (LPS) was obtained from Sigma-Aldrich (Saint Louis, MO, USA). Recombinant macrophage colony-stimulating factor (M-CSF) was from MedChemExpress (Shanghai, China). All other reagents used were analytical grade from Sinopharm Chemical Reagent Co., Ltd. (Shanghai, China).

4.2. Aspergillus Ochraceus Cultured Condition

Aspergillus ochraceus was deposited at the Marine Medicinal Bioresources Center (MMBC) (Ocean University of China, China), and was collected from Antarctic Weddell Sea Island and stored at the Ocean University of China's Marine Derived Species Bank with a case number of HDN1829900. It was identified according to its morphological characteristics and 18S rRNA sequences. The marine fungus *Aspergillus ochraceus* was initially cultivated on potato dextrose water medium and grown in a Petri dish sample (One week for the growth of the strains) at 28 °C for 7 days, then inoculated into a conical flask from a total of 2 L of culture medium comprising potato dextrose water. This culture was agitated on a rotary shaker at 178 rpm and 28 °C for 9 days. Finally, the broth was then separated from the filtrate by centrifugation at 5000 rpm for 25 min to isolate the supernatant; the resulting precipitate or pellet was obtained.

4.3. Preparation of AOP

Autolysis of *Aspergillus ochraceus*: Freshly precipitated *Aspergillus ochraceus* cells are combined with 10 times the volume of distilled water and thoroughly mixed. The mixture is then filtered through a 100-mesh gauze to remove any impurities. The filtrate is centrifuged,

and the resulting precipitate is washed three times with distilled water. The precipitate is then dried overnight in an oven at 60 °C, mixed with a 1 M sodium acetate buffer solution at a 1:5 mass ratio. The pH is adjusted to 5.5 using acetic acid, and solid sodium chloride is added to achieve a 3% mass fraction. The mixture is stirred at 55 °C for 24 h, then neutralized to pH 7 with 0.5 M sodium hydroxide solution and centrifuged. The precipitate is washed three times with distilled water, yielding *Aspergillus ochraceus* cell walls. Alkali Treatment: The precipitate is treated with a 0.5 M NaOH solution at a 1:5 mass ratio, heated, and stirred at 80 °C for 2 h. The mixture is then neutralized with HCl to a pH of 7 and centrifuged. The supernatant is concentrated under vacuum and dialyzed. The dialysate is further concentrated under vacuum and freeze-dried. Subsequently, an alkaline extract was fractionated on a DEAE Sepharose Fast Flow column (50 × 5 cm, Cl^-) with a gradient elution of 0.2 M NaCl, and was further purified with Sephacryl S-200 HR (100 cm × 1.6 cm) column to obtain a homogeneous fraction AOP.

4.4. Monosaccharide Composition

The monosaccharide composition was determined using a modified 1-phenyl-3-methyl-5-pyrazolone (PMP)-HPLC method. Each marine fungi strain was hydrolyzed briefly with 2 M trifluoroacetic acid (TFA) at 110 °C for 6 h. The hydrolysate was then dried to remove the excess TFA. Next, the hydrolysate or monosaccharide standard was separately dissolved in water, followed by the addition of sodium hydroxide and PMP in methanol. The mixture was incubated at 70 °C for 1 h. After cooling, the reaction mixture was neutralized with hydrochloric acid and extracted with chloroform three times. HPLC analysis was performed on an Agilent ZORBAX Eclipse XDB-C18 column at a constant flow rate of 1.0 mL/min, with the column temperature maintained at 30 °C. The mobile phase comprised 17% acetonitrile in a 0.1 M phosphate buffer solution. The entire process was monitored using a Diode array detector.

4.5. NMR Analysis

The dried sample (30 mg) was dissolved with D_2O (500 μL, 99.8% D), and 0.2 μL with acetone as an internal standard (2.225 ppm for ^1H and 31.07 ppm for ^{13}C). Then, a Bruker AVANCE III NMR spectrometer (Billerica, GermanyUSA), operating at 500 MHz at 333 K, was used to detect the NMR spectra (^1H NMR, ^{13}C NMR spectra, ^1H-^{13}C HMBC and HSQC) of the sample.

4.6. Mass Spectrometry

To elucidate the structural features of AOP, controlled acidic hydrolysis was performed under optimized conditions. Briefly, 10 mg/mL of AOP was dissolved in a 0.05 M H_2SO_4 aqueous solution and incubated at 80 °C for 1 h. The reaction was immediately quenched by neutralization with 0.1 M $Ba(OH)_2$. The centrifuged hydrolysate was diluted with an equal volume of acetonitrile (1:1, *v*/*v*) prior to ESI-MS/MS analysis by LTQ Orbitrap XL (Thermo, Waltham, MA, USA). Fragment ion profiles were acquired using electrospray ionization-tandem mass spectrometry (ESI-MS/MS) in negative ion mode, with the collision-induced dissociation (CID) energy set to 20–35 eV to optimize the spectral resolution of glycosidic bond cleavage patterns. The mass data were analyzed by Xcalibur 4.0.

4.7. Cell Lines and Extraction of Primary BMDM Cells

B16-F10 cells were cultured in Roswell Park Memorial Institute (RPMI-1640), containing 10% fetal bovine serum (FBS, Gibco, Grand Island, NY, USA) and 1% penicillin/streptomycin; A357 cells were maintained with Dulbecco's modified Eagle's medium (DMEM) containing 10% (FBS, Gibco, USA) and 1% penicillin/streptomycin.

Briefly, C57BL/6 mouse bone marrow (C57BL/6 mice were purchased from GemPharmatech (Nanjing, China)) was washed to obtain a single-cell suspension, followed by steps such as red blood cell lysis and washing, and then stimulated with M-CSF (20 ng/mL) for 5 days to differentiate into BMDM, and cultured with DMEM. All cells were cultured at 37 °C in a humidified incubator with 5% CO_2.

4.8. Cell Proliferation and Apoptosis Detection

The cell proliferation and apoptosis of B16-F10 and A375 cells were tested by CCK8 assay, flow cytometry assay, and clone formation assay. Briefly, cells were seeded into a 96-well plate (4×10^3 cells/well) and treated with different concentrations of AOP for the intended time; then, 10 μL CCK8 was added to each well, and the optical density was measured by a spectrophotometer (Epoch 2, BioTe, Irving, TX, USA) at 450 nm. On the other hand, cells were plated into the 6-well plate (2×10^5 cells/well); then, AOP was added to the cells after cells adhered, and the cell apoptosis rate was tested by Annexin V-FITC Apoptosis Detection Kit (Beyotime, Shanghai, China), following the instructions. Subsequently, flow cytometry (Novocyte 3000, Agilent, Santa Clara, CA, USA) was used for detection, and data analysis was conducted using software NovoExpress (Version 1.5.8).

As for the clone formation assay, B16-F10 cells were incoluted into a 6-well plate (600 cells/well) and continued to culture for 14 days. The medium containing AOP (or not) was changed every 3 days and the cell status was observed; after cloning, washing with PBS was performed. Then, 1 mL of 4% paraformaldehyde (Servicebio, Wuhan, China) was added to each well for 15 min and washed once with PBS; 1 mL of crystal violet staining solution (Servicebio, Wuhan, China) was added to each well and incubated for 20 min; Cells were then washed several times with PBS and photos were taken with a digital camera.

4.9. Cell Migration Ability Detection

The migration ability of cells was tested by wound-healing experiments and transwell experiments. Cells were plated into 6-well plate (1×10^6 cells/well); after the cells are fully attached to the wall, a 10 μL pipette tip was used to draw a straight line that intersected with the marked line, and gentle rinsing with PBS buffer was performed to remove the scratched cells; culture medium containing AOP or not was added, and an Olympus CKX41 microscope (Olympus, Tokyo, Japan) was used to observe the healing of the wound. Finally, an edge analysis was conducted using ImageJ software 2.9 (NIH, Bethesda, MD, USA).

A transwell with an aperture of 8 μm was purchased from Corning (Corning, New York, NY, USA). Generally, the cells were pre-starved for 4 h, and 600 μL of culture medium containing 10% FBS was added to the lower chamber of a 24-well plate. Then, 100 μL of cell suspension (5×10^4) was added to the upper chamber of the transwell, significantly, with or without AOP in both chambers. Incubation was continued for 24 h, followed by crystal violet staining as described in 4.7, and observation under a microscope.

4.10. RT-qPCR Assay

Cells were treated with different concentrations of AOP, total RNA was extracted by Tissue/Cell Fast RNA Extraction Kit for Animal (Abclonal, Wuhan, China), and then ABScript III RT Master Mix for qPCR with gDNA Remover (Abclonal, Wuhan, China) was used for the reverse transcription of RNA and qPCR assay. Finally, a thermocycler (Bio-Rad, Hercules, CA, USA) was used for the qPCR test. Primers (Table 1) were synthesized by Sangon Biotech (Shanghai, China).

Table 1. RT-qPCR primer sequences.

Target Gene	Forward Primer	Reverse Primer
E-cadherin	CAGTTCCGAGGTCTACACCTT	TGAATCGGGAGTCTTCCGAAAA
N-cadherin	AGGCTTCTGGTGAAATTGCAT	GTCCACCTTGAAATCTGCTGG
vimentin	CGTCCACACGCACCTACAG	GGGGGATGAGGAATAGAGGCT
snail	CACACGCTGCCTTGTGTCT	GGTCAGCAAAAGCACGGTT
GAPDH	AGGTCGGTGTGAACGGATTTG	GGGGTCGTTGATGGCAACA
CD86	TCAATGGGACTGCATATCTGCC	GCCAAAATACTACCAGCTCACT
CD206	CTCTGTTCAGCTATTGGACGC	TGGCACTCCCAAACATAATTTGA
iNOS	GTTCTCAGCCCAACAATACAAGA	GTGGACGGGTCGATGTCAC
IFN-γ	GACAACTACACCCTAAAGTGGAG	GCTCTGACACGAAACTGTGTTTT
COX-2	TTCCAATCCATGTCAAAACCGT	AGTCCGGGTACAGTCACACTT
IL-4	GGTCTCAACCCCCAGCTAGT	GCCGATGATCTCTCTCAAGTGAT
Arg1	CTCCAAGCCAAAGTCCTTAGAG	GGAGCTGTCATTAGGGACATCA
TGF-β1	CCACCTGCAAGACCATCGAC	CTGGCGAGCCTTAGTTTGGAC

4.11. ELISA Assay

Raw264.7 and BMDM cells were seeded into a 24-well plate and treated with different concentrations of AOP for 24 h. Then, the supernatant was collected and centrifugation at 13,000 rpm at 4 °C for 15 min. The contents of TNF-α, IL-1β, and IL-6 were detected using the ELISA kit (Thermo Fisher Scientific, Waltham, MA, USA) according to the manufacturer's instructions.

4.12. Tumor and Immune Cell Co-Incubation Assay

A B16-F10-luc stable cell line was constructed through the lentiviral infection method. Briefly, plasmids containing the luc-EGFP sequence were transfected into cells to construct the stable transgenic cell line with a 1 week screening of puromycin, and then the killing effect was evaluated under a co-incubation system through direct contact and transwell (0.4 μm) indirect contact. After incubation with AOP-trained or untrained BMDMs, luciferase substrate was added, and the luminescence value was measured to evaluate tumor cell viability.

4.13. Statistics Assay

Data were displayed as mean ± S.D. and analyzed by GraphPad Prism 9.0 software using an unpaired *t*-test and one-way ANOVA. All experiments were conducted independently at least 3 times and p values less than 0.05 were considered significant differences (*, $p < 0.05$; **, $p < 0.01$; ***, $p < 0.001$, ****, $p < 0.0001$).

5. Conclusions

In conclusion, a novel homogeneous polysaccharide, designated as AOP, was successfully extracted and purified from *Aspergillus ochraceus*. Our studies demonstrated that the AOP directly inhibits the proliferation and migration of B16-F10 and A375 cells, inducing apoptosis at higher concentrations, while also exerting immune anti-tumor activity by activating macrophages at lower concentrations. These findings provide a strong rationale for further in vivo experiments. Mechanistic investigations indicated that the inhibition of migration induced by AOP may be linked to its ability to suppress the activation of the

epithelial-mesenchymal transition (EMT) process. Therefore, our results lay a theoretical foundation for the development of anti-tumor lead compounds derived from marine fungi.

Author Contributions: Conceptualization, G.L. and G.Y.; methodology, J.H. and P.G.; software, K.k.W.A.; validation, J.W. and W.Z.; formal analysis, K.D. and Q.L.; investigation, H.G.; resources, G.L. and G.Y.; data curation, J.H. and P.G.; writing—original draft preparation, P.G.; writing—review and editing, P.G.; visualization, K.k.W.A.; supervision, G.L. and G.Y.; project administration, J.H.; funding acquisition, G.L. and G.Y. All authors have read and agreed to the published version of the manuscript.

Funding: This research was funded by the National Natural Science Foundation of China (81991522), the Fundamental Research Funds for the Central Universities (202441010), Qingdao Marine Science and Technology Center (2022QNLM030003-4), Taishan Scholar Project (TSQN202408073, TSPD20210304), Qingdao Key Technology Research and Development and Industrialization Demonstration Program (No. 22-7-3-hygg-1-nsh), and Key Scientific and Technological Projects of Shandong Province (2021ZDSYS22 and 2021KJ012).

Institutional Review Board Statement: The animal study protocol was approved by the Guidelines of Ocean university of China and conformed to experimental animal ethics. Animal experiments were permitted by the institutional animal care and use committee of Ocean University of China (OUC-SMP-2023-02-01).

Data Availability Statement: Data will be made available on request.

Acknowledgments: *Aspergillus ochraceus* were deposited at the Marine Medicinal Bioresources Center (MMBC), (Ocean University of China, China) and collected from Antarctic Weddell Sea Island and store at the Ocean University of China's Marine Derived Species Bank with a case number of HDN1829900.

Conflicts of Interest: The authors declare no conflicts of interest.

Abbreviations

The following abbreviations are used in this manuscript:

BMDM	bone marrow-derived macrophage
TNF-α	Tumor necrosis factor alpha
IL-6	Interleukin-6hree letter acronym
DAMPs	Damage-associated molecular patterns
IL-1β	Interleukin-1β
TAMs	Tumor-associated macrophages
EMT	Epithelial-to-mesenchymal transition

References

1. Zhou, R.; Wang, M.; Li, X.; Liu, Y.; Yao, Y.; Wang, A.; Chen, C.; Zhang, Q.; Wu, Q.; Zhang, Q.; et al. TBK1-Zyxin signaling controls tumor-associated macrophage recruitment to mitigate antitumor immunity. *EMBO J.* **2024**, *43*, 4984–5017. [CrossRef] [PubMed]
2. Fan, C.Y.; Zheng, J.S.; Hong, L.L.; Ling, Z.-Q. Macrophage crosstalk and therapies: Between tumor cells and immune cells. *Int. Immunopharmacol.* **2024**, *141*, 113037. [CrossRef] [PubMed]
3. Zhang, W.; Wang, M.; Ji, C.; Liu, X.; Gu, B.; Dong, T. Macrophage polarization in the tumor microenvironment: Emerging roles and therapeutic potentials. *Biomed. Pharmacother.* **2024**, *177*, 116930. [CrossRef]
4. Hinshaw, D.C.; Shevde, L.A. The Tumor Microenvironment Innately Modulates Cancer Progression. *Cancer Res.* **2019**, *79*, 4557–4566. [CrossRef] [PubMed]
5. Gu, X.; Zhu, Y.; Su, J.; Wang, S.; Su, X.; Ding, X.; Jiang, L.; Fei, X.; Zhang, W. Lactate-induced activation of tumor-associated fibroblasts and IL-8-mediated macrophage recruitment promote lung cancer progression. *Redox Biol.* **2024**, *74*, 103209. [CrossRef]
6. Wang, J.; Zhu, N.; Su, X.; Gao, Y.; Yang, R. Novel tumor-associated macrophage populations and subpopulations by single cell RNA sequencing. *Front. Immunol.* **2024**, *14*, 1264774. [CrossRef]
7. Wang, H.; Wang, X.; Zhang, X.; Xu, W. The promising role of tumor-associated macrophages in the treatment of cancer. *Drug Resist. Updates* **2024**, *73*, 101041. [CrossRef]

8. Liu, Y.; Fu, W.X.; Wang, W.W.; Zhou, C.L.; Ding, X.D.; Zhang, Q. A novel 12bp deletion in the ITGB5 gene is strongly associated with Escherichia coli F4ac adhesion and increased susceptibility to infection in pigs. *Livest. Sci.* **2015**, *172*, 1–4. [CrossRef]
9. Yeung, O.W.H.; Lo, C.M.; Ling, C.C.; Qi, X.; Geng, W.; Li, C.X.; Ng, K.T.P.; Forbes, S.J.; Guan, X.Y.; Poon, R.T.P.; et al. Alternatively activated (M2) macrophages promote tumor growth and invasiveness in hepatocellular carcinoma. *J. Hepatol.* **2015**, *62*, 607–616. [CrossRef]
10. Hua, H.K.; Zhu, H.M.; Zhang, Z.G. Clinical significance of downregulated NISCH expression in skin cutaneous melanoma: Modulation of tumor cell invasion, migration, and EMT via PAK1 inhibition. *Tissue Cell* **2024**, *88*, 102399. [CrossRef]
11. Dai, L.H.; Zhang, G.R.; Ou, Y.H.; Liu, X.J.; Yao, H.L.; Hu, W.H.; Li, H.J.; Lan, W.J. Five New Indole Alkaloid Derivatives from Deep-Sea Fungus *Aspergillus fumigatus* AF1. *Mar. Drugs* **2024**, *23*, 4. [CrossRef] [PubMed]
12. Park, M.S.; Son, S.U.; Kim, T.E.; Shim, S.H.; Jang, B.K.; Park, S.; Shin, K.S. Polysaccharide Fraction Isolated from Saccharina japonica Exhibits Anti-Cancer Effects Through Immunostimulating Activities. *Mar. Drugs* **2025**, *23*, 38. [CrossRef]
13. Zou, Z.B.; Li, Y.; Wang, Y.; Xie, C.L.; Li, Z.Q.; Nie, S.S.; Li, Y.; Fang, S.Y.; Zhong, T.H.; Li, L.S.; et al. Stephaochratidin A, a Rare Stephacidin-Asperochratide Hybrid with Ferroptosis Inhibitory Activity from the Deep-Sea-Derived *Aspergillus ochraceus*. *Org. Lett.* **2024**, *26*, 5695–5699. [CrossRef] [PubMed]
14. Nasr, A.R.; Komarevtsev, S.K.; Baidamshina, D.R.; Ryskulova, A.B.; Makarov, D.A.; Stepanenko, V.N.; Trizna, E.Y.; Gorshkova, A.S.; Osmolovskiy, A.A.; Miroshnikov, K.A.; et al. Targeting mono- and dual-species biofilms of Staphylococcus aureus and Pseudomonas aeruginosa by the recombinant anticoagulant enzyme PAPC from micromycete *Aspergillus ochraceus*. *Biochimie* **2025**, *230*, 33–42. [CrossRef]
15. Guo, S.; Mao, W.; Yan, M.; Zhao, C.; Li, N.; Shan, J.; Lin, C.; Liu, X.; Guo, T.; Guo, T.; et al. Galactomannan with novel structure produced by the coral endophytic fungus *Aspergillus ochraceus*. *Carbohydr. Polym.* **2014**, *105*, 325–333. [CrossRef]
16. Leonard-Murali, S.; Bhaskarla, C.; Yadav, G.S.; Maurya, S.K.; Galiveti, C.R.; Tobin, J.A.; Kann, R.J.; Ashwat, E.; Murphy, P.S.; Chakka, A.B.; et al. Uveal melanoma immunogenomics predict immunotherapy resistance and susceptibility. *Nat. Commun.* **2024**, *15*, 2863. [CrossRef]
17. Fontaine, T.; Latgé, J.-P. Galactomannan Produced by *Aspergillus fumigatus*: An Update on the Structure, Biosynthesis and Biological Functions of an Emblematic Fungal Biomarker. *J. Fungi* **2020**, *6*, 283. [CrossRef] [PubMed]
18. Chen, Y.; Wang, T.; Zhang, X.; Zhang, F.; Linhardt, R.J. Structural and immunological studies on the polysaccharide from spores of a medicinal entomogenous fungus *Paecilomyces cicadae*. *Carbohydr Polym.* **2021**, *254*, 117462. [CrossRef]
19. Fontana, C.; Widmalm, G. Primary Structure of Glycans by NMR Spectroscopy. *Chem. Rev.* **2023**, *123*, 1040–1102. [CrossRef]
20. Álvarez-Martínez, I.; Pfrengle, F. On the structure, conformation and reactivity of β-1,4-linked plant cell wall glycans: Why are xylan polysaccharides or furanosyl substituents easier to hydrolyze than cellulose? *Cellulose* **2025**, *32*, 2145–2165. [CrossRef]
21. Boutros, A.; Croce, E.; Ferrari, M.; Gili, R.; Massaro, G.; Marconcini, R.; Arecco, L.; Tanda, E.T.; Spagnolo, F. The treatment of advanced melanoma: Current approaches and new challenges. *Crit. Rev. Oncol. Hematol.* **2024**, *196*, 104276. [CrossRef] [PubMed]
22. Li, S.; Wu, F.; Gao, P.; Jin, C.; Wang, Y.; Liao, W.; Ding, K. A novel peptidoglycan isolated from Semiaquilegia adoxoides inhibits Aβ42 production via activating autophagy. *Fitoterapia* **2023**, *169*, 105552. [CrossRef] [PubMed]
23. Fedele, M.; Sgarra, R.; Battista, S.; Cerchia, L.; Manfioletti, G. The Epithelial–Mesenchymal Transition at the Crossroads Between Metabolism and Tumor Progression. *Int. J. Mol. Sci.* **2022**, *23*, 800. [CrossRef] [PubMed]
24. Chen, Z.; Hu, T.; Zhou, J.; Gu, X.; Chen, S.; Qi, Q.; Wang, L. Overview of tumor immunotherapy based on approved drugs. *Life Sci.* **2024**, *340*, 122419. [CrossRef]
25. Wu, M.; Wu, L.; Wu, W.; Zhu, M.; Li, J.; Wang, Z.; Li, J.; Ding, R.; Liang, Y.; Li, L.; et al. Phagocytosis of Glioma Cells Enhances the Immunosuppressive Phenotype of Bone Marrow–Derived Macrophages. *Cancer Res.* **2023**, *83*, 771–785. [CrossRef]
26. Marchese, P.; Garzoli, L.; Young, R.; Allcock, L.; Barry, F.; Tuohy, M.; Murphy, M. Fungi populate deep-sea coral gardens as well as marine sediments in the Irish Atlantic Ocean. *Environ. Microbiol.* **2021**, *23*, 4168–4184. [CrossRef]
27. Hareeri, R.H.; Aldurdunji, M.M.; Abdallah, H.M.; Alqarni, A.A.; Mohamed, S.G.A.; Mohamed, G.A.; Ibrahim, S.R.M. *Aspergillus ochraceus*: Metabolites, Bioactivities, Biosynthesis, and Biotechnological Potential. *Molecules* **2022**, *27*, 6759. [CrossRef]
28. Bardalaye, P.; Nordin, J. Chemical structure of the galactomannan from the cell wall of *Aspergillus niger*. *J. Biol. Chem.* **1977**, *252*, 2584–2591. [CrossRef]
29. Gomez-Miranda, B. Extracellular and cell wall polysaccharides of *Aspergillus alliaceus*. *Trans. Br. Mycol. Soc.* **1981**, *76*, 249–253. [CrossRef]

Disclaimer/Publisher's Note: The statements, opinions and data contained in all publications are solely those of the individual author(s) and contributor(s) and not of MDPI and/or the editor(s). MDPI and/or the editor(s) disclaim responsibility for any injury to people or property resulting from any ideas, methods, instructions or products referred to in the content.

marine drugs

MDPI

Article

Dihydrogeodin from *Fennellia flavipes* Modulates Platelet Aggregation via Downregulation of Calcium Signaling, αIIbβ$_3$ Integrins, MAPK, and PI3K/Akt Pathways

Abdul Wahab Akram [1], Dae-Cheol Choi [2], Hyung-Kyu Chae [1], Sung Dae Kim [1], Dongmi Kwak [1], Bong-Sik Yun [2,*] and Man Hee Rhee [1,3,*]

[1] Department of Veterinary Medicine, College of Veterinary Medicine, Kyungpook National University, Daegu 41566, Republic of Korea; ab.wahab226@gmail.com (A.W.A.)
[2] Division of Biotechnology and Advanced Institute of Environment and Bioscience, College of Environmental and Bioresource Sciences, Jeonbuk National University, Gobong-ro 79, Iksan 54596, Republic of Korea
[3] Institute for Veterinary Biomedical Science, College of Veterinary Medicine Kyungpook National University, Daegu 41566, Republic of Korea
* Correspondence: bsyun@jbnu.ac.kr (B.-S.Y.); rheemh@knu.ac.kr (M.H.R.); Tel.: +82-53-950-5967 (B.-S.Y. & M.H.R.); Fax: +82-53-950-5955 (B.-S.Y. & M.H.R.)

Abstract: Cardiovascular disease remains a leading cause of morbidity and mortality worldwide, frequently arising from platelet hyperactivation and subsequent thrombus formation. Although conventional antiplatelet therapies are available, challenges, such as drug resistance and bleeding complications, require the development of novel agents. In this study, dihydrogeodin (DHG) was isolated from *Fennellia flavipes* and evaluated using platelets derived from Sprague–Dawley rats. Platelet aggregation induced by collagen, adenosine diphosphate, or thrombin was assessed by light transmission aggregometry; DHG significantly reduced aggregation in a dose-dependent manner. Further assays demonstrated that DHG suppressed intracellular calcium mobilization, adenosine triphosphate release, and integrin αIIbβ$_3$-dependent fibrinogen binding, thereby impairing clot retraction. Western blot analysis revealed that DHG reduced the phosphorylation of mitogen-activated protein kinases (ERK, JNK, p38) and PI3K/Akt, indicating inhibition across multiple platelet-signaling pathways. Additionally, SwissADME-assisted pharmacokinetics predicted favorable properties without violations of the Lipinski (Pfizer) filter, Muegge (Bayer) filter, Ghose filter, Veber filter, and Egan filter, and network pharmacology revealed inhibition of calcium and MAPK pathways. These results highlight the potential of DHG as a novel antiplatelet agent with broad-spectrum activity and promising drug-like characteristics. Further studies are warranted to assess its therapeutic window, safety profile, and potential for synergistic use with existing antiplatelet drugs.

Keywords: dihydrogeodin; *Fennellia flavipes*; platelet aggregation; MAPK and PI3K/Akt pathways; marine natural products

1. Introduction

Cardiovascular disease encompasses a broad spectrum of conditions, including atherosclerosis, coronary heart disease, hypertension, and stroke [1]. A key contributor to cardiovascular disease pathophysiology is platelet hyperactivation, which facilitates atherosclerotic plaque development, plaque rupture, and thrombus formation [2]. Under physiological conditions, platelets play a critical role in maintaining hemostasis [3]; however, when excessively activated, they can form occlusive thrombi that impair blood flow,

potentially resulting in myocardial infarction, stroke, or other ischemic complications [4]. Accordingly, pharmacological inhibition of platelet function remains a well-established approach for both the treatment and prevention of cardiovascular disease [5–8]. While synthetic antiplatelet agents have been instrumental in managing cardiovascular diseases, their use is often accompanied by significant adverse effects. For instance, clopidogrel has been associated with rare but severe hematological disorders, such as aplastic anemia and thrombotic thrombocytopenic purpura. Similarly, long-term aspirin therapy is linked to gastrointestinal complications, including ulcer formation and an increased risk of bleeding [9]. Considering this, the ethnomedical approach could be a promising strategy for preventing cardiovascular disease and its complications [6].

Platelets contain dense (δ) and alpha (α) granules. δ granules store adenosine diphosphate (ADP), adenosine triphosphate (ATP), Ca^{2+}, and serotonin, whereas α granules contain fibronectin, fibrinogen, von Willebrand factor (vWF), and P-selectin [6,10]. Multiple signaling pathways control granule secretion, including Src family kinases (early platelet activation), intracellular Ca^{2+} mobilization, the cAMP-VASP-PKA pathway, protein kinase C (PKC) activation, the mitogen-activated protein kinase (MAPK) and phosphoinositide 3-kinase (PI3K)/protein kinase B (Akt) cascades, and RhoA-regulated cytoskeletal reorganization [10]. The increase in intracellular Ca^{2+} is essential for platelet function, initiating downstream signaling that promotes aggregation and thrombus formation [11]. Platelet activation also depends on integrin $\alpha IIb\beta_3$, which undergoes conformational changes during inside–out signaling and binds fibrinogen, a critical step in the formation of stable thrombi [12]. Fibronectin enhances aggregation by interacting with integrins and recruiting signaling molecules to the cytoplasmic tails [13]. Additionally, Rho GTPases and Rho kinases (ROCKs) regulate cytoskeletal remodeling through myosin light chain phosphorylation, influencing platelet morphology, motility, and clot retraction [14]. Notably, treatment with natural products has been shown to reduce Ca^{2+} mobilization, ATP and serotonin release, fibrinogen binding, fibronectin adhesion, and clot retraction, indicating that such compounds exert antiplatelet effects through the inhibition of granule secretion and integrin $\alpha IIb\beta_3$ signaling [12,15]. Despite the effectiveness of current antiplatelet agents, such as aspirin and clopidogrel, these drugs are frequently associated with adverse effects and complications [16,17]. Aspirin, for instance, may cause severe gastric ulcers and prolonged bleeding, whereas clopidogrel has been linked to aplastic anemia and thrombocytopenic purpura [6]. Moreover, a substantial proportion of patients exhibit resistance to these therapies [18,19]. Factors contributing to aspirin resistance include genetic polymorphisms in cyclooxygenase-1 (COX-1) and other thromboxane-related genes, upregulated thromboxane biosynthesis from non-platelet sources, elevated platelet turnover, and interindividual variability in drug absorption [5]. These limitations highlight the pressing need for safer and more efficacious antiplatelet agents.

Natural products have historically been a rich source of bioactive molecules [20–22]. Numerous plant-derived and microbial metabolites demonstrate potent antiplatelet activity by targeting key enzymes or receptors involved in platelet aggregation [20,23–25]. These multitarget mechanisms reflect the broader therapeutic potential of natural compounds, which often exert bidirectional regulatory effects on physiological processes and tend to produce fewer side effects. Several marine fungi have previously been reported to possess bioactive natural products and significantly beneficial antiplatelet activities; for example, *Epicoccum sorghinum* metabolites inhibit platelet aggregation and inflammation [26], and *Aspergillus* species have been reported to exhibit antiplatelet as well as anticancer properties [27]. Moreover, marine fungal lipid bioactives display anti-inflammatory and antithrombotic effects, underscoring their promise as sources of novel antiplatelet agents [28].

Among microbial sources, *Aspergillus* species are well known for producing a wide variety of secondary metabolites with therapeutic potential, including antiviral xanthones, diphenyl ether and butenolide derivatives with α-glucosidase inhibitory activity, and benzophenones with antimicrobial properties [29]. Chlorinated diphenyl ethers, in particular, serve as chemical markers of *Aspergillus* spp. and are generally believed to originate from anthraquinone precursors, such as emodin, via intermediates, such as sulochrin and grisandienes (e.g., geodin) [29]. The genus *Fennellia* (family Trichocomaceae), which includes *F. flavipes* and *F. nivea*, has been identified as the teleomorph of *Aspergillus flavipes* [30]. Although *A. flavipes* has been extensively studied for its production of cytochalasins, alkaloids, polyketides, butenolides, meroterpenoids, diphenyl ethers, benzophenones, and xanthones [31], some of which exhibit cytotoxic, antibacterial, or glucosidase-inhibiting properties, relatively little is known about the bioactive compounds specifically produced by *F. flavipes* [31]. This study began to address this gap by identifying several notable metabolites from *F. flavipes*, including a newly characterized dimeric 1,3-dihydroisobenzofuran and five previously known compounds, such as dihydrogeodin (DHG) [31,32]. In the present study, we isolated DHG from the culture broth of *F. flavipes* and evaluated its in vitro antiplatelet activity. Our findings demonstrate that DHG functions as a potent inhibitor of platelet aggregation, highlighting the potential of *F. flavipes* as a source of novel antiplatelet agents and pharmacologically active natural products.

2. Results

2.1. Structural Elucidation

The known compound dihydrogeodin was identified through the comprehensive analysis of its ^{1}H and ^{13}C NMR spectra and HPLC data (Supplementary Figures S1–S5), which were consistent with both recent [31] and previously published reports [32,33].

2.2. DHG Inhibits Agonist-Induced Platelet Aggregation

Platelet aggregation can be induced by various agonists, each activating distinct signaling pathways. Collagen initiates platelet adhesion and aggregation at sites of vascular injury [34], ADP promotes platelet activation through P_2Y receptors [35], and thrombin induces robust platelet responses via protease-activated receptors [36]. To assess the antiplatelet potential of DHG, we evaluated platelet aggregation induced by each of these three agonists. Figure 1A presents the chemical structure of DHG. As shown in Figure 1B–D, DHG significantly inhibited platelet aggregation induced by collagen, ADP, and thrombin in a dose-dependent manner. Notably, DHG exerted its strongest inhibitory effect on collagen-induced aggregation. In collagen-stimulated platelets (Figure 1B), DHG at 10 μM significantly reduced aggregation compared with collagen alone (* $p < 0.05$) and completely inhibited aggregation at 40 μM (*** $p < 0.001$). In contrast, ADP-induced aggregation (Figure 1C) required a concentration of 80 μM to achieve significant reduction (* $p < 0.05$), whereas thrombin-induced aggregation (Figure 1D) was significantly inhibited at 40 μM (* $p < 0.05$). These findings indicate that DHG more strongly targets the collagen-mediated pathway of platelet activation, while also exhibiting broader inhibitory effects against ADP- and thrombin-induced activation, highlighting its potential as a novel therapeutic agent for the prevention of platelet-mediated thrombotic events. The IC_{50} of DHG for collagen-induced platelet aggregation was calculated to be 18.5 μM (Figure 1E). No potential cytotoxicity was observed at the indicated concentration (Supplementary Figure S7).

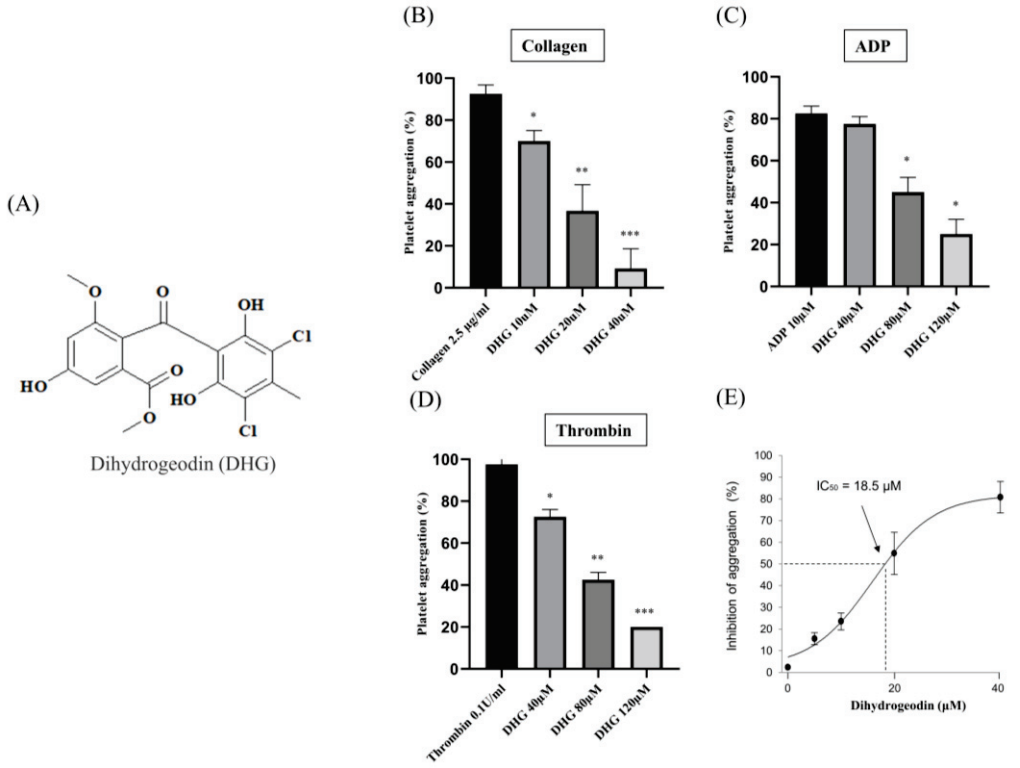

Figure 1. Dihydrogeodin (DHG) inhibits agonist-induced platelet aggregation. Washed platelets were incubated for 1 min with DHG in the presence of 1 mM $CaCl_2$. Aggregation was initiated by the addition of agonists. (**A**) Chemical structure of DHG. (**B**) Effect of DHG on collagen-induced platelet aggregation. (**C**) Effect of DHG on ADP-induced platelet aggregation. (**D**) Effect of DHG on thrombin-induced platelet aggregation. (**E**) IC_{50} of DHG for collagen-induced platelet aggregation. Data are expressed as means ± SD (n = 3). Statistical significance was determined by one-way ANOVA followed by a post hoc Dunnett's test. * $p < 0.05$, ** $p < 0.01$, *** $p < 0.001$ versus agonist.

2.3. DHG Inhibits ATP Release and $[Ca^{2+}]_i$ Mobilization

To determine whether DHG affects dense granule secretion, we measured ATP release from platelets stimulated with collagen (2.5 μg/mL). As shown in Figure 2 (left panel), collagen substantially increased ATP release compared with resting platelets, whereas DHG at 10, 20, and 40 μM significantly reduced ATP secretion in a dose-dependent manner (* $p < 0.05$, ** $p < 0.01$, *** $p < 0.001$ versus collagen-stimulated controls). In parallel, intracellular Ca^{2+} mobilization, a key event in platelet activation, was assessed using Fura-2/AM-loaded platelets. Collagen stimulation induced a substantial increase in Ca^{2+} levels relative to resting platelets (Figure 2, right panel). DHG at 10, 20, and 40 μM significantly attenuated this collagen-induced Ca^{2+} mobilization (** $p < 0.01$, *** $p < 0.001$ versus collagen-stimulated controls). These findings suggest that DHG suppresses both dense granule secretion and intracellular calcium signaling, providing further mechanistic evidence for its potent antiplatelet activity.

2.4. DHG Downregulates Inside–Out and Outside–In Signaling and Prevents Platelet Shape Change

Inside–out signaling in platelets is primarily mediated by the activation of integrin $\alpha IIb\beta_3$, which promotes fibrinogen binding and supports platelet aggregation [37]. As shown in Figure 3 (left), collagen stimulation (2.5 μg/mL) substantially increased the proportion of platelets binding fibrinogen compared with resting conditions. Pretreatment with DHG at 10, 20, and 40 μM significantly reduced fibrinogen binding in a dose-dependent manner (* $p < 0.05$, ** $p < 0.01$, *** $p < 0.001$ versus collagen-stimulated controls). Notably,

DHG at 40 μM nearly abolished fibrinogen binding, producing an effect comparable to that of EGTA (100 μM), which chelates calcium and prevents integrin activation [38]. These results indicate that DHG potently inhibits the inside–out signaling pathway leading to $\alpha IIb\beta_3$ activation, thereby blocking fibrinogen binding and platelet aggregation.

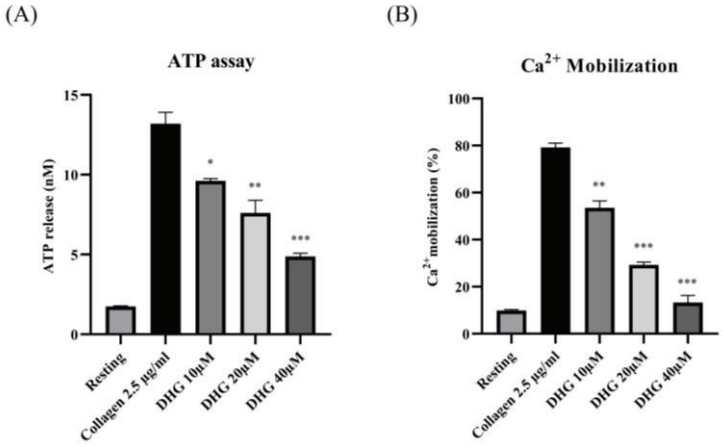

Figure 2. DHG inhibits platelet granule release. (**A**) Platelets were preincubated with DHG, stimulated with collagen, and the supernatant was analyzed for ATP using a standard ATP assay kit. (**B**) Intracellular Ca^{2+} levels were assessed using Fura-2/AM-loaded platelets. Data are presented as means ± SD (n = 3). * $p < 0.05$, ** $p < 0.01$, *** $p < 0.001$ versus collagen alone.

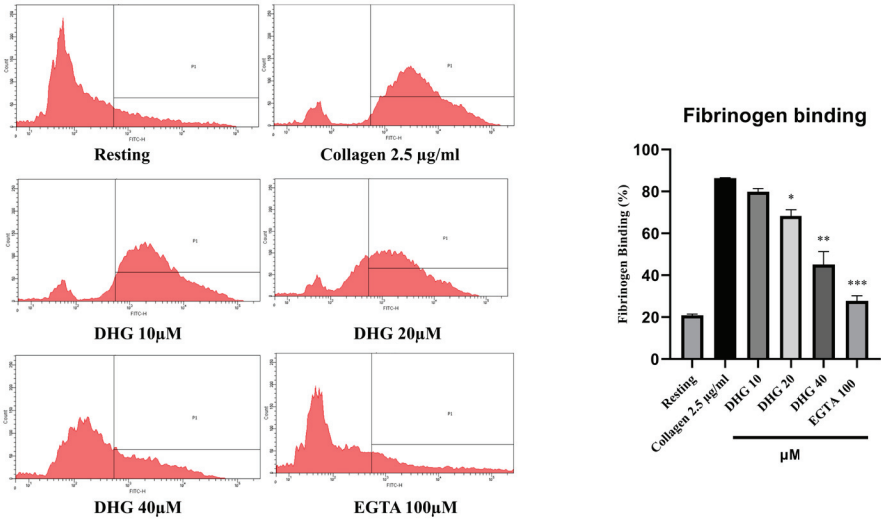

Figure 3. DHG inhibits integrin αIIbβ3-mediated inside–out signaling pathway. (**Left**) Flow cytometry histograms showing fibrinogen binding in resting and collagen-stimulated platelets (2.5 μg/mL) in the presence or absence of DHG (10, 20, 40 μM) or EGTA (100 μM). (**Right**) Quantification of fibrinogen binding. Data are presented as means ± SD (n = 3). * $p < 0.05$, ** $p < 0.01$, *** $p < 0.001$ versus collagen alone.

After integrin activation and aggregation, outside–in signaling via $\alpha IIb\beta_3$ coordinates platelet spreading, cytoskeletal reorganization, and clot retraction, a critical process for thrombus stabilization [12]. To assess whether DHG interferes with outside–in signaling, we performed a clot retraction assay using thrombin (1 U/mL) as the stimulus (Figure 4). In the absence of DHG, clot retraction was substantial, resulting in a compact thrombus (Figure 4A). In contrast, treatment with DHG at 20 and 40 μM significantly impaired clot retraction (* $p < 0.05$, ** $p < 0.01$, *** $p < 0.001$ versus thrombin alone), yielding larger, less compact, and heavier clots (Figure 4B). The degree of inhibition was comparable to that observed with Y-27632 (10 μM), a known ROCK inhibitor, suggesting that DHG interferes

with Rho-dependent signaling pathways. These findings demonstrate that DHG disrupts both inside–out and outside–in signaling in platelets. Further scanning electron microscopy (SEM) was performed to visualize the platelet shape change (Figure 4C). Collagen-induced platelets show clear fibrin meshwork formation which was significantly prevented after treatment with the indicated concentration of DHG.

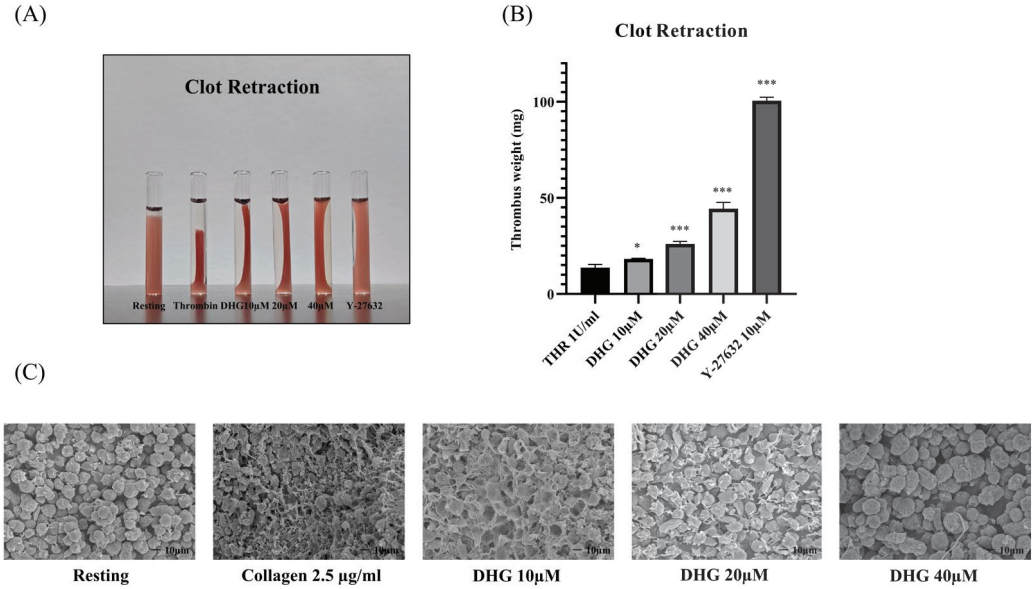

Figure 4. DHG inhibits clot retraction. Platelet-rich plasma (PRP) was incubated for 2 min with DHG or Y-27632. Human thrombin (1 U/mL) was then added, and (**A**) clot retraction and clot shape change were assessed at room temperature for 90 min. (**B**) The clot weight was assessed * $p < 0.05$, *** $p < 0.001$ versus thrombin alone. (**C**) Platelet shape change was visualized with scanning electron microscopy (SEM). SEM images of the platelet shape revealed a change in morphology from discoid to a rounded shape containing filopodia upon activation with collagen, which was prevented by treatment with DHG.

2.5. DHG Attenuates MAPK and PI3K/Akt Phosphorylation

To determine whether DHG modulates the MAPK and PI3K/Akt pathways, both of which are essential for platelet activation [5], platelets were pretreated with DHG (10, 20, or 40 μM) and subsequently stimulated with collagen (2.5 μg/mL). Phosphorylation levels of extracellular signal-regulated kinase (ERK), Janus kinase (JNK), p38, PI3K, and Akt were assessed by Western blotting (Figure 5). Collagen stimulation substantially increased the phosphorylation of these proteins compared with resting platelets. In contrast, DHG reduced phosphorylation in a dose-dependent manner, whereas total protein levels (T-ERK, T-JNK, T-p38, T-PI3K, T-Akt) remained largely unchanged. Notably, DHG at 40 μM reduced phospho-ERK, phospho-JNK, phospho-PI3K, and phospho-Akt levels to near-basal values, indicating a strong inhibitory effect on MAPK and PI3K/Akt signaling. These results suggest that suppression of these key pathways contributes to the antiplatelet mechanism of DHG.

2.6. Pharmacokinetics, Drug-Likeliness Analysis

To assess the drug-likeness and pharmacokinetic potential of DHG, we utilized SwissADME to predict its physicochemical and pharmacokinetic properties. The analysis revealed that DHG complies with Lipinski's rule of five, suggesting good oral bioavailability. Additionally, DHG demonstrated favorable lipophilicity (LogP), solubility, and gastrointestinal (GI) absorption, supporting its potential for systemic administration. No violations of drug-likeness criteria were predicted, reinforcing its suitability as a bioactive

compound. The pharmacokinetic profile also suggested a low probability of BBB permeability, which may reduce the risk of central nervous system side effects. DHG was also predicted to be a non-substrate for P-glycoprotein (P-gp) efflux transporters, potentially enhancing its bioavailability. However, predicted interactions with cytochrome P450 (CYP) isoforms warrant consideration in future metabolism studies (Figure 6A,B).

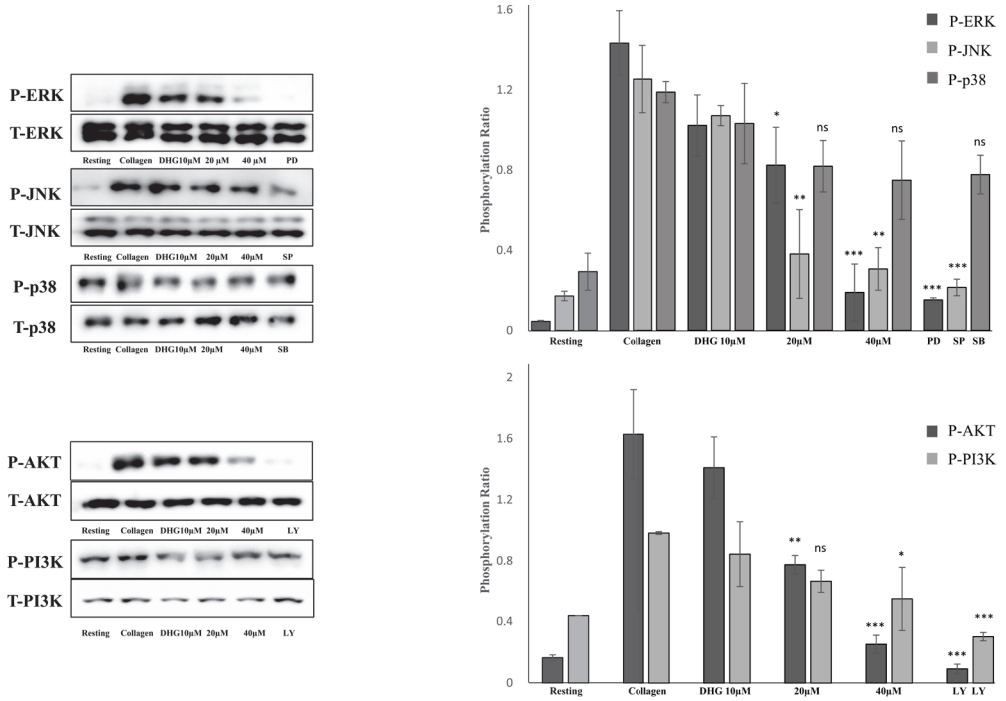

Figure 5. DHG inhibits protein phosphorylation. Platelets were preincubated with DHG and stimulated with collagen. Aggregation was halted by the addition of lysis buffer, after which protein concentrations were measured. Proteins were separated by SDS-PAGE, transferred to PVDF membranes, and probed with specific antibodies after membrane blocking. Visualization was performed using enhanced chemiluminescence. Representative Western blots (**left panels**) and corresponding quantification (**right panels**) show the phosphorylation levels of MAPK (ERK, JNK, p38) and PI3K/Akt in platelets pretreated with DHG (10, 20, 40 μM) or a reference inhibitor. Data are presented as means ± SD. Statistical significance was determined by one-way ANOVA followed by a post hoc Dunnett's test * $p < 0.05$, ** $p < 0.01$, *** $p < 0.001$, and ns = non-significant versus collagen alone.

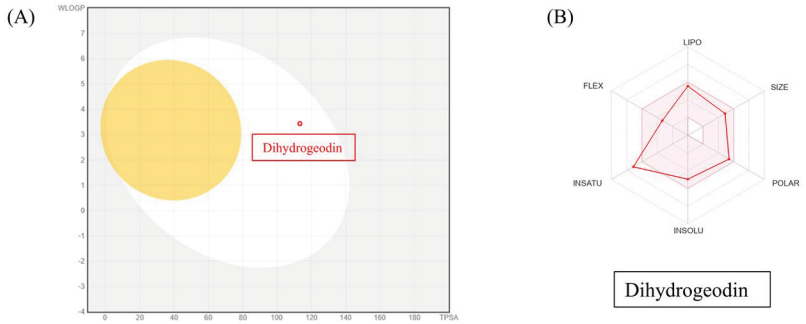

Figure 6. SwissADME analysis of DHG. The canonical SMILES for DHG were retrieved from PubChem and entered into SwissADME. Output files and visualizations were directly from the website. (**A**) The BOILED-Egg model evaluated human intestinal absorption (HIA) and blood–brain barrier (BBB) permeability based on lipophilicity and polarity, generating a WLOGP versus tPSA plot. (**B**) SwissADME predictions showed that DHG complies with Lipinski's rule of five, indicating good oral bioavailability.

2.7. Network Pharmacology

To explore the potential mechanism of DHG in platelet modulation, a network pharmacological approach was employed. A Venn diagram (Figure 7A) was constructed to identify overlapping targets between DHG and platelet activation-related genes, revealing 25 common targets, suggesting a potential pharmacological link between the compound and platelet function. A protein–protein interaction (PPI) network of these overlapping targets was constructed using the STRING database (Figure 7B). Notably, NFKB1, PDGFRA, RXRA, and PTPN11 emerged as key hub nodes, indicating their potential central roles in mediating the effects of DHG. The network shows that these targets are functionally interconnected and may be critical in signal transduction processes related to platelet activity. Further, a compound–target–pathway network (Figure 7C) demonstrated that DHG targets are significantly enriched in several signaling pathways. These include the calcium signaling pathway, MAPK signaling pathway, adipocytokine signaling pathway, and insulin resistance pathways. Notably, these pathways are not only relevant to cardiovascular diseases but also play crucial roles in platelet activation and aggregation, highlighting the therapeutic potential of DHG in thrombosis or related disorders.

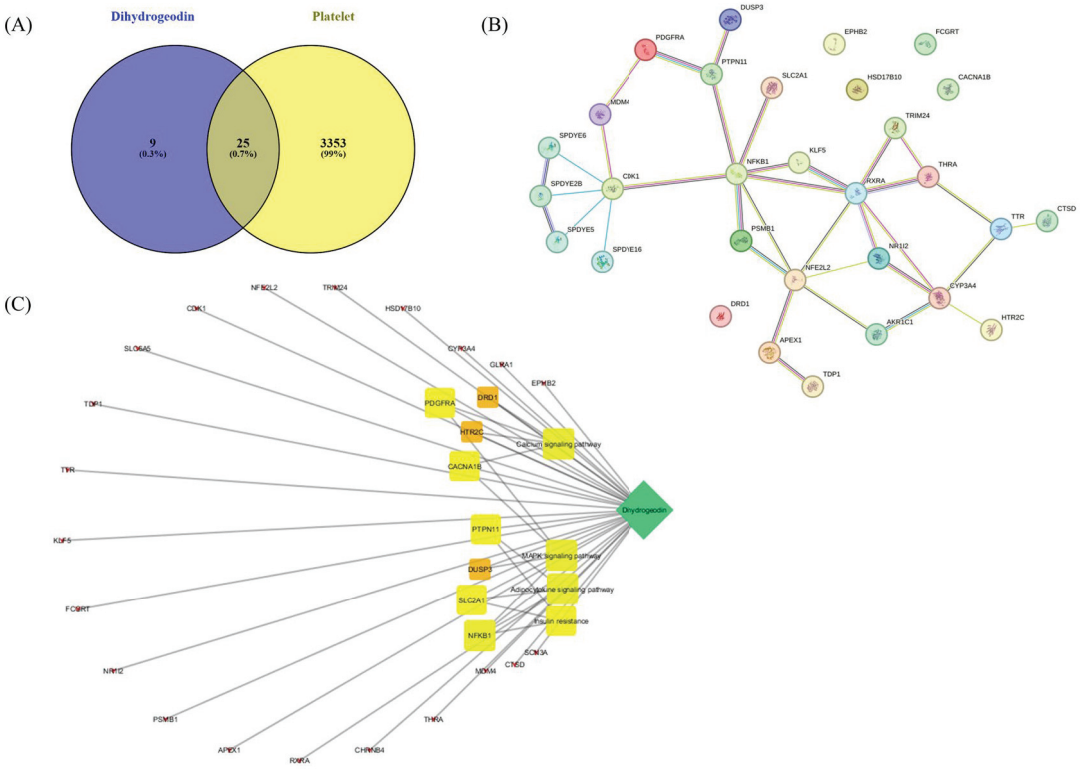

Figure 7. Network pharmacological assessment of DHG. (**A**) Venn diagram showing the intersection between predicted targets of DHG and platelet-related genes, where 25 overlapping genes were identified. (**B**) Protein–protein interaction (PPI) network of the 25 common targets constructed using the STRING database. (**C**) Compound–target–pathway network illustrating the association between DHG, its core targets, and enriched KEGG pathways.

3. Discussion

Natural products have attracted considerable interest due to their multitarget activities and relatively low incidence of adverse effects [39]. Recent studies have identified marine-derived compounds as promising sources of antiplatelet agents [40–43]. Similarly, various herbal medicines and their purified constituents have demonstrated potent antiplatelet activity [6,44,45]. For example, in our recently published study, ginsenoside Rg5

regulates GPVI signaling pathways by inhibiting collagen-induced platelet aggregation. The cryptotanshinone from *Salvia miltiorrhiza* Bunge exerts $P2Y_{12}$-independent antiplatelet effects by downregulating the PI3K/Akt, MAPK, and STAT3 pathways [46]. Tryptanthrin from *Isatidis Radix* interferes with both inside–out and outside–in $\alpha IIb\beta_3$ signaling, thus preventing stable thrombus formation [45]. Additionally, dieckol from *Eisenia bicyclis* inhibits platelet aggregation by suppressing granule secretion, integrin $\alpha IIb\beta_3$ function, and the RhoA/ROCK pathway [12]. Similarly, in our study, DHG attenuated integrin $\alpha IIb\beta_3$–mediated fibrinogen binding and clot retraction, as well as the phosphorylation of MAPK (ERK, JNK, p38) and PI3K/Akt, underscoring its multifaceted mode of action.

Platelet activation depends on a coordinated network of signaling events triggered by vascular injury [47]. Collagen, ADP, and thrombin activate distinct platelet receptors, GPVI, $P2Y_{12}$, and protease-activated receptors, respectively, to initiate granule secretion, integrin $\alpha IIb\beta_3$ activation, and cytoskeletal reorganization [48]. DHG significantly inhibited platelet aggregation induced by collagen, ADP, and thrombin in a dose-dependent manner, indicating broad inhibitory activity across multiple platelet activation pathways (Figure 1). In addition to its inhibition of aggregation, DHG substantially reduced intracellular Ca^{2+} mobilization and ATP release in response to collagen stimulation (Figure 2). Given the critical role of Ca^{2+} in platelet granule secretion, these results suggest that DHG disrupts upstream signaling events essential for platelet activation and may prevent thrombus formation at an early stage. DHG significantly reduced fibrinogen binding to platelets, indicating strong inhibition of $\alpha IIb\beta_3$ activation. By blocking this step, DHG prevents the formation of stable platelet plugs (Figure 3). Furthermore, DHG attenuated human thrombin-induced clot retraction, mirroring the effects of established ROCK inhibitors and also prevented collagen-induced platelet shape change (Figure 4). DHG also reduced the phosphorylation of key signaling proteins in a dose-dependent manner without significantly altering total protein levels (Figure 5). Additionally, DHG satisfies Lipinski's rule of five, suggesting good oral bioavailability. It also demonstrated favorable lipophilicity, solubility, and gastrointestinal absorption, along with a low probability of blood–brain barrier permeability (Figure 6A,B). The Venn diagram in Figure 7A shows the intersection between DHG-predicted targets and genes associated with platelet activation. Among the 34 DHG-related genes and 3353 platelet activation-related genes, 25 common genes were identified, representing potential targets through which DHG may influence platelet function. Figure 7B presents a protein–protein interaction (PPI) network constructed from the 25 overlapping genes using the STRING database. The network reveals a tightly connected hub centered around key nodes, such as NFKB1, CDK1, RXRA, PDGFRA, and PTPN11, indicating their crucial roles in mediating the interaction between DHG and platelet-related signaling. These core targets are functionally linked through multiple biological processes, suggesting DHG may exert multi-targeted modulation. Further, Figure 7C shows the compound–target–pathway network constructed using Cytoscape. DHG is connected to several targets, including NFKB1, PDGFRA, DRD1, PTPN11, and HTR2C, which are further linked to relevant pathways, such as the MAPK signaling pathway, calcium signaling pathway, adipocytokine signaling pathway, and insulin resistance. These enriched pathways have established roles in platelet function, inflammation, and cardiovascular regulation, supporting the potential of DHG to modulate platelet activity through multiple signaling cascades. Taken together, these pharmacological properties support DHG as a promising candidate for antithrombotic drug development.

Unlike many conventional antiplatelet agents, which typically target a single receptor or enzyme (e.g., $P2Y_{12}$ for clopidogrel or COX-1 for aspirin), DHG appears to modulate multiple pathways integral to platelet function. Our results demonstrate that DHG inhibits platelet aggregation while reducing ATP release, intracellular Ca^{2+} mobilization, $\alpha IIb\beta_3$

integrin activation, clot retraction, and activation of the MAPK and PI3K/Akt pathways (see schematic in Figure 8). Collectively, these findings suggest a broad-spectrum antiplatelet mechanism, similar to that of other recently reported multitarget natural compounds, such as ginsenoside Rg5 [15] cryptotanshinone [46], dieckol [12], and tryptanthrin [45], which also inhibit platelet activation by modulating multiple signaling cascades. However, in vivo studies are necessary to further elucidate the pharmacological effects of DHG in animal models or human platelets. Although the in vitro findings strongly support its antiplatelet efficacy, translation of these results to in vivo systems requires additional investigation. Therefore, future studies using animal models of arterial thrombosis (e.g., $FeCl_3$-induced vascular injury) or venous thrombosis are essential to establish its therapeutic potential.

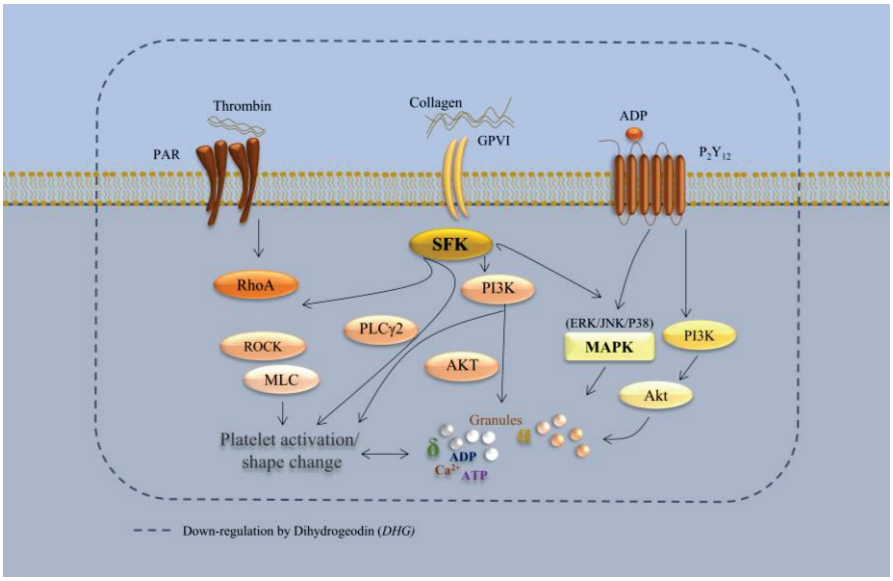

Figure 8. Schematic representation of DHG-mediated inhibition of platelet signaling pathways. DHG inhibits platelet aggregation while reducing ATP release, intracellular Ca^{2+} mobilization, αIIbβ3 integrin activation, clot retraction, and activation of the MAPK and PI3K/Akt pathways.

4. Materials and Methods

4.1. Reagents

Collagen, ADP, and thrombin were obtained from Chrono-Log Co. (Geffen, The Netherlands). Human plasma-derived thrombin and glutaraldehyde were purchased from Sigma-Aldrich. ATP assay kits were acquired from Cayman Chemical (Ann Arbor, MI, USA). Paraformaldehyde, Fura 2-AM, and Alexa Fluor 488-conjugated fibrinogen were obtained from Invitrogen (Eugene, OR, USA). Avertin was prepared as the anesthetic by dissolving 2,2,2-tribromoethanol (Sigma-Aldrich, Darmstadt, Germany, catalog no. T48402-5G) in 2-methyl-2-butanol (Sigma-Aldrich, Darmstadt, Germany, catalog no. 152463). All antibodies for western blotting were purchased from Cell Signaling Technology (Danvers, MA, USA).

4.2. Fungal Material and Fermentation

A fungal strain of *F. flavipes* (FU00000759) was obtained from the National Marine Biodiversity Institute of Korea (MABIK) (Seocheon-gun, Chungcheongnam-do 33662). This strain was isolated from a tidal flat in Incheon, located on the Western Coast of Korea. The strain was cultured in twenty 5 L flasks, each containing 1 L of potato dextrose broth, at 27 °C for 4 weeks under stationary conditions.

4.3. Extraction, Isolation, and Structure Determination

The extraction, isolation, and structure determination of the active compounds from *F. flavipes* were performed as described in our recent publication [31] and Supplementary Material Section 1.1. The ^{1}H and ^{13}C NMR spectra matched those known for dihydrogeodin [31,32], and complete data are provided in Supplementary Material Figures S1–S5.

4.4. Experimental Animals

Seven-week-old male Sprague–Dawley rats weighing 240–260 g were used for in vitro platelet experiments. The animals were acclimated in an environmentally controlled room maintained at approximately 23 ± 2 °C and 50% ± 10% humidity, with a 12 h light/dark cycle. All animal procedures were performed in accordance with institutional guidelines and approved by the Animal Care Committee of the College of Veterinary Medicine, Kyungpook National University, Daegu, Republic of Korea (Permit no KNU 2022-0083).

4.5. Light Transmission Aggregometry and Scanning Electron Microscopy (SEM)

Blood was collected from Sprague–Dawley rats via cardiac puncture using a syringe containing acid-citrate-dextrose to isolate purified platelets [6]. The collected blood was transferred into round-bottom tubes containing Tyrode's buffer and acid-citrate-dextrose at a 1:4 (*v*/*v*) ratio. Washed platelets were separated from whole blood by centrifugation at 170× *g* for 7 min, followed by a second centrifugation at 350× *g* for 10 min. The platelet suspension was adjusted to a concentration of 3×10^8 cells/mL for aggregometry analysis. Platelets were incubated for 1 min with DHG (10, 20, or 40 μM) or with DMSO as a control in the presence of 1 mM $CaCl_2$. Aggregation was then induced by the addition of agonists (collagen at 2.5 μg/mL, ADP at 10 μM, or thrombin at 0.1 U/mL) for 5 min. This method enabled precise quantification of the platelet response under defined experimental conditions, providing valuable insights into the effects of dihydrogeodin on platelet function. Platelets incubated with DHG and agonist (collagen) were fixed in 0.5% paraformaldehyde and 0.5% osmium tetroxide, dehydrated, and freeze-dried at –55 °C before being mounted for field-emission scanning electron microscopy (Hitachi SU8220, Tokyo, Japan) to assess ultrastructural shape changes.

4.6. ATP Release Assay, $[Ca^{2+}]_i$ Mobilization Assay, and Fibrinogen Binding Assay

Platelets were preincubated with dihydrogeodin and then stimulated with collagen to induce activation. Subsequently, ATP release, intracellular calcium mobilization, and fibrinogen binding were assessed as previously described [6]. ATP secretion was measured in the supernatant using an ATP assay kit to evaluate platelet function. Intracellular calcium concentration ($[Ca^{2+}]_i$) was determined in Fura-2/AM-loaded platelets using the following formula: $224\ nM \times (F - F_{min})/(F_{max} - F)$. For the fibrinogen binding assay, platelets were stained with an anti-fibrinogen antibody, and activation levels were evaluated by flow cytometry after collagen stimulation in the presence or absence of dihydrogeodin.

4.7. Clot Retraction

Platelet-rich plasma (PRP, 250 μL) was incubated for 2 min with DHG or Y-27632 (a ROCK inhibitor). A final volume of 1 mL was achieved by adding red blood cells (5 μL) and Tyrode's buffer. Thrombin (1 U/mL) was then added, and clot retraction was assessed at room temperature. Thrombin-induced clots were weighed to compare clot retraction among treatment groups.

4.8. Western Blotting

After preincubation with DHG and stimulation with collagen, lysis buffer was added to initiate lysis, and protein concentrations were quantified. Whole platelet proteins were isolated for subsequent analysis. Proteins were separated by sodium dodecyl sulfate–polyacrylamide gel electrophoresis (SDS-PAGE) and transferred onto polyvinylidene fluoride (PVDF) membranes. Membranes were blocked and incubated overnight with primary antibodies, followed by incubation with secondary antibodies for 3 h. The membranes were then washed three times and visualized using enhanced chemiluminescence. This procedure enabled evaluation of changes in protein expression induced by dihydrogeodin treatment.

4.9. Pharmacokinetics, Drug-Likeliness Analysis, and Network Pharmacology

SwissADME, a freely accessible web-based tool, was used to evaluate the pharmacokinetic properties and drug-likeness of DHG, as previously reported [49]. Briefly, the canonical SMILES notation for DHG was retrieved from PubChem (PC-ID 612831 https://pubchem.ncbi.nlm.nih.gov/compound/Dihydrogeodin, accessed on 20 March 2025) and entered into the SwissADME platform (http://www.swissadme.ch/, accessed on 20 March 2025). The resulting output files and images were directly imported from the website. The BOILED-Egg (Brain or Intestinal Estimated permeation predictive) model provides a rapid and straightforward method for assessing human intestinal absorption (HIA) and blood–brain barrier (BBB) permeation by calculating the lipophilicity and polarity of molecules, followed by generation of a water partition coefficient (WLOGP) versus topological polar surface area (tPSA) plot. For network pharmacology, the potential target proteins of DHG were predicted using the SuperPred web server, and the results were downloaded as CSV files. Corresponding UniProt IDs for Homo sapiens were retrieved and used for protein mapping via the STRING database to identify protein names (preferred names) associated with DHG. To identify disease-related targets, the keyword "platelet activation" was searched in the GeneCards database, and relevant human gene targets were extracted. The predicted DHG target genes (compound-related genes) and platelet activation-related genes (disease target genes) were compared using Venny 2.1. This analysis identified overlapping targets (common genes) between DHG and platelet activation. These overlapping targets were input into the STRING database (organism: Homo sapiens) to generate a protein–protein interaction (PPI) network and assess potential biological connections. KEGG pathway enrichment analysis was also performed through STRING to identify key signaling pathways associated with the overlapping genes. Finally, the network of DHG, overlapping target genes, and enriched pathways was constructed and visualized using Cytoscape software (version 3.7.2).

4.10. Statistical Analysis

Data were analyzed by one-way analysis of variance (ANOVA), followed by post hoc Dunnett's test (SAS Institute, Inc., Cary, NC, USA) to determine statistical significance. Results are presented as means ± standard deviation (SD). A p-value of 0.05 or less was considered statistically significant.

5. Conclusions

Overall, the findings of this study position dihydrogeodin as a promising natural antiplatelet agent capable of multifaceted inhibition of platelet function. By targeting central signaling pathways (MAPK and PI3K/Akt) and integrin αIIbβ_3 activation, DHG interferes with both the early and late stages of platelet activation. Coupled with its favorable in silico drug-likeness profile, these results support DHG as a strong candidate

for future pharmacological development. Rigorous in vivo studies and detailed mechanistic investigations will be required to fully characterize its therapeutic efficacy and safety in the prevention or treatment of thrombotic diseases.

Supplementary Materials: The following supporting information can be downloaded at: https://www.mdpi.com/article/10.3390/md23050212/s1, Figure S1. Compound 1, Figure S2. ^{1}H NMR spectrum of compound 1, Figure S3. ^{13}C NMR spectrum of compound 1, Figure S4. High-resolution ESI-mass spectrometry of compound 1, Figure S5. HPLC analysis of compound 1, Figure S6. Western blot bands, Figure S7. Cytotoxicity of DHG.

Author Contributions: Conceptualization, A.W.A., D.-C.C., B.-S.Y. and M.H.R.; methodology, A.W.A., D.-C.C., B.-S.Y. and M.H.R.; software, A.W.A., B.-S.Y. and M.H.R.; validation, B.-S.Y. and M.H.R.; formal analysis, A.W.A.; investigation, M.H.R.; resources, D.-C.C., B.-S.Y. and M.H.R.; data curation, A.W.A. and D.-C.C.; writing—original draft preparation, A.W.A., D.-C.C., H.-K.C., S.D.K. and D.K.; writing—review and editing, A.W.A., D.-C.C., H.-K.C., S.D.K., D.K., B.-S.Y. and M.H.R.; visualization, B.-S.Y. and M.H.R.; supervision, B.-S.Y. and M.H.R.; project administration, B.-S.Y. and M.H.R.; funding acquisition, B.-S.Y. and M.H.R. All authors have read and agreed to the published version of the manuscript.

Funding: This work was supported by the National Research Foundation of Korea (NRF) grant funded by the Korean government (MSIT) (No. 2022R1A2C1012963). We are thankful to the National Research Foundation of Korea (NRF) for the grants.

Institutional Review Board Statement: All animal procedures were performed in accordance with institutional guidelines and approved by the Animal Care Committee of the College of Veterinary Medicine, Kyungpook National University, Daegu, South Korea (Permit no. KNU 2022-0083).

Data Availability Statement: The original contributions presented in the study are included in the article/Supplementary material; further inquiries can be directed to the corresponding authors.

Conflicts of Interest: The authors declare no conflicts of interest.

References

1. Lockhart, P.B.; Sun, Y.P. Diseases of the cardiovascular system. In *Burket's Oral Medicine*; John Wiley & Sons: Hoboken, NJ, USA, 2021; pp. 505–552.
2. Caffrey, C.; Leamy, A.; O'Sullivan, E.; Zabetakis, I.; Lordan, R.; Nasopoulou, C. Cardiovascular diseases and marine oils: A focus on omega-3 polyunsaturated fatty acids and polar lipids. *Mar. Drugs* **2023**, *21*, 549. [CrossRef] [PubMed]
3. Scridon, A. Platelets and their role in hemostasis and thrombosis—From physiology to pathophysiology and therapeutic implications. *Int. J. Mol. Sci.* **2022**, *23*, 12772. [CrossRef] [PubMed]
4. Młynarska, E.; Czarnik, W.; Fularski, P.; Hajdys, J.; Majchrowicz, G.; Stabrawa, M.; Rysz, J.; Franczyk, B. From atherosclerotic plaque to myocardial infarction—The leading cause of coronary artery occlusion. *Int. J. Mol. Sci.* **2024**, *25*, 7295. [CrossRef]
5. Zhou, Y.; Zhang, D.; Tan, P.; Xian, B.; Jiang, H.; Wu, Q.; Huang, X.; Zhang, P.; Xiao, X.; Pei, J. Mechanism of platelet activation and potential therapeutic effects of natural drugs. *Phytomedicine* **2023**, *108*, 154463. [CrossRef]
6. Akram, A.W.; Saba, E.; Rhee, M.H. Antiplatelet and antithrombotic activities of Lespedeza cuneata via Pharmacological inhibition of integrin αIIbβ3, MAPK, and PI3K/AKT pathways and FeCl3-induced murine thrombosis. *Evid.-Based Complement. Altern. Med.* **2024**, *2024*, 9927160. [CrossRef]
7. Chen, C.; Yang, F.-Q.; Zhang, Q.; Wang, F.-Q.; Hu, Y.-J.; Xia, Z.-N. Natural products for antithrombosis. *Evid.-Based Complement. Altern. Med.* **2015**, *2015*, 876426. [CrossRef]
8. Li, D.; Li, Y.; Yang, S.; Yu, Z.; Xing, Y.; Wu, M. Mechanism and potential target of blood-activating Chinese botanical drugs combined with anti-platelet drugs: Prevention and treatment of atherosclerotic cardiovascular diseases. *Front. Pharmacol.* **2022**, *13*, 811422. [CrossRef]
9. Krishnan, K.; Nguyen, T.N.; Appleton, J.P.; Law, Z.K.; Caulfied, M.; Cabrera, C.P.; Lenthall, R.; Hewson, D.; England, T.; McConachie, N. Antiplatelet resistance: A review of concepts, mechanisms, and implications for management in acute ischemic stroke and transient ischemic attack. *Stroke Vasc. Interv. Neurol.* **2023**, *3*, e000576. [CrossRef]
10. Mussbacher, M.; Kral-Pointner, J.B.; Salzmann, M.; Schrottmaier, W.C.; Assinger, A. Mechanisms of hemostasis: Contributions of platelets, coagulation factors, and the vessel wall. In *Fundamentals of Vascular Biology*; Springer: Berlin/Heidelberg, Germany, 2024; pp. 167–203.

11. Shehwar, D.; Barki, S.; Aliotta, A.; Calderara, D.B.; Veuthey, L.; Portela, C.P.; Alberio, L.; Alam, M.R. Platelets and mitochondria: The calcium connection. *Mol. Biol. Rep.* **2025**, *52*, 276. [CrossRef]
12. Irfan, M.; Kwon, T.-H.; Kwon, H.-W.; Rhee, M.H. Pharmacological actions of dieckol on modulation of platelet functions and thrombus formation via integrin αIIbβ3 and cAMP signaling. *Pharmacol. Res.* **2022**, *177*, 106088. [CrossRef]
13. Kanchanawong, P.; Calderwood, D.A. Organization, dynamics and mechanoregulation of integrin-mediated cell–ECM adhesions. *Nat. Rev. Mol. Cell Biol.* **2023**, *24*, 142–161. [CrossRef] [PubMed]
14. Ngo, A.T.P.; Parra-Izquierdo, I.; Aslan, J.E.; McCarty, O.J.T. Rho GTPase regulation of reactive oxygen species generation and signalling in platelet function and disease. *Small GTPases* **2021**, *12*, 440–457. [CrossRef]
15. Akram, A.W.; Shin, J.-H.; Batmunkh, U.; Saba, E.; Kang, Y.-M.; Jung, S.; Han, J.E.; Kim, S.D.; Kwak, D.; Kwon, H.-W. Ginsenoside Rg5 inhibits platelet aggregation by regulating GPVI signaling pathways and ferric chloride-induced thrombosis. *J. Ginseng Res.* 2025. [CrossRef]
16. Li, Z.; Wang, Z.; Shen, B.; Chen, C.; Ding, X.; Song, H. Effects of aspirin on the gastrointestinal tract: Pros vs. cons. *Oncol. Lett.* **2020**, *20*, 2567–2578. [CrossRef]
17. Bebars, A.E.; Alhazmi, A.A.; Aldajan, M.Y.; Alhujeri, N.A.F.; Alhaidari, R.M. Gastrointestinal side effects of antiplatelet drugs (Aspirin and Clopidogrel) in Medina, Saudi Arabia. *Int. J. Med. Dev. Ctries.* **2021**, *5*, 210. [CrossRef]
18. Ferreira, M.; Freitas-Silva, M.; Assis, J.; Pinto, R.; Nunes, J.P.; Medeiros, R. The emergent phenomenon of aspirin resistance: Insights from genetic association studies. *Pharmacogenomics* **2020**, *21*, 125–140. [CrossRef]
19. Hidayat, R.; Nabilah, R.A.; Rasyid, A.; Harris, S.; Harahap, A.R.; Louisa, M.; Listyaningsih, E.; Rambe, A.S.; Loho, T. Clopidogrel resistance among ischemic stroke patients and its risk factors in Indonesia. *Acta Medica Acad.* **2022**, *51*, 29. [CrossRef]
20. Chaachouay, N.; Zidane, L. Plant-derived natural products: A source for drug discovery and development. *Drugs Drug Candidates* **2024**, *3*, 184–207. [CrossRef]
21. Aware, C.B.; Patil, D.N.; Suryawanshi, S.S.; Mali, P.R.; Rane, M.R.; Gurav, R.G.; Jadhav, J.P. Natural bioactive products as promising therapeutics: A review of natural product-based drug development. *South Afr. J. Bot.* **2022**, *151*, 512–528. [CrossRef]
22. Ahmed, H.A.; Hashmi, H.A.; Muzammal, U.; Akram, A.W.; Alvi, M.A.; Talib, M.T.; Basharat, A.; Rauf, U.; Rahman, H.M.S.; ur Rahman, H.M.H. Use of natural feed additives as a remedy for diseases in veterinary medicine. In *Complementary and Alternative Medicine: Feed Additives*; Unique Scientific Publisher: Faisalabad, Pakistan, 2024; p. 104. [CrossRef]
23. Wang, H.; He, D.; Duan, L.; Lv, L.; Gao, Q.; Wang, Y.; Yang, S.; Lv, Z. In Vivo anticoagulant and antithrombic activity of depolymerized glycosaminoglycan from Apostichopus japonicus and dynamic effect–exposure relationship in rat plasma. *Mar. Drugs* **2022**, *20*, 631. [CrossRef]
24. Zhang, H.; Sun, C.; Xia, Q.; Li, P.; Liu, K.; Zhang, Y. Brevianamide F exerts antithrombotic effects by modulating the MAPK signaling pathway and coagulation cascade. *Mar. Drugs* **2024**, *22*, 439. [CrossRef] [PubMed]
25. Sun, H.; Zhu, G.; Li, S.; Li, P.; Zhang, J.; Yin, R.; Yuan, L.; Gao, N.; Zhao, J. Fucosylated glycosaminoglycan oligosaccharide HS14, derived from Sea Cucumbers, is a novel inhibitor of platelet Toll-like receptor 2. *Mar. Drugs* **2025**, *23*, 110. [CrossRef] [PubMed]
26. Li, C.-Y.; Chang, C.-C.; Tsai, Y.-H.; El-Shazly, M.; Wu, C.-C.; Wang, S.-W.; Hwang, T.-L.; Wei, C.-K.; Hohmann, J.; Yang, Z.-J. Anti-inflammatory, antiplatelet aggregation, and antiangiogenesis polyketides from Epicoccum sorghinum: Toward an understating of its biological activities and potential applications. *ACS Omega* **2020**, *5*, 11092–11099. [CrossRef]
27. Zhao, L.; Lin, X.; Fu, J.; Zhang, J.; Tang, W.; He, Z. A novel bi-functional fibrinolytic enzyme with anticoagulant and thrombolytic activities from a marine-derived fungus Aspergillus versicolor ZLH-1. *Mar. Drugs* **2022**, *20*, 356. [CrossRef]
28. Papikinou, M.-A.; Pavlidis, K.; Cholidis, P.; Kranas, D.; Adamantidi, T.; Anastasiadou, C.; Tsoupras, A. Marine fungi bioactives with anti-inflammatory, antithrombotic and antioxidant health-promoting properties against inflammation-related chronic diseases. *Mar. Drugs* **2024**, *22*, 520. [CrossRef]
29. Ji, Y.B.; Chen, W.J.; Shan, T.Z.; Sun, B.Y.; Yan, P.C.; Jiang, W. Antibacterial diphenyl ether, benzophenone and xanthone derivatives from Aspergillus flavipes. *Chem. Biodivers.* **2020**, *17*, e1900640. [CrossRef]
30. Peterson, S.W. Phylogenetic analysis of Aspergillus species using DNA sequences from four loci. *Mycologia* **2008**, *100*, 205–226. [CrossRef]
31. Choi, D.-C.; Ki, D.-W.; Kim, J.-Y.; Lee, I.-K.; Yun, B.-S. New dimeric 1, 3-dihydroisobenzofuran from culture broth of Fennellia flavipes. *Phytochem. Lett.* **2025**, *65*, 141–144. [CrossRef]
32. Hamed, A.; Ismail, M.; El-Metwally, M.M.; Frese, M.; Stammler, H.G.; Sewald, N.; Shaaban, M. X-ray, structural assignment and molecular docking study of dihydrogeodin from *Aspergillus Terreus* TM8. *Nat. Prod. Res.* **2019**, *33*, 117–121. [CrossRef]
33. Sato, S.; Okusa, N.; Ogawa, A.; Ikenoue, T.; Seki, T.; Tsuji, T. Identification and preliminary SAR studies of (+)-geodin as a glucose uptake stimulator for rat adipocytes. *J. Antibiot.* **2005**, *58*, 583–589. [CrossRef]
34. Lemmens, T.P.; Luo, Q.; Wielders, S.J.H.; Scheijen, J.; Al-Nasiry, S.; Koenen, R.R.; Wenzel, P.; Cosemans, J. Platelet collagen receptors and their role in modulating platelet adhesion patterns and activation on alternatively processed collagen substrates. *Thromb. Res.* **2024**, *244*, 109201. [CrossRef] [PubMed]

35. Gachet, C.; Hechler, B. Platelet purinergic receptors in thrombosis and inflammation. *Hämostaseologie* **2020**, *40*, 145–152. [CrossRef] [PubMed]
36. Zou, J.; Wu, J.; Roest, M.; Heemskerk, J.W.M. Long-term platelet priming after glycoprotein VI stimulation in comparison to protease-activating receptor (PAR) stimulation. *PLoS ONE* **2021**, *16*, e0247425. [CrossRef]
37. Huang, W.-C.; Lin, K.-C.; Hsia, C.-W.; Hsia, C.-H.; Chen, T.-Y.; Bhavan, P.S.; Sheu, J.-R.; Hou, S.-M. The antithrombotic agent pterostilbene interferes with integrin αIIbβ3-mediated inside-out and outside-in signals in human platelets. *Int. J. Mol. Sci.* **2021**, *22*, 3643. [CrossRef]
38. Xiang, B.; Zhang, G.; Zhang, Y.; Wu, C.; Joshi, S.; Morris, A.J.; Ware, J.; Smyth, S.S.; Whiteheart, S.W.; Li, Z. Calcium ion chelation preserves platelet function during cold storage. *Arterioscler. Thromb. Vasc. Biol.* **2021**, *41*, 234–249. [CrossRef]
39. Lichota, A.; Szewczyk, E.M.; Gwozdzinski, K. Factors affecting the formation and treatment of thrombosis by natural and synthetic compounds. *Int. J. Mol. Sci.* **2020**, *21*, 7975. [CrossRef]
40. Pan, N.; Li, Z.-C.; Li, Z.-H.; Chen, S.-H.; Jiang, M.-H.; Yang, H.-Y.; Liu, Y.-S.; Hu, R.; Zeng, Y.-W.; Dai, L.-H. Antiplatelet and antithrombotic effects of isaridin E isolated from the marine-derived fungus via downregulating the PI3K/Akt signaling pathway. *Mar. Drugs* **2021**, *20*, 23. [CrossRef]
41. Vasconcelos, A.A.; Sucupira, I.D.; Guedes, A.L.; Queiroz, I.N.; Frattani, F.S.; Fonseca, R.J.; Pomin, V.H. Anticoagulant and antithrombotic properties of three structurally correlated sea urchin sulfated glycans and their low-molecular-weight derivatives. *Mar. Drugs* **2018**, *16*, 304. [CrossRef]
42. Cao, S.; He, X.; Qin, L.; He, M.; Yang, Y.; Liu, Z.; Mao, W. Anticoagulant and antithrombotic properties in vitro and in vivo of a novel sulfated polysaccharide from marine green alga Monostroma nitidum. *Mar. Drugs* **2019**, *17*, 247. [CrossRef]
43. Moura, L.d.A.; Marqui de Almeida, A.C.; Francielle Souza Domingos, T.; Ortiz-Ramirez, F.; Negrão Cavalcanti, D.; Laneuville Teixeira, V.; Lopes Fuly, A. Antiplatelet and anticoagulant effects of diterpenes isolated from the marine alga, Dictyota menstrualis. *Mar. Drugs* **2014**, *12*, 2471–2484. [CrossRef]
44. Gholkar, A.A.; Nikam, Y.P.; Zambare, K.K.; Reddy, K.V.; Ghorpade, A.D. Potential anticoagulant herbal plants: A review. *Asian J. Pharm. Sci.* **2020**, *10*, 51–55. [CrossRef]
45. Gao, H.; Huang, J.; Huang, X.; Lin, X.; Li, X.; Deng, H.; Zhou, Y.; Wu, L.; Xi, X.; Jin, J. Tryptanthrin impairs platelet function and thrombus formation by reducing Gp1bα expression. *Eur. J. Pharmacol.* **2025**, *991*, 177332. [CrossRef] [PubMed]
46. Xiao, Y.; Zhang, R.; Hua, C.; Wu, M.; Yuan, Y.; Zhang, L.; Guo, F.; Liu, J.; Yang, Z.; Liu, G. P2Y12 receptor-independent antiplatelet mechanism of cryptotanshinone: Network pharmacology and experimental validation of multi-target signaling pathways. *J. Ethnopharmacol.* **2025**, *341*, 119321. [CrossRef] [PubMed]
47. Suades, R.; Padró, T.; Vilahur, G.; Badimon, L. Platelet-released extracellular vesicles: The effects of thrombin activation. *Cell. Mol. Life Sci.* **2022**, *79*, 190. [CrossRef]
48. Zou, J.; Swieringa, F.; de Laat, B.; de Groot, P.G.; Roest, M.; Heemskerk, J.W.M. Reversible platelet integrin αIIbβ3 activation and thrombus instability. *Int. J. Mol. Sci.* **2022**, *23*, 12512. [CrossRef]
49. Quah, Y.; Lee, Y.Y.; Lee, S.-J.; Kim, S.D.; Rhee, M.H.; Park, S.-C. In silico investigation of *Panax ginseng* lead compounds against COVID-19 associated platelet activation and thromboembolism. *J. Ginseng Res.* **2023**, *47*, 283–290. [CrossRef]

Disclaimer/Publisher's Note: The statements, opinions and data contained in all publications are solely those of the individual author(s) and contributor(s) and not of MDPI and/or the editor(s). MDPI and/or the editor(s) disclaim responsibility for any injury to people or property resulting from any ideas, methods, instructions or products referred to in the content.

marine drugs

MDPI

Article

New Polyketides from a Marine Sponge-Derived Fungus, *Neopestalotiopsis* sp., with Anti-Renal Fibrosis Activity

Xinlong Li [1,†], Jianglian She [2,3,4,†], Meiqun Cai [3], Xinqi Chen [2,4], Rongxiang Qiu [3,5], Xiaowei Luo [1], Yonghong Liu [1,2], Xuefeng Zhou [1,2,4,*] and Lan Tang [3,*]

[1] Guangxi Key Laboratory of Marine Drugs, Institute of Marine Drugs, Guangxi University of Chinese Medicine, Nanning 530200, China; 13409379936@163.com (X.L.); luoxiaowei1991@126.com (X.L.); yonghongliu@scsio.ac.cn (Y.L.)
[2] CAS Key Laboratory of Tropical Marine Bio-Resources and Ecology, Guangdong Key Laboratory of Marine Materia Medica, South China Sea Institute of Oceanology, Chinese Academy of Sciences, Guangzhou 510301, China; shejianglian20@mails.ucas.ac.cn (J.S.); scsiochenxinqi@163.com (X.C.)
[3] NMPA Key Laboratory for Research and Evaluation of Drug Metabolism, Guangdong Provincial Key Laboratory of New Drug Screening, School of Pharmaceutical Sciences, Southern Medical University, Guangzhou 510515, China; meiquncai@163.com (M.C.); 18707678946@163.com (R.Q.)
[4] University of Chinese Academy of Sciences, Beijing 100049, China
[5] School of Chinese Materia Medica, Guangdong Pharmaceutical University, Guangzhou 510006, China
* Correspondence: xfzhou@scsio.ac.cn (X.Z.); tl405@smu.edu.cn (L.T.)
† These authors contributed equally to this work.

Abstract: Sixteen polyketides, including six new compounds (**1**–**2**, and **5**–**8**), were isolated from the culture of the marine sponge-associated fungus *Neopestalotiopsis* sp. SCSIO 41422. Their structures were elucidated through NMR, MS spectroscopic analyses, calculated electronic circular dichroism, quantum chemical NMR calculations, and X-ray single-crystal diffraction. To screen and evaluate the inhibitory activity of these polyketides in renal fibrosis, a TGF-β1-stimulated HK-2 cell model was used. All tested compounds (**1**, **5**–**8**, and **11**–**12**) at 10 μM showed obvious anti-fibrotic activity by inhibiting TGF-β1-induced α-SMA expression and extracellular matrix production (collagen I and fibronectin). Among them, gamahorin A (**1**) was shown to be the most potent and the most promising inhibitor against renal fibrosis.

Keywords: sponge-associated fungi; polyketides; *Neopestalotiopsis*; anti-renal fibrosis

1. Introduction

Chronic kidney disease (CKD) has become a significant global health concern, affecting roughly 700 million individuals [1,2]. Chronic inflammation and renal fibrosis drive the disease, with conditions like chronic glomerulonephritis, diabetic nephropathy, and hypertensive nephropathy sharing common pathological features of fibrosis, leading to end-stage renal failure [3,4]. Kidney damage causes nephron shrinkage, fibroblast transformation into myofibroblasts, and excessive extracellular matrix (ECM) accumulation [5]. The ECM consists of a fibrous network with gel-like components, including collagen, elastin, fibronectin, and laminin. Collagen, mainly produced by myofibroblasts, plays a central role in fibrosis. Fibroblast-to-myofibroblast conversion is key in renal fibrosis and a therapeutic target [6]. Current clinical trials of anti-fibrosis drugs show limited efficacy and significant side effects [7]. Pirfenidone (PFD) showed only a transient improvement in Phase II trials, with some patients discontinuing due to adverse effects, such as rash and gastrointestinal issues [8]. PFD's pharmacokinetics depend on renal function, limiting its

clinical applicability [9]. Therefore, developing novel, effective, and safe anti-fibrosis drugs is crucial.

Marine natural products are a new source for drug discovery, and studies show that many of them have potent anti-inflammatory and antioxidant properties, which are crucial in mitigating renal fibrosis. Penicilliumin B, a methyl cyclopentadienone from a deep-sea *Penicillium* strain, inhibits high-glucose-induced fibrosis in renal tubular cells. It also reduces oxidative stress and has strong anti-fibrotic and anti-proliferative properties [10]. Extreme marine environments have driven the evolution of marine fungi with exceptional adaptability, facilitating the production of diverse secondary metabolites with notable biological activity [11–14]. More than 3166 new compounds have been derived from sponges and their associated microorganisms, making them the second-largest source of marine natural products [15,16]. In the pursuit of anti-renal fibrosis lead compounds, six new and ten reported polyketides (Figure 1) were isolated from the sponge-associated fungus *Neopestalotiopsis* sp. SCSIO 41422. This study details the isolation, structural elucidation, and evaluation of the anti-renal fibrosis activity of the compounds, providing new insights into potential treatments for renal fibrosis.

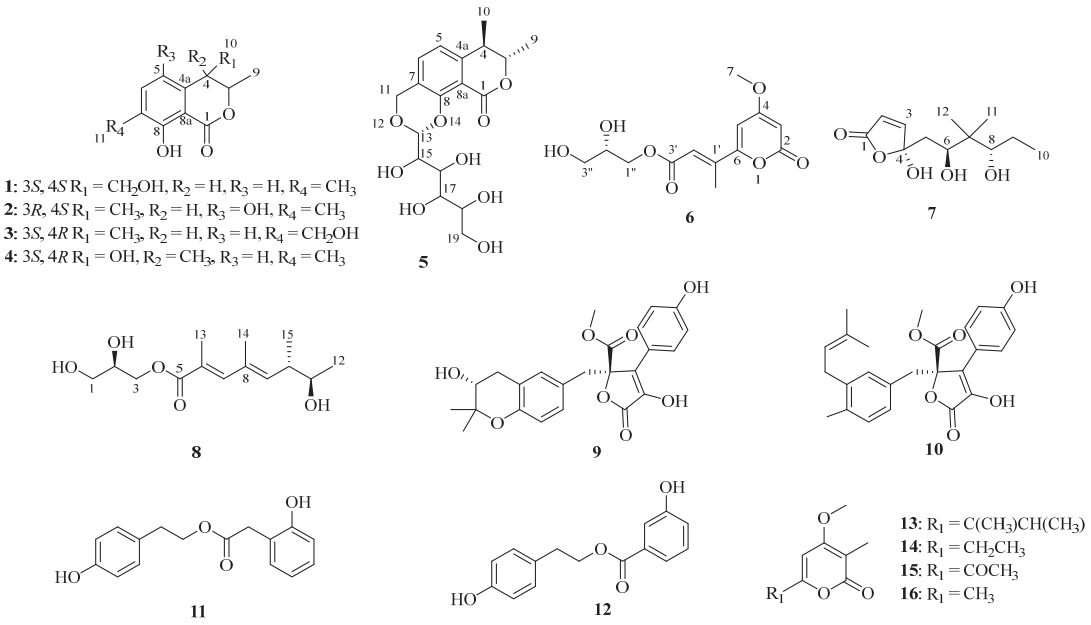

Figure 1. Structures of compounds **1**–**16**.

2. Results and Discussion

2.1. Structural Determination

Compound **1** was isolated as a brown oil, and its molecular formula was established as $C_{12}H_{14}O_4$ based on HRESIMS data, indicating six degrees of unsaturation. The 1D NMR and HSQC spectra (Table 1) revealed the following characteristic signals: two methyl groups [$\delta_{C/H}$ 19.9/1.37 (CH_3-9), 15.5/2.22 (CH_3-11)], two olefinic methine carbons [$\delta_{C/H}$ 120.1/6.79 (CH-5), 138.4/7.39 (CH-6)], one methylene carbon [$\delta_{C/H}$ 64.7/3.66 (CH_2-10)], and two methine carbons [$\delta_{C/H}$ 77.6/5.05 (CH-3), 46.7/2.89 (CH-4)], along with five quaternary carbons [δ_C 170.5 (C-1), 137.9 (C-4a), 126.6 (C-7), 161.3 (C-8), 108.2 (C-8a)]. The ^{1}H and ^{13}C NMR data of **1** closely resembled those of gamahorin [17], with the primary difference being the conversion of the methyl group at C-10 into a hydroxymethyl group and the hydroxymethyl group at C-11 into a methyl group, respectively. The HMBC (Figure 2) correlations of H-11/C-6, C-8 and H-10/C-3, C-4a further supported this deduction. Furthermore, the ^{1}H-^{1}H COSY spectrum revealed a correlation between H-10 and H-4, which

provided additional confirmation of the proposed structure. The NOESY spectrum showed a correlation between H-4 and H-9, indicating that H-4 and CH_3-9 were positioned on the same face of the molecule. The vicinal coupling constant (J = 5.6 Hz) between the two methine protons (H-3 and H-4) at position 3 supports the *threo* stereochemistry [17]. Based on this, the relative configuration of **1** was determined as 3*S**, 4*S**-**1**, 3*R**, 4*R**-**1**. The absolute configurations were subsequently established through computational electronic circular dichroism (ECD) analysis. The calculated ECD spectrum of 3*S*, 4*S*-**1** closely matched the experimental ECD spectrum (Figure 3), confirming the absolute configuration as 3*S*, 4*S*. In conclusion, the structure of **1** was elucidated as depicted in Figure 1, and it was named gamahorin A (**1**).

Table 1. ^{1}H (700MHz) and ^{13}C (175MHz) NMR data of **1-2** and **5** in CD_3OD.

Pos.	1		2		5	
	δ_C, Type	δ_H, (J in Hz)	δ_C, Type	δ_H, (J in Hz)	δ_C, Type	δ_H, (J in Hz)
1	170.5, C		170.7, C		170.9, C	
3	77.6, CH	5.05, qd, (6.7, 2.0)	83, CH	4.73, q, (6.7)	82.6, CH	4.57, m
4	46.7, CH	2.89, ddd, (7.6, 5.6, 1.8)	32.7, CH	3.19, q, (6.8)	38.5, CH	2.96, p, (7.0)
4a	137.9, C		126.5, C		145.3, C	
5	120.1, CH	6.79, d, (7.5)	147, C		117.9, CH	6.90, d, (7.7)
6	138.4, CH	7.39, d, (7.5)	126.6, CH	6.95, s	137.6, CH	7.74, d, (7.7)
7	126.6, C		126, C		125.9, C	
8	161.3, C		154.7, C		160.9, C	
8a	108.2, C		107, C		108.2, C	
9	19.9, CH_3	1.37, d, (6.7)	20.3, CH_3	1.30, d, (6.7)	19.9, CH_3	1.43, d, (6.5)
10	64.7, CH_2	3.66, m	19.9, CH_3	1.27, d, (7.1)	18.2, CH_3	1.36, d, (6.9)
11	15.5, CH_3	2.22, s	15.5, CH_3	2.17, s	64.7, CH_2	4.85, d, (12.5) 4.61, d, (12.5)
13					100.0, CH	4.95, d, (3.8)
15					73.7, CH	3.44, dd, (9.7, 3.8)
16					75.1, CH	3.70, m
17					71.7, CH	3.34, m
18					73.8, CH	3.66, td, (4.9, 2.1)
19					62.5, CH_2	3.77, dd, (11.2, 2.1) 3.70, m

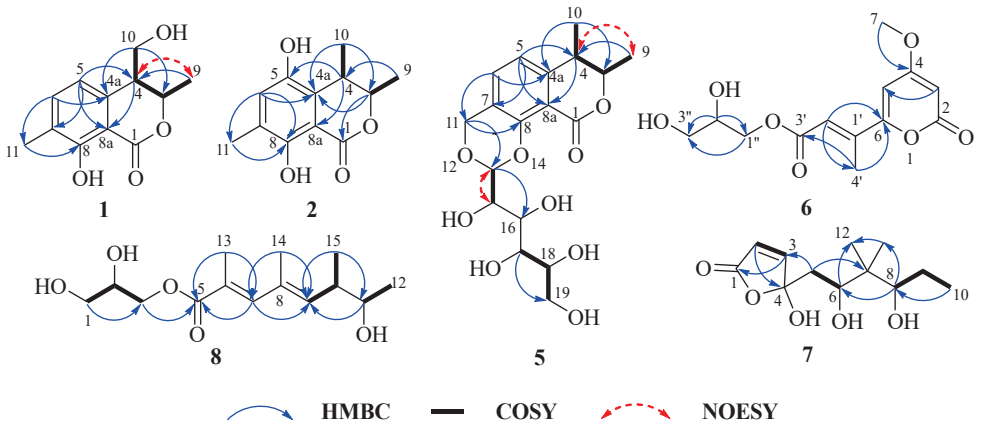

Figure 2. Key HMBC, COSY, and NOESY correlations of compounds **1**–**2** and **5**–**8**.

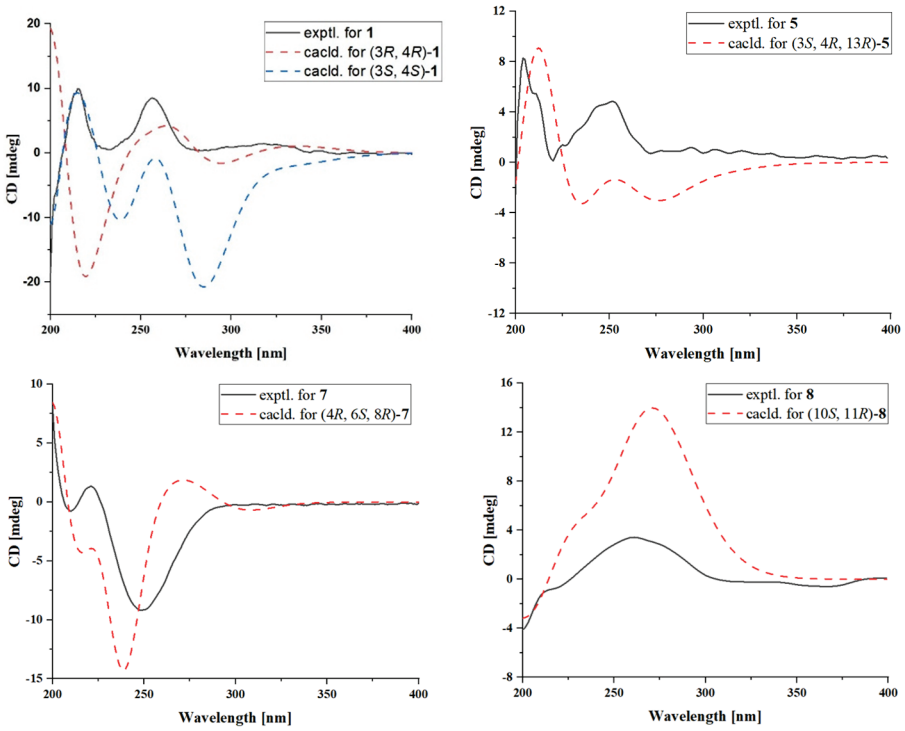

Figure 3. Experimental and calculated ECD spectra of compounds **1**, **5**, and **7**–**8**.

Compound **2** was isolated as a yellow solid, with its molecular formula established as $C_{12}H_{14}O_4$ based on HRESIMS data. The one-dimensional NMR and HSQC spectra (Table 1) displayed the following characteristic signals: three methyl groups [$\delta_{C/H}$ 20.3/1.30 (CH_3-9), 19.9/1.27 (CH_3-10), 15.5/2.17 (CH_3-11)], one olefinic methine carbon [$\delta_{C/H}$ 126.6/6.95 (CH-6)], two methine carbons [$\delta_{C/H}$ 83.0/4.73 (CH-3), 32.7/3.19 (CH-4)], and six quaternary carbons [δ_C 170.7 (C-1), 126.5 (C-4a), 147.0 (C-5), 126.0 (C-7), 154.7 (C-8), 107.0 (C-8a)]. The structure of **2** closely resembled that of **1**, with the primary difference being the location of the hydroxyl group. In the structure of **1**, the hydroxyl group is located at C-10, whereas, in **2**, it is attached to C-5. The proposed structure of **2** was further substantiated by ^{1}H-^{1}H COSY and HMBC correlations (Figure 2). The ^{1}H-^{1}H COSY correlations observed between H-3/H-9 and H-4/H-10, together with the HMBC correlations of H-10/C-3, C-4a, H-4/C-5, C-8a and H-3/C-10, C-4a, and C-1, provided strong support for the structural assignment. To determine the absolute configuration of the compound, X-ray diffraction analysis was performed, confirming both the planar structure and the absolute configuration as (3*R*, 4*S*-**2**) (Figure 4). Consequently, **2** was identified as gamahorin B (**2**).

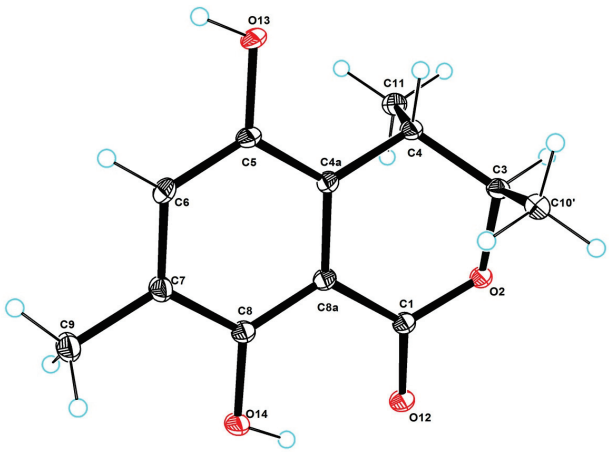

Figure 4. X-ray single-crystal diffraction of **2**.

Compound **5** was isolated as a yellow solid, with its molecular formula established as $C_{18}H_{24}O_9$ based on HRESIMS data, suggesting seven degrees of unsaturation. The one-dimensional NMR (Table 1) and HSQC spectra displayed characteristic signals, including two methyl groups [$\delta_{C/H}$ 19.9/1.43 (CH_3-9), 18.2/1.36 (CH_3-10)], two olefinic methines [$\delta_{C/H}$ 117.9/6.90 (CH-5), 137.6/7.74 (CH-6)], two methylene groups [$\delta_{C/H}$ 64.7/4.89, 4.61 (CH_2-11); 62.5/3.77, 3.70 (CH_2-19)], seven methine groups [$\delta_{C/H}$ 82.6/4.57 (CH-3), 38.5/2.96 (CH-4); 100.0/4.95 (CH-13), 73.7/3.44 (CH-15), 75.1/3.70 (CH-16), 71.7/3.34 (CH-17), 73.8/3.66 (CH-18)], and five quaternary carbons [δ_C 170.9 (C-1), 145.3 (C-4a), 125.9 (C-7), 160.9 (C-8), 108.2 (C-8a)]. The ^{1}H and ^{13}C NMR spectral data of **5** revealed structural similarities to gamahorin [17]. The NOESY spectrum revealed a correlation between H-4 and H-9, indicating that H-4 and CH_3-9 are positioned on the same face of the molecule. The vicinal coupling constant (J = 7.0 Hz) between the two methine protons (H-3 and H-4) at position 4 supports the *threo* stereochemistry. To determine the absolute configurations at the C-3, C-4, and C-13 rigid-ring positions of **5**, we employed DP4$^+$ probability analysis combined with NMR calculations utilizing the GIAO method. Through the prediction and analysis of NMR chemical shifts for four potential isomers (3*S**,4*R**,13*R**-**5**, 3*R**,4*S**,13*R**-**5**, 3*S**,4*R**,13*S**-**5**, 3*R**,4*S**,13*S**-**5**), the results identified 3*S**,4*R**,13*R**-**5** (Figure 5) as the most probable configuration, with a DP4$^+$ probability of 96.22%. Furthermore, the experimental CD curve of **5** exhibited a strong match with the calculated ECD curve, thereby providing additional confirmation of its absolute configuration. Consequently, the absolute configuration of compound 5 was conclusively determined to be 3*S*,4*R*,13*R*-**5** (Figure 3). The HMBC spectrum (Figure 2) exhibited key correlations between H-6/C-11, H-11/C-8, C-13, confirming the formation of a six-membered ring through two ether bonds at C-7 and C-8 in 5. Additionally, a polyhydroxy side chain was identified as being substituted at C-13 of the six-membered ring. This substitution was supported by HMBC correlations between H-13/C-16, H-17/C-19, together with ^{1}H-^{1}H COSY correlations between H-13/H-15, H-17/H-18. The polyhydroxylated side chain in **5** suggests that it may be a glycosylated natural product, where the stereochemistry of its chiral centers is governed by the glycosylation process, typically consistent with the D-glucose configuration. The observed specific rotation ([α]25 D +11.05) and the presence of multiple chiral centers may influence the optical activity. A literature analysis revealed that coretinphenol (structurally analogous to **5**) releases its aglycone and D-glucose upon 2M HCl hydrolysis [18]. The hydrolysate was derivatized into trimethylsilyl (TMS) ethers and analyzed by GC-MS, with retention time matching against authentic references confirming the β-D-glucopyranosyl configuration. Attempts to isolate the side chain via acid hydrolysis were unsuccessful due to insufficient compound quantities. Collectively, while the core stereochemistry (3*S*,4*R*,13*R*) has been rigorously supported, the side-chain configuration remains unassigned, necessitating further structural characterization. Consequently, **5** was identified and named as gamahorin C (**5**).

Compound **6** was isolated as a yellow crystalline solid, with its molecular formula established as $C_{13}H_{16}O_7$ based on HRESIMS data. The one-dimensional NMR (Table 2) and HSQC spectra displayed characteristic signals, including one methyl group [$\delta_{C/H}$ 13.6/2.37 (CH_3-4′)], one methoxy group [$\delta_{C/H}$ 57.3/3.90 (7-OCH_3)], two oxygenated methylene groups [$\delta_{C/H}$ 64.2/3.59 (CH_2-1″), $\delta_{C/H}$ 64.2/3.51 (CH_2-3″)], three olefinic methine groups [$\delta_{C/H}$ 91.3/5.74 (CH-3), $\delta_{C/H}$ 104.0/6.55 (CH-5), $\delta_{C/H}$ 120.8/6.65 (CH-2′)], one oxygenated secondary methine group [$\delta_{C/H}$ 73.9/3.65 (CH-2″)], and five sp^2 carbon signals [δ_C 165.6 (C-2), 172.9 (C-4), 160.1 (C-6), 144.0 (C-1′), 167.9 (C-3′)]. The NMR spectra of **6** showed a strong resemblance to those of pestalotiopyrone I [19], suggesting that both compounds share the same planar structure. This hypothesis was further supported by key HMBC (Figure 2) correlations in **6**, including H-3/C-5, H_3-7/C-4, H-2′/C-6 and C-4′, H_3-4′/C-3′ and C-6, H-1″/C-3″, and H-2″/C-1″ and C-2″. A closer examination of the 1D NMR

spectra of the two compounds revealed a significant difference at the C-1″, 2″, and 3″ positions. As C-2″ is the only chiral center on the side chain and is conformationally flexible, it was inferred that the absolute configuration of C-2″ in **6** is the opposite to that in pestalotiopyrone I. To verify the previous assumption and determine the absolute configuration of **6**, we first attempted to use the Mosher reaction to determine its configuration at the 2″ position. However, the experiment was unsuccessful, resulting in an insufficient compound quantity to proceed with further chemical verification. To address this issue, we successfully determined the absolute configuration of **6** by combining specific rotation measurements with literature comparisons. We found that **6** shared the same planar structure with the known compound pestalotiopyrone I, with the opposite specific rotation signs. Specifically, the specific rotation of **6** was measured as $[\alpha]_D^{25}$ +1.6 (c 0.1, MeOH), while that of pestalotiopyrone I was $[\alpha]_D^{20}$ –13.1 (c 0.2, MeOH). Based on this observation and the literature support, we concluded that the absolute configuration of compound **6** at the 2″ position was *S*. Consequently, **6** was identified as epi-pestalotiopyrone I (**6**).

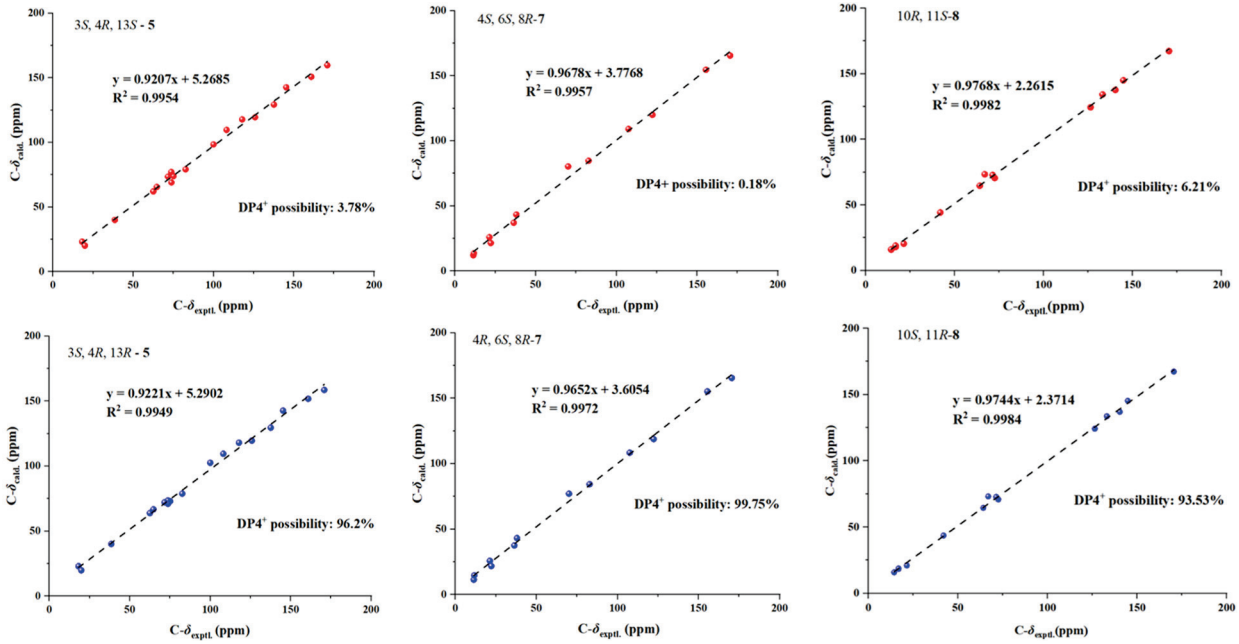

Figure 5. Linear regression and DP4 possibility analysis between the experimental and calculated ^{1}H and ^{13}C chemical shifts of the diastereomers of (3*S*,4*R*,13*R*)-**5**/(3*S*,4*R*,13*S*)-**5**, (4*S*,6*S*,8*R*)-**7**/(4*R*,6*S*,8*R*)-**7**, and (10*R*,11*S*)-**8**/ (10*S*,11*R*)-**8**.

Table 2. ^{1}H (500MHz) and ^{13}C (125MHz) NMR data of **6** in CD_3OD.

Pos.	6	
	δ_C, Type	δ_H, (*J* in Hz)
2	165.6, C	
3	91.3, CH	5.74, d, (1.9)
4	172.9, C	
5	104, CH	6.55, d, (2.1)
6	160.1, C	
7	57.3, CH_3	3.9, s
1′	144, C	
2′	120.8, CH	6.65, d, (1.6)
3′	167.9, C	
4′	13.6, CH_3	2.37, d, (1.1)
1″	64.4, CH_2	3.59, dd, (11.2, 4.9)
2″	73.9, CH	3.65, m
3″	64.4, CH_2	3.51, dd, (11.2, 6.0)

The new compound **7** was isolated as a yellow crystalline solid, with its molecular formula established as $C_{12}H_{20}O_5$ based on HRESIMS data. The ^{1}H NMR spectrum (Table 3) displayed characteristic signals, including three methyl groups [$\delta_{C/H}$ 11.4/0.83 (CH_3-10), $\delta_{C/H}$ 11.7/0.77 (CH_3-11), $\delta_{C/H}$ 22.2/0.90 (CH_3-12)], two olefinic methine groups [$\delta_{C/H}$ 122.4/6.29 (CH-2), $\delta_{C/H}$ 155.5/7.55 (CH-3)], two methylene groups [$\delta_{C/H}$ 36.4/1.91, 1.65 (CH_2-5), $\delta_{C/H}$ 21.3/1.55, 1.26 (CH_2-9)], two methine groups [$\delta_{C/H}$ 70.2/3.54 (CH-6), $\delta_{C/H}$ 82.8/3.36 (CH-8)], and three quaternary carbons [δ_C 170.5 (C-1), 107.5 (C-4), 38.1 (C-7)]. The ^{1}H and ^{13}C NMR spectral data of **7** revealed the presence of a five-membered lactone group and a long-chain structure. The planar structure was established through HMBC and COSY spectra (Figure 2). Key HMBC correlations included H-3/C-1, H-2/C-4, H-5/C-3, C-7, H-6/C-12, H-8/C-6, C-11, and H3-10/C-8. Additionally, ^{1}H-^{1}H COSY correlations between H-2/H-3, H-5/H-6, and H-9/H-8, H-10 provided further support for the proposed structure. To determine the absolute configurations at C-4, C-6, and C-8, a DP4$^+$ probability analysis was performed in combination with NMR calculations using the GIAO method. The NMR chemical shifts of eight possible isomers (4*R**,6*R**,8*R**-**7**, 4*R**,6*R**,8*S**-**7**, 4*R**,6*S**,8*S**-**7**, 4*R**,6*S**,8*R**-**7**, 4*S**,6*R**,8*R**-**7**, 4*S**,6*S**,8*R**-**7**, 4*S**,6*R**,8*S**-**7**, 4*S**,6*S**,8*S**-**7**) were predicted and analyzed via DP4$^+$ probability analysis. The results identified 4*R**, 6*S**, 8*S**-**7** (Figure 5) as the most likely configuration, with a DP4$^+$ probability of 99%. The experimental CD curve of **7** closely matched the calculated ECD curve, further confirming its absolute configuration. In conclusion, the absolute configuration of **7** was determined to be 4*R*, 6*S*, 8*S*-**7** (Figure 3). Consequently, **7** was identified as epiclactone C (**7**).

Table 3. ^{1}H (500MHz) and ^{13}C (125MHz) NMR data of **7** (DMSO-d_6) and **8** (CD_3OD).

Pos.	**7**		**8**	
	δ_C, Type	**δ_H, (*J* in Hz)**	**δ_C, Type**	**δ_H, (*J* in Hz)**
1	170.5, C		64.1, CH_2	3.61, m
2	122.4, CH	6.29, d, (5.6)	71.3, CH	3.90, m
3	155.5, CH	7.55, d, (5.6)	66.9, CH_2	4.25, dd, (11.4, 4.8) 4.16, dd, (11.4, 6.1)
4	107.5, C			
5	36.4, CH_2	1.91, m 1.65, dd, (13.5, 4.9)	170.5, C	
6	70.2, CH	3.54, dd, (11.8, 4.7)	126.4, C	
7	38.1, C		144.8, CH	7.21, s
8	82.8, CH	3.36, m	133.1, C	
9	21.3, CH_2	1.55, m 1.26, m	140.3, CH	5.51, d, (10.0)
10	11.4, CH_3	0.83, t, (7.3)	41.9, CH	2.5, m
11	11.7, CH_3	0.77, s	72.5, CH	3.58, m
12	22.2, CH_3	0.90, s	21.4, CH_3	1.17, d, (6.3)
13			14.3, CH_3	2.04, s
14			16.8, CH_3	1.91, s
15			16.8, CH_3	1.07, d, (6.7)

Compound **8** was isolated as a brown oily substance, with its molecular formula established as $C_{14}H_{24}O_5$ based on HRESIMS data, indicating three degrees of unsaturation. The ^{1}H NMR spectrum (Table 3) displayed characteristic signals, including four methyl groups [$\delta_{C/H}$ 21.4/1.17 (CH_3-12), $\delta_{C/H}$ 14.3/2.04 (CH_3-13), $\delta_{C/H}$ 16.8/1.91 (CH_3-14), $\delta_{C/H}$ 16.8/1.07 (CH_3-15)], two olefinic methine groups [$\delta_{C/H}$ 144.8/7.21 (CH-7), $\delta_{C/H}$ 140.3/5.51 (CH-9)], two methylene groups [$\delta_{C/H}$ 64.1/3.61 (CH_2-1), $\delta_{C/H}$ 66.9/4.25, 4.16 (CH_2-3)], three methine groups [$\delta_{C/H}$ 71.3/3.90 (CH-2), $\delta_{C/H}$ 41.9/2.53 (CH-10), $\delta_{C/H}$ 72.5/3.58 (CH-11)], and three quaternary carbons [δ_C 170.5 (C-5), 126.4 (C-6), 133.1 (C-8)]. The ^{1}H and ^{13}C NMR spectral data of **8** revealed the presence of an α, β-dihydroxy ester unit, similar to pestalotiopyrone I [19], suggesting that it is a long-chain compound with conjugated dienes and an ester group. The planar structure was established through HMBC and COSY spectra (Figure 2). Key HMBC correlations included H-1/C-3, H-3/C-5, H-12/C-5, C-7, H-13/C-7,

C-9, H-15/C-9, C-11, and H-7/C-5, C-9. Additionally, ^{1}H-^{1}H COSY correlations between H-2/H-1, H-3, H-10/H-9, H-15 further supported the proposed structure. A comparison of the NMR data for the *α*, *β*-dihydroxy ester unit indicated strong similarity to pestalotiopyrone I, suggesting the same R-configuration at C-2. To determine the absolute configurations at C-10 and C-11, a DP4^{+} probability analysis was conducted using NMR calculations via the GIAO method. Among the four possible isomers (10*R**,11*R**-**8**, 10*R**,11*S**-**8**, 10*S**,11*R**-**8**, 10*S**,11*S**-**8**), the analysis identified 10*S**, 11*R**-**8** (Figure 5) as the most likely configuration, with a DP4^{+} probability of 93.53%. The experimental CD curve of **8** closely matched the calculated ECD curve, providing further confirmation of the absolute configuration. In summary, the absolute configuration of **8** was determined to be 10*S*, 11*R*-**8** (Figure 3). Consequently, **8** was identified as pestalotiopyrone M (**8**).

By comparing the 1D NMR data in detail with previously reported literature values, the identified known compounds were confirmed as gamahorin (**3**) [17], pestalotiopisorin B (**4**) [20], pestalotiopyrones J (**13**) [21], pestalotiopyrones C (**14**) [21], vermopyrone (**15**) [22], 4-methoxy-3,6-dimethylpyran-2-one (**16**) [23], butyrolactone-V (**9**) [24], butyrolactone I (**10**) [25], aspergillol A (**11**) [26], and 4-hydroxyphenethyl 3-hydroxybenzoate (**12**) [27].

2.2. Bioactivity Assay

To investigate the therapeutic potential of the compounds in renal fibrosis, we established a TGF-*β*1-induced HK-2 cell model to simulate epithelial–mesenchymal transition (EMT) and extracellular matrix (ECM) deposition. As a result, seven tested compounds (**1**, **5**–**8**, and **11**−**12**) at 10 μM revealed obvious anti-fibrotic activity through the suppression of TGF-*β*1-induced *α*-smooth muscle actin (*α*-SMA) expression and ECM component production (collagen I and fibronectin) (Figure 6). Among these compounds, compound **1** was shown to be the most potent and the most promising inhibitor against renal fibrosis, being even better than the positive control pirfenidone (PFD), which is the current clinical standard for fibrosis treatment. This lead compound also demonstrated the strongest ECM-modulatory effects, significantly suppressing fibronectin and collagen I accumulation to a greater extent than all other derivatives.

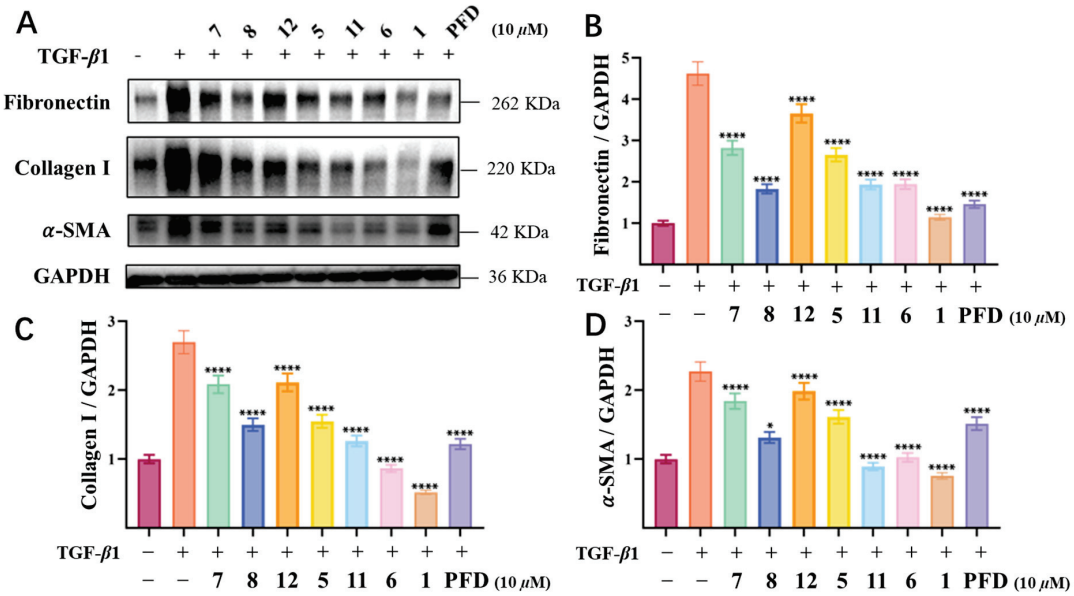

Figure 6. Evaluation of the renal-fibrosis-inhibitory activity of polyketides (**1**, **5**–**8**, and **11**–**12**) in a TGF-*β*1-stimulated HK-2 cell model. (**A**) The effects of polyketides (10 μM) on fibronectin, collagen I, and *α*-SMA in the cell model. (**B**–**D**) Quantification of the immunoblot data of (**A**). Data were analyzed using one-way ANOVA followed by Bonferroni's multiple-comparisons test. * $p < 0.05$, **** $p < 0.0001$.

Compounds **1**–**16** were also evaluated for their antibacterial and antioxidant activity. The results showed that all compounds were inactive against *Escherichia coli*, *Staphylococcus aureus*, *Streptococcus* spp., and *Salmonella* spp. Compounds **2** and **9**–**10** exhibited weak antioxidant activity, with EC_{50} values of 45.24, 37.96, and 52.53 μg/mL against DPPH radicals, respectively (positive control: ascorbic acid, 3.5 μg/mL).

3. Materials and Methods

3.1. General Experimental Procedures

The infrared spectra were recorded using a Shimadzu IR Affinity-1 Fourier transform infrared spectrophotometer (the FT-IR analysis was performed using the ATR method, with 25 scans, a resolution of 4 cm^{-1}, and a scanning range of 400–4000 cm^{-1}). Optical rotation measurements were performed with an Anton Paar MPC 500 polarimeter (Anton, Graz, Austria). UV and circular dichroism (CD) spectra were analyzed using a Chirascan circular dichroism spectrometer (Applied Photophysics, Leatherhead, U.K.). High-resolution electrospray ionization mass spectrometry (HRESIMS) data were acquired with a Bruker maxis Q-TOF mass spectrometer. Nuclear magnetic resonance (NMR) spectra were obtained on Bruker Avance-500 and Avance-700 MHz spectrometers, using tetramethylsilane (TMS) as an internal standard (Bruker BioSpin International AG, Fällanden, Switzerland); solvent peaks of methanol-d_4 (δ_H 3.31 and δ_C 49.0) and DMSO-d_6 (δ_H 2.50 and δ_C 39.52) were used as references. Semi-preparative high-performance liquid chromatography (HPLC) was carried out on a Hitachi Primaide system equipped with a diode-array detector (DAD) and an octadecylsilane (ODS) column (YMC-pack ODS-A, YMC Co. Ltd., Kyoto, Japan, 10 mm × 250 mm, 5 μm). For column chromatography (CC), silica gel (200−300 mesh) (Qingdao Ocean Chemical Plant, Qingdao, China) and ODS (50 μm) (Merck, Darmstadt, Germany) were utilized. Thin-layer chromatography (TLC) spots were visualized under 254 nm UV light on plates from the Qingdao Ocean Chemical Factory. Additionally, semi-preparative HPLC employed an ODS column (YMC-pack ODS-A, YMC Co. Ltd., Kyoto, Japan, 10 mm × 250 mm, 5 μm) operating at a flow rate of 2.5 mL/min.

3.2. Fungal Material

Strain SCSIO 41422 was obtained from an endophytic fungus associated with a sponge sample collected in the waters surrounding Weizhou Island, in the Beibu Gulf of the South China Sea. The sequence analysis of the internal transcribed spacer (ITS) region of its rDNA (GenBank accession number: NR_OQ120420) confirmed that this fungal strain belonged to the genus *Neopestalotiopsis*. The strain has been preserved at the Key Laboratory of Tropical Marine Biological Resources and Ecology, South China Sea Institute of Oceanology, Chinese Academy of Sciences, located in Guangzhou, China.

3.3. Fermentation and Extraction

The fungal strain *Neopestalotiopsis* sp. SCSIO 41422 was initially cultivated under static conditions on MB solid medium before being transferred to seed medium (250 mL; 1.5% malt extract, 2.4% sea salt) in 1 L Erlenmeyer flasks. The seed cultures were incubated at 28 °C on a rotary shaker set to 180 rpm for three days. For large-scale fermentation, the fungus was grown for 30 days at 26 °C under static conditions using a rice-based medium, which consisted of 200 g of rice, 2.4% sea salt, and 250 mL of water per flask. A total of 300 Erlenmeyer flasks (1 L each) were utilized for this process. The entire fermentation culture was extracted three times with ethyl acetate, producing 288 g of a brown, oily crude extract.

3.4. Isolation and Purification

The ethyl acetate extract was fractionated through silica gel medium-pressure liquid chromatography (MPLC) using a stepwise gradient elution. Initially, petroleum ether (PE) and dichloromethane (DCM) mixtures were applied as eluents in varying volume ratios of 1:0, 3:1, 2:1, 1:1, and 0:1. Subsequently, gradient elution with dichloromethane and methanol (DCM-CH_3OH) was conducted, incorporating methanol concentrations of 1%, 3%, 5%, 10%, 50%, and 70%. Thin-layer chromatography (TLC) analysis guided the combination of the eluates, resulting in 16 fractions (designated as Frs. 1–16). Frs. 3–7 were subjected to fractionation using an ODS silica gel column with methanol–water (CH_3OH/H_2O) gradient elution ranging from 5% to 100%, resulting in 16 subfractions (Frs. A-1–A-16). Fr. A-3 was purified by semi-preparative HPLC (50% CH_3OH/H_2O, flow rate of 3 mL/min), yielding **1** (1.9 mg, t_R = 26 min). Similarly, Fr. A-4 underwent semi-preparative HPLC purification (35% CH_3OH/H_2O, flow rate of 3 mL/min) to produce **13** (4.4 mg, t_R = 12 min). Fr. A-4-1 was further purified via HPLC (35% CH_3OH/H_2O, flow rate of 3 mL/min), yielding **3** (5.4 mg, t_R = 5 min), while Fr. A-4-4 was processed by HPLC (26% CH_3CN/H_2O, flow rate of 3 mL/min), isolating **14** (93.1 mg, t_R = 10 min). The further purification of Fr. A-5 by HPLC (23% CH_3CN/H_2O, flow rate of 3 mL/min) yielded **5** (1.48 mg, t_R = 21 min). Fr. A-7 was processed using HPLC (69% CH_3OH/H_2O, flow rate of 3 mL/min), yielding **8** (6.7 mg, t_R = 11 min), while Fr. A-7-2 was purified by semi-preparative HPLC (70% CH_3CN/H_2O, flow rate of 3 mL/min), producing **16** (89 mg, t_R = 9 min). Fr. A-8-1 underwent HPLC separation (40% CH_3CN/H_2O, flow rate of 3 mL/min), yielding compound **2** (36 mg, t_R = 8 min). Finally, Fr. A-10-3 was separated by HPLC (46% CH_3CN/H_2O, flow rate of 3 mL/min), resulting in **4** and **15** (8.4 mg and 119.8 mg, t_R = 8 and 12 min, respectively).

Frs. 8–10 were fractionated using an ODS silica gel column with methanol–water gradient elution (5–100%), producing 14 subfractions (Frs. B-1–B-14). Fr. B-6-6 was purified via HPLC (45% CH_3CN/H_2O, flow rate of 3 mL/min), isolating **7** (11 mg, t_R = 12 min). Similarly, Fr. B-7 was processed using HPLC (69% CH_3OH/H_2O, flow rate of 3 mL/min), yielding **9** (6.72 mg, t_R = 11 min), and Fr. B-9 was purified by HPLC (65% CH_3OH/H_2O, flow rate of 3 mL/min), producing **10** (43.6 mg, t_R = 18 min). Lastly, Frs. 11–13 were separated using an ODS silica gel column with methanol–water gradient elution (5–100%), yielding 12 subfractions (Frs. C-1–C-12). Fr. C-2 underwent HPLC purification (30% CH_3CN/H_2O, flow rate of 3 mL/min), producing **11** (6 mg, t_R = 35 min). Fr. C-5 was processed by HPLC (35% CH_3CN/H_2O, flow rate of 3 mL/min), yielding **12** (6 mg, t_R = 7 min), while Fr. C-6-3 was purified by HPLC (15% CH_3CN/H_2O, flow rate of 3 mL/min), producing **6** (6 mg, t_R = 7 min).

3.5. Spectroscopic Data of Compounds

Gamahorin A (**1**): Brown oily substance; $[\alpha]_D^{25}$ –5.3 (*c* 0.1, MeOH); UV (MeOH) λ_{max} (log ε) 210 (6.09), 237 (2.33), 250 (2.46), 276 (1.93), 320 (2.26) nm; ECD (0.3 mg/mL, MeOH) λmax ($\Delta\varepsilon$) 215 (+9.96), 233 (+0.53), 256 (+8.50) nm; IR (film) ν_{max} 3356, 2943, 2835, 2974, 1663, 1423, 1136, 1018, 286 cm^{-1}; ^1H and ^{13}C NMR data available in Table 1; HRESIMS *m*/*z* 223.0969 $[M+H]^+$ (calculated for $C_{12}H_{15}O_4^+$, 223.0965).

Gamahorin B (**2**): Yellow crystalline solid; $[\alpha]_D^{25}$ +35.5 (*c* 0.1, MeOH); UV (MeOH) λ_{max} (log ε) 204 (2.95), 220 (2.76), 256 (2.43), 349 (2.25) nm; ECD (0.3 mg/mL, MeOH) λmax ($\Delta\varepsilon$) 215 (–5.41), 238 (+3.87), 259 (+14.98) nm; IR (film) ν_{max} 3612, 3566, 2362, 1921, 1867, 1649, 1556, 1458, 682 cm^{-1}; ^1H and ^{13}C NMR data available in Table 1; HRESIMS *m*/*z* 223.0968 $[M+H]^+$ (calculated for $C_{12}H_{15}O_4^+$, 223.0965).

Gamahorin C (**5**): Yellow solid; $[\alpha]_D^{25}$ +11.05 (*c* 0.1, MeOH); UV (MeOH) λ_{max} (log ε) 211 (3.30), 236 (2.53), 249 (2.64), 275 (2.00) nm; ECD (0.3 mg/mL, MeOH) λmax ($\Delta\varepsilon$) 203 (+9.90), 210 (+4.73), 212 (+6.06), 252 (+4.99) nm; IR (film) ν_{max} 3342, 2949, 2837, 1658, 1408,

1111, 1020, 590 cm^{-1}; ^{1}H and ^{13}C NMR data available in Table 1; HRESIMS *m*/*z* 385.1496 $[M+H]^+$ (calculated for $C_{18}H_{25}O_9^+$, 385.1493).

epi-Pestalotiopyrone I (**6**): Yellow crystalline solid; $[\alpha]_D^{25}$ +1.6 (*c* 0.1, MeOH); UV (MeOH) λ_{max} (log ε) 212 (2.94), 232 (3.29), 259 (2.62), 215 (2.79) nm; ECD (0.3 mg/mL, MeOH) λmax ($\Delta\varepsilon$) 204 (–2.75), 212 (–2.22), 225 (–1.44), 240 (–0.96) nm; IR (film) ν_{max} 3587, 3564, 2924, 2358, 1716, 1598, 1417, 1039, 667 cm^{-1}; ^{1}H and ^{13}C NMR data available in Table 2; HRESIMS *m*/*z* 285.0964 $[M+H]^+$ (calculated for $C_{13}H_{17}O_7^+$, 285.0969).

Epiclactone C (**7**): Yellow crystalline solid; $[\alpha]_D^{25}$ –52.4 (*c* 0.1, MeOH); UV (MeOH) λ_{max} (log ε) 204 (2.93), 224 (2.33), 253 (1.90) nm; ECD (0.3 mg/mL, MeOH) λmax ($\Delta\varepsilon$) 210 (–0.78), 221 (+1.36), 248 (–9.18), 284 (–0.91) nm; IR (film) ν_{max} 3589, 3564, 2372, 2320, 1867, 1716, 1556, 1031, 592 cm^{-1}; ^{1}H and ^{13}C NMR data available in Table 3; HRESIMS *m*/*z* 243.1244 $[M-H]^-$ (calculated for $C_{12}H_{19}O_5^-$, 243.1238).

Pestalotiopyrone M (**8**): Yellow solid; $[\alpha]_D^{25}$ +8.74 (*c* 0.1, MeOH); UV (MeOH) λ_{max} (log ε) 234 (2.82), 267 (3.08), 317 (3.04) nm; ECD (0.3 mg/mL, MeOH) λmax ($\Delta\varepsilon$) 258 (+3.91) nm; IR (film) ν_{max} 3350, 2951, 2837, 1645, 1450 1408, 1117, 1015, 673 cm^{-1}; ^{1}H and ^{13}C NMR data available in Table 3; HRESIMS *m*/*z* 273.1701 $[M+H]^+$ (calculated for $C_{12}H_{25}O_5^+$, 273.1697).

3.6. X-Ray Crystallographic Analysis

Crystallographic data for **2** were collected using an XtaLAB PRO single-crystal diffractometer with Cu Kα radiation, following the slow evaporation of the compound in methanol. The X-ray crystal structures were solved using the *SHELXS97* program, expanded through difference Fourier methods, and refined via full-matrix least-squares calculations. Non-hydrogen atoms were subjected to anisotropic refinement, while hydrogen atoms were constrained to calculated positions. The crystallographic data for **2** have been deposited in the Cambridge Crystallographic Data Centre (CCDC).

Crystal Data for $C_{12}H_{14}O_4$ (*M* = 222.23 g/mol): orthorhombic, space group $P2_12_12_1$ (no. 19), *a* = 6.91550(10) Å, *b* = 8.21390(10) Å, *c* = 19.3752(2) Å, *V* = 1100.57(2) $Å^3$, *Z* = 4, *T* = 100.00(10) K, μ (Cu Kα) = 0.837 mm^{-1}, *Dcalc* = 1.341 g/cm^3, 10,749 reflections measured ($9.128^\circ \leq 2\Theta \leq 148.58^\circ$), 2196 unique ($R_{int}$ = 0.0314, R_{sigma} = 0.0212), which were used in all calculations. The final R_1 was 0.0291 ($I > 2\sigma(I)$) and the wR_2 was 0.0777 (all data) (Figure 4, Flack parameter −0.08(8) and CCDC 2429168).

3.7. ECD Computational and DP4+ Probability Analysis Methods

Random conformational searches for molecules **1**, **5**, and **7**−**8** were conducted using the MMFF94s molecular force field implemented in Spartan ′14 V1.1.4. The identified stable conformers were further optimized in Gaussian09 at the B3LYP/6-31G(d) level under gas-phase conditions. These optimized conformers were subsequently utilized for ECD calculations in methanol at the B3LYP/6-311G (d, p) level of theory [28]. The resulting ECD data were weighted based on the Boltzmann distribution with a half-bandwidth of 0.3 eV, processed using GaussView6.0, and the ECD curves were plotted in OriginPro 2021 following UV corrections.

First, an initial conformational search was performed using the Spartan'14 software with the MIMFF94 force field, yielding a set of low-energy conformations within a 5 kcal/mol range. Subsequently, each conformation was optimized using the TDDFT quantum chemistry method at the B3LYP/6-31G (d, p) level of theory with Gaussian 09. NMR shieldings were then calculated using the GIAO method at the same B3LYP/6-31G (d, p) level, employing the PCM solvent model. Finally, Boltzmann weights were calculated using Molclus, and a $DP4^+$ probability analysis was conducted [29].

3.8. Antioxidant Activity Assay

The DPPH radical scavenging assay was used to assess the antioxidant capacity of the compounds. Test compounds at concentrations of 1000, 500, 100, 50, and 10 μg/mL, with ascorbic acid as a positive control, were dissolved in MeOH and mixed with fresh DPPH in a methanol solution. The assay was performed in triplicate, and, after a 30 min reaction in the absence of light, the absorbance was measured at 517 nm using an Enspire Genios microplate reader. The blank solution contained only MeOH, while the control solution contained MeOH instead of the sample. The DPPH scavenging activity (%) was calculated using the formula [1 − (sample absorbance − blank absorbance)/control absorbance] × 100. EC_{50} values, representing the concentration causing 50% of the maximum effect, were determined using the Origin 2022 software [30].

3.9. Antimicrobial Activity Assay

Compounds were evaluated for antibacterial activity against Escherichia coli, Staphylococcus aureus, Streptococcus spp., and Salmonella spp. using a modified broth microdilution method in 96-well plates [31].

3.10. TGF-β1-Stimulated HK-2 Cell Model

The HK-2 cells were cultured in a 37 °C, 5% CO_2 cell incubator, maintained with DMEM/F12 (Gibco, New York, NY, USA) supplemented with 10% fetal bovine serum (FBS) (ExCell, FSP500, Suzhou, China). HK-2 cells were inoculated for 12 h in 6-well (2×10^5 cells per well) plates. Subsequently, to establish the TGF-β1-stimulated HK-2 cell model, the cells were starved in serum-free medium for 24 h and then were treated with 10 ng mL^{-1} recombinant TGF-β1 (R&D Systems, 240-B-002, Minneapolis, MN, USA), with or without compounds, for 48 h.

3.11. Western Blot (WB) Analysis

The kidney tissue, HK-2, or 293T cells were lysed in RIPA (Ncmblo, WB3100, Suzhou, China) with proteinase inhibitors (Meilunbio, MB2678-1, Dalian, China) and then centrifuged (13,000× *g*, 15 min, 4 °C). A BCA kit (Epizyme, ZJ102, Shanghai, China) was employed to measure the concentration of total protein. Quantified protein-mixed loading buffer (Epizyme, LT101S) was boiled for 10 min at 100 °C, separated by SDS-PAGE, and transferred onto PVDF membranes (Millipore, ISEQ00010, Burlington, MA, USA). After incubation with blocking buffer for 1 h at room temperature, the membranes were incubated overnight at 4 °C with antibodies specific to the indicated proteins. Then, the washed membranes were incubated with the secondary antibodies (anti-rabbit or anti-mouse IgG) for 2 h at room temperature. Western blot bands were detected by the ECL (Fdbio, FD8020, Hangzhou, China) substrates and analyzed by the Image-J 1.52a software [32].

3.12. Statistical Analysis

All experiments, except the in vivo mouse studies, were performed at least three times. All data are expressed as the mean ± standard deviation (SD). Statistical analysis was performed using the Prism 7 software (GraphPad, San Diego, CA, USA), including Student's *t*-test, one-way ANOVA, and two-way ANOVA. $p < 0.05$ was considered to be significant (* $p < 0.05$, ** $p < 0.01$, *** $p < 0.001$, **** $p < 0.0001$).

4. Conclusions

Sixteen polyketide compounds were isolated from the sponge-associated fungus *Neopestalotiopsis* sp. SCSIO 41422, including six new compounds (**1**−**2** and **5**−**8**). Their chemical structures were fully determined through NMR and HRESIMS, with quantum

chemical calculations used to assign the absolute configurations of compounds **1** and **5**−**8** and X-ray diffraction confirming the absolute configuration of compound **2**. All tested compounds (**1**, **5**–**8**, and **11**–**12**) at 10 μM exhibited significant anti-fibrotic activity by inhibiting TGF-β1-induced α-SMA expression and ECM component production (collagen I and fibronectin). Among them, gamahorin A (**1**) has been shown to be the most potent and the most promising inhibitor against renal fibrosis, being even better than the positive control PFD. This lead compound also demonstrated the strongest ECM-modulatory effects, significantly suppressing fibronectin and collagen I accumulation to a greater extent than all other derivatives. This study provides promising lead compounds for the discovery of marine-derived renal fibrosis inhibitors and candidate drugs for the prevention and treatment of chronic kidney disease.

Supplementary Materials: The following supporting information can be downloaded at https://www.mdpi.com/article/10.3390/md23040148/s1: Figures S1–S58: The NMR, HRESIMS, UV, and IR spectra of **1**–**2** and **5**–**8**; physicochemical data of **3**–**4** and **11**–**16**; ITS sequence data of the strain.

Author Contributions: Funding acquisition, L.T. and X.Z.; investigation, X.L. (Xinlong Li) and J.S.; methodology, X.L. (Xinlong Li), J.S., M.C., X.C. and R.Q.; project administration, L.T. and X.Z.; supervision, X.L. (Xiaowei Luo), Y.L., L.T. and X.Z.; writing—original draft, X.L. (Xinlong Li) and J.S.; writing—review and editing, M.C., L.T. and X.Z. All authors have read and agreed to the published version of the manuscript.

Funding: This research was funded by the Special Project for Marine Economic Development of the Department of Natural Resources of Guangdong Province (GDNRC [2024]25), the National Natural Science Foundation of China (U24A20809), the Natural Science Foundation of Guangdong Province (2024A1515012477, 2024A1515011051), and the Guangdong Local Innovation Team Program (2019BT02Y262).

Institutional Review Board Statement: Not applicable.

Informed Consent Statement: Not applicable.

Data Availability Statement: Data are contained within the article and Supplementary Materials.

Acknowledgments: We are grateful to Z. Xiao, X. Zheng, A. Sun, Y. Zhang, and X. Ma at the analytical facility at SCSIO for recording the spectroscopic data.

Conflicts of Interest: The authors declare no conflicts of interest.

References

1. Carney, E.F. The impact of chronic kidney disease on global health. *Nat. Rev. Nephrol.* **2020**, *16*, 251. [CrossRef] [PubMed]
2. Cockwell, P.; Fisher, L.-A. The global burden of chronic kidney disease. *Lancet* **2020**, *395*, 662–664. [CrossRef]
3. Ruiz-Ortega, M.; Rayego-Mateos, S.; Lamas, S.; Ortiz, A.; Rodrigues-Diez, R.R. Targeting the progression of chronic kidney disease. *Nat. Rev. Nephrol.* **2020**, *16*, 269–288. [CrossRef]
4. Xiang, Y.; Yuan, Z.; Deng, Q.; Xie, L.; Yu, D.; Shi, J. Potential therapeutic medicines for renal fibrosis: Small-molecule compounds and natural products. *Bioorg. Chem.* **2024**, *143*, 106999. [CrossRef] [PubMed]
5. Webster, A.C.; Nagler, E.V.; Morton, R.L.; Masson, P. Chronic Kidney Disease. *Lancet* **2017**, *389*, 1238–1252. [CrossRef]
6. Horowitz, J.C.; Thannickal, V.J. Mechanisms for the Resolution of Organ Fibrosis. *Physiology* **2019**, *34*, 43–55. [CrossRef]
7. Ruiz-Ortega, M.; Lamas, S.; Ortiz, A. Antifibrotic Agents for the Management of CKD: A Review. *Am. J. Kidney Dis.* **2022**, *80*, 251–263. [CrossRef]
8. Kim, E.S.; Keating, G.M. Pirfenidone: A review of its use in idiopathic pulmonary fibrosis. *Drugs* **2015**, *75*, 219–230. [CrossRef] [PubMed]
9. Maher, T.M.; Corte, T.J.; Fischer, A.; Kreuter, M.; Lederer, D.J.; Molina-Molina, M.; Axmann, J.; Kirchgaessler, K.-U.; Samara, K.; Gilberg, F.; et al. Pirfenidone in patients with unclassifiable progressive fibrosing inte rstitial lung disease: A double-blind, randomised, placebo-controlled, phase 2 trial. *Lancet Respir. Med.* **2020**, *8*, 147–157. [CrossRef]
10. Lin, X.; Wu, Q.; Yu, Y.; Liang, Z.; Liu, Y.; Zhou, L.; Tang, L.; Zhou, X. Penicilliumin B, a novel sesquiterpene methylcyclopentenedione from a deep sea-derived Penicillium strain with renoprotective activities. *Sci. Rep.* **2017**, *7*, 10757. [CrossRef]

11. Zhong, M.; Li, Y.; Deng, L.; Fang, J.; Yu, X. Insight into the adaptation mechanisms of high hydrostatic pressure in physiology and metabolism of hadal fungi from the deepest ocean sediment. *mSystems* **2024**, *9*, e01085-23. [CrossRef] [PubMed]
12. Venkatachalam, M.; Gérard, L.; Milhau, C.; Vinale, F.; Dufossé, L.; Fouillaud, M. Salinity and Temperature Influence Growth and Pigment Production in the Marine-Derived Fungal Strain Talaromyces albobiverticillius 30548. *Microorganisms* **2019**, *7*, 10. [CrossRef]
13. Giordano, D. Bioactive Molecules from Extreme Environments. *Mar. Drugs* **2020**, *18*, 640. [CrossRef]
14. Jones, E.B.G.; Ramakrishna, S.; Vikineswary, S.; Das, D.; Bahkali, A.H.; Guo, S.-Y.; Pang, K.-L. How Do Fungi Survive in the Sea and Respond to Climate Change? *J. Fungi* **2022**, *8*, 291. [CrossRef]
15. Li, P.; Lu, H.; Zhang, Y.; Zhang, X.; Liu, L.; Wang, M.; Liu, L. The natural products discovered in marine sponge-associated microorgan isms: Structures, activities, and mining strategy. *Front. Mar. Sci.* **2023**, *10*, 1191858. [CrossRef]
16. Carroll, A.R.; Copp, B.R.; Davis, R.A.; Keyzers, R.A.; Prinsep, M.R. Marine natural products. *Nat. Prod. Rep.* **2020**, *37*, 175–223. [CrossRef]
17. Koshino, H.; Yoshihara, T.; Okuno, M.; Sakamura, S.; Tajimi, A.; Shimanuki, T. Gamahonolides A, B, and Gamahorin, Novel Antifungal Compounds from Str omata of *Epichloe typhina* on *Phleum pratense*. *Biosci. Biotechnol. Biochem.* **1992**, *56*, 1096–1099. [CrossRef] [PubMed]
18. Wang, W.; Chen, W.; Yang, Y.; Liu, T.; Yang, H.; Xin, Z. New phenolic compounds from Coreopsis tinctoria Nutt. and their antiox idant and angiotensin i-converting enzyme inhibitory activities. *J. Agric. Food Chem.* **2015**, *63*, 200–207. [CrossRef] [PubMed]
19. Rönsberg, D.; Debbab, A.; Mándi, A.; Wray, V.; Dai, H.; Kurtán, T.; Proksch, P.; Aly, A.H. Secondary metabolites from the endophytic fungus Pestalotiopsis virgat ula isolated from the mangrove plant Sonneratia caseolaris. *Tetrahedron Lett.* **2013**, *54*, 3256–3259. [CrossRef]
20. Xu, Z.; Wu, X.; Li, G.; Feng, Z.; Xu, J. Pestalotiopisorin B, a new isocoumarin derivative from the mangrove en dophytic fungus *Pestalotiopsis* sp. HHL101. *Nat. Prod. Res.* **2020**, *34*, 1002–1007. [CrossRef]
21. Xu, J.; Aly, A.H.; Wray, V.; Proksch, P. Polyketide derivatives of endophytic fungus Pestalotiopsis sp. isolate d from the Chinese mangrove plant Rhizophora mucronata. *Tetrahedron Lett.* **2011**, *52*, 21–25. [CrossRef]
22. Bi, Y.-M.; Bi, X.-B.; Fang, A.; Zhao, Q.-R. Metabolites from the fungus *Cephalosporium* sp. AL031. *Arch. Pharm. Res.* **2007**, *30*, 267–269. [CrossRef]
23. Hirota, A.; Nemoto, A.; Tsuchiya, Y.; Hojo, H.; Abe, N. Isolation of a 2-Pyrone Compound as an Antioxidant from a Fungus and Its New Reaction Product with 1,1-Diphenyl-2-picrylhydrazyl Radical. *Biosci. Biotechnol. Biochem.* **1999**, *63*, 418–420. [CrossRef]
24. Nagia, M.M.; El-Metwally, M.M.; Shaaban, M.; El-Zalabani, S.M.; Hanna, A.G. Four butyrolactones and diverse bioactive secondary metabolites from t errestrial Aspergillus flavipes MM2: Isolation and structure determination. *Org. Med. Chem. Lett.* **2012**, *2*, 9. [CrossRef]
25. Zhang, Y.Y.; Zhang, Y.; Yao, Y.-B.; Lei, X.-L.; Qian, Z.-J. Butyrolactone-I from Coral-Derived Fungus *Aspergillus terreus* Attenuates Neuro-Inflammatory Response via Suppression of NF-κB Pathway in BV-2 Cells. *Mar. Drugs* **2018**, *16*, 202. [CrossRef] [PubMed]
26. Pettit, G.; Du, J.; Pettit, R.; Knight, J.C.; Doubek, D.L. Antineoplastic Agents. 575. The Fungus Aspergillus phoenicis. *Heterocycles* **2009**, *79*, 909. [CrossRef]
27. Zhang, L.; Xu, Q.; Zhu, J.; Xia, G.; Zang, H. Synthesis, α-Glucosidase inhibition and molecular docking studies of tyrosol derivatives. *Nat. Prod. Res.* **2021**, *35*, 1596–1604. [CrossRef] [PubMed]
28. Yang, B.; Tao, H.; Lin, X.; Wang, J.; Liao, S.; Dong, J.; Zhou, X.; Liu, Y. Prenylated indole alkaloids and chromone derivatives from the fungus *Penicillium* sp. SCSIO041218. *Tetrahedron* **2018**, *74*, 77–82. [CrossRef]
29. Grimblat, N.; Zanardi, M.M.; Sarotti, A.M. Beyond DP4: An Improved Probability for the Stereochemical Assignment of Isomeric Compounds using Quantum Chemical Calculations of NMR Shifts. *J. Org. Chem.* **2015**, *80*, 12526–12534. [CrossRef]
30. Huang, Z.; Nong, X.; Ren, Z.; Wang, J.; Zhang, X.; Qi, S. Anti-HSV-1, antioxidant and antifouling phenolic compounds from the de ep-sea-derived fungus Aspergillus versicolor SCSIO 41502. *Bioorg. Med. Chem. Lett.* **2017**, *27*, 787–791. [CrossRef]
31. Huang, Z.-H.; Nong, X.-H.; Liang, X.; Qi, S.-H. New tetramic acid derivatives from the deep-sea-derived fungus *Cladosp orium* sp. SCSIO z0025. *Tetrahedron* **2018**, *74*, 2620–2626. [CrossRef]
32. Gan, L.; Jiang, Q.; Huang, D.; Wu, X.; Zhu, X.; Wang, L.; Xie, W.; Huang, J.; Fan, R.; Jing, Y.; et al. A natural small molecule alleviates liver fibrosis by targeting apolip oprotein L2. *Nat. Chem. Biol.* **2025**, *21*, 80–90. [CrossRef] [PubMed]

Disclaimer/Publisher's Note: The statements, opinions and data contained in all publications are solely those of the individual author(s) and contributor(s) and not of MDPI and/or the editor(s). MDPI and/or the editor(s) disclaim responsibility for any injury to people or property resulting from any ideas, methods, instructions or products referred to in the content.

marine drugs

MDPI

Article

Bioprospecting Marine Fungi from the Plastisphere: Osteogenic and Antiviral Activities of Fungal Extracts

Matteo Florio Furno [1], Vincent Laizé [2], Irene Arduino [3], Giang Nam Pham [4,†], Federica Spina [1], Mohamed Mehiri [4], David Lembo [3], Paulo J. Gavaia [2] and Giovanna Cristina Varese [1,*]

[1] Department of Life Sciences and Systems Biology, University of Turin, Mycotheca Universitatis Taurinensis (MUT), Viale Mattioli 25, 10125 Turin, Italy; matteo.floriofurno@unito.it (M.F.F.); federica.spina@unito.it (F.S.)
[2] Centre of Marine Sciences, University of Algarve, 8005-139 Faro, Portugal; vlaize@ualg.pt (V.L.); pgavaia@ualg.pt (P.J.G.)
[3] Department of Clinical and Biological Sciences, University of Turin, Regione Gonzole, 10, Orbassano, 10043 Turin, Italy; irene.arduino@unito.it (I.A.); david.lembo@unito.it (D.L.)
[4] Marine Natural Products Team, UMR 7272, Institut de Chimie de Nice, Université Côte d'Azur, CNRS, 06108 Nice, France; nam.phamgiang@phenikaa-uni.edu.vn (G.N.P.); mohamed.mehiri@univ-cotedazur.fr (M.M.)
* Correspondence: cristina.varese@unito.it; Tel.: +39-011-670-59-84
† Present address: Faculty of Pharmacy, PHENIKAA University, Yen Nghia, Ha Dong, Hanoi 12116, Vietnam.

Abstract: Marine microplastics (MPs) represent a novel ecological niche, populated by fungi with high potential for pharmaceutical discovery. This study explores the bioactivity of fungal strains isolated from MPs in Mediterranean sediments, focusing on their osteogenic and antiviral activities. Crude extracts prepared via solid-state and submerged-state fermentation were tested for their effects on extracellular matrix mineralization in vitro and bone growth in zebrafish larvae, and for their activity against the respiratory syncytial virus (RSV) and herpes simplex virus type 2 (HSV-2). Several extracts exhibited significant mineralogenic and osteogenic activities, with *Aspergillus jensenii* MUT6581 and *Cladosporium halotolerans* MUT6558 being the most performing ones. Antiviral assays identified extracts from *A. jensenii* MUT6581 and *Bjerkandera adusta* MUT6589 as effective against RSV and HSV-2 at different extents, with no cytotoxic effect. Although chemical profiling of *A. jensenii* MUT6581 extract led to the isolation of decumbenones A and B, they did not reproduce the observed bioactivities, suggesting the involvement of other active compounds or synergistic effects. These results highlight the plastisphere as a valuable resource for novel bioactive compounds and suggest the need for further fractionation and characterization to identify the molecules responsible for these promising activities.

Keywords: secondary metabolites; plastisphere; *Aspergillus jensenii*; SSF; SmF; microplastics

1. Introduction

Marine fungi have evolved remarkable biodiversity and unique biological metabolic pathways to adapt to a range of ecological conditions, including extreme environments characterized by high pressure, low temperature, anoxia, and light limitation [1]. These adaptations came along with the synthesis of new metabolites, many of them yet to be discovered, that could present novel biological activities [2]. The antibiotic cephalosporin C was the first drug isolated from marine fungi in the 1950s [3]. Subsequently, more active metabolites were isolated from marine fungi [1,4,5]. The biochemical diversity of these metabolites is complex and rich, ranging from linear peptides and fatty acids to

complex alkaloids, terpenes, and polyketides, which have shown antitumoral, antioxidant, antifungal, antibacterial, antiviral, and anticancer properties [1,2,6–8].

Among the various marine-associated habitats, sediments represent one of the most microorganism-rich environments. However, they are also highly competitive ecosystems, constantly challenged by factors such as nutrient limitation, pressure, anoxia, and the presence of toxic compounds. In the last decades, the persistent accumulation of microplastics (MPs) has emerged as a major concern [9]. The mycobiota associated with MPs in marine sediments of the Mediterranean Sea was recently investigated [10], leading to the identification of several yeast and filamentous fungal taxa. Furthermore, comparisons with the surrounding sediment-associated fungal communities revealed potential substrate specificity, underscoring the complexity of MP-associated fungal assemblages. Besides their ecological value, these MP-associated fungal strains could represent a valuable resource for innovative biochemical properties. In fact, MP-associated fungi have shown versatile metabolism, including the ability to degrade hydrocarbons, dyes, and xenobiotics (i.e., plastics), to produce biosurfactants (thus increasing the bioavailability of organic compounds), or being halotolerant and osmo-protective.

In this new human-made environment (i.e., the plastisphere), the competition for space and nutrients is very high, and the entire microbiome may be affected by this constant fight for survival. Although bacteria are known to produce bioactive compounds [11–14], marine fungi associated with the plastisphere could prevail by producing bioactive molecules involved in defense or antagonistic mechanisms. In fact, the ecological role of bioactive molecules has been associated with chemical defenses, where they act as potent inhibitors of physiological processes, promoting competition with other marine organisms to ensure their survival [15–17]. The biosynthetic pathways for secondary metabolites have evolved to produce chemical structures that specifically interact with biological targets. As a result, it can be inferred that many secondary metabolites possess inherent biological activities [18–20]. Therefore, bioprospecting plays a crucial role in deciphering the bioactive potential of these metabolites from marine microorganisms.

Although the ecological role of fungal secondary metabolites may be complex and not fully understood yet, the regulatory networks governing natural product production can be manipulated during fermentation processes to generate different bioactive compounds. Fermentation has been mainly classified into solid-state fermentation (SSF) and submerged fermentation (SmF) based on the type of substrate used. Studies have shown that SSF and SmF could activate different metabolic pathways, resulting in higher production of certain bioactive compounds in SSF, while SmF thrives on others [21–23]. Consequently, selecting the appropriate fermentation method is crucial, as it can significantly influence the outcomes.

The present study aims at investigating the MPs-associated marine fungi from Mediterranean sediments as possible sources of novel bioactive molecules of pharmaceutical interest, evaluating their potential in regenerative and infectivity medicine. Two different fermentation techniques, SSF and SmF, were evaluated for the production of bioactive molecules. Fungal crude extracts produced were screened using different assays for (1) osteoactive compounds using a fish bone-derived cell line capable of in vitro mineralization and the developing opercular bone of zebrafish larvae; and (2) compounds with antiviral activity against the respiratory syncytial virus (RSV) and herpes simplex virus type 2 (HSV-2).

2. Results and Discussion

Crude polar extracts of 15 marine fungi associated with the plastisphere of Mediterranean sediments (Table 1) were produced using SSF and SmF. In most cases, the productivity was 20–40-fold higher in SSF than in SmF. These differences in productivity across

the two different methods are documented in the literature and attributed to the variations in fermentation techniques, which can trigger distinct metabolic responses [24,25]. However, in SSF conditions, the extract yield strongly depended on the fungus, ranging from 374.6 mg of *Vishniacozyma carnescens* MUT6591 down to 15.4 mg for *Aureobasidium pullulans* MUT6584. These differences were much less pronounced in SmF, where most extract yields were below 10 mg. The only outliers were *A. pullulans* MUT6584 and *Penicillium griseofulvum* MUT6588 (e.g., 12.0 mg and 108.2 mg, respectively). An average crude extract dry weight of 187.9 mg and 12.4 mg was achieved for SSF and SmF, respectively (Table 1).

Table 1. List of fungi and crude extract dry weight associated with solid-state fermentation (SSF) and submerged-state fermentation (SmF).

Taxa	Id. Crude Extract SSF	Productivity for SSF (mg)	Id. Crude Extract SmF	Productivity for SmF (mg)
Cystobasidium slooffiae MUT6565	1S	121.9	1L	5.5
Cladosporium cladosporioides MUT6583	2S	188.8	2L	8.8
Aspergillus domesticus MUT6603	3S	131.7	3L	3.1
Bjerkandera adusta MUT6589	4S	43.0	4L	5.4
Parengydontium album MUT6579	5S	197.4	5L	4.1
Cladosporium ramotenellum MUT6556	6S	159.4	6L	2.7
Sesquicillium microsporum MUT6592	7S	37.4	7L	4.2
Cladosporium halotolerans MUT6558	8S	132.1	8L	3.8
Aspergillus jensenii MUT6581	9S	176.8	9L	9.0
Sakaguchia dacryoidea MUT6569	10S	355.3	10L	7.0
Aureobasidium pullulans MUT6584	11S	15.4	11L	12.0
Vishniacozyma carnescens MUT6591	12S	374.6	12L	6.9
Kondoa aeria MUT6563	13S	119.3	13L	3.4
Cladosporium pseudocladosporioides MUT6586	14S	132.2	14L	2.8
Penicillium griseofulvum MUT6588	15S	293.8	15L	108.2
Average productivity		187.9		12.4

2.1. Mineralogenic and Osteogenic Activities

2.1.1. In Vitro Mineralogenic Assay

Initial approaches for screening osteoactive compounds involved in vitro, ex vivo, and in vivo systems that have been developed and recently optimized [26–28]. In this study, the mineralogenic activity of extracts was assessed in vitro by testing the effect of the highest non-toxic concentration on extracellular matrix (ECM) mineralization of the gilthead seabream vertebra-derived cell line VSa13 for 17 days. The non-toxic concentration was determined by initially testing all extracts at 100 μg/mL and subsequently reducing the concentration to 10 μg/mL for extracts 9S and 15S when signs of cytotoxicity were observed. This stepwise approach ensured that the assessment of mineralogenic activity was conducted under non-toxic conditions. A total of 12 extracts exhibited mineralogenic activity (Figure 1). Among those, extracts 9L, 7S, and 14S increased ECM mineralization (42.17%, 35.16%, and 18.00% over the control, respectively) over the control, suggesting the presence of pro-mineralogenic compounds in these extracts. The osteoactive potential of marine fungi has already been assessed using in vitro cell systems [29–33]. Of special interest for this work, Marchese et al. [29] recently reported the osteogenic potential of the fungal community associated with the marine sea cucumber *Holothuria poli* in human mesenchymal stem cells. Among the 48 fungi tested in their study, *Penicillium chrysogenum* MUT1115 and *Penicillium citrinum* MUT1071 extracts promoted osteogenic differentiation, as demonstrated by increased alkaline phosphatase activity and ECM mineralization. Several compounds isolated from the marine fungi *Aspergillus jensenii*, *Sesquicillium microsporum*, and *Cladosporium pseudocladosporioides* were also tested in the same in vitro system [24–27], but none of them exhibited mineralogenic and/or osteogenic

activity [34–37]. The present study instead identified 9L, 7S, and 14S as among the most active extracts, highlighting once again the crucial role of each single strain and the difficulties of generalizing the research findings on the whole species.

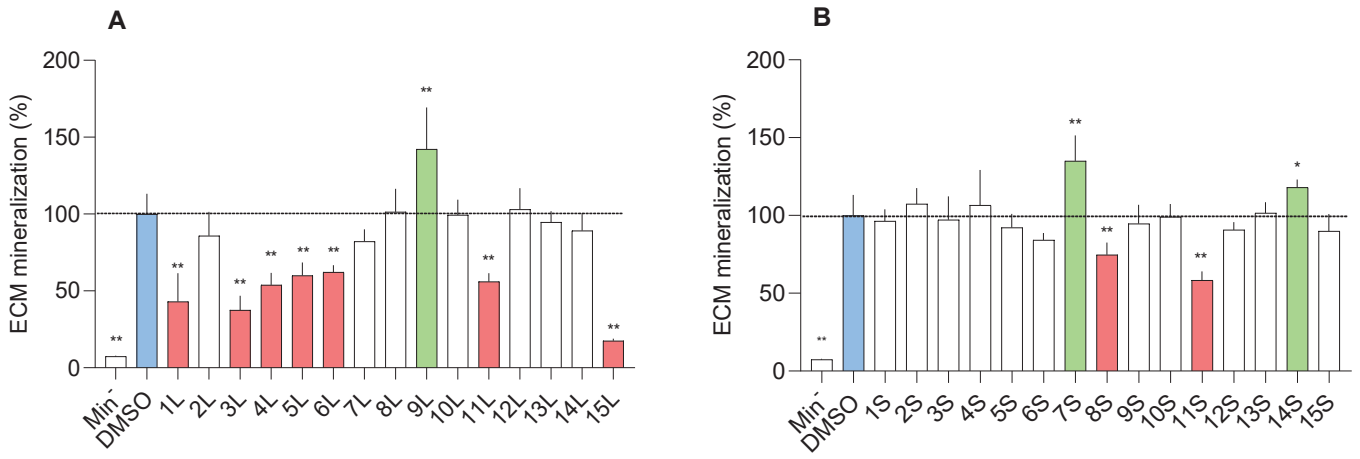

Figure 1. Mineralogenic effect of submerged fermentation (**A**) and solid-state fermentation (**B**) extracts assessed in VSa13 cells. All extracts were tested at 100 μg/mL, with the only exceptions of 9S and 15S that were tested at 10 μg/mL. Values are presented as mean ± standard deviation and as a percentage over the control group (DMSO, in blue). Normality was tested through Anderson–Darling test ($p < 0.05$). Asterisks indicate values significantly different (one-way ANOVA followed by Kruskal–Wallis test; * $p < 0.001$ and ** $p < 0.0001$). Each experimental group was tested against the control group (DMSO). Anti-mineralogenic extracts are represented in red, while pro-mineralogenic extracts are represented in green. Min^{-} indicates the control group not exposed to the mineralogenic cocktail n = 7.

For some fungi, this study represents an outbreak in the field, being the first time that *Cystobasidium slooffiae, Aspergillus domesticus*, and *Parengydontium album* (extract 1-3-5) were identified as producers of compounds with osteogenic activity. However, it should be noted that these species have been poorly investigated in literature for their metabolic properties, in contrast to more studied genera, such as *Cladosporium* and *Penicillium.* No previous reports could be found also for *Cladosporium ramotenellum*, *Cladosporium halotolerans*, *C. pseudocladosporioides* (extract 6-8-14), *Bjerkandera adusta* (extract 4), and *P. griseofulvum* (extract 15). It is remarkable that despite the general interest in these taxa, osteogenic activity has never been reported before. *Cladosporium* species have been subjected to several metabolomic studies, and 244 (up to 286) compounds have been extracted [38,39], displaying mostly antimicrobial and cytotoxic activity [38]. Osteogenic bioactive molecules have not been identified yet.

As for *B. adusta*, despite its widely known capacity to degrade pollutants, has very little information available about its production of bioactive compounds. The synergistic interactions between natural phenolics and flavonoids in the *B. adusta* extract was directly correlated to a strong antimicrobial activity against pathogenic bacteria and yeast [40]. To the best of our knowledge, no other reports are currently available about other bioactive functions. A more complex scenario can be depicted for *Penicillium* spp. During 2021–2023 alone, more than 450 natural products from marine-derived *Penicillium* strains have been discovered [4], many of them showing cytotoxic, antiproliferative, and antimicrobial activity [41]. However, the involvement of *Penicillium*-derived molecules in osteoclastogenesis and osteogenesis is rare and was currently reported only for a few species, e.g., *Penicillium antarcticum* and *P. citrinum* [42,43], that do not include those investigated in the present study.

In this study, 9 extracts significantly reduced ECM mineralization when compared to the control. Notably, 7 of those were produced from SmF, a fermentation condition that may have triggered the production of compounds with anti-mineralogenic activity. These extracts should be further characterized to gain insights into the mechanisms and molecules responsible for this effect.

Interestingly, *A. pullulans* metabolome was insensitive to the growth conditions, since both SSF and SmF extracts (extract 11) exhibited anti-mineralogenic effects. This finding did not come as a surprise, as *A. pullulans* is known for its active metabolites, with many of them being used to set novel osteoporosis therapies. For instance, calcium polymalate (PMA-Ca) and beta-glucan polycan can enhance osteoblast proliferation, ECM mineralization, and osteogenic gene expression in vitro. In vivo, PMA-Ca can also promote bone growth and calcium conversion, while polycan improves bone density and reduces osteoporosis in mice [44–46]. However, Ca-PMA production in *A. pullulans* varies among strains and remains taxonomically unclear [47–49]. Some strains exhibit high Ca-PMA synthesis, while others lack characterization in this regard [50,51]. It can be hypothesized that the strain in this study may belong to a low or non-producing variety, explaining its anti-mineralogenic activity. Future genomic and metabolomic analyses should confirm this, helping to identify metabolites responsible for the anti-osteogenic effect.

2.1.2. In Vivo Osteogenic Assay

To assess the osteoactive effects of fungal extracts on a whole organism, 3-day post-fertilization (dpf) zebrafish larvae were exposed for 3 days to each extract, starting at 100 µg/mL (n = 7). In general, SSF extracts were found to be more toxic than SmF extracts (Figure S1). Consequently, only 4 SSF extracts were tested at 100 µg/mL, and the remaining 11 SSF extracts were tested at 10 µg/mL, while 9 SmF extracts were tested at 100 µg/mL, and the other 5 SmF extracts were tested at 10 µg/mL. Extract 9L exhibited the highest level of cytotoxicity and was tested at 1 µg/mL. As shown in Figure S1, extracts 8S, and 9L significantly increased the mineralized area of the opercular bone and were further tested at different concentrations and using a higher number of larvae (n = 15). Extract 8S and 9L increased the area of the operculum by 28.27% (at 10 µg/mL) and 27.62% (at 1 µg/mL), respectively (Figure 2).

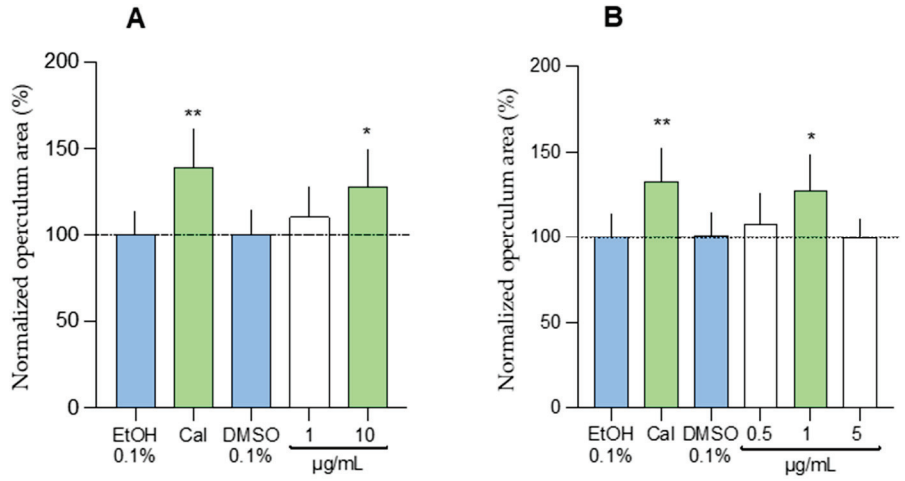

Figure 2. Osteogenic effect of extracts 8S (**A**) and 9L (**B**) assessed in the developing operculum of 6-dpf zebrafish larvae larvae through alizarin red S staining. DMSO and ethanol (EtOH) were used as negative controls for extracts and calcitriol (Cal), respectively. Changes in operculum area are expressed as percentages over the negative controls. Asterisks indicate values statistically different (one-way ANOVA followed by Dunnett's multiple comparison test for extracts and DMSO, Student's *t*-test for calcitriol and EtOH; * $p < 0.001$ and ** $p < 0.0001$) n = 15.

A comparative analysis of in vitro and in vivo datasets identified extract 9L as both mineralogenic and osteogenic, highlighting the osteoactive potential of SmF extract from *A. jensenii*, which has never been reported in the literature before. Shin et al. isolated several secondary metabolites from *Aspergillus flocculosus* associated with the marine sponge *Stylissa* sp. [33]. Two of these metabolites, spertetranone D and wasabidienone E, weakly inhibited osteoclast differentiation, while a third metabolite, mactanamide, showed potent inhibition of osteoclast differentiation without any indications of cytotoxicity at effective concentrations. This compound was also isolated from a not-yet-described marine fungus of the genus *Aspergillus* associated with the brown seaweed *Sargassum* sp. [52] and could represent a taxon-specific metabolite. Future work should assess its presence in extract 9L and gain more insights into a possible role in osteoblast differentiation.

Extracts of 8S prepared from *C. halotolerans* exhibited a peculiar osteoactive effect characterized by an anti-mineralogenic activity in vitro and a pro-osteogenic activity in vivo. These opposite effects are per se intriguing, as one would expect a similar mineralogenic effect in vitro and in vivo. However, the extract could have different targets at cellular and organismal levels and affect ECM and bone mineralization in a direct or indirect manner. It is also possible that both activities originate from different molecules. Future studies should aim at evaluating all these hypotheses. Mohamed et al. have recently reviewed the secondary metabolites and the biotechnological potential of marine-derived *Cladosporium* species [38]. Among the nearly 300 compounds identified, none have been reported to have mineralogenic or osteogenic potential. However, the polyketide 7,4′-dihydroxy isoflavone (daidzein) isolated from the Antarctic fungus *Cladosporium* sp. NJF-6 was shown to decrease the expression of inflammatory markers like NF-kB, TGF β, TNF-α, IL-6, IL-8, and COX-2 using different systems both in vitro and in vivo [53], a result that may indicate a therapeutic potential to treat different diseases including osteoporosis [34,54]. The mineralogenic and osteogenic activities observed in fungal extracts, particularly those from *A. jensenii* MUT6581 and *C. halotolerans* MUT6558, suggest their potential involvement in key pathways regulating bone formation and extracellular matrix mineralization. Although the precise molecular mechanisms remain to be fully elucidated, we hypothesize that these extracts may influence osteoblast differentiation and activity through the WNT/β-catenin signaling pathway, which is essential for bone formation, or by modulating the RANK/RANKL/OPG axis, which governs osteoclast-mediated bone resorption [55–57]. The presence of bioactive secondary metabolites, such as polyketides or terpenoids, could underlie these effects, potentially acting as signaling modulators or enzyme inhibitors [58,59].

2.2. Antiviral Potential

The antiviral activity of the fungal extracts was assessed against RSV and HSV-2, important causes of diseases that can seriously impact human health [60–65]. These viruses were selected as prototypes for RNA and DNA viruses, respectively. In the first set of experiments, viral infectivity was assayed against cells exposed to increasing amounts of extracts to generate dose-response curves. Among the 30 extracts tested, 16 (53%) showed dose-dependent activity against RSV, with EC_{50} (half maximal effective concentration, or concentration of a compound that reduces viral infectivity by 50%) values ranging from 1.1 to 407.7 μg/mL (Table S1). Among those, extracts 4S, 4L, 9L, 15S, and 15L exhibited the best EC_{50} values (1.18–43.5 μg/mL). Similarly, 11 extracts (36.6%) significantly inhibited HSV-2 infectivity in a dose-dependent manner, exhibiting EC_{50} values ranging from 9.5 to 560.1 μg/mL, and only extracts 7S, 9S, and 9L resulted in EC_{50} values lower than 100 μg/mL (9.5–38.7 μg/mL). Extracts 4 and 9 of both SSF and SmF showed antiviral activities, suggesting a strain-specific production of antiviral molecule(s).

To assess the possibility that the observed antiviral activity may be due to the cytotoxicity of the extracts, cell viability was determined using the MTS assay. Several extracts demonstrated a high cytocompatibility, exhibiting CC_{50} (half-maximal cytotoxic concentration) values higher than 2000 μg/mL, while others exhibited some degree of toxicity at lower concentrations (Table S1). In particular, extracts 15L and 9S showed the lowest CC_{50} values on Hep-2 and Vero cells, respectively. It should be noted that cytotoxicity was not observed at the antiviral effective doses for all active extracts, indicating that the inhibitory activity was not due to cytotoxic effects.

While this study is the first report of antiviral activity for most of the fungi tested (12 out of 15), the presence of antiviral compounds in extracts prepared from *Cladosporium cladosporioides* (extract 2) and *P. griseofulvum* (extract 15) has already been documented [66,67]. Tang et al. showed that 4 compounds produced in the biotransformation of patchouli alcohol by *C. cladosporioides* exerted potent anti-influenza virus activity, with EC_{50} values in the range of 2.1–20.9 μM [68]. An inhibitor of the viral protease of the hepatitis C virus was also isolated from *P. griseofulvum*, showing an EC_{50} (concentration of a compound that inhibits viral infectivity by 50%) value of 3.8 μg/mL [68]. According to these previous observations, our work showed that extracts from both *C. cladosporioides* (extract 2) and *P. griseofulvum* (extract 15) exert inhibitory activity against another virus, i.e., RSV. This is the first time that an antiviral activity against RSV has been demonstrated for these two fungal strains. However, Yu et al. previously highlighted that the strain *Cladosporium* sp. WZ-2008-0042, associated with the gorgonian *Dichotella gemmacea*, produced a new pregnane (3α-hydroxy-7-ene-6,20-dione), which exhibited potent antiviral activity against RSV with an EC_{50} value of 0.12 mM [68]. Moreover, oxalierpenes A and B, produced by the mantis-shrimp-derived *Penicillium oxalicum*, showed antiviral activity against the H1N1 virus and RSV, with EC_{50} values ranging from 2.8 to 9.4 μM [69].

Extracts 4S, 4L, and 9L were selected, based on their high selectivity indices (SIs), to further characterize in vitro for their antiviral activity (Figures 3 and 4). To gain insights into the mechanisms underlying the antiviral activity of these fungal extracts, time-of-addition assays were performed treating cells with the extract before, during, or after virus infection.

Results reported in Figure 3 show that extracts 4S and 4L inhibited RSV infectivity when added during the infection, with EC_{50} values similar to those obtained in the first antiviral assay (49.0–76.9 μg/mL). RSV replication was also partially inhibited by these two extracts when treatment was performed after the infection. Extract 9L was found to be active on both viruses and significantly inhibited RSV infectivity when added after infection (EC_{50} = 4.9 μg/mL) and, although to a lesser extent, before infection (EC_{50} = 17.9 μg/mL; Figure 3F). On the contrary, as reported in Figure 4, 9Ls ability to inhibit HSV-2 activity was observed independently of the time of exposure (i.e., it was effective when added before, during, and after infection), and EC_{50} values were in the same range as for the first antiviral assay (25.9–36.1 μg/mL; Figure 4B). The inhibitory activity herein observed at the different phases of virus replication may be ascribed to the well-known broad and diverse population of metabolites present in fungal extracts, which could account for the multiple targets of action of the extracts [70].

While this study reports for the first time antiviral activity in extracts prepared from *B. adusta* (extract 4) and *A. jensenii* (extract 9), other bioactivities have already been documented for fungi of the genera *Bjerkandera* and *Aspergillus*, e.g., antibacterial and antioxidant activity [40,71]. For instance, Georgousaki et al. also showed that benzoic acid derivatives isolated from *B. adusta* promoted the activity of two protein degradation systems, namely the ubiquitin-proteasome (UPP) and the autophagy-lysosome pathway [72]. Yi et al. recently reviewed the antiviral activity of compounds produced by marine microorganisms

and highlighted the dominant position of species belonging to the genus *Aspergillus* as providers of antiviral natural products [73]. In this regard, Chen et al. recently reported an anti-RSV activity for compounds isolated from the gorgonian-associated *Aspergillus* sp. XS-20090B15 [74]. Xu-Hua Nong et al. also reported an anti-HSV type 1 (HSV-1) activity from territrem and butyrolactone derivatives purified from the marine fungus *Aspergillus terreus* SCSGAF0162 [75]. Among them, 12a-dehydroxyisoterreulactone A, arisugacin A, isobutyrolactone II, and aspernolide A demonstrated significant inhibitory effects, with EC_{50} values of 16.4, 6.34, 21.8, and 28.9 mg/mL, respectively [75]. Moreover, *Aspergillus* sp. SCSIO 41501, associated with gorgonians, produced aspergillipeptides D and E, which successfully inhibited HSV-1 with EC_{50} values of 9.5 and 19.8 μM, respectively; of note, aspergillipeptide D also demonstrated activity against an acyclovir-resistant strain of HSV-1 [76].

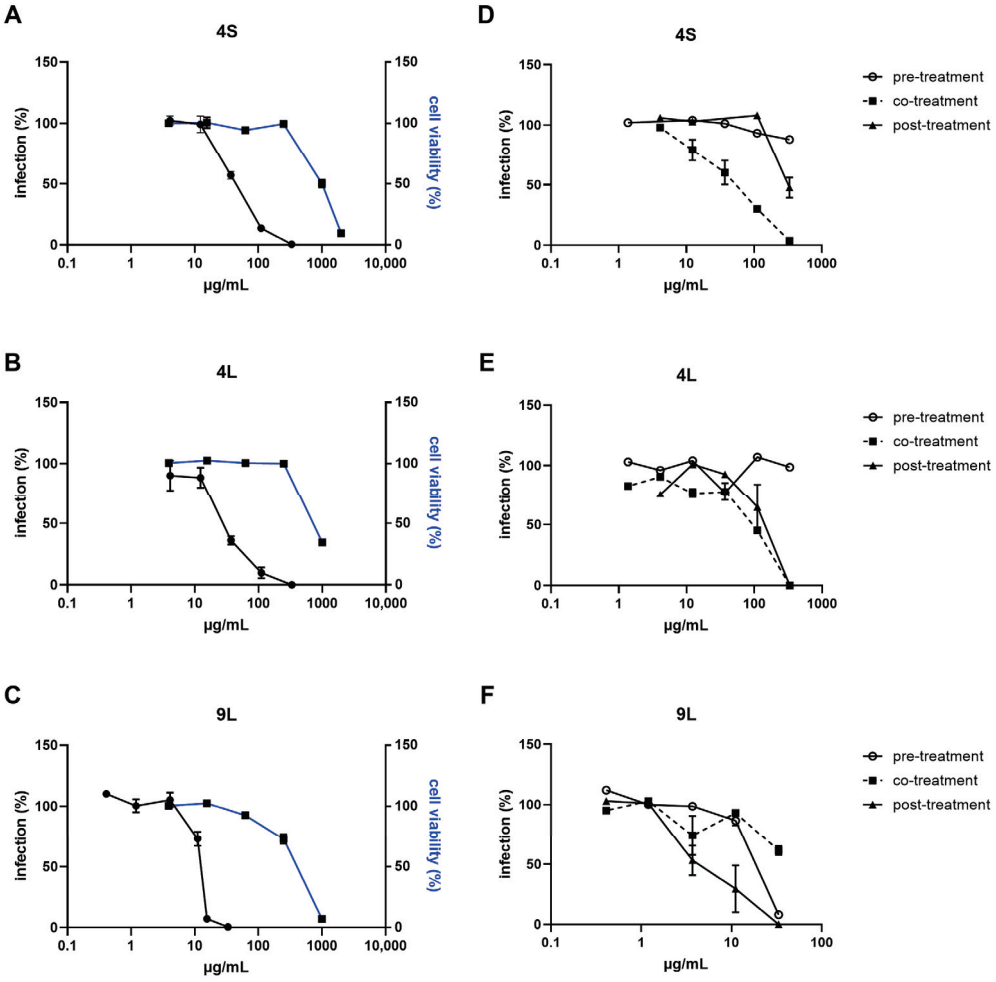

Figure 3. Antiviral activity of lead extracts 4S, 4L, and 9L against respiratory syncytial virus (RSV). (**A**–**C**) Antiviral activity was evaluated in cells infected with RSV and exposed to increasing concentrations of each extract. Virus infectivity (black) was assessed at 24 h post-infection, and cell viability (blue) was determined in the absence of viral inoculum. Both infection and viability were calculated by comparing extract-treated to DMSO-treated samples. (**D**–**F**) Time-of-addition assays were performed exposing cells to increasing concentrations of each extract for 2 h before infection (pre-treatment), for 2 h during infection (co-treatment), or for 24 h after removal of the virus inoculum (post-treatment). Virus infectivity was assessed at 24 h post-infection and was calculated by comparing extract-treated to DMSO-treated samples. Values are presented as mean ± standard error of the mean (SEM); n = 3.

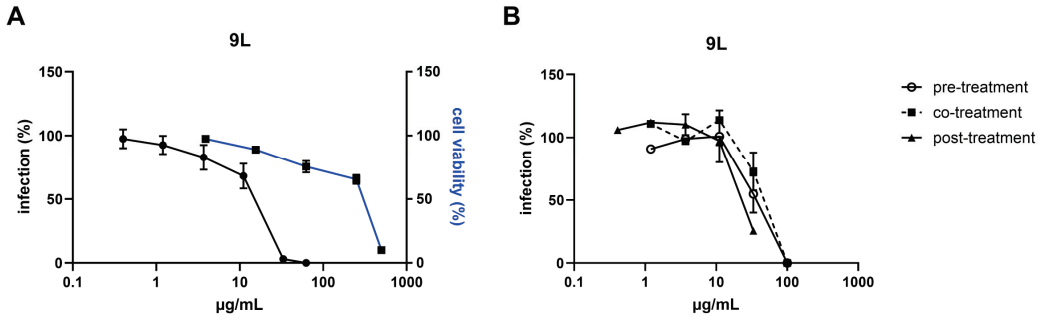

Figure 4. Antiviral activity of lead extract 9L against herpes simplex virus type 2 (HSV-2). (**A**) Antiviral activity was evaluated in cells infected with HSV-2 and exposed to increasing concentrations of the extract. Virus infectivity (black) was assessed at 24 h post-infection, and cell viability (blue) was determined in the absence of viral inoculum. Both infection and viability were calculated by comparing extract-treated and DMSO-treated samples. (**B**) Time-of-addition assays were performed in cells exposed to increasing concentrations of the extract for 2 h before infection (pre-treatment), for 2 h during infection (co-treatment), or for 24 h after removal of the virus inoculum (post-treatment). Virus infectivity was assessed at 24 h post-infection and calculated by comparing extract-treated and DMSO-treated samples. Values are presented as mean ± standard error of the mean (SEM); n = 3.

2.3. Extraction and Purification of Bioactives

Since it exhibited promising pro-osteogenic and antiviral activities, the crude extract 9L was further analyzed by HPLC-UV/ELSD (Figure 5). Two compounds, predominant in the extract, were purified by HPLC and identified as decumbenones A and B by HRMS, NMR, and specific rotation values with literature (Figures S4–S10) [77].

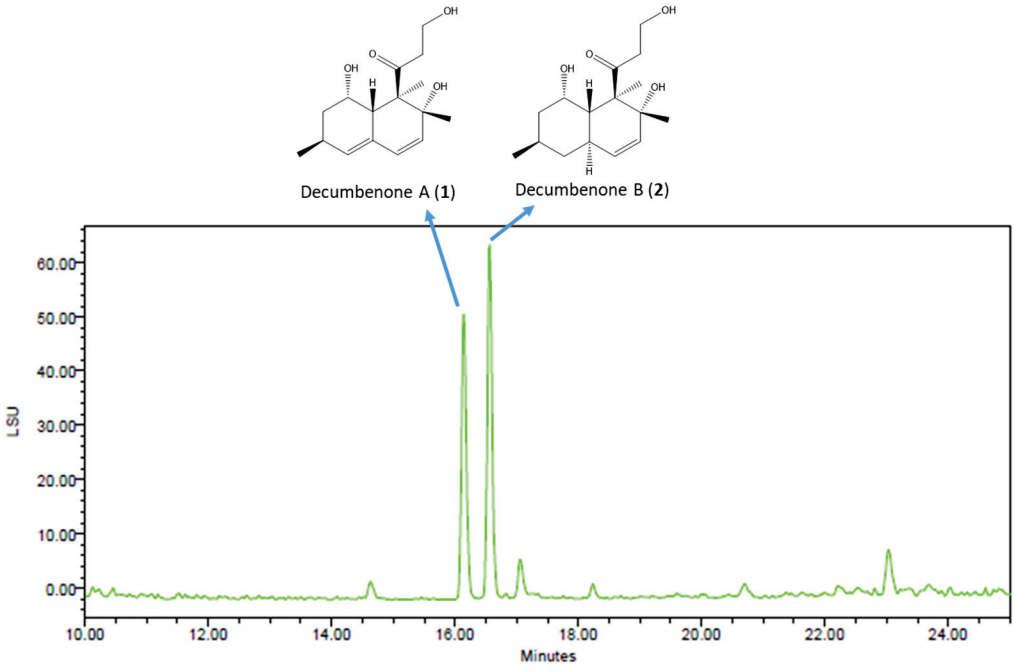

Figure 5. HPLC–ELSD chromatogram of *A. jensenii* extract 9L and the chemical structures of the two most abundant compounds: decumbenones A (**1**) and decumbenone B (**2**) (Column: NUCLEODUR Sphinx RP 250 × 4.6 mm; mobile phase: H_2O-acetonitrile 90:10 for 5 min, then 90:10 to 0:100 for 25 min, containing 0.1% formic acid; flow rate: 1 mL.min^{-1}; injection volume: 20 µL).

Decumbenones are polyketides initially isolated from the terrestrial fungus *Penicillium decumbens* [77]; as shown in Table 2, they are also found in marine and terrestrial fungal species and have been assessed for several bioactivities.

Table 2. Decumbenones A and B: producing organisms and biological activities.

Organism	Source	Bioactivity	Bioassay	Activity	Ref.
Decumbenone A					
Penicillium decumbens	Terrestrial	Melanin inhibition	-	Active	[77]
Aspergillus sulphureus	Marine	Cytotoxicity Antiproliferation Antitumoral	Cancer cell lines (SK-MEL-28, SK-MEL-5, HCT 116)	Cytotoxic against SK-MEL-5, SK-MEL-28 Inhibitor for all Antitumoral on SK-MEL-5 and HCT 116	[78–80]
		Stimulators of development of agricultural plants	-	Stimulating effect on root growth of spring wheat	
Aspergillus versicolor	Marine	Antimicrobial	ATCC bacterial and yeasts	None	[81]
		Antioxidant	DPPH and FRAP	None	
Aspergillus versicolor	Marine	Cytotoxicity	A549, SKOV-3, SK-MEL-2, XF498, HTC15 cell lines	None	[82]
		Antibacterial	meticillin-resistent clinical strains	None	
Aspergillus versicolor	Marine	Antitumoral	TDP1 inhibition assay	None	[83]
Aspergillus versicolor	Marine	-	-	-	[84]
Aspergillus carneus	Marine	Cytotoxicity	MTT assay	None	[85]
		Antiradical activities	DPPH assay	None	
		Influence on fertilized sea urchin ovum	-	None	
Craterellus odoratus	Terrestrial	Glucocorticoid metabolism regulation	Inhibition of 11β-HSD1	None	[86]
		Cytotoxicity	Cancer cell lines	None	
Synthesized molecule	-	Cytotoxicity	Cancer cell lines	None	[87]
Decumbenone B					
Penicillium decumbens	Terrestrial	Melanin inhibition	-	Inactive	[77]
Aspergillus sulphureus	Marine	Cytotoxicity, Antiproliferation Antitumoral	Cancer cell lines (SK-MEL-28, SK-MEL-5, HCT 116)	Cytotoxicity against SK-MEL-5, SK-MEL-28, Antiproliferative for all Antitumoral on SK-MEL-5 and HCT 116.	[78–80]
		Stimulators of development of agricultural plants	-	Stimulatory growth effect on roots of buckwheat	
Aspergillus versicolor	marine	Antimicrobial	ATCC bacterial and yeasts	None	[81]
		Antioxidant	DPPH and FRAP	None	
Aspergillus versicolor	marine	Cytotoxicity agains human solid tumor cell lines	A549, SKOV-3, SK-MEL-2, XF498, HTC15 cell lines	None	[82]
		Antibacterial	20 meticillin-resistent clinical strains	None	
Aspergillus versicolor	Marine	Antitumoral	TDP1 inhibition assay	None	[83]
Aspergillus versicolor	Marine	-	-	-	[84]
Aspergillus carneus	Marine	Cytotoxicity	MTT assay	None	[85]
		Antiradical	DPPH assay	None	
		Influence on fertilized sea urchin ovum	-	None	
Aspergillus flavus	Marine	Antimicrobial	ATCC bacterial and yeasts	None	[88]
Craterellus odoratus	Terrestrial	Glucocorticoid metabolism regulation	Inhibition of 11β-HSD1	None	[86]
		Cytotoxicity	Cancer cell lines	None	

Decumbenone A and B were described here for the first time as metabolites of the marine species of *A. jensenii*, even though they have already been found involved in many processes (Table 2). For instance, decumbenone A inhibited the melanization in *Magnaporthe grisea*, a rice blast pathogen [77], while decumbenones A and B selectively affected the human cancer esophageal cell line ECA109 with EC_{50} values of 12.41 and 15.60 μM, respectively [89]. In the present study, decumbenones A and B were hence evaluated for mineralogenic, osteogenic, and antiviral activities. However, neither of them replicated

the observed bioactivities (e.g., mineralogenic, osteogenic, and antiviral) observed for the crude extract (Figures S2 and S3). This finding suggests that other compounds present in trace amounts or potential synergistic interactions among different metabolites could be responsible for the biological effects. Future studies should focus on a more comprehensive metabolomic approach, employing advanced techniques such as high-resolution mass spectrometry and tandem mass spectrometry to detect and characterize minor bioactive compounds. Additionally, fractionation strategies combined with bioassay-guided screening could help identify active metabolites that may work in synergy. Multi-omics approaches, integrating metabolomics with transcriptomics and proteomics, could provide insights into the regulatory pathways involved in the observed bioactivities. These methods would not only clarify the identity of the active compounds but also reveal possible mechanisms of action, paving the way for the development of novel therapeutic agents from marine fungal extracts.

3. Materials and Methods

The experimental setup of this study is summarized in Table 3, which provides an overview of the assays performed and their corresponding conditions.

Table 3. Overview of the experimental design and conditions.

15 Strains Recovered from Marine Microplastics
Solid State Fermentation: 15 crude extracts
Submerged Fermentation: 15 crude extracts
Mineralogenic and Osteogenic Activities
In vitro mineralogic assay
Endpoint: extracellular matrix mineralization using gilthead seabream vertebra-derived cell line VSa13
Conditions: highest non-toxic concentration (100 μg/mL for most extracts; 10 μg/mL for extracts 9S and 15S)
In vivo osteogenic assay
Endpoint: mineralized operculum area using 6-day post-fertilization zebrafish larvae
Conditions: highest non-toxic concentration (1, 10, and 100 μg/mL depending on the extracts)
Antiviral Activities Against RSV And HSV-2
Endpoint #1: viral infectivity reduction assay, based on the number of infected cells exposed to increasing extract concentrations
Conditions: extracts from 0.1 to 1000 μg/mL covering all steps of infection
Endpoint #2: time-of-addition assay, exposing cells to extracts before, during, or after viral infection
Conditions: the most active extracts
Identification of Bioactive Molecules
Endpoint #1: HPLC-UV/ELSD analysis of the crude extract
Conditions: Extract of Aspergillus jensenii 9L with pro-osteogenic and antiviral activities
Endpoint #2: purification of predominant compounds in 9L extract by HPLC and evaluation of mineralogic, osteogenic, and antiviral activities

3.1. Fungal Strains

A total of 15 fungal strains were isolated from MPs sampled in three areas of the Tyrrhenian Sea in Tuscany (Italy) in November 2019, as previously described by Florio Furno et al. [10]. Fungi were preserved at the *Mycotheca Universitatis Taurinensis* (MUT) of the University of Turin.

3.2. Growth of the Fungal Strains and Preparation of the Crude Extracts

Fifteen fungal strains were cultivated using SSF and SmF, following a protocol adapted from Yue et al. [90]. Briefly, fungi were pre-grown in 9 cm Petri dishes containing Malt Extract Agar (MEA) medium for 7–14 days at 24 °C. For both SSF and SmF, the inoculation was performed according to a modified Biolog protocol [91]. Whenever possible, a conidia suspension was prepared into a suspension medium (FF inoculation fluid, Biolog, Hayward, CA, USA), and the density, measured using a turbidimeter (Biolog, Hayward,

CA, USA), was adjusted to the recommended value of 75%. The mycelium homogenate was prepared as follows: fungal biomass was collected from MEA plates with a sterile scalpel and homogenized using an UltraTurrax homogenizer (IKA, Staufen, Germany). The homogenate was transferred into the suspension medium using a sterile Pasteur pipette to achieve 40–60% transmittance.

For SmF, 3 mL of suspension was inoculated into 100 mL flasks containing 40 mL of Potato Dextrose Broth (PDB) for fermentation. After 2 weeks at 24 °C, the mycelium was separated from the broth by passing the fungal culture through a filter paper in a Buchner funnel under vacuum. In a separatory funnel, the broth was mixed twice with 100% ethyl acetate (EtOAc) at a proportion of 1:1 (v/v) to separate the aqueous phase and the organic phase and enhance the extraction yield. The organic phase was collected, and the solvent was removed using a rotary evaporator Re100-Pro (DLAB Scientific Inc., Beijing, China).

For SSF, 3 mL of suspension was inoculated into 100 mL flasks containing solid Rice Media (RM: 20 g of rice + 20 mL of mineral medium). The Mineral Medium (MM) was prepared as follows:10 mL/L of Mineral Solution (MS) and 1 mL/L of Trace Metal Solution (TMS). MS: 5 g of KCl, 5 g of $MgSO_4 | 7H_2O$, 0.1 g of $FeSO_4 | 7H_2O$ in 100 mL of deionized water; TMS: 1 g of $ZnSO_4 | 7H_2O$ and 0.5 g of $CuSO_4$. After 2 weeks of cultivation at 24 °C, the fungus was homogenized using a sterile spatula and macerated in 100% EtOAc (1:1 v/v). After an overnight maceration, the organic phase was collected. The previous step was repeated with shorter incubation times (180 min). All the organic phases were pooled, and the solvent was removed using a rotary evaporator Re100-pro. Extracts were resuspended in 100% dimethyl sulfoxide (DMSO) and stored at 4 °C until used.

3.3. Assessment of Mineralogenic Activity

Gilthead seabream (*Sparus aurata*) bone-derived cell line VSa13 (Cellosaurus ID number CVCL_S952) [92] was maintained in Dulbecco's modified Eagle medium (DMEM) supplemented with 10% fetal bovine serum (FBS), 1% penicillin–streptomycin, 1% L-glutamine, and 0.2% fungizone at 33 °C in a 10% CO_2-humidified atmosphere [92,93]. Pre-confluent cell cultures were sub-cultured 1:4 twice a week using a trypsin–EDTA solution (0.2% trypsin, 1.1 mM EDTA, pH 7.4). Mineralization assays were conducted in 48-well NUNC plates seeded with 1.25×10^4 cells per well and further incubated for 4 days until the culture reached confluency. The ECM mineralization was induced by supplementing culture medium with L-ascorbic acid (50 μg/mL), β-glycerophosphate (10 mM), and calcium chloride (4 mM). All extracts were initially tested at a concentration of 100 μg/mL. In case of cytotoxicity (e.g., cell death and altered morphology), extract concentration was lowered to 10 μg/mL and further evaluated. This stepwise approach allowed us to assess bioactivity while minimizing interference from toxic responses. Mineralizing cell cultures were exposed for 17 days to SmF or SSF extracts at the highest non-toxic concentration, or to 0.1% DMSO (vehicle) thereafter designed as the control group (CTRL). Cells cultured in non-supplemented medium (i.e., without mineralogenic cocktail and extracts) were also used as a negative control (Min^-). Mineral deposition was assessed through alizarin red S (AR-S) staining and quantified by spectrophotometry as previously described [92].

3.4. Assessment of Osteogenic Activity

Zebrafish (*Danio rerio*) larvae at 3 dpf were exposed for 3 days to the fungal extracts as described by Tarasco et al. [94]. Briefly, freshly hatched 3-dpf larvae were transferred into 12-well plates at a density of 7 larvae per well; each well was filled with 5 mL of filtrated system water (i.e., water collected from the fish housing system) and supplemented with the extracts at the non-toxic concentrations or with 0.1% DMSO (vehicle/negative control sample). A group of larvae exposed to 10 pg/mL calcitriol dissolved in ethanol was used as

positive control. Approximately 70% of the treatment was renewed daily. All the extracts were first tested at 100 µg/mL. Mortality and malformations were monitored for 3 days, and lower doses (10 or 1 µg/mL) were tested in case of severe toxic effects. After 3 days of exposure, larvae were given a lethal dose of anesthetic (MS-222 at 0.6 mM, pH 7.0, Merck KGaA, Darmstadt, Germania), washed in system water, and then stained with 0.01% of alizarin red S. Larvae were positioned laterally on a 2% agarose gel and then imaged using an MZ 7.5 fluorescence stereomicroscope (Leica, Wetzlar, Germany) equipped with a green light filter (λ_{ex} = 530–560 nm and λ_{em} = 580 nm) and a black-and-white F-View II camera (Olympus, Hamburg, Germany). The morphometric analysis of the operculum was performed using the fluorescence images and ZFBONE plugin for ImageJ [94]. The operculum area was corrected for interspecimen variability using the head area. After an initial screening, extracts exhibiting an osteogenic activity were retested using multiple concentrations and a higher number of larvae (n = 15), placed in a 6-well plate with 10 mL of system water per well.

3.5. Assessment of Antiviral Activity

Human epithelial cells (Hep-2; ATCC ID number CCL-23) and African green monkey fibroblastoid kidney cells (Vero; ATCC ID number CCL-81) were grown as monolayers in DMEM supplemented with 10% of FBS and 1% of antibiotic-antimycotic solution (Sigma-Aldrich, St. Louis, MO, USA). Cells were maintained at 37 °C in a 5% CO_2-atmosphere. The RSV strain A2 (ATCC ID number VR-1540) and the HSV-2 strain MS (ATCC ID number VR-540) were propagated in Hep-2 and Vero cells, respectively. After propagation, viral progenies were clarified out of cell debris, aliquoted, and stored at −80 °C prior to virus titration by standard plaque assay.

All antiviral assays were performed in DMEM supplemented with 2% of FBS. For the antiviral assays, sub-confluent Hep-2 or Vero cells were seeded at a density of 1×10^4 cells per well in 96-well plates and infected with a fixed inoculum of RSV or HSV-2 (multiplicities of infection—MOI of 0.01 or 0.005, respectively), while exposed to increasing amounts of extracts. After 24 h at 37 °C, cells were fixed in acetone:methanol (1:1), and infective events were visualized with an indirect immunocytochemistry procedure using specific primary antibodies directed against viral antigens, as described previously [95]. Infective events were microscopically counted, and viral infectivity was expressed as the mean % of infection ± standard error of the mean (SEM) of the extract-treated sample compared to the DMSO-treated sample (corresponding to 100% of infection).

Cell viability was measured using the MTS assay, as previously described [64]. Briefly, sub-confluent Hep-2 or Vero cells in 96-well plates were overlaid with serial dilutions of extracts and treated for the antiviral assay, without virus infection. The effect on cell viability of extracts was expressed as a mean % ± SEM, calculated by comparing the absorbances of treated cells with those of cells incubated with DMSO alone. Values of EC_{50}, EC_{90} (concentration of a compound that reduces viral infectivity by 90%), $CC_{50,}$ and relative 95% confidence intervals (CIs) were calculated. Where possible, selectivity indices of POMs were calculated as SI = CC_{50}/EC_{50}.

For time-of-addition assays that evaluate the virus replicative phase inhibited by a compound, sub-confluent Hep-2 or Vero cells were seeded at a density of 1×10^4 cells per well in 96-well plates and incubated with increasing concentrations of extracts at 37 °C for 2 h before infection (pre-treatment), for 2 h during infection (co-treatment), or for 24 h after removal of the virus inoculum (post-treatment). Cells were concurrently infected with RSV or HSV-2 and treated for the antiviral assay.

3.6. Isolation of Secondary Metabolites from A. Jensenii Extract 9L

The culture broth (250 mL) of *A. jensenii* extract 9L was extracted as previously described. The crude extract (32.0 mg) was purified by HPLC (column: NUCLEODUR Sphinx RP 250 × 4.6 mm) using acetonitrile/water (25:75, 1 mL/min) containing 0.1% formic acid, to yield **1** (3.3 mg, Rt = 10.5 min) and **2** (2.1 mg, Rt = 12.3 min).

Decumbenone A (**1**): Yellow gum. $[\alpha]_D^{20}$ + 35.0 (c 0.1, MeOH) (reported as $[\alpha]_D^{20}$ + 54.0 (*c* 0.5, EtOH) [80]. Molecular formula: $C_{16}H_{24}O_4$. ^{1}H NMR (400 MHz, CD_3OD) δ_H 5.93 (d, *J* = 9.9 Hz, H-11), 5.59 (s, H-9), 5.35 (d, *J* = 9.9 Hz, H-12), 4.22 (m, H-6), 3.83 (t, *J* = 6.2 Hz, H-1), 3.05 (dt, *J* = 18.0, 6.2 Hz, H-2a), 2.93 (q, *J* = 3.5 Hz, H-5), 2.85 (dt, *J* = 18.0, 6.4 Hz, H-2b), 2.52 (m, H-8), 1.86 (ddd, *J* = 9.9, 8.5, 4.2 Hz, H-7a), 1.46 (s, H-15), 1.24 (m, H-7b), 1.12 (s, H-14), 1.03 (d, *J* = 7.1 Hz, H-16). ^{13}C NMR (400 MHz, CD_3OD) δ_C 215.9 (C-3), 134.9 (C-12), 134.2 (C-9), 132.7 (C-10), 129.6 (C-11), 75.4 (C-13), 67.2 (C-6), 58.8 (C-1), 58.6 (C-4), 45.2 (C-2), 43.4 (C-5), 40.7 (C-7), 26.9 (C-14), 26.6 (C-8), 21.7 (C-16), 14.8 (C-15). HRESIMS *m/z* 303.1564 $[M + Na]^+$ (calcd for $C_{16}H_{24}O_4Na^+$ 303.1567), 263.1640 $[M - H_2O + H]^+$ (calcd for $C_{16}H_{23}O_3^+$ 263.1642).

Decumbenone B (**2**): Yellow gum. $[\alpha]_D^{20}$ + 10.0 (c 0.1, MeOH) (reported as $[\alpha]_D^{20}$ + 8.0 (*c* 0.5, EtOH) [80]. Molecular formula: $C_{16}H_{26}O_4$. ^{1}H NMR (400 MHz, CD_3OD) δ_H 5.39 (dd, *J* = 10.0, 1.8 Hz, H-11), 5.31 (dd, *J* = 10.0, 2.5 Hz, H-12), 4.09 (br s, H-6), 3.80 (td, *J* = 6.3, 2.8 Hz, H-1), 3.04 (dt, *J* = 18.3, 6.4 Hz, H-2a), 2.82 (dt, *J* = 18.3, 6.3 Hz, H-2b), 2.37 (m, H-10), 1.92 (dd, *J* = 10.7, 4.4 Hz, H-8), 1.82 (m, H-9a), 1.70 (m, H-7a), 1.52 (s, H-15), 1.15 (td, *J* = 13.5, 2.5 Hz, H-7b), 1.06 (s, H-14), 0.89 (d, *J* = 6.6 Hz, H-16), 0.73 (q, *J* = 12.2 Hz, H-9b). ^{13}C NMR (400 MHz, CD_3OD) δ_C 216.2 (C-3), 134.5 (C-12), 131.8 (C-11), 75.1 (C-13), 68.0 (C-6), 58.3 (C-1), 58.3 (C-4), 47.7 (C-5), 45.7 (C-2), 44.9 (C-7), 43.2 (C-9), 32.6 (C-10), 27.9 (C-14), 27.6 (C-8), 22.6 (C-16), 14.1 (C-15). HRESIMS *m/z* 305.1721 $[M + Na]^+$ (calcd for $C_{16}H_{26}O_4Na^+$ 305.1724), 265.1797 $[M - H_2O + H]^+$ (calcd for $C_{16}H_{25}O_3^+$ 265.1799).

3.7. Statistical Analyses

Prism version 10.0 (GraphPad Software, Inc., La Jolla, CA, USA) was used for statistical analysis. For all the experiments, normality was tested with a D'Agostino-Pearson omnibus normality test or with an Anderson-Darling test ($p < 0.05$). Homoscedasticity was tested through the Brown-Forsythe test ($p < 0.05$). When the distribution of the data of all the experimental groups resulted normal and homogeneous, statistical differences between the control and the extracts were tested with a one-way ANOVA followed by Dunnett's multiple comparison test ($p < 0.05$). If the distribution of the data of any of the experimental conditions resulted in non-normal or non-homogeneous statistical differences between the control and the extracts, they were tested with a non-parametric ANOVA test followed by Dunn's multiple comparison test ($p < 0.05$). Sample sizes can be found in figure legends.

4. Conclusions

The bioprospection of the marine plastisphere has resulted in the identification of fungi able to produce different bioactive molecules with interesting pharmacological activities (i.e., osteogenic and antiviral). This work primarily underlines the hidden potential of marine fungi, with many species demonstrating bioactivities for the first time, supporting the importance of exploring the mycobiota associated with unique ecological niches such as the plastisphere. Moreover, it was demonstrated that fermentation techniques may affect the ability to activate distinct metabolic pathways. Both process yield and diversity of bioactive compounds could vary, highlighting the importance of optimizing cultivation strategies.

The extract prepared from *A. jensenii* has demonstrated promising pro-osteogenic and antiviral activities. Two abundant molecules, decumbenones A and B, were purified from this extract. However, none of these molecules exhibited the bioactivity found in the extract tested, both for osteogenic/mineralogenic and antiviral assays. The precise identity

of the molecule or group of molecules responsible for the observed bioactivities remains unknown. As a result, it is imperative to conduct a comprehensive investigation into the compounds present in the extract, even those found in trace amounts, as these lesser-known constituents may play a significant role. Special consideration should be given to the possibility of synergistic effects, where the interaction between different molecules could amplify the bioactive properties. In the future, the systematic fractionation of the extract, followed by detailed validation of each bioactive fraction, will be critical for the successful identification and characterization of the specific molecules driving the reported biological effects.

Supplementary Materials: The following supporting information can be downloaded at: https://www.mdpi.com/article/10.3390/md23030115/s1, Figure S1: Osteogenic activity of Liquid (A) and Solid (B) extracts in zebrafish larvae; Figure S2: Antiviral activity of decumbenone A and B from extract *A. jensenii* 9L; Figure S3: Osteogenic activity of decumbenone A and B from extract *A. jensenii* 9L; Figure S4: HPLC-ELSD-UV/VIS chromatograms of the EtOAc extract of *A. jensenii*-9L; Figure S5: HRESIMS of 1; Figure S6: 1H NMR (400 MHz) spectrum of 1 in CD3OD; Figure S7: 13C NMR (100 MHz) spectrum of 1 in CD3OD; Figure S8: HRESIMS of 2; Figure S9: 1H NMR (400 MHz) spectrum of 2 in CD3OD; Figure S10: 13C NMR (100 MHz) spectrum of 2 in CD3OD; Table S1: Antiviral activity of extracts.

Author Contributions: Conceptualization, M.F.F., V.L., G.N.P., F.S., I.A., M.M., P.J.G., D.L. and G.C.V.; methodology M.F.F., V.L., G.N.P., F.S., I.A., M.M., P.J.G., D.L. and G.C.V.; software, M.F.F., V.L., I.A.; G.N.P.; validation, V.L., P.J.G., M.M., D.L. and G.C.V.; formal analysis, M.F.F., G.N.P. and I.A.; investigation, M.F.F., V.L., G.N.P. and I.A.; resources, V.L., P.J.G., D.L., M.M. and G.C.V.; data curation, M.F.F., I.A. and G.N.P.; writing—original draft preparation, M.F.F., I.A. and G.N.P.; writing—review and editing, V.L., M.M., D.L. and G.C.V.; visualization, M.F.F.; supervision, G.C.V.; project administration, G.C.V.; funding acquisition, V.L. and G.C.V. All authors have read and agreed to the published version of the manuscript.

Funding: This research was funded by EU funding to D.L. within the MUR PNRR Extended Partnership Initiative on Emerging Infectious Diseases (Project no. PE00000007, INF-ACT). V.L. and P:J.G: were financed by the Portuguese Foundation for Science and Technology (FCT) through the projects UIDB/04326/2020 (DOI:10.54499/UIDB/04326/2020), UIDP/04326/2020 (DOI:10.54499/UIDP/04326/2020) and LA/P/0101/2020 (DOI:10.54499/LA/P/0101/2020) and by the operational programmes CRESC Algarve 2020 and COMPETE 2020 through project EMBRC.PT ALG-01-0145-FEDER-022121. This work was granted by the European Commission—NextGenerationEU, Project SUS-MIRRI.IT "Strengthening the MIRRI Italian Research Infrastructure for Sustainable Bioscience and Bioeconomy", code n. IR0000005.

Institutional Review Board Statement: Procedures involving animals were performed following the EU and Portuguese legislation for animal experimentation and welfare (Directives 86/609/CEE and 2010/63/EU; Portaria 1005/92, 466/95 and 1131/97; Decreto-Lei 113/2013). Animal handling and experimentation were performed by qualified operators accredited by the Portuguese Direção-Geral de Alimentação e Veterinária (DGAV) under the authorization no. 012769/2021. All efforts were made to minimize pain, distress, and discomfort. Experiments were terminated (fish were returned to normal conditions or euthanized) whenever adverse effects were observed.

Data Availability Statement: Datasets generated during and/or analyzed during the current study are available from the corresponding author on reasonable request.

Acknowledgments: A special thanks to the MIRRI-IT Research Infrastructure for the technical and scientific support. The authors would like to thank Jolanda Perugini and Angelica Laera for their useful suggestions and scientific support in fungal preservation at MUT.

Conflicts of Interest: The authors declare no conflicts of interest.

Abbreviations

The following abbreviations are used in this manuscript:

MP	Microplastic
RSV	Respiratory Syncytial Virus
HSV-1	Herpes Simplex Virus Type 1
HSV-2	Herpes Simplex Virus Type 2
SSF	Solid State Fermentation
SmF	Submerged Fermentation
ECM	Extracellular Matrix
PMA-Ca	Calcium Polymalate
EtOH	Ethanol
SI	Selectivity Indices
MEA	Malt Extract Agar
PDB	Potato Dextrose Broth
MM	Mineral Medium
TMS	Trace Metal Solution
MS	Mineral Solution
EtOAc	Ethyl Acetate
RM	Rice Media
DMSO	Dimethylsulfoxide
AR-S	Alizarin Red S
EC_{50}	Concentration of a compound that reduces viral infectivity by 50%
EC_{90}	Concentration of a compound that reduces viral infectivity by 90%
CC_{50}	Half maximal cytotoxic concentration
IC_{50}	Concentration of a compound that inhibit viral infectivity by 50%
CI	Confidence Interval
dpf	Days Post-Fertilization
FBS	Fetal Bovine Serum
DMEM	Dulbecco's Modified Eagle medium

References

1. Ameen, F.; AlNadhari, S.; Al-Homaidan, A.A. Marine Microorganisms as an Untapped Source of Bioactive Compounds. *Saudi J. Biol. Sci.* **2021**, *28*, 224–231. [CrossRef] [PubMed]
2. Saravanakumar, K.; Rajendren, N.; Kathiresan, K.; Wang, M.H. Medicinal Drug-Related Bioactive Agents from Marine Fungi. *Encycl. Mar. Biotechnol.* **2020**, *4*, 2173–2190. [CrossRef]
3. Newton, G.G.F.; Abraham, E.P. Cephalosporin C, a New Antibiotic Containing Sulphur and D-α-Aminoadipic Acid [1]. *Nature* **1955**, *175*, 548. [CrossRef]
4. Lv, F.; Zeng, Y. Novel Bioactive Natural Products from Marine-Derived Penicillium Fungi: A Review (2021–2023). *Mar. Drugs* **2024**, *22*, 191. [CrossRef] [PubMed]
5. Wang, Z.; Qader, M.; Wang, Y.; Kong, F.; Wang, Q.; Wang, C. Progress in the Discovery of New Bioactive Substances from Deep-Sea Associated Fungi during 2020–2022. *Front. Mar. Sci.* **2023**, *10*, 1232891. [CrossRef]
6. Choudhary, A.; Naughton, L.M.; Montánchez, I.; Dobson, A.D.W.; Rai, D.K. Current Status and Future Prospects of Marine Natural Products (MNPs) as Antimicrobials. *Mar. Drugs* **2017**, *15*, 272. [CrossRef]
7. Negi, B.; Kumar, D.; Rawat, D.S. Marine Peptides as Anticancer Agents: A Remedy to Mankind by Nature. *Curr. Protein Pept. Sci.* **2016**, *18*, 885–904. [CrossRef]
8. Corzo, L.; Fernández-Novoa, L.; Carrera, I.; Martínez, O.; Rodríguez, S.; Alejo, R.; Cacabelos, R. Nutrition, Health, and Disease: Role of Selected Marine and Vegetal Nutraceuticals. *Nutrients* **2020**, *12*, 747. [CrossRef] [PubMed]
9. Browne, M.A.; Crump, P.; Niven, S.J.; Teuten, E.; Tonkin, A.; Galloway, T.; Thompson, R. Accumulation of Microplastic on Shorelines Woldwide: Sources and Sinks. *Environ. Sci. Technol.* **2011**, *45*, 9175–9179. [CrossRef]
10. Florio Furno, M.; Poli, A.; Ferrero, D.; Tardelli, F.; Manzini, C.; Oliva, M.; Pretti, C.; Campani, T.; Casini, S.; Fossi, M.C.; et al. The Culturable Mycobiota of Sediments and Associated Microplastics: From a Harbor to a Marine Protected Area, a Comparative Study. *J. Fungi* **2022**, *8*, 927. [CrossRef]

11. Roager, L.; Sonnenschein, E.C. Bacterial Candidates for Colonization and Degradation of Marine Plastic Debris. *Environ. Sci. Technol.* **2019**, *53*, 11636–11643. [CrossRef] [PubMed]
12. Sharma, H.; Neelam, D.K. Understanding Challenges Associated with Plastic and Bacterial Approach toward Plastic Degradation. *J. Basic. Microbiol.* **2023**, *63*, 292–307. [CrossRef] [PubMed]
13. Urbanek, A.K.; Rymowicz, W.; Mirończuk, A.M. Degradation of Plastics and Plastic-Degrading Bacteria in Cold Marine Habitats. *Appl. Microbiol. Biotechnol.* **2018**, *102*, 7669–7678. [CrossRef]
14. Beloe, C.J.; Browne, M.A.; Johnston, E.L. Plastic Debris as a Vector for Bacterial Disease: An Interdisciplinary Systematic Review. *Environ. Sci. Technol.* **2022**, *56*, 2950–2958. [CrossRef] [PubMed]
15. Puglisi, M.P.; Sneed, J.M.; Ritson-Williams, R.; Young, R. Marine Chemical Ecology in Benthic Environments. *Nat. Prod. Rep.* **2019**, *36*, 410–429. [CrossRef]
16. Kamat, S.; Kumar, S.; Philip, S.; Kumari, M. Secondary Metabolites from Marine Fungi: Current Status and Application. In *Microbial Biomolecules: Emerging Approach in Agriculture, Pharmaceuticals and Environment Management*; Academic Press: Cambridge, MA, USA, 2022. [CrossRef]
17. Hay, M.E. Marine Chemical Ecology: Chemical Signals and Cues Structure Marine Populations, Communities, and Ecosystems. *Ann. Rev. Mar. Sci.* **2009**, *1*, 193–212. [CrossRef]
18. Sekurova, O.N.; Schneider, O.; Zotchev, S.B. Novel Bioactive Natural Products from Bacteria via Bioprospecting, Genome Mining and Metabolic Engineering. *Microb. Biotechnol.* **2019**, *12*, 574–575. [CrossRef]
19. Karthikeyan, A.; Joseph, A.; Nair, B.G. Promising Bioactive Compounds from the Marine Environment and Their Potential Effects on Various Diseases. *J. Genet. Eng. Biotechnol.* **2022**, *20*, 1–38. [CrossRef]
20. Brakhage, A.A.; Schroeckh, V. Fungal Secondary Metabolites—Strategies to Activate Silent Gene Clusters. *Fungal Genet. Biol.* **2011**, *48*, 15–22. [CrossRef]
21. Singh, A.; Bajar, S.; Devi, A.; Bishnoi, N.R. Evaluation of Cellulase Production from *Aspergillus Niger* and *Aspergillus Heteromorphus* under Submerged and Solid-state Fermentation. *Environ. Sustain.* **2021**, *4*, 437–442. [CrossRef]
22. Asther, M.; Haon, M.; Roussos, S.; Record, E.; Delattre, M.; Lesage-Meessen, L.; Labat, M.; Asther, M. Feruloyl Esterase from *Aspergillus Niger* a Comparison of the Production in Solid State and Submerged Fermentation. *Process Biochem.* **2002**, *38*, 685–691. [CrossRef]
23. Vintila, T.; Dragomirescu, M.; Jurcoane, S.; Vintila, D.; Caprita, R.; Maniu, M. Production of Cellulase by Submerged and Solid-State Cultures and Yeasts Selection for Conversion of Lignocellulose to Ethanol. *Rom. Biotechnol. Lett.* **2009**, *14*, 4275–4281.
24. Ravichandran, S. Solid State and Submerged Fermentation for the Production of Bioactive Substances: A Comparative Study. *Int. J. Sci. Nat.* **2012**, *3*, 480–486.
25. Hölker, U.; Höfer, M.; Lenz, J. Biotechnological Advantages of Laboratory-Scale Solid-State Fermentation with Fungi. *Appl. Microbiol. Biotechnol.* **2004**, *64*, 175–186. [CrossRef] [PubMed]
26. Rosa, J.T.; Tarasco, M.; Gavaia, P.J.; Cancela, M.L.; Laizé, V. Screening of Mineralogenic and Osteogenic Compounds in Zebrafish—Tools to Improve Assay Throughput and Data Accuracy. *Pharmaceuticals* **2022**, *15*, 983. [CrossRef] [PubMed]
27. Carson, M.A.; Nelson, J.; Cancela, M.L.; Laizé, V.; Gavaia, P.J.; Rae, M.; Heesch, S.; Verzin, E.; Maggs, C.; Gilmore, B.F.; et al. Red Algal Extracts from *Plocamium Lyngbyanum* and *Ceramium Secundatum* Stimulate Osteogenic Activities in Vitro and Bone Growth in Zebrafish Larvae. *Sci. Rep.* **2018**, *8*, 7725. [CrossRef]
28. Laizé, V.; Gavaia, P.J.; Tarasco, M.; Viegas, M.N.; Caria, J.; Luis, N.; Cancela, M.L. Osteotoxicity of 3-Methylcholanthrene in Fish. *Ecotoxicol. Environ. Saf.* **2018**, *161*, 721–728. [CrossRef]
29. Marchese, P.; Garzoli, L.; Gnavi, G.; O'Connell, E.; Bouraoui, A.; Mehiri, M.; Murphy, J.M.; Varese, G.C. Diversity and Bioactivity of Fungi Associated with the Marine Sea Cucumber Holothuria Poli: Disclosing the Strains Potential for Biomedical Applications. *J. Appl. Microbiol.* **2020**, *129*, 612–625. [CrossRef]
30. Chen, C.; Xiao, L.; Luo, X.; Cai, J.; Huang, L.; Tao, H.; Zhou, X.; Tan, Y.; Liu, Y. Identifying Marine-Derived Tanzawaic Acid Derivatives as Novel Inhibitors against Osteoclastogenesis and Osteoporosis via Downregulation of NF-KB and NFATc1 Activation. *J. Med. Chem.* **2024**, *67*, 2602–2618. [CrossRef]
31. Kim, K.J.; Lee, J.; Wang, W.; Lee, Y.; Oh, E.; Park, K.H.; Park, C.; Woo, G.E.; Son, Y.J.; Kang, H. Austalide k from the *Fungus Penicillium* Rudallense Prevents Lps-Induced Bone Loss in Mice by Inhibiting Osteoclast Differentiation and Promoting Osteoblast Differentiation. *Int. J. Mol. Sci.* **2021**, *22*, 5493. [CrossRef]
32. Cai, J.; Gao, L.; Wang, Y.; Zheng, Y.; Lin, X.; Zhou, P.; Chen, C.; Liu, K.; Tang, L.; Liu, Y.; et al. Discovery of a Novel Anti-Osteoporotic Agent from Marine Fungus-Derived Structurally Diverse Sirenins. *Eur. J. Med. Chem.* **2024**, *265*, 116068. [CrossRef] [PubMed]
33. Shin, H.J.; Choi, B.K.; Trinh, P.T.H.; Lee, H.S.; Kang, J.S.; Van, T.T.T.; Lee, H.S.; Lee, J.S.; Lee, Y.J.; Lee, J. Suppression of RANKL-Induced Osteoclastogenesis by the Metabolites from the Marine *Fungus Aspergillus* Flocculosus Isolated from a *Sponge Stylissa* Sp. *Mar. Drugs* **2018**, *16*, 14. [CrossRef] [PubMed]

34. Li, Y.; Wang, Y.; Wang, H.; Shi, T.; Wang, B. The Genus Cladosporium: A Prospective Producer of Natural Products. *Int. J. Mol. Sci.* **2024**, *25*, 1652. [CrossRef]
35. Yu, H.Y.; Chen, Y.S.; Wang, Y.; Zou, Z.B.; Xie, M.M.; Li, Y.; Li, L.S.; Meng, D.L.; Wu, L.Q.; Yang, X.W. Anti-Necroptosis and Anti-Ferroptosis Compounds from the Deep-Sea-Derived *Fungus Aspergillus* Sp. MCCC 3A00392. *Bioorg Chem.* **2024**, *144*, 107175. [CrossRef]
36. Zhu, G.; Kong, F.; Wang, Y.; Fu, P.; Zhu, W. Cladodionen, a Cytotoxic Hybrid Polyketide from the Marine-Derived *Cladosporium* Sp. OUCMDZ-1635. *Mar. Drugs* **2018**, *16*, 71. [CrossRef]
37. Hafez Ghoran, S.; Taktaz, F.; Sousa, E.; Fernandes, C.; Kijjoa, A. Peptides from Marine-Derived Fungi: Chemistry and Biological Activities†. *Mar. Drugs* **2023**, *21*, 510. [CrossRef]
38. Mohamed, G.A.; Ibrahim, S.R.M. Untapped Potential of Marine-Associated Cladosporium Species: An Overview on Secondary Metabolites, Biotechnological Relevance, and Biological Activities. *Mar. Drugs* **2021**, *19*, 645. [CrossRef] [PubMed]
39. Salvatore, M.M.; Andolfi, A.; Nicoletti, R. The Genus Cladosporium: A Rich Source of Diverse and Bioactive Natural Compounds. *Molecules* **2021**, *26*, 3959. [CrossRef] [PubMed]
40. Soliman, E.R.S.; El-Sayed, H. Molecular Identification and Antimicrobial Activities of Some Wild Egyptian Mushrooms: Bjerkandera Adusta as a Promising Source of Bioactive Antimicrobial Phenolic Compounds. *J. Genet. Eng. Biotechnol.* **2021**, *19*, 106. [CrossRef]
41. Nicoletti, R.; Trincone, A. Bioactive Compounds Produced by Strains of Penicillium and Talaromyces of Marine Origin. *Mar. Drugs* **2016**, *14*, 37. [CrossRef]
42. Marchese, P.; Mahajan, N.; O'Connell, E.; Fearnhead, H.; Tuohy, M.; Krawczyk, J.; Thomas, O.P.; Barry, F.; Murphy, M.J. A Novel High-Throughput Screening Platform Identifies Itaconate Derivatives from Marine Penicillium Antarcticum as Inhibitors of Mesenchymal Stem Cell Differentiation. *Mar. Drugs* **2020**, *18*, 192. [CrossRef] [PubMed]
43. Zhang, Y.; Zhang, J.; Du, Q.; Wu, X.M.; Chen, Y.; Tan, R.X. Citrisorbicillinol, an Undescribed Hybrid Sorbicillinoid with Osteogenic Activity from *Penicillium Citrinum* ZY-2. *Fitoterapia* **2024**, *173*, 105836. [CrossRef]
44. Li, F.; Xie, X.; Xu, X.; Zou, X. Water-Soluble Biopolymers Calcium Polymalate Derived from Fermentation Broth of Aureobasidium Pullulans Markedly Alleviates Osteoporosis and Fatigue. *Int. J. Biol. Macromol.* **2024**, *268*, 132013. [CrossRef] [PubMed]
45. Suzuki, T.; Kusano, K.; Kondo, N.; Nishikawa, K.; Kuge, T.; Ohno, N. Biological Activity of High-Purity β-1,3-1,6-Glucan Derived from the Black Yeast *Aureobasidium Pullulans*: A Literature Review. *Nutrients* **2021**, *13*, 242. [CrossRef]
46. Shin, H.D.; Yang, K.J.; Park, B.R.; Son, C.W.; Jang, H.J.; Ku, S.K. Antiosteoporotic Effect of Polycan, β-Glucan from Aureobasidium, in Ovariectomized Osteoporotic Mice. *Nutrition* **2007**, *23*, 853–860. [CrossRef] [PubMed]
47. Liu, S.; Steinbüchel, A. Investigation of Poly(β-L-Malic Acid) Production by Strains of *Aureobasidium Pullulans*. *Appl. Microbiol. Biotechnol.* **1996**, *46*, 273–278. [CrossRef]
48. Zhang, H.; Cai, J.; Dong, J.; Zhang, D.; Huang, L.; Xu, Z.; Cen, P. High-Level Production of Poly (β-L-Malic Acid) with a New Isolated *Aureobasidium Pullulans* Strain. *Appl. Microbiol. Biotechnol.* **2011**, *92*, 295–303. [CrossRef]
49. Zou, X.; Zhou, Y.; Yang, S.T. Production of Polymalic Acid and Malic Acid by *Aureobasidium Pullulans* Fermentation and Acid Hydrolysis. *Biotechnol. Bioeng.* **2013**, *110*, 2105–2113. [CrossRef]
50. Gostinčar, C.; Ohm, R.A.; Kogej, T.; Sonjak, S.; Turk, M.; Zajc, J.; Zalar, P.; Grube, M.; Sun, H.; Han, J.; et al. Genome Sequencing of Four *Aureobasidium Pullulans* Varieties: Biotechnological Potential, Stress Tolerance, and Description of New Species. *BMC Genom.* **2014**, *15*, 1–29. [CrossRef]
51. Li, Y.; Chi, Z.; Wang, G.Y.; Wang, Z.P.; Liu, G.L.; Lee, C.F.; Ma, Z.C.; Chi, Z.M. Taxonomy of *Aureobasidium* Spp. and Biosynthesis and Regulation of Their Extracellular Polymers. *Crit. Rev. Microbiol.* **2015**, *41*, 132013. [CrossRef]
52. Lorenz, P.; Jensen, P.R.; Fenical, W. Mactanamide, a New Fungistatic Diketopiperazine Produced by a Marine *Aspergillus* Sp. *Nat. Prod. Lett.* **1998**, *12*, 55–60. [CrossRef]
53. Laddha, A.P.; Kulkarni, Y.A. Pharmacokinetics, Pharmacodynamics, Toxicity, and Formulations of Daidzein: An Important Isoflavone. *Phytother. Res.* **2023**, *37*, 2578–2604. [CrossRef] [PubMed]
54. Junnan, C.; Xiaoqing, T.; Chengqi, F.; Jinchang, H.; Yanan, L.; Qinghua, H. Secondary Metabolites from the Antarctic Fungi *Cladosporium* Sp. NJF4 and NJF6. *Chin. J. Polar Res.* **2020**, *32*, 60. [CrossRef]
55. Carletti, A.; Gavaia, P.J.; Cancela, M.L.; Laizé, V. Metabolic Bone Disorders and the Promise of Marine Osteoactive Compounds. *Cell. Mol. Life Sci.* **2024**, *81*, 11. [CrossRef]
56. Marcadet, L.; Bouredji, Z.; Argaw, A.; Frenette, J. The Roles of RANK/RANKL/OPG in Cardiac, Skeletal, and Smooth Muscles in Health and Disease. *Front. Cell Dev. Biol.* **2022**, *10*, 903657. [CrossRef] [PubMed]
57. Yu, M.; Qin, K.; Fan, J.; Zhao, G.; Zhao, P.; Zeng, W.; Chen, C.; Wang, A.; Wang, Y.; Zhong, J.; et al. The Evolving Roles of Wnt Signaling in Stem Cell Proliferation and Differentiation, the Development of Human Diseases, and Therapeutic Opportunities. *Genes. Dis.* **2024**, *11*, 101026. [CrossRef] [PubMed]
58. González-Hernández, R.A.; Valdez-Cruz, N.A.; Macías-Rubalcava, M.L.; Trujillo-Roldán, M.A. Overview of Fungal Terpene Synthases and Their Regulation. *World J. Microbiol. Biotechnol.* **2023**, *39*, 1–21. [CrossRef]

59. Wang, Q.; Zhao, X.; Jiang, Y.; Jin, B.; Wang, L. Functions of Representative Terpenoids and Their Biosynthesis Mechanisms in Medicinal Plants. *Biomolecules* **2023**, *13*, 1725. [CrossRef]
60. Looker, K.J.; Magaret, A.S.; Turner, K.M.E.; Vickerman, P.; Gottlieb, S.L.; Newman, L.M. Global Estimates of Prevalent and Incident Herpes Simplex Virus Type 2 Infections in 2012. *PLoS ONE* **2015**, *10*, e114989. [CrossRef]
61. Gupta, R.; Warren, T.; Wald, A. Genital Herpes. *Lancet* **2007**, *370*, 2127–2137. [CrossRef]
62. Zou, G.; Cao, S.; Gao, Z.; Yie, J.; Wu, J.Z. Current State and Challenges in Respiratory Syncytial Virus Drug Discovery and Development. *Antiviral Res.* **2024**, *221*, 105791. [CrossRef] [PubMed]
63. Bechini, A.; Salvati, C.; Bonito, B.; Del Riccio, M.; Stancanelli, E.; Bruschi, M.; Ionita, G.; Iamarino, J.A.; Bentivegna, D.; Buscemi, P.; et al. Costs and Healthcare Utilisation Due to Respiratory Syncytial Virus Disease in Paediatric Patients in Italy: A Systematic Review. *Public. Health* **2024**, *227*, 103–111. [CrossRef] [PubMed]
64. Argenziano, M.; Arduino, I.; Rittà, M.; Molinar, C.; Feyles, E.; Lembo, D.; Cavalli, R.; Donalisio, M. Enhanced Anti-Herpetic Activity of Valacyclovir Loaded in Sulfobutyl-Ether-β-Cyclodextrin-Decorated Chitosan Nanodroplets. *Microorganisms* **2023**, *11*, 2460. [CrossRef] [PubMed]
65. Kim, T.; Choi, S.H. Epidemiology and Disease Burden of Respiratory Syncytial Virus Infection in Adults. *Infect. Chemother.* **2024**, *56*, 1. [CrossRef]
66. Yu, M.L.; Guan, F.F.; Cao, F.; Jia, Y.L.; Wang, C.Y. A New Antiviral Pregnane from a Gorgonian-Derived *Cladosporium* Sp. Fungus. *Nat. Prod. Res.* **2018**, *32*, 1260–1266. [CrossRef]
67. Zhang, Y.H.; Li, L.; Li, Y.Q.; Luo, J.H.; Li, W.; Li, L.F.; Zheng, C.J.; Cao, F. Oxalierpenes A and B, Unusual Indole-Diterpenoid Derivatives with Antiviral Activity from a Marine-Derived Strain of the Fungus *Penicillium Oxalicum*. *J. Nat. Prod.* **2022**, *85*, 1880–1885. [CrossRef]
68. Tang, J.; Su, L.; He, X.; Liu, D.; Zhao, C.; Zhang, S.; Li, Q.; Li, R.; Li, H. Biotransformation of Patchouli Alcohol by Cladosporium Cladosporioides and the Anti-Influenza Virus Activities of Biotransformation Products. *J. Agric. Food Chem.* **2024**, *72*, 7991–8005. [CrossRef] [PubMed]
69. Chu, M.; Mierzwa, R.; He, L.; King, A.; Patel, M.; Pichardo, J.; Hart, A.; Butkiewicz, N.; Puar, M.S. Isolation and Structure of Sch 351633: A Novel Hepatitis C Virus (HCV) NS3 Protease Inhibitor from the Fungus *Penicillium Griseofulvum*. *Bioorg. Med. Chem. Lett.* **1999**, *9*, 1949–1952. [CrossRef]
70. Ngamcharungchit, C.; Chaimusik, N.; Panbangred, W.; Euanorasetr, J.; Intra, B. Bioactive Metabolites from Terrestrial and Marine Actinomycetes. *Molecules* **2023**, *28*, 5915. [CrossRef]
71. Nowacka, N.; Nowak, R.; Drozd, M.; Olech, M.; Los, R.; Malm, A. Antibacterial, Antiradical Potential and Phenolic Compounds of Thirty-One Polish Mushrooms. *PLoS ONE* **2015**, *10*, e0140355. [CrossRef]
72. Georgousaki, K.; Tsafantakis, N.; Gumeni, S.; Lambrinidis, G.; González-Menéndez, V.; Tormo, J.R.; Genilloud, O.; Trougakos, I.P.; Fokialakis, N. Biological Evaluation and in Silico Study of Benzoic Acid Derivatives from Bjerkandera Adusta Targeting Proteostasis Network Modules. *Molecules* **2020**, *25*, 666. [CrossRef] [PubMed]
73. Yi, M.; Lin, S.; Zhang, B.; Jin, H.; Ding, L. Antiviral Potential of Natural Products from Marine Microbes. *Eur. J. Med. Chem.* **2020**, *207*, 112738. [CrossRef]
74. Chen, M.; Shao, C.L.; Meng, H.; She, Z.G.; Wang, C.Y. Anti-Respiratory Syncytial Virus Prenylated Dihydroquinolone Derivatives from the Gorgonian-Derived Fungus *Aspergillus* Sp. XS-20090B15. *J. Nat. Prod.* **2014**, *77*, 2720–2724. [CrossRef]
75. Nong, X.H.; Wang, Y.F.; Zhang, X.Y.; Zhou, M.P.; Xu, X.Y.; Qi, S.H. Territrem and Butyrolactone Derivatives from a Marine-Derived Fungus *Aspergillus Terreus*. *Mar. Drugs* **2014**, *12*, 6113–6124. [CrossRef]
76. Ma, X.; Nong, X.H.; Ren, Z.; Wang, J.; Liang, X.; Wang, L.; Qi, S.H. Antiviral Peptides from Marine Gorgonian-Derived Fungus *Aspergillus* Sp. SCSIO 41501. *Tetrahedron Lett.* **2017**, *58*, 1151–1155. [CrossRef]
77. Fujii, Y.; Asahara, M.; Ichinoe, M.; Nakajima, H. Fungal Melanin Inhibitor and Related Compounds from *Penicillium Decumbens*. *Phytochemistry* **2002**, *60*, 703–708. [CrossRef] [PubMed]
78. Anisimov, M.M.; Klykov, A.G. Metabolites of Terrestrial Plants and Marine Organisms as Potential Regulators of Growth of Agricultural Plants in the Russian Far East. *J. Agric. Sci.* **2014**, *6*, 1019–1022. [CrossRef]
79. Zhuravleva, O.I.; Afiyatullov, S.S.; Vishchuk, O.S.; Denisenko, V.A.; Slinkina, N.N.; Smetanina, O.F. Decumbenone C, a New Cytotoxic Decaline Derivative from the Marine Fungus *Aspergillus Sulphureus* KMM 4640. *Arch. Pharm. Res.* **2012**, *35*, 1757–1762. [CrossRef] [PubMed]
80. Anisimov, M.M.; Chaikina, E.L.; Afiyatullov, S.S.; Zhuravleva, O.I.; Klykov, A.G.; Kraskovskaja, N.A.; Aminin, D.L. Decumbenones A–C from Marine Fungus *Aspergillus Sulphureus* as Stimulators of the Initial Stages of Development of Agricultural Plants. *Agric. Sci.* **2012**, *3*, 1019–1022. [CrossRef]
81. Yang, L.J.; Peng, X.Y.; Zhang, Y.H.; Liu, Z.Q.; Li, X.; Gu, Y.C.; Shao, C.L.; Han, Z.; Wang, C.Y. Antimicrobial and Antioxidant Polyketides from a Deep-Sea-Derived Fungus *Aspergillus Versicolor* SH0105. *Mar. Drugs* **2020**, *18*, 636. [CrossRef]
82. He, Y.P.; Zhang, Z.K.; Li, Z.J.; Wu, P.P.; Hu, J.S.; Fan, H.; Zhang, C.X. Two New Types of Structures from Soft Coral-Associated Epiphytic Fungus *Aspergillus Versicolor* CGF9-1-2. *Fitoterapia* **2024**, *177*, 106136. [CrossRef] [PubMed]

83. Yoon, M.L.; Mansoor, T.A.; Hong, J.; Lee, C.O.; Kyung, S.B.; Jung, J.H. Polyketides from a Sponge-Derived Fungus, *Aspergillus Versicolor*. *Nat. Product. Sci.* **2007**, *13*, 90–96.
84. Fu, Y.; Wu, P.; Xue, J.; Wei, X.; Li, H. Versicorin, a New Lovastatin Analogue from the Fungus *Aspergillus Versicolor* SC0156. *Nat. Prod. Res.* **2015**, *29*, 1363–1368. [CrossRef]
85. Yurchenko, A.A.; Smetanina, O.F.; Kalinovsky, A.I.; Kirichuk, N.N.; Pivkin, M.V.; Ivanets, E.V.; Yurchenko, E.A.; Afiyatullov, S.S. New Metabolites from a Marine Sediment-Derived Fungus, *Aspergillus Carneus*. *Nat. Prod. Commun.* **2015**, *10*, 1247–1250. [CrossRef]
86. Guo, H.; Feng, T.; Li, Z.H.; Liu, J.K. Five New Polyketides from the Basidiomycete *Craterellus Odoratus*. *Nat. Prod. Bioprospect.* **2012**, *2*, 170–173. [CrossRef]
87. National Center for Biotechnology Information. Primary High Throughput Screening by Co-Culture Imaging for Identification Hits as a Selective Cytotoxic Compound to Cancer Cells in an EMT-Like State. PubChem Bioassay Record for AID 1345086, Source: University of Iowa High-Throughput Screening Core (UIHTS). Available online: https://pubchem.ncbi.nlm.nih.gov/bioassay/1345086 (accessed on 24 February 2025).
88. Zhuravleva, O.I.; Kirichuk, N.N.; Denisenko, V.A.; Dmitrenok, P.S.; Pivkin, M.V.; Afiyatullov, S.S. New Kipukasin from Marine Isolate of the Fungus *Aspergillus Flavus*. *Chem. Nat. Compd.* **2016**, *52*, 266–268. [CrossRef]
89. Niu, S.; Xia, M.; Chen, M.; Liu, X.; Li, Z.; Xie, Y.; Shao, Z.; Zhang, G. Cytotoxic Polyketides Isolated from the Deep-Sea-Derived Fungus *Penicillium Chrysogenum* MCCC 3A00292. *Mar. Drugs* **2019**, *17*, 686. [CrossRef]
90. Yue, Y.; Yu, H.; Li, R.; Hu, L.; Liu, S.; Xing, R.; Li, P. Isolation and Identification of Antimicrobial Metabolites from Sea Anemone-Derived Fungus *Emericella* Sp. SMA01. *J. Oceanol. Limnol.* **2021**, *39*, 1010–1019. [CrossRef]
91. Shea, A.; Wolcott, M.; Daefler, S.; Rozak, D.A. Biolog Phenotype Microarrays. *Methods Mol. Biol.* **2012**, *881*, 331–373. [CrossRef]
92. Pombinho, A.R.; Laizé, V.; Molha, D.M.; Marques, S.M.P.; Cancela, M.L. Development of Two Bone-Derived Cell Lines from the Marine Teleost Sparus Aurata; Evidence for Extracellular Matrix Mineralization and Cell-Type-Specific Expression of Matrix Gla Protein and Osteocalcin. *Cell Tissue Res.* **2004**, *315*, 393–406. [CrossRef]
93. Marques, C.L.; Rafael, M.S.; Cancela, M.L.; Laizé, V. Establishment of Primary Cell Cultures from Fish Calcified Tissues. *Cytotechnology* **2007**, *55*, 9–13. [CrossRef] [PubMed]
94. Tarasco, M.; Laizé, V.; Cardeira, J.; Cancela, M.L.; Gavaia, P.J. The Zebrafish Operculum: A Powerful System to Assess Osteogenic Bioactivities of Molecules with Pharmacological and Toxicological Relevance. *Comp. Biochem. Physiol. Part. C Toxicol. Pharmacol.* **2017**, *197*, 115480. [CrossRef] [PubMed]
95. Arduino, I.; Francese, R.; Civra, A.; Feyles, E.; Argenziano, M.; Volante, M.; Cavalli, R.; Mougharbel, A.M.; Kortz, U.; Donalisio, M.; et al. Polyoxometalate Exerts Broad-Spectrum Activity against Human Respiratory Viruses Hampering Viral Entry. *Antivir. Res.* **2024**, *226*, 105897. [CrossRef] [PubMed]

Disclaimer/Publisher's Note: The statements, opinions and data contained in all publications are solely those of the individual author(s) and contributor(s) and not of MDPI and/or the editor(s). MDPI and/or the editor(s) disclaim responsibility for any injury to people or property resulting from any ideas, methods, instructions or products referred to in the content.

marine drugs

MDPI

Article

An Investigation of Quorum Sensing Inhibitors against *Bacillus cereus* in The Endophytic Fungus *Pithomyces sacchari* of the *Laurencia* sp.

Shi-Liang Xiang, Kai-Zhong Xu, Lu-Jun Yin and Ai-Qun Jia *

Key Laboratory of Tropical Biological Resources of Ministry of Education, School of Pharmaceutical Sciences, Hainan University, Haikou 570228, China
* Correspondence: ajia@hainanu.edu.cn; Tel./Fax: +86-0898-66254967

Abstract: *Bacillus cereus*, a common food-borne pathogen, forms biofilms and generates virulence factors through a quorum sensing (QS) mechanism. In this study, six compounds (dankasterone A, demethylincisterol A_3, zinnimidine, cyclo-(L-Val-L-Pro), cyclo-(L-Ile-L-Pro), and cyclo-(L-Leu-L-Pro)) were isolated from the endophytic fungus *Pithomyces sacchari* of the *Laurencia* sp. in the South China Sea. Among them, demethylincisterol A_3, a sterol derivative, exhibited strong QS inhibitory activity against *B. cereus*. The QS inhibitory activity of demethylincisterol A_3 was evaluated through experiments. The minimum inhibitory concentration (MIC) of demethylincisterol A_3 against *B. cereus* was 6.25 μg/mL. At sub-MIC concentrations, it significantly decreased biofilm formation, hindered mobility, and diminished the production of protease and hemolysin activity. Moreover, RT-qPCR results demonstrated that demethylincisterol A_3 markedly inhibited the expression of QS-related genes (*plcR* and *papR*) in *B. cereus*. The exposure to demethylincisterol A3 resulted in the downregulation of genes (*comER*, *tasA*, *rpoN*, *sinR*, *codY*, *nheA*, *hblD*, and *cytK*) associated with biofilm formation, mobility, and virulence factors. Hence, demethylincisterol A_3 is a potentially effective compound in the pipeline of innovative antimicrobial therapies.

Keywords: *Laurencia* sp.; endophytic fungus; *Pithomyces sacchari*; demethylincisterol A_3; *Bacillus cereus*; quorum sensing

1. Introduction

Seaweeds, the largest group of oceanic plants, are capable of producing various metabolites, including polysaccharides, terpenes, and lectins [1]. Algal metabolites exhibit a range of beneficial effects, such as antibacterial, antiviral, antioxidant, and anticancer properties [1–4]. Endophytic fungi, residing within the plant body, coexist without harming the host and can synthesize compounds similar to those produced by the host plant [5]. For instance, the fungal endophyte *Taxomyces andreanae*, found within the inner bark of the *Taxus brevifolia* (Pacific yew tree), is capable of synthesizing paclitaxel derivatives [6]. Similarly, *Diaporthe longicolla*, an endophyte from the leaves of *Saraca asoca*, produces metabolites with noted antibacterial and antioxidant properties [7]. The ethyl acetate extract from *Nigrospora sphaerica*, another endophytic fungus, exhibits potent antioxidant activities, effectively combating free radicals [8]. Additionally, *Hyllosticta capitalensis*, an endophyte, is known for generating a variety of bioactive compounds that possess both antibacterial and antitumor potential [9]. Recent studies reveal that bioactive substances from endophytic fungi, known for their antioxidant, antibacterial, anti-inflammatory, and cancer cell inhibitory effects, have become a prominent focus for screening and research [10].

Foodborne diseases stemming from pathogens constitute a widespread global public health concern [11]. *Bacillus cereus* is a Gram-positive bacterium known for its ability to cause food poisoning [12]. Widely distributed in air, water, and soil, *B. cereus* may be present in various foods, including potatoes, rice, and beans [12]. *B. cereus* can produce

enterotoxins and emetic toxins, leading to symptoms such as diarrhea and vomiting in affected individuals [13]. At the same time, it can form biofilms, enhancing its efficiency in producing harmful metabolites [14]. With the assistance of biofilms, *B. cereus* can evade the decomposition of digestive enzymes [15]. The flagella of *B. cereus* aid in movement to suitable locations and the formation of *B. cereus* biofilm is intricately connected to this locomotion process [16]. It can modulate gene expression through quorum sensing (QS), exercising control over biofilm formation, virulence factors, and spore production [17].

Given that the production of harmful toxins, as well as functions like mobility and membrane activity in *B. cereus*, rely on QS, addressing its impact on human health underscores the importance of developing treatments to disrupt its QS. Therefore, this study aimed to identify compounds from marine algal endophytic fungi that can inhibit the QS function of *B. cereus*, thereby attenuating its pathogenicity.

2. Results

2.1. Identification of Active Strains

Mycelium grown on potato dextrose agar (PDA) exhibited a white coloration and adopted a coarse and cotton-like texture. With the progression of growth, the central color could progressively transform to yellow (Figure 1a). The cells of the conidia exhibited microscopic features such as yellow coloration, oval or slightly oval shape, and 3–5 diaphragms (Figure 1b). The spore wall was smooth. The conidia were septate, elongated, and pale brown in color (Figure 1c). The strain was determined as *Pithomyces* by comparing its gene sequences to those in the gene library (Figure S9). The most closely related strain of W2-F1 was *Pithomyces sacchari* (99.00%) (Figure 1d).

2.2. The Elucidation of Compounds

The isolated six compounds were identified using nuclear magnetic resonance (NMR) and mass spectrum (MS) techniques, and their structures were determined by comparing them with the literature data (Figure 2). The NMR and MS spectra of the six compounds are shown in the Supporting Information (Figures S3–S8).

Compound **1** (4.8 mg) was identified as follows. Dankasterone A ($C_{28}H_{40}O_3$, *m/z* = 425.3058 $[M + H]^+$, cald. for 425.3050) [18]. ^{1}H-NMR (400 MHz, MeOD) δ 6.16 (s, H-4, 1H), 5.35–5.31 (m, 2H), 2.87 (td, *J* = 8.9, 1.5 Hz, 1H), 2.69–2.60 (m, 2H), 2.60–2.53 (m, 2H), 2.51–2.46 (m, 1H), 2.41–2.39 (m, 1H), 2.38–2.34 (m, 1H), 2.09–1.99 (m, 3H), 1.95–1.84 (m, 3H), 1.78–1.68 (m, 3H), 1.56–1.38 (m, 2H), 1.29 (s, H-19, 3H), 1.13 (d, *J* = 7.1 Hz, H-21, 3H), 0.99 (s, H-18, 3H), 0.94 (d, *J* = 6.8 Hz, H-27, 3H), 0.86 (d, *J* = 6.7 Hz, H-26, 3H), 0.84 (d, *J* = 6.8 Hz, H-28, 3H). ^{13}C-NMR (101 MHz, MeOD) δ 217.53 (q, C-14), 202.21 (q, C-6), 201.68 (q, C-3), 159.33 (q, C-5), 136.00 (CH, C-23), 134.28 (CH, C-22), 126.55 (CH, C-4), 64.05[a] (q, C-8), 55.68[a] (q, C-13), 50.96 (CH, C-9), 49.50 (CH, C-17), 44.70 (CH, C-24), 41.42 (CH_2, C-7), 39.96 (CH_2, C-1), 38.99 (CH_2, C-12), 38.63 (CH_2, C-15), 38.49 (CH, C-20), 37.39 (q, C-10), 35.17 (CH_2, C-2), 34.37 (CH, C-25), 25.91 (CH_2, C-11), 24.74 (CH_3, C-19), 24.18 (CH_3, C-21), 24.09 (CH_2, C-16), 20.55 (CH_3, C-27), 20.14 (CH_3, C-26), 18.10 (CH_3, C-28), 17.35 (CH_3, C-18) ([a] assignments could be switched).

Compound **2** (8.7 mg) was identified as follows. Demethylincisterol A_3 ($C_{21}H_{32}O_3$, *m/z* = 331.2271 $[M - H]^-$, cald. for 331.2279) [19,20]. ^{1}H-NMR (400 MHz, $CDCl_3$) δ 5.61 (d, *J* = 4.2 Hz, H-2 1H), 5.25 (dd, *J* = 15.2, 7.5 Hz, H-16, 1H), 5.16 (dd, *J* = 15.3, 8.2 Hz, H-15, 1H), 2.68–2.61 (m, H-8, 1H), 2.33–2.26 (m, 1H), 2.06–2.00 (m, 1H), 1.99–1.94 (m, 1H), 1.90–1.80 (m, 3H), 1.71–1.65 (m, 1H), 1.65–1.60 (m, 1H), 1.52–1.42 (m, 4H), 1.03 (d, *J* = 6.2 Hz, H-14, 3H), 0.91 (d, *J* = 6.4 Hz, H-21, 3H), 0.83 (d, *J* = 6.7 Hz, H-19, 3H), 0.82 (d, *J* = 6.6 Hz, H-20, 3H), 0.60 (s, H-12, 3H). ^{13}C-NMR (101 MHz, $CDCl_3$) δ 171.56 (q, C-1), 170.98 (q, C-3), 134.80 (CH, C-15), 132.96 (CH, C-16), 112.29 (CH, C-2), 105.39 (q, C-4), 55.46 (CH, C-11), 50.51 (CH, C-8), 48.98 (q, C-7), 42.96 (CH, C-17), 40.25 (CH, C-13), 35.37 (CH_2, C-5), 35.19 (CH_2, C-6), 33.17 (CH, C-18), 28.99 (CH_2, C-10), 21.50 (CH_2, C-9), 21.13 (CH_3, C-14), 20.09 (CH_3, C-20), 19.78 (CH_3, C-19), 17.73 (CH_3, C-21), 11.88 (CH_3, C-12).

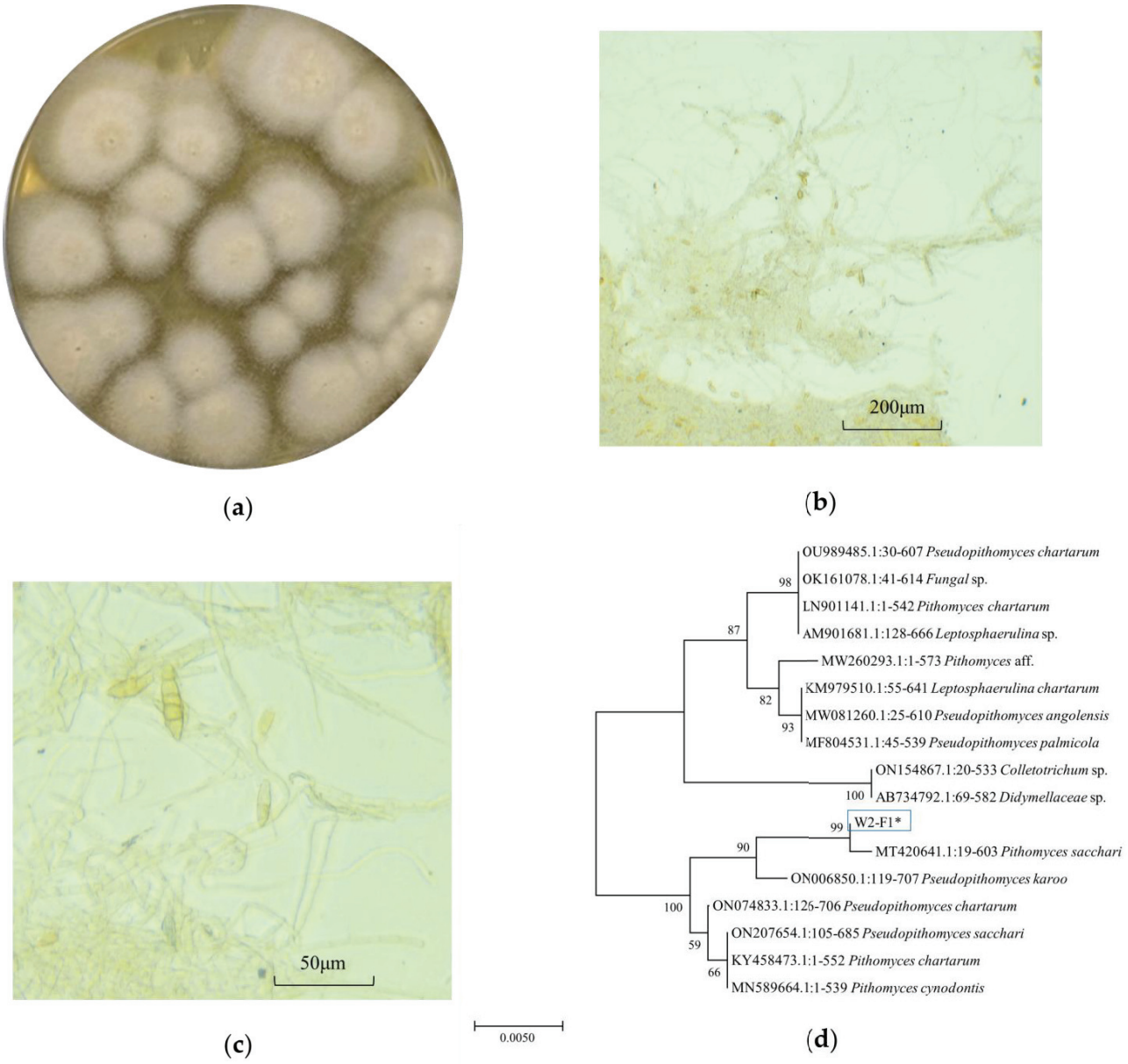

Figure 1. Morphological and phylogenetic tree of *P. sacchari* strain. (**a**) Colonies grown on a PDA. (**b**,**c**) The spores and mycelia were under a microscope with 40× and 100× magnification. (**d**) Phylogenetic tree.

Compound **3** (3.2 mg) was identified as follows. Zinnimidine ($C_{15}H_{19}NO_3$, *m/z* = 262.1435 $[M + H]^+$, cald. for 262.1438) [21]. ^{1}H-NMR (400 MHz, MeOD) δ 7.05 (s, H-6, 1H), 5.49 (t, *J* = 6.6 Hz, H-12, 1H), 4.60 (d, *J* = 6.1 Hz, H-11, 2H), 4.50 (s, H-8, 2H), 3.89 (s, H-9, 3H), 2.16 (s, H-10, 3H), 1.79 (s, H-14, 3H), 1.76 (s, H-15, 3H). ^{13}C-NMR (101 MHz, MeOD) δ 173.70 (q, C-7), 159.86 (q, C-3), 155.15 (q, C-5), 138.94 (q, C-13), 132.43 (q, C-1), 127.47 (q, C-2), 124.43 (q, C-4), 120.93 (CH, C-12), 101.74 (CH, C-6), 66.59 (CH_2, C-11), 60.11 (CH_3, C-9), 45.06 (CH_2, C-8), 25.87 (CH_3, C-14), 18.26 (CH_3, C-15), 9.68 (CH_3, C-10).

Compound **4** (10.8 mg) was identified as follows. Cyclo-(L-Val-L-Pro) ($C_{10}H_{16}N_2O_2$, *m/z* = 197.1296 $[M + H]^+$, cald. for 197.1285) [22–24]. ^{1}H-NMR (400 MHz, MeOD) δ 4.20 (t, *J* = 7.2 Hz, H-2, 1H), 4.03 (s, H-4, 1H), 3.63–3.45 (m, H-5, 2H), 2.56–2.42 (m, 1H), 2.39–2.20 (m, 1H), 2.07–1.82 (m, 3H), 1.09 (d, *J* = 7.3 Hz, H-9, 3H), 0.93 (d, *J* = 6.9 Hz, H-10, 3H). ^{13}C-NMR (101 MHz, MeOD) δ 172.60 (q, C-3), 167.57 (q, C-1), 61.51 (CH, C-4), 60.03 (CH,

C-2), 46.18 (CH_2, C-5), 29.87 (CH, C-8), 29.52 (CH_2, C-7), 23.25 (CH_2, C-6), 18.85 (CH_3, C-9), 16.65 (CH_3, C-10).

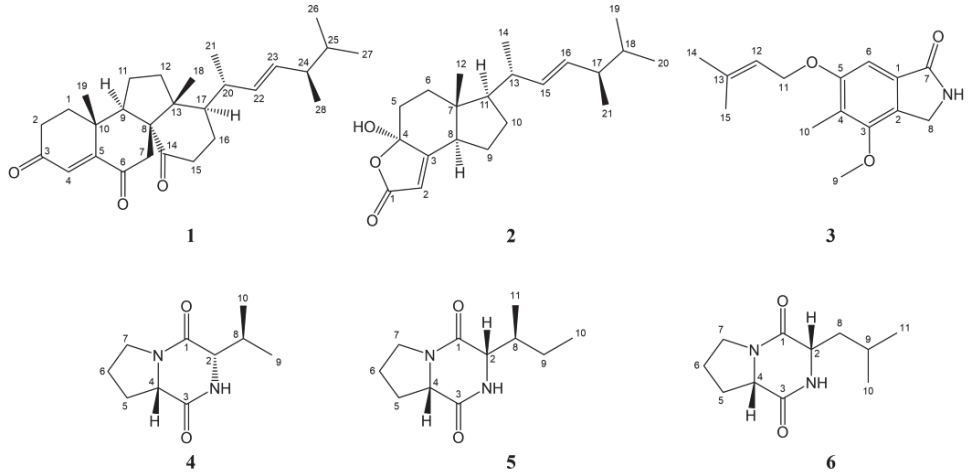

Figure 2. The chemical structures of the isolated six compounds (**1**–**6**).

Compound **5** (7.4 mg) was identified as follows. Cyclo-(L-Ile-L-Pro) ($C_{11}H_{18}N_2O_2$, *m/z* = 211.1413 $[M + H]^+$, cald. For 211.1441) [25,26]. ^{1}H-NMR (400 MHz, MeOD) δ 4.19 (t, *J* = 7.0 Hz, H-2, 1H), 4.07 (s, H-4, 1H), 3.60–3.45 (m, H-5, 2H), 2.36–2.26 (m, H-8, 1H), 2.20–2.12 (m, H-7a, 1H), 2.05–1.98 (m, H-7b, 1H), 1.97–1.87 (m, H-6, 2H), 1.50–1.27 (m, H-9, 2H), 1.06 (d, *J* = 7.2 Hz, H-10, 3H), 0.93 (t, *J* = 7.4 Hz, H-11, 3H). ^{13}C-NMR (101 MHz, MeOD) δ 172.45 (q, C-3), 167.59 (q, C-1), 61.30 (CH, C-4), 59.99 (CH, C-2), 46.17 (CH_2, C-5), 37.06 (CH, C-8), 29.54 (CH_2, C-7), 25.41 (CH_2, C-9), 23.22 (CH_2, C-6), 15.52 (CH_3, C-10), 12.57 (CH_3, C-11).

Compound **6** (7.5 mg) was identified as follows. Cyclo-(L-Leu-L-Pro) ($C_{11}H_{18}N_2O_2$, *m/z* = 211.1409 $[M + H]^+$, cald. for 211.1441) [26,27]. ^{1}H-NMR (400 MHz, MeOD) δ 4.25 (t, *J* = 7.1 Hz, H-2, 1H), 4.12 (dd, *J* = 6.8, 3.7 Hz, H-4, 1H), 3.56–3.44 (m, H-7, 2H), 2.36–2.23 (m, 1H), 2.10–1.78 (m, 5H), 1.58–1.44 (m, 1H), 0.95 (dd, *J* = 6.3, 2.5 Hz, H-10, 11, 6H). ^{13}C-NMR (101 MHz, MeOD) δ 172.81 (q, C-3), 168.92 (q, C-1), 60.28 (CH, C-4), 54.63 (CH, C-2), 46.44 (CH_2, C-5), 39.39 (CH_2, C-8), 29.07 (CH_2, C-7), 25.76 (CH, C-9), 23.65 (CH_2, C-6), 23.30 (CH_3, C-10), 22.20 (CH_3, C-11).

2.3. The Growth Profiles of B. cereus at Sub-Minimum Inhibitory Concentrations of Demethylincisterol A$_3$

After quorum sensing inhibitory (QSI)-screening the isolated compounds with *B. cereus*, it was found that only demethylincisterol A_3 had antibacterial and QSI activities. Its minimum inhibitory concentration (MIC) was 6.25 μg/mL. At sub-MICs (3.12, 1.56, and 0.78 μg/mL), there was no effect on the growth of *B. cereus* (Figure 3).

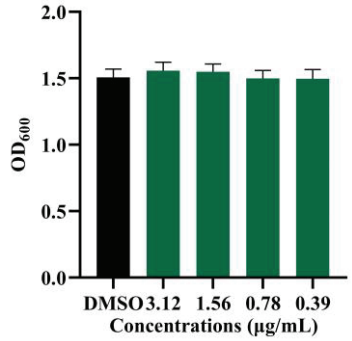

Figure 3. The growth of *B. cereus* at sub-MICs of demethylincisterol A_3. *B. cereus* grew for 24 h in different sub-MICs (3.12, 1.56, and 0.78 μg/mL) of demethylincisterol A_3; DMSO was used as the negative control. Error bars represent the standard deviation (*n* = 3).

2.4. Demethylincisterol A_3 Inhibits the Biofilm Formation of B. cereus

The results of crystal violet staining indicated a significant reduction in biofilm formation in the demethylincisterol A_3 treatment group when compared to the control group (Figure 4a). When the demethylincisterol A_3 concentration was 3.12, 1.56, and 0.78 μg/mL, the biofilm decreased by 50.2%, 37.9%, and 15.2%, respectively. A substantial reduction in bacterial density after treatment with demethylincisterol A_3 was observed using scanning electron microscopy (SEM) (Figure 4b).

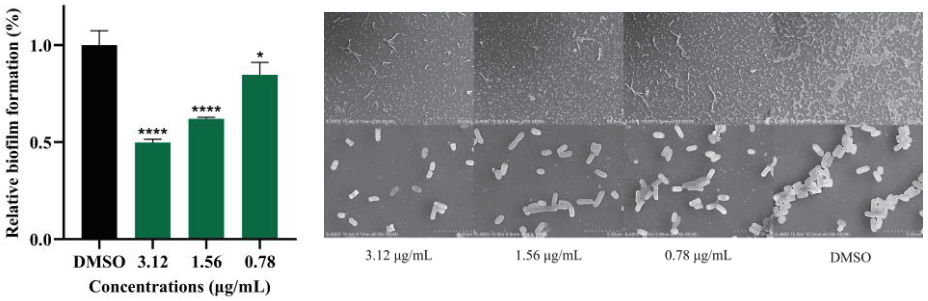

(**a**) (**b**)

Figure 4. The effect of demethylincisterol A_3 on the biofilm formation of *B. cereus*. *B. cereus* was treated with different concentrations (3.12, 1.56, and 0.78 μg/mL) of demethylsterol A_3 for 24 h, with DMSO as the negative control. (**a**) Biofilm formation. (**b**) SEM images of biofilms. Error bars represent the standard deviation (n = 3). * $p < 0.05$, **** $p < 0.0001$.

2.5. Demethylincisterol A_3 Inhibits the Swimming of B. cereus

The swimming behavior of *B. cereus* was notably hindered after exposure to demethylincisterol A_3 (Figure 5). Under the action of demethylincisterol A_3 at 3.12, 1.56, and 0.78 μg/mL, the swimming ability of *B. cereus* was reduced by 53.9%, 14.7%, and 4.4%, respectively.

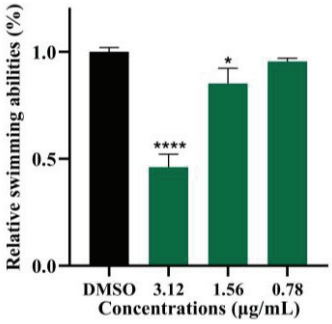

Figure 5. The effect of demethylincisterol A_3 on the swimming of *B. cereus* was examined using a swimming medium. The swimming behavior of *B. cereus* for 24 h of treatment with demethylsterol A_3 at various concentrations (3.12, 1.56, and 0.78 μg/mL) was tested. DMSO served as a negative control. After 24 h of incubation, the swimming diameter was observed and recorded. Values are represented as mean ± standard deviation (n = 3). Significant differences are denoted by * $p < 0.05$ and **** $p < 0.0001$, respectively.

2.6. Demethylincisterol A_3 Inhibits the Protease and Hemolytic Activity of B. cereus

After treatment with demethylincisterol A_3, the protease of *B. cereus* was significantly inhibited (Figure 6a). Under the action of demethylincisterol A_3 at 3.12, 1.56, and 0.78 μg/mL, the protease activities of *B. cereus* were reduced by 22.1%, 18.1%, and 10.7%, respectively. The hemolytic activity of *B. cereus* was significantly inhibited when treated with demethylincisterol A_3 (Figure 6b). Under the action of demethylincisterol A_3 at 3.12, 1.56, and 0.78 μg/mL, the hemolytic activities of *B. cereus* were reduced by 15.3%, 11.0%, and 7.6%, respectively.

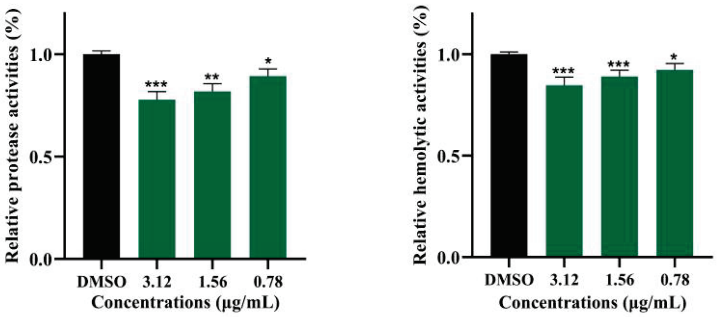

Figure 6. The effect of demethylincisterol A_3 on the virulence factors of *B. cereus*. The virulence factor produced by *B. cereus* after 24 h of treatment with different concentrations (3.12, 1.56, and 0.78 μg/mL) of demethylsterol A_3 was evaluated. DMSO was used as a negative control. (**a**) The protease activity was assessed by examining the clear zone on the skim milk agar plates. (**b**) The hemolysin activities were analyzed by examining the hemolysis zone on the blood agar plates. Values are represented as mean ± standard deviation (n = 3). Significant differences are denoted by * $p < 0.05$, ** $p < 0.01$, and *** $p < 0.001$, respectively.

2.7. Demethylincisterol A_3 Inhibits the Expression of Key Virulence-Related Genes of B. cereus

The expression of virulence-related genes of *B. cereus* was significantly inhibited when treated with demethylincisterol A_3 (Figure 7). Under the action of demethylincisterol A_3 at 3.12 μg/mL, the expression of the *sinR*, *tasA*, *papR*, *cytK*, *rpoN*, *hblD*, *comER*, *codY*, *plcR*, and *nheA* genes in *B. cereus* was significantly reduced.

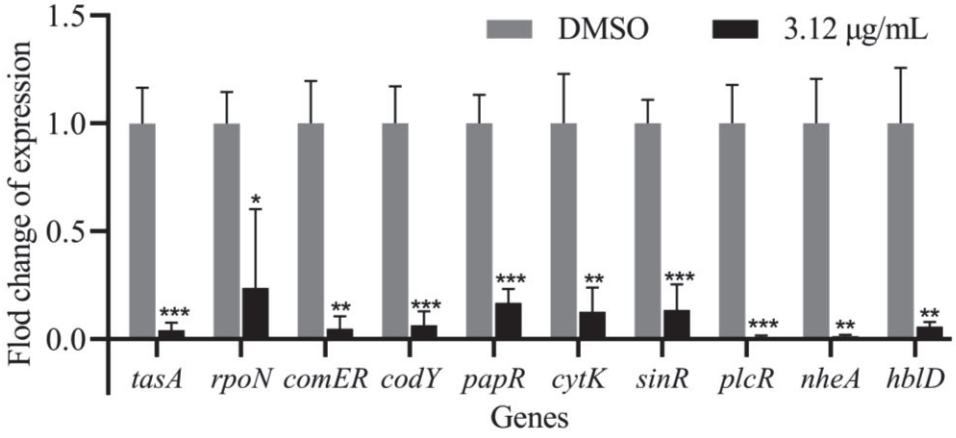

Figure 7. The effect of demethylincisterol A_3 on *B. cereus* gene transcription was investigated. The expression of QS-related genes in *B. cereus* was examined after treatment with 3.12 μg/mL of demethylsterol A_3 for 24 h. DMSO was the negative control. Three biological replicates were conducted and are represented as mean ± standard deviation (n = 3). Significant differences are denoted by * $p < 0.05$, ** $p < 0.01$, and *** $p < 0.001$, respectively.

2.8. Demethylincisterol A_3 Reduces the Mortality Rate of B. cereus

As shown in Figure 8, the supernatant of *B. cereus* treated with demethylincisterol A_3 was injected into a *Galleria mellonella* larval model. Only 25% of the larvae in the DMSO group survived after 72 h. However, the survival rate of the experimental group treated with demethylincisterol A_3 was significantly improved, with a survival rate of 88% for the larvae at a concentration of 3.12 μg/mL.

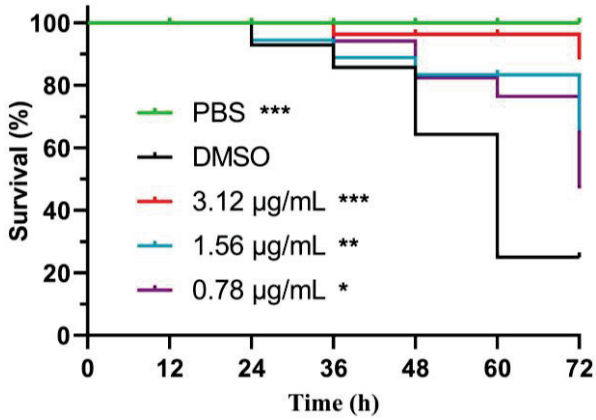

Figure 8. The effect of demethylincisterol A_3 on the survival rate of *G. mellonella* larval models was observed. PBS was the blank control. DMSO was used as a negative control. Statistical analyses were carried out using the log-rank (Mantel–Cox) test. Three biological replicates were conducted and are represented as mean ± standard deviation ($n = 3$). Significant differences are denoted by * $p < 0.05$, ** $p < 0.01$, and *** $p < 0.001$, respectively.

3. Discussion

In this study, demethylincisterol A_3, along with five other compounds, was initially isolated from *P. sacchari*. As an incisterol-type steroid, demethylincisterol A_3 has been identified in various fungi, possibly representing a common metabolite in fungal processes [28–30]. Notably, demethylincisterol A_3 exhibits significant anti-tumor and anti-inflammatory effects [31,32]. Studies have demonstrated that the rate of inhibition exhibited by demethylincisterol A_3 towards *Helicobacter pylori* is 11% greater than that of 100 μM quercetin [33]. Despite its recognized therapeutic potential, there has been limited research on its QS inhibitory effect against pathogens. Therefore, this study pioneers the investigation of demethylincisterol A_3's impact on QS, biofilm formation, and virulence factors in *B. cereus*.

At the MIC, *B. cereus* growth was inhibited, but at sub-MICs, there was no significant effect (Figure 3). *B. cereus* biofilms contribute to equipment adhesion, increased resistance, and toxicity [34]. Following demethylincisterol A_3 treatment, biofilm formation was significantly inhibited, decreasing production by 50.2% at 3.12 μg/mL. Our research is consistent with that pertaining to Siphonocholin, which can effectively inhibit biofilm formation at 1/2 MIC [35]. At the same time, diallyl disulfide can also inhibit the biofilm formation of *B. cereus* at 1/2 MIC [36]. The downregulation of *rpoN* and *comER*, important regulators of *B. cereus* biofilms, is associated with reduced biofilm production [37,38]. Additionally, the decrease in *tasA* expression directly correlates with a reduction in biofilm matrix protein synthesis [39].

B. cereus utilizes its swimming ability to navigate and reach the target host [36], and this mobility is intertwined with its biofilm formation [16]. Upon the addition of demethylincisterol A_3, both the swimming ability and the biofilm production of *B. cereus* decreased. Genes associated with flagella or mobility, including *rpoN*, *codY*, and *sinR* [38,40], showed significant downregulation after demethylincisterol A_3 treatment.

Proteases and hemolysin serve as virulence factors produced by *B. cereus*, aiding in immune system evasion [41]. Hemolysins induce red blood cell rupture, leading to hemolysis [42]. Following demethylincisterol A_3 treatment, *B. cereus* exhibited a significant reduction in protease and hemolysin production. In *B. cereus*, *nhe* represents non-hemolytic enterotoxin, *hbl* represents hemolysin BL, and *cytK* represents cytotoxin, regulated by *plcR* [42]. *papR* can produce PapR peptides to activate the PlcR protein [43]. Demethylincisterol A_3 reduced the mortality rate of *B. cereus* in the *G. mellonella* larval model from 75% to 12%. Furthermore, demethylincisterol A_3 diminished the transcription of the *nheA*, *hblD*, *cytK*, *plcR*, and *papR* genes in *B. cereus*. Therefore, demethylincisterol A_3 may mitigate the

production of virulence factors in *B. cereus*, weakening its pathogenicity by inhibiting the transcription of the *nheA*, *hblD*, *cytK*, *plcR*, and *papR* genes.

In the current study, cyclo-(L-Pro-L-Leu) was also extracted from *P. sacchari*. This cyclodipeptide was identified as a signaling molecule that facilitates communication between *B. cereus* and *Cronobacter sakazakii* [44]. It was already known whether or not it was a molecular signaling pathway in *B. cereus*; further research will be conducted to determine the above.

4. Materials and Methods

4.1. General

B. cereus (ATCC11778) was cultured using LB medium at 37 °C. Fresh *Laurencia* sp. was collected from the Nansha Islands area in the South China Sea (Figure S1), identified by Prof. X.L. Wang (Institute of Oceanology, CAS, China). The test compound was firstly dissolved in dimethyl sulfoxide (DMSO) to 1 mg/mL and sterilized using a filter membrane (0.22 μm) to obtain the stock solution. During all the experiments, an equal volume of DMSO was added as the negative control. The NMR was the Bruker Avance neo 400 (Bruker BioSpin AG, Ettlingen, Germany). The MS was ion trap time-of-flight mass spectrometry liquid chromatography-mass spectrometry (Shimadzu, Kyoto, Japan). All used chemicals in this work were analytical reagents.

4.2. Seaweed Sample Collection and Morphological Identification

The seaweed samples were collected by researcher Zhi-Kai Guo from the Institute of Biology, Chinese Academy of Tropical Agricultural Sciences, from the reef of Zhaoshu Island in the Xisha Xuande Islands. The algae species were identified by Professor Xu-Lei Wang from the Qingdao Institute of Oceanography, Chinese Academy of Sciences. The algal body was purplish red in appearance, with cylindrical branches—mostly forked or trifurcate branches, dense and clustered—with forked or threefold apical branchlets, and a concave apical center with trichonema. The tetrasporangium divides cruciform or conical. Identified as *Laurencia* sp. (Figure S1). Endophytes were extracted from algae. After placing fresh *Laurencia* sp. in a petri dish and disinfecting it three times with sterile water, it was rinsed with sterile water and alcohol for 30 seconds. It was then immersed in a 1% (*w*/*w*) NaClO solution for three minutes and then rinsed five times with sterile water. Once it was dried with filter paper, it was chopped into small segments. Mixed the small segments with sterile quartz sand. Then grinded the mixture in a sterile phosphate-buffered saline (PBS) environment. Diluted the grinding solution using a PBS gradient. A layer of 100 μL dilution solution (evenly distributed) was coated onto the culture plate containing PDA, Gause's Synthetic Agar No.1 (GSA) and LB. LB plate was cultured at 37 °C, while PDA and GSA plates were cultured at 28 °C. Colonies with different morphologies were selected for purification and preservation during the cultivation process.

4.3. Identification of QSI Active-Strain W2-F1

The QSI activities of the crude extract of ethyl acetate from the isolated strain were evaluated by using the indicator strain *Chromobacterium violaceum* CV026. Among these 7 isolates, W2-F1 showed the best QSI activity (Figure S2). The morphological characteristics of strain W2-F1 cultivated in PDA medium (Hope Bio, Qingdao, China) were examined [45]. Further, the genomic DNA was extracted and amplified using ITS primers (5′-TCCGTAGGTGGAACCTGGG-3′ and 5′-TCTCCGCTTATTGCT-3′) and the obtained sequence was aligned in the NCBI. Based on the sequence similarities, the phylogenetic tree was constructed by the neighbor-joining method with the 1000-bootstrap value using MEGA 7.0 software [46]. The W2-F1 strain was identified as *P. sacchari*.

4.4. Scale-Up Fermentation of QSI Active-Strain P. sacchari and Isolation, Purification, and Elucidation of Compounds under Bio-Guided Screenings

P. sacchari was activated on a PDA plate, then inoculated into a solid PDA medium containing 3% sea salt and cultured at 28 °C for 14 days. After the culture was completed, the mycelium was broken together with the culture medium. Absolute ethanol was added to the mixture and treated with ultrasonic for 12 h and then filtered, repeated three times. The ethanol in the filtrate was removed by evaporation under reduced pressure. The residual liquid was extracted three times by equal ethyl acetate (EtOAc) and concentrated under reduced pressure to give a crude extract (110.1 g), which was subjected to column chromatography (CC) over a silica gel (100–200 mesh) eluted with a gradient of CH_2Cl_2/MeOH (100:0–0:100) to obtain fractions (R1-R11). The fraction R4 (5.26 g) showing QSI activity was further submitted to silica gel (200–300 mesh) column chromatography (CC) and eluted with a gradient system of petroleum ether/CH_2Cl_2 (20:1–1:1) and CH_2Cl_2/MeOH (100:1–10:1) to obtain twenty-two subfractions (R4–1–22). Fraction R4–9 (0.24 g) showing QSI activity was purified by reversed-phase C_{18} CC and semi-preparation HPLC equipped with a preparative column (5 μm, 21.2 × 250mm; Beijing, China) to obtain compounds **1** and **2** (eluting conditions: 100% MeOH, flow rate = 8 mL/min; yields: 4.8 and 8.7 mg). QSI-active R4–18 were eluted by silica gel column chromatography and semi-preparation HPLC to obtain compound **3** (eluting conditions: 90% MeOH, flow rate = 8 mL/min; yield: 3.2 mg) and R4–18–6. Compound **4** (yield: 10.8 mg) was obtained from R4–18–6 with a 60% MeOH eluting solution and a flow rate of 8 mL/min. Compounds **5** and **6** (yields: 7.4 and 7.5 mg) were obtained from R4–18–6 with a 50% MeOH elution solution and flow rate of 6 mL/min.

4.5. MIC of Demethylincisterol A_3 against B. cereus

MIC of demethylincisterol A_3 was measured by using the double dilution method [35]. The seed solution of *B. cereus* that was cultured overnight was added to LB medium at a rate of 1% (*v*/*v*). The compounds were added and the mixture was diluted and incubated at 37 °C and 180 rpm for 24 h. DMSO was used as the negative control. Growth profiles were measured at 620 nm.

4.6. Growth Measurement of B. cereus

The planktonic cell growth measurement was performed by the reported methods, with some modifications [47]. The *B. cereus* culture was inoculated into LB medium at a ratio of 1% (*v*/*v*). Demethylincisterol A_3 was then added to achieve final concentrations of 3.12, 1.56, and 0.78 μg/mL. After 24 hours of cultivation at 37 °C and 180 rpm, OD_{620} was measured (Biotech Epoch 2, Santa Clara, CA, USA).

4.7. The Effects of Biofilm Formation

The biofilm formation assays were conducted following established procedures with slight modifications, as outlined in the report by [48]. *B. cereus* cultures that had been grown overnight were introduced into LB medium at a 1% (*v*/*v*) ratio, and demethylincisterol A_3 was added. A 200 μL aliquot of this mixed culture was then transferred to a 96-well polystyrene microtiter plate. The final concentrations of demethylincisterol A_3 in the wells were 3.12, 1.56, and 0.78 μg/mL. The plate was then incubated at 37 °C for 24 h. After this period, the culture medium was carefully removed and the wells were washed three times with sterile PBS to eliminate planktonic cells. The remaining water in the wells was evaporated at 60 °C. The biofilms that had adhered to the bottom of the wells were fixed with cool methanol for 15 min. The liquid was then removed and the plate was dried again at 60 °C. Each well was stained with 200 μL of a 0.05% (*w*/*v*) crystal violet solution. After 10 min staining, any excess crystal violet was removed and the wells were washed three times with PBS. Once the plate had dried at 60 °C, 200 μL of 95% (*v*/*v*) ethanol was added to each well and the plate was decolorized for 15 min on a shaker set at 37 °C and

180 rpm. A 150 μL sample of the decolorizing solution was then taken from each well and the absorbance was measured at 570 nm.

SEM measurement: The coating was fixed on the glass slide with 2.5% (*v*/*v*) glutaraldehyde for 12 h. After fixation, it was washed at once with ultrapure water and then gradient dehydration was performed with 50%, 60%, 70%, 80%, 90%, and 100% (*v*/*v*) ethanol in sequence. After drying, it was sprayed gold and observed under a SEMn microscope.

4.8. Swimming Motility Assay

The swimming motility assay was evaluated by established protocols and reports, as per the study by [46]. Swimming medium (10 g/L peptone, 5 g/L NaCl, 3 g/L agar) was added to demethylincisterol A_3 to the final concentrations of 3.12, 1.56, and 0.78 μg/mL, respectively. It was mixed well and poured evenly into a petri dish. Sterile water served as a negative control. After solidification, 2 μL of *B. cereus* bacterial solution was inoculated in the center of the swimming medium. The migration diameter was recorded after 24 h of cultivation at 37 °C.

4.9. Measurement of Protease Production

Protease activities were measured by reported methods, with some modifications [49]. *B. cereus* cultures that had been grown overnight were introduced into LB medium at a 1% (*v*/*v*) ratio, and demethylincisterol A_3 was added. The final concentrations of desmethylergosterol A_3 were 3.12, 1.56, and 0.78 μg/mL, respectively. The solution was incubated at 37 °C and 180 rpm for 24 h. The fermentation broth was centrifuged (8000× *g*, 4 °C, 15 min) to collect the supernatant. The supernatant was filtered through a 0.22 μm membrane. Skim milk agar was prepared (1/4-strength LB broth with 4% (*w*/*v*) skim milk and 1.5% (*w*/*v*) agar). Added 50 μL of supernatant to the wells of a skim milk agar plate and incubated at 37 °C for 24 h. The protease activity was assessed by examining the clear zone on the skim milk agar plates.

4.10. Measurement of Hemolytic Activities

Hemolytic activities were measured by reported methods, with some modifications [50]. Hemolysis experiments were performed using a trypticase soy sheep blood agar plate (Huankai Microbial, Guangzhou, China). The supernatant was prepared according to the previous method. Then, 50 μL of cultured supernatant was added after drilling, incubated at 37 °C for 24 h, and the size of the hemolytic halo was observed.

4.11. Quantitative Real-Time PCR

Quantitative real-time PCR (RT-qPCR) was performed according to reported methods, with minor modifications [48]. The bacterial solution cultured overnight was diluted to a 0.5 Michaelis turbidimetric unit with sterile LB broth. Overnight cultured *B. cereus* was added in a 1% (*v*/*v*) ratio to LB medium. The experimental group was supplemented with demethylincisterol A_3 to make its concentration 3.12 μg/mL, and the same volume of DMSO was used as the negative control group. The solution was incubated at 37 °C and 180 rpm for 24 h. The fermentation broth was centrifuged (8000× *g*, 4 °C, 15 min) to collect cells and washed thrice with diethylpyrocarbonate (DEPC)-treated water. The total RNA of *B. cereus* was extracted using an Eastern® Super Total RNA Extraction Kit (Promega, Beijing, China) and transformed into cDNA by a Reverse Transcription Kit (Biosharp, Beijing, China). The real-time PCR reaction was performed using a TB Green® Premix Ex Taq™ II FAST qPCR Mix (TaKaRa, Dalian, China) with a Bio-Rad CFX Connect System (Bio-Rad, Hercules, CA, USA). The primers used for real-time PCR are listed in Table 1. Gene *16S* rRNA was used as an internal control [36].

Table 1. PCR primers for RT-qPCR.

Primer	Sequence (5′-3′)
16S rRNA_F	GGAGGAAGGTGGGGATGAC
16S rRNA_R	ATGGTGTGACGGGCGGTGTG
*sinR*_F	AGCGAGCGCCGATATGATAG
*sinR*_R	TCGAGCGCATTCGTAACCAT
*tasA*_F	ACTCGCCACATGGAAACACA
*tasA*_R	ACGATTTGTTCGTTTTCTTCGT
*papR*_F	TGTACCTCTTGATCACTGTGAGA
*papR*_R	AACGTTAGCAATGGCATGGG
*cytK*_F	CGATGACCCAAGCGCTGATA
*ctyK*_R	GTTGCACTAGCACCAGGGAT
*rpoN*_F	CACTTGAACGAGCTTTCGCC
*rpoN*_R	GGGGCGCGTAATATTCAGGA
*hblD*_F	GGTCCAGATGGGAAAGGTGG
*hblD*_R	AAGTTGTGGGATCGTTGCCT
*comER*_F	CAAGTTGCGGTCCTGCTTTC
*comER*_R	AATTTCCCCATCCCCACGAC
*codY*_F	CCACGACGGCTAACTACGAA
*codY*_R	GCGTTATTACAGAGCGCAGC
*plcR*_F	GGGTGATGCGGGGATTAACA
*plcR*_R	GGCTCACTTCCGATTGGTGA
*nheA*_F	TCTTGCAACAGCCAGACATT
*nheA*_R	CTCTCGCACATTCGCCTTTG

4.12. Evaluating the Inhibitory Effect of Demethylincisterol A_3 in a G. mellonella Model

A *G. mellonella* larval model was used to evaluate the toxic inhibitory effect of demethylincisterol A_3 on *B. cereus* [51]. The supernatant was prepared as described above. The larvae were randomly divided into 15 groups (n = 10 per group) and 5 μL of supernatant was injected into the posterior part of the left abdominal foot. Then, the larvae were cultured at room temperature for 72 h, and their growth was recorded every 12 h. PBS served as a blank control.

4.13. Statistical Analysis

Unless otherwise stated, all experiments described were performed in triplicate independently. The data shown in the figures are the mean ± standard deviation (± SD) of the replicates. Statistical differences were determined using one-way ANOVA or *t*-test using GraphPad Prism 8, where $p < 0.05$ was considered statistically significant.

5. Conclusions

Demethylincisterol A_3 exhibits significant inhibitory effects on *B. cereus*, encompassing reduced biofilm formation, diminished bacterial mobility, and lowered production of virulence factors. This multifaceted impact has the potential to attenuate the pathogenicity of *B. cereus*. Based on these results, it can be inferred that demethylincisterol A_3 exhibits potential as a valuable compound in the development of novel antibacterial therapies.

Supplementary Materials: The following supporting information can be downloaded at https://www.mdpi.com/article/10.3390/md22040161/s1: Figure S1: *Laurencia* sp. was collected from the Nansha Islands area in the South China Sea; Figure S2: Evaluated QSI activities using the indicator strain of *Chromobacterium violaceum* CV026; Figure S3–S8: ^{1}H, ^{13}C NMR, and HRMS data of compounds **1**–**6**; Figure S9: Sequence comparison results of strain W2-F1; Figure S10–S13: Preparation spectrum of compounds **1**–**6**; Table S1: The chemical shifts of each hydrogen-bearing chiral carbon.

Author Contributions: Conceptualization, S.-L.X.; data curation, S.-L.X. and K.-Z.X.; formal analysis, S.-L.X. and K.-Z.X.; funding acquisition, A.-Q.J.; investigation, S.-L.X.; methodology, S.-L.X. and L.-J.Y.; project administration, A.-Q.J.; resources, A.-Q.J.; software, S.-L.X. and L.-J.Y.; supervision, A.-Q.J.; writing—original draft, S.-L.X., K.-Z.X. and L.-J.Y.; writing—review and editing, A.-Q.J. All authors have read and agreed to the published version of the manuscript.

Funding: This research was funded by the Hainan Province Science and Technology Special Fund (ZDYF2024SHFZ103), the National Natural Science Foundation of China (82160664), and Innovative Research Projects for Postgraduates in Hainan Province (Qhyb2021-38, Qhyb2022-46).

Institutional Review Board Statement: Not applicable.

Data Availability Statement: The data presented in this study are available from the corresponding author upon request.

Acknowledgments: We thank the Hainan University for its support.

Conflicts of Interest: The authors declare no conflicts of interest.

References

1. Pagarete, A.; Ramos, A.S.; Puntervoll, P.; Allen, M.J.; Verdelho, V. Antiviral potential of slgal metabolites—A comprehensive review. *Mar. Drugs* **2021**, *19*, 94. [CrossRef] [PubMed]
2. Nagamalla, L.; Shanmukha Kumar, J.V.; Sanjay, C.; Alsamhan, A.M.; Shaik, M.R. In-silico study of seaweed secondary metabolites as AXL kinase inhibitors. *Saudi J. Biol. Sci.* **2022**, *29*, 689–701. [CrossRef] [PubMed]
3. Vairagkar, U.; Mirza, Y. Antagonistic activity of antimicrobial metabolites produced from seaweed-associated *Bacillus amyloliquefaciens* MTCC 10456 against *Malassezia* spp. *Probiotics Antimicrob. Proteins* **2021**, *13*, 1228–1237. [CrossRef] [PubMed]
4. Catarino, M.D.; Silva-Reis, R.; Chouh, A.; Silva, S.; Braga, S.S.; Silva, A.M.S.; Cardoso, S.M. Applications of antioxidant secondary metabolites of *Sargassum* spp. *Mar. Drugs* **2023**, *21*, 172. [CrossRef]
5. Digra, S.; Nonzom, S. An insight into endophytic antimicrobial compounds: An updated analysis. *Plant Biotechnol. Rep.* **2023**, *17*, 427–457. [CrossRef] [PubMed]
6. Stierle, A.; Strobel, G.; Stierle, D. Taxol and taxane production by *Taxomyces andreanae*, an endophytic fungus of Pacific yew. *Science* **1993**, *260*, 214–216. [CrossRef] [PubMed]
7. Nishad, J.H.; Singh, A.; Gautam, V.S.; Kumari, P.; Kumar, J.; Yadav, M.; Kharwar, R.N. Bioactive potential evaluation and purification of compounds from an endophytic fungus *Diaporthe longicolla*, a resident of *Saraca asoca* (Roxb.) Willd. *Arch. Microbiol.* **2021**, *203*, 4179–4188. [CrossRef] [PubMed]
8. Gautam, V.S.; Singh, A.; Kumari, P.; Nishad, J.H.; Kumar, J.; Yadav, M.; Bharti, R.; Prajapati, P.; Kharwar, R.N. Phenolic and flavonoid contents and antioxidant activity of an endophytic fungus *Nigrospora sphaerica* (EHL2), inhabiting the medicinal plant *Euphorbia hirta* (dudhi) L. *Arch. Microbiol.* **2022**, *204*, 140. [CrossRef]
9. Xu, Z.; Xiong, B.; Xu, J. Chemical investigation of secondary metabolites produced by mangrove endophytic fungus *Phyllosticta capitalensis*. *Nat. Prod. Res.* **2021**, *35*, 1561–1565. [CrossRef]
10. Singh, V.K.; Kumar, A. Secondary metabolites from endophytic fungi: Production, methods of analysis, and diverse pharmaceutical potential. *Symbiosis* **2023**, *90*, 111–125. [CrossRef]
11. Akinpelu, D.A.; Aiyegoro, O.A.; Akinpelu, O.F.; Okoh, A.I. Stem bark extract and fraction of *Persea americana* (Mill.) exhibits bactericidal activities against strains of *Bacillus cereus* associated with food poisoning. *Molecules* **2015**, *20*, 416–429. [CrossRef] [PubMed]
12. Eglezos, S.; Huang, B.; Dykes, G.A.; Fegan, N. The prevalence and concentration of *Bacillus cereus* in retail food products in Brisbane, Australia. *Foodborne Pathog. Dis.* **2010**, *7*, 867–870. [CrossRef] [PubMed]
13. Leong, S.S.; Korel, F.; King, J.H. *Bacillus cereus*: A review of "fried rice syndrome" causative agents. *Microb. Pathog.* **2023**, *185*, 106418. [CrossRef] [PubMed]
14. Lin, Y.; Briandet, R.; Kovács, Á.T. *Bacillus cereus* sensu lato biofilm formation and its ecological importance. *Biofilm* **2022**, *4*, 100070. [CrossRef] [PubMed]
15. Huang, Y.; Flint, S.H.; Palmer, J.S. *Bacillus cereus* spores and toxins–the potential role of biofilms. *Food Microbiol.* **2020**, *90*, 103493. [CrossRef] [PubMed]
16. Zhao, L.; Duan, F.; Gong, M.; Tian, X.; Guo, Y.; Jia, L.; Deng, S. (+)-Terpinen-4-ol Inhibits *Bacillus cereus* biofilm formation by upregulating the interspecies quorum sensing signals diketopiperazines and diffusing signaling factors. *J. Agric. Food Chem.* **2021**, *69*, 3496–3510. [CrossRef] [PubMed]
17. Gorgan, M.; Vanunu Ofri, S.; Engler, E.R.; Yehuda, A.; Hutnick, E.; Hayouka, Z.; Bertucci, M.A. The importance of the PapR7 C-terminus and amide protons in mediating quorum sensing in *Bacillus cereus*. *Res. Microbiol.* **2023**, *174*, 104139. [CrossRef] [PubMed]

18. Amagata, T.; Tanaka, M.; Yamada, T.; Doi, M.; Minoura, K.; Ohishi, H.; Yamori, T.; Numata, A. Variation in cytostatic constituents of a sponge-derived *Gymnascella dankaliensis* by manipulating the carbon source. *J. Nat. Prod.* **2007**, *70*, 1731–1740. [CrossRef] [PubMed]
19. Mansoor, T.A.; Hong, J.; Lee, C.-O.; Bae, S.-J.; Im, K.S.; Jung, J.H. Cytotoxic sterol derivatives from a marine sponge *Homaxinella* sp. *J. Nat. Prod.* **2005**, *68*, 331–336. [CrossRef]
20. Yajima, A.; Kagohara, Y.; Shikai, K.; Katsuta, R.; Nukada, T. Synthesis of two osteoclast-forming suppressors, demethylincisterol A_3 and chaxine A. *Tetrahedron* **2012**, *68*, 1729–1735. [CrossRef]
21. Yang, X.-L.; Zhang, S.; Hu, Q.-B.; Luo, D.-Q.; Zhang, Y. Phthalide derivatives with antifungal activities against the plant pathogens isolated from the liquid culture of *Pestalotiopsis photiniae*. *J. Antibiot.* **2011**, *64*, 723–727. [CrossRef]
22. Mehnaz, S.; Saleem, R.S.Z.; Yameen, B.; Pianet, I.; Schnakenburg, G.; Pietraszkiewicz, H.; Valeriote, F.; Josten, M.; Sahl, H.-G.; Franzblau, S.G.; et al. Lahorenoic acids A–C, *ortho*-dialkyl-substituted aromatic acids from the biocontrol strain *Pseudomonas aurantiaca* PB-St2. *J. Nat. Prod.* **2013**, *76*, 135–141. [CrossRef]
23. Campbell, J.; Lin, Q.; Geske, G.D.; Blackwell, H.E. New and Unexpected Insights into the Modulation of LuxR-Type Quorum Sensing by Cyclic Dipeptides. *ACS Chem. Bio.* **2009**, *4*, 1051–1059. [CrossRef]
24. Fdhila, F.; Vázquez, V.; Sánchez, J.L.; Riguera, R. $_{DD}$-Diketopiperazines: Antibiotics Active against *Vibrio anguillarum* Isolated from Marine Bacteria Associated with Cultures of *Pecten maximus*. *J. Nat. Prod.* **2003**, *66*, 1299–1301. [CrossRef]
25. Song, S.; Fu, S.; Sun, X.; Li, P.; Wu, J.E.; Dong, T.; He, F.; Deng, Y. Identification of cyclic dipeptides from *Escherichia coli* as new antimicrobial agents against *Ralstonia solanacearum*. *Molecules* **2018**, *23*, 214. [CrossRef]
26. Yang, B.; Dong, J.; Zhou, X.; Yang, X.; Lee, K.J.; Wang, L.; Zhang, S.; Liu, Y. Proline-containing dipeptides from a marine sponge of a *Callyspongia* Species. *Helv. Chim. Acta* **2009**, *92*, 1112–1117. [CrossRef]
27. Han, Y.; Li, Y.Y.; Shen, Y.; Li, J.; Li, W.J.; Shen, Y.M. Oxoprothracarcin, a novel pyrrolo[1,4]benzodiazepine antibiotic from marine *Streptomyces* sp. M10946. *Drug Discov. Ther.* **2013**, *7*, 243–247. [CrossRef] [PubMed]
28. Yang, X.; Wu, P.; Xue, J.; Li, H.; Wei, X. Seco-pimarane diterpenoids and androstane steroids from an endophytic *Nodulisporium* fungus derived from *Cyclosorus parasiticus*. *Phytochemistry* **2023**, *210*, 113679. [CrossRef]
29. Li, D.X.; Cheng, X.; Ma, F.P.; Chen, J.Y.; Chen, Y.P.; Zhao, X.S.; Luo, Q. Identification of metabolites from edible mushroom *Morchella sextelata* and their biological evaluation. *Nat. Prod. Res.* **2023**, *37*, 1774–1781. [CrossRef] [PubMed]
30. Jiang, C.; Ji, J.; Li, P.; Liu, W.; Yu, H.; Yang, X.; Xu, L.; Guo, L.; Fan, Y. New lanostane-type triterpenoids with proangiogenic activity from the fruiting body of *Ganoderma applanatum*. *Nat. Prod. Res.* **2022**, *36*, 1529–1535. [CrossRef]
31. Su, J.-C.; Pan, Q.; Xu, X.; Wei, X.; Lei, X.; Zhang, P. Structurally diverse steroids from an endophyte of *Aspergillus tennesseensis* 1022LEF attenuates LPS-induced inflammatory response through the cholinergic anti-inflammatory pathway. *Chem.-Biol. Interact.* **2022**, *362*, 109998. [CrossRef] [PubMed]
32. Liu, Y.; Fu, H.; Zuo, L. Synergistic cytotoxicity effect of 5-Fluorouracil and SHP2 Inhibitor demethylincisterol A_3 on cervical cancer cell. *Anti-Cancer Agents Med. Chem.* **2022**, *22*, 1313–1319. [CrossRef] [PubMed]
33. Na, M.W.; Lee, E.; Kang, D.-M.; Jeong, S.Y.; Ryoo, R.; Kim, C.-Y.; Ahn, M.-J.; Kang, K.B.; Kim, K.H. Identification of antibacterial sterols from Korean wild mushroom *Daedaleopsis confragosa* via bioactivity- and LC-MS/MS profile-guided fractionation. *Molecules* **2022**, *27*, 1865. [CrossRef] [PubMed]
34. Huang, Y.; Flint, S.H.; Loo, T.S.; Palmer, J.S. Emetic toxin production of *Bacillus cereus* in a biofilm. *LWT-Food Sci. Technol.* **2022**, *154*, 112840. [CrossRef]
35. Alam, P.; Alqahtani, A.S.; Mabood Husain, F.; Tabish Rehman, M.; Alajmi, M.F.; Noman, O.M.; El Gamal, A.A.; Al-Massarani, S.M.; Shavez Khan, M. Siphonocholin isolated from red sea sponge *Siphonochalina siphonella* attenuates quorum sensing controlled virulence and biofilm formation. *Saudi Pharm. J.* **2020**, *28*, 1383–1391. [CrossRef] [PubMed]
36. Jin, Z.; Li, L.; Zheng, Y.; An, P. Diallyl disulfide, the antibacterial component of garlic essential oil, inhibits the toxicity of *Bacillus cereus* ATCC 14579 at sub-inhibitory concentrations. *Food Control* **2021**, *126*, 108090. [CrossRef]
37. Hayrapetyan, H.; Tempelaars, M.; Nierop Groot, M.; Abee, T. *Bacillus cereus* ATCC 14579 RpoN (Sigma 54) Is a pleiotropic regulator of growth, carbohydrate metabolism, motility, biofilm formation and toxin production. *PLoS ONE* **2015**, *10*, e0134872. [CrossRef] [PubMed]
38. Yan, F.; Yu, Y.; Wang, L.; Luo, Y.; Guo, J.-h.; Chai, Y. The *comER* gene plays an Important role in biofilm formation and sporulation in both *Bacillus subtilis* and *Bacillus cereus*. *Front. Microbiol.* **2016**, *7*, 1025. [CrossRef] [PubMed]
39. Caro-Astorga, J.; Pérez-García, A.; de Vicente, A.; Romero, D. A genomic region involved in the formation of adhesin fibers in *Bacillus cereus* biofilms. *Front. Microbiol.* **2015**, *5*, 745. [CrossRef]
40. Coburn, P.S.; Miller, F.C.; Enty, M.A.; Land, C.; LaGrow, A.L.; Mursalin, M.H.; Callegan, M.C. The *Bacillus virulome* in endophthalmitis. *Microbiology* **2021**, *167*, 001057. [CrossRef]
41. Dietrich, R.; Jessberger, N.; Ehling-Schulz, M.; Märtlbauer, E.; Granum, P.E. The food poisoning toxins of *Bacillus cereus*. *Toxins* **2021**, *13*, 98. [CrossRef]
42. Enosi Tuipulotu, D.; Mathur, A.; Ngo, C.; Man, S.M. *Bacillus cereus*: Epidemiology, virulence factors, and host-pathogen interactions. *Trends Microbiol.* **2021**, *29*, 458–471. [CrossRef]
43. Huillet, E.; Bridoux, L.; Barboza, I.; Lemy, C.; André-Leroux, G.; Lereclus, D. The signaling peptide PapR is required for the activity of the quorum-sensor PlcRa in *Bacillus thuringiensis*. *Microbiology* **2020**, *166*, 398–410. [CrossRef]

44. Bofinger, M.R.; de Sousa, L.S.; Fontes, J.E.N.; Marsaioli, A.J. Diketopiperazines as cross-communication quorum-sensing signals between *Cronobacter sakazakii* and *Bacillus cereus*. *ACS Omega* **2017**, *2*, 1003–1008. [CrossRef] [PubMed]
45. Shafique, S.; Javed, A.; Shafique, S.; Hussain, A.; Rafique, R.; Mubarak, A. Isolation and identification of *Pithomyces sacchari* as a leaf spot pathogen of *Helianthus annuus* from Pakistan. *Sci. Rep.* **2022**, *12*, 22033. [CrossRef]
46. Zeng, Y.X.; Liu, J.S.; Wang, Y.J.; Tang, S.; Wang, D.Y.; Deng, S.M.; Jia, A.Q. Actinomycin D: A novel *Pseudomonas aeruginosa* quorum sensing inhibitor from the endophyte *Streptomyces cyaneochromogenes* RC1. *World J. Microbiol. Biotechnol.* **2022**, *38*, 170. [CrossRef] [PubMed]
47. Inaba, M.; Matsuda, N.; Banno, H.; Jin, W.; Wachino, J.-i.; Yamada, K.; Kimura, K.; Arakawa, Y. In vitro reduction of antibacterial activity of tigecycline against multidrug-resistant *Acinetobacter baumannii* with host stress hormone norepinephrine. *Int. J. Antimicrob. Agents* **2016**, *48*, 680–689. [CrossRef] [PubMed]
48. Xu, K.-Z.; Xiang, S.-L.; Wang, Y.-J.; Wang, B.; Jia, A.-Q. Methyl gallate isolated from partridge tea (*Mallotus oblongifolius* (Miq.) Müll.Arg.) inhibits the biofilms and virulence factors of *Burkholderia thailandensis*. *J. Ethnopharmacol.* **2024**, *320*, 117422. [CrossRef]
49. Chu, W.; Zhou, S.; Jiang, Y.; Zhu, W.; Zhuang, X.; Fu, J. Effect of traditional Chinese herbal medicine with antiquorum sensing activity on *Pseudomonas aeruginosa*. *Evid.-Based Complement. Altern. Med.* **2013**, *2013*, 648257. [CrossRef]
50. Zhao, Y.; Chen, C.; Gu, H.-j.; Zhang, J.; Sun, L. Characterization of the genome feature and toxic capacity of a *Bacillus wiedmannii* isolate from the hydrothermal field in Okinawa Trough. *Front. Cell. Infect. Microbiol.* **2019**, *9*, 370. [CrossRef]
51. Yin, L.; Wang, Y.; Xiang, S.; Xu, K.; Wang, B.; Jia, A.-Q. Tyramine, one quorum sensing inhibitor, reduces pathogenicity and restores tetracycline susceptibility in *Burkholderia cenocepacia*. *Biochem. Pharmacol.* **2023**, *218*, 115906. [CrossRef] [PubMed]

Disclaimer/Publisher's Note: The statements, opinions and data contained in all publications are solely those of the individual author(s) and contributor(s) and not of MDPI and/or the editor(s). MDPI and/or the editor(s) disclaim responsibility for any injury to people or property resulting from any ideas, methods, instructions or products referred to in the content.

marine drugs

MDPI

Review

Insights into Natural Products from Marine-Derived Fungi with Antimycobacterial Properties: Opportunities and Challenges

Muhammad Azhari [1], Novi Merliani [1], Marlia Singgih [1], Masayoshi Arai [2] and Elin Julianti [1,*]

[1] School of Pharmacy, Bandung Institute of Technology, Jl. Ganesha No. 10, Bandung 40132, Indonesia; mazhari@itb.ac.id (M.A.); novimrl@gmail.com (N.M.); marlia@itb.ac.id (M.S.)
[2] Laboratory of Natural Products for Drug Discovery, Graduate School of Pharmaceutical Sciences, Osaka University, 1-6 Yamadaoka, Osaka 565-0871, Japan; araim@phs.osaka-u.ac.jp
* Correspondence: elin_julianti@itb.ac.id

Abstract

Tuberculosis (TB) poses a persistent global health threat exacerbated by the emergence of drug-resistant strains; hence, there is a continuous quest for novel antimicrobial agents. Despite efforts to develop effective therapies, existing treatments require a relatively long duration of therapy to eradicate the pathogen due to its virulence factors, pathogenesis patterns, and ability to enter dormant states. This can lead to a higher risk of treatment failure due to poor patient adherence to the complex regimen. As a result, considerable research is necessary to identify alternative antituberculosis agents. The marine environment, particularly marine-derived fungi, has recently gained interest due to its potential as an abundant source of bioactive natural products. This review covers 19 genera of marine-derived fungi and 139 metabolites, 131 of which exhibit antimycobacterial activity. The integrated dataset pinpoints the fungal genera and chemical classes that most frequently yield potent antimycobacterial hits while simultaneously exposing critical gaps, such as the minimal evaluation of compounds against dormant bacilli and the presence of underexplored ecological niches and fungal genera. Several compounds exhibit potent activity through uncommon mechanisms, including the inhibition of mycobacterial protein tyrosine phosphatases (MptpB/MptpA), protein kinase PknG, ATP synthase and the disruption of mycobacterial DNA via G-quadruplex stabilization. Structure–activity relationship (SAR) trends are highlighted for the most potent agents, illuminating how specific functional groups underpin target engagement and potency. This review also briefly proposes a dereplication strategy and approaches for toxicity mitigation in the exploration of marine-derived fungi's natural products. Through this analysis, we offer insights into the potency and challenges of marine-derived fungi's natural products as hit compounds or scaffolds for further antimycobacterial research.

Keywords: tuberculosis; marine-derived fungi; natural products; antimycobacterial; dormant

1. Introduction

Mycobacterium tuberculosis, the causative agent of tuberculosis, was first reported on in March 1882 by Robert Koch, though the history of tuberculosis began thousands of years ago [1]. The WHO Global Tuberculosis Report 2022 revealed 10.6 million cases, with Southeast Asia being the highest contributing number, followed by Africa and the Western Pacific, indicating that most patients were found in developing countries [2]. Factors such

as poverty, limited access to healthcare, HIV co-infection, malnutrition, and overcrowded living conditions are thought to underlie these high case numbers. Tuberculosis spreads easily via droplets, so such conditions greatly increase the possibility of local epidemics [3]. Additionally, *M. tuberculosis*'s virulence factors, unique pathogenesis, and capacity to enter a non-replicating (dormant) state are major reasons for the disease's persistence and the complexity of its therapy, despite the availability of current medications and nationwide prevention strategies [4–6]. This phenomenon urges the need to find alternatives with a better mode of action to shorten the duration of therapy and simplify the therapy regimen. Also, the emergence of antibiotic-resistant *M. tuberculosis* strains makes the search for alternative antituberculosis agents more imperative than ever.

Marine organism diversity offers rich opportunities to explore novel and medically promising NPs. Although only a tiny fraction of active MF NPs have been identified, they show higher successful application rates than other natural resources, indicating underexplored yet valuable assets [7]. Among various microorganisms that reside independently or in association with other organisms (such as sponges and coral reefs), fungi occupy most of the marine environment. In 2019, marine-derived fungi (MF) NPs accounted for almost 47% of the total marine-derived NPs reported, indicating that MF could be a promising source for NP research, with diverse biological activities encompassing antifungal, antibacterial, cytotoxic, and other biological activities [8]. This suggests that continuing the study of MF is essential to discover new and potentially beneficial bioactive compounds that can help tackle various global challenges, including infectious diseases.

Marine-derived fungi represent a promising source of antimycobacterial activity because they can be cultivated and, in many cases, genetically manipulated to support gram-to-kilogram-scale metabolite production. This review collates and summarizes secondary metabolites with confirmed antimycobacterial activity that have been isolated from marine fungi recovered from diverse habitats, including coastal sediments, mangroves, sponges, and deep-sea environments. Relevant primary papers were retrieved by prioritizing original reports reporting minimum inhibitory (MIC) or half-maximal inhibitory (IC_{50}) concentrations against *Mycobacterium* or validated mycobacterial enzyme targets, with the objective of identifying compounds that warrant further evaluation as lead compounds for alternative antituberculosis development. In this article, we present extensive coverage over the period of 2002–2023, with 131 out of 139 MF NPs exhibiting antimycobacterial properties reported from various MF genera. The compounds are presented in groups based on the common chemical structures, namely, polyketides, peptides, alkaloids, terpenoids, and steroids. We also highlight the novelty of the MF NPs at the time of their being reported as having antimycobacterial properties. The mechanisms of action of some compounds are discussed and the structure–activity relationships of the most potent compounds are also briefly outlined.

2. Antimycobacterial Compounds from Marine-Derived Fungi

2.1. Marine-Derived Fungi and Their Marine Sources

The antimycobacterial MF discussed in this review consist of polyketides (57.58%), alkaloids and peptides (25.76%), terpenoids and steroids (13.64%), and miscellaneous compounds (3.03%) (Figure 1). Polyketides are some of the most varied metabolites, with distinct bioactivities identified in the fungi, which are known to house an immense number of biosynthetic gene clusters coding for numerous secondary metabolites, including polyketide synthase [9,10].

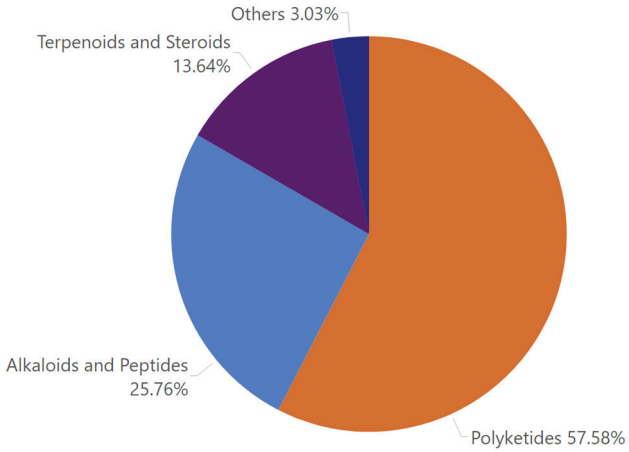

Figure 1. Antimycobacterial compounds from marine-derived fungi according to structure types.

Those antimycobacterials originate from 19 genera, including *Alternaria*, *Arthrinium*, *Ascochyta*, *Aspergillus*, *Coniothyrium*, *Diaporthe*, *Fusarium*, *Gliomastix*, *Metarhizium*, *Nigrospora*, *Penicillium*, *Phoma*, *Pleosporales*, *Sporendonema*, *Talaromyces*, *Tolypocladium*, *Trichoderma*, *Zopfiella*, and *Xylaria*, which were isolated from various marine sources such as marine sediment, mangrove, sponge, alga, coral, sea fan, anemone, and ascidian (Figure 2).

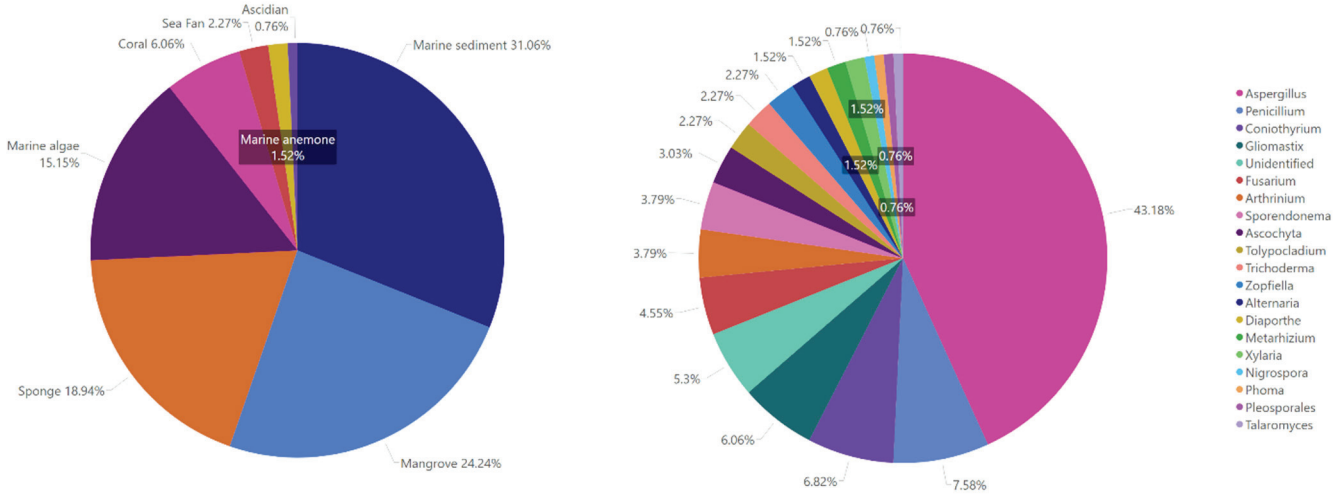

Figure 2. Marine sources of the fungi (**left**) and the antimycobacterial-producing genera (**right**).

2.2. Novel Antimycobacterials from Marine-Derived Fungi

Between 2002 and 2023, roughly half of all marine-fungal antimycobacterial compounds reported each year were new (novel) structures (Figure 3). The majority of these novel compounds were found in 2019, which had the highest number of marine-fungal antimycobacterial compounds reported in a single year. Novel compounds were found more dominantly in the alkaloid and peptide groups compared to other compound types (Figure 4). Polyketides, being the largest group of MF antimycobacterials, are composed of more known compounds than novel ones (Figure 3). This is partly due to polyketides being one of the most abundant metabolites in fungi, leading to their more frequent discovery compared to other compound groups [11].

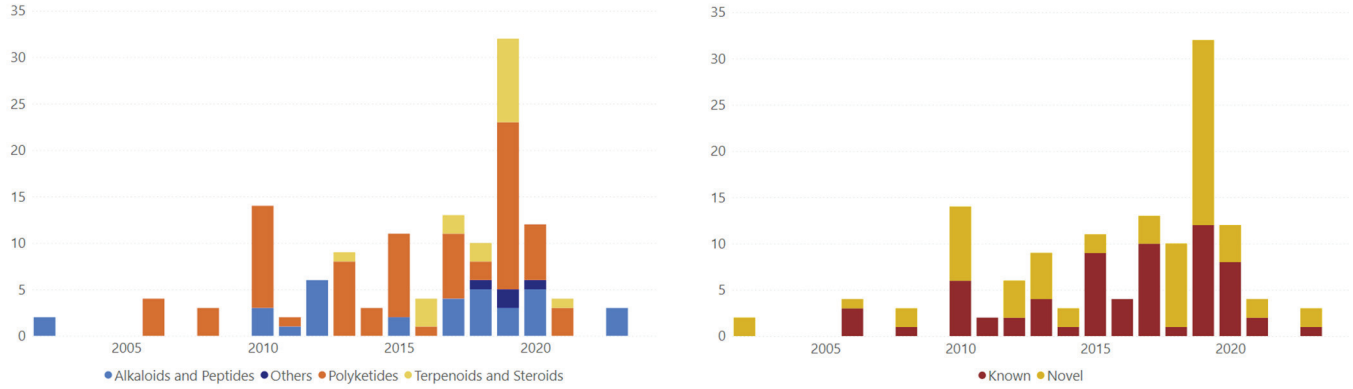

Figure 3. All marine-derived fungi metabolites by type/year (**left**) and novelty/year (**right**).

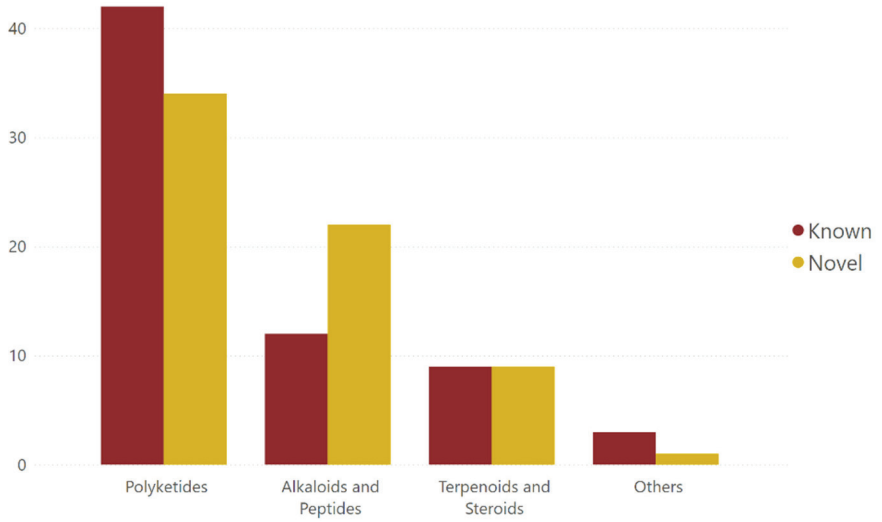

Figure 4. Antimycobacterial compounds based on the novelty as per structure types.

2.3. Antimycobacterial Assay

We found that a total of 131 MF metabolites (out of 139) exhibited antimycobacterial activity, ranging from strong to weak activity (in the sections below, compounds with strong activity will be discussed in more detail; weak compounds will be described more briefly). The compounds were investigated against various *Mycobacterium* strains, such as *M. tuberculosis*, *M. smegmatis*, *M. bovis* BCG, *M. phlei*, and *M. marinum*. Another method that is commonly used to investigate antitubercular activity is the mycobacterial enzyme inhibitor assay. Here, we plot the activity against the *Mycobacterium* strain or specific enzyme (Figure 5).

Our review showed that 39.4% of compounds were tested only against non-*M. tuberculosis* species. Of those tests, *M. phlei* was the most common surrogate (accounting for 43.9% of the non-*M.tb* assays), followed by *M. smegmatis* (28.8%), *M. bovis* BCG (22.7%), and *M. marinum* (4.5%). In comparison, 26.3% of the compounds were tested against *M. tuberculosis* itself, and 25.0% were evaluated in enzymatic assays (e.g., against MptpB, MptpA, or PknG). A smaller fraction of compounds was tested in multiple model types: 7.6% against both *M. tuberculosis* and a surrogate species, 0.76% against both *M. tuberculosis* and a mycobacterial enzyme, and 0.76% against both a surrogate species and an enzyme. This suggests that surrogate models are highly valued as front-line, high-throughput surrogates that combine speed, safety, and cost-efficiency.

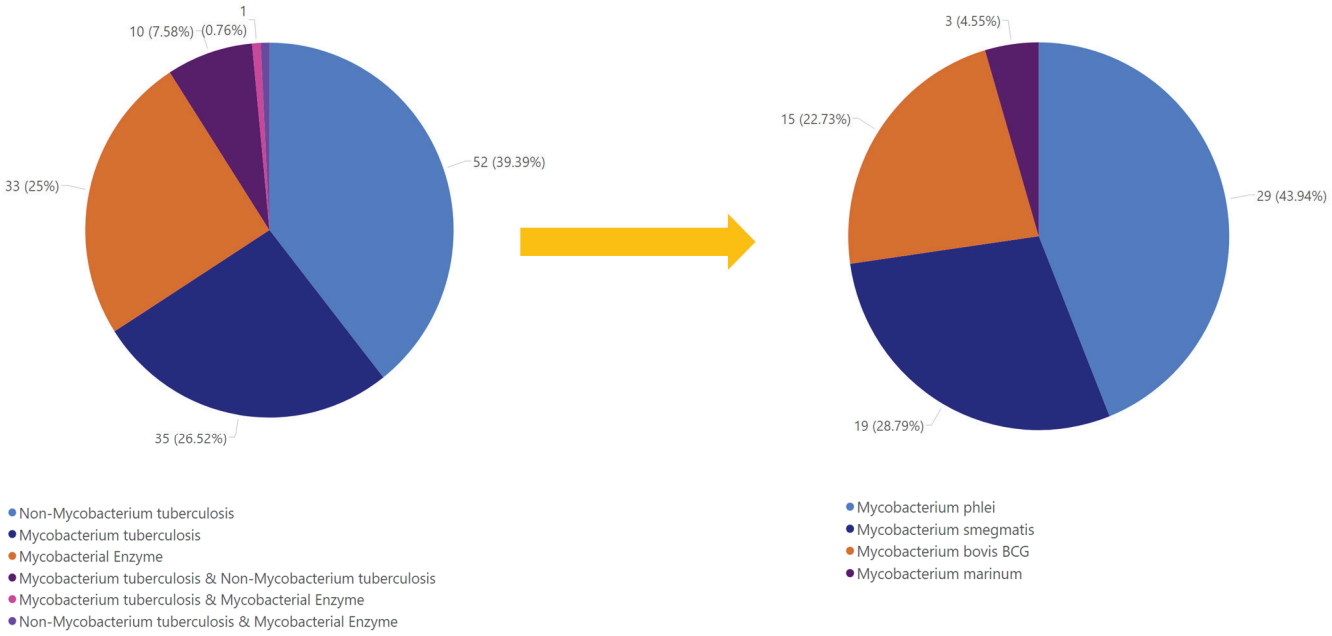

Figure 5. The *Mycobacterium* strains and enzymes used in the antimycobacterial assay.

2.4. Antimycobacterials Against Dormant Phenotypes

Tuberculosis infection is known to be highly influenced by the host's immune status, indicating that the outcome post-invasion may differ from one individual to another. In immunocompetent individuals, infection can remain latent or become active, whereas immunocompromised hosts (e.g., HIV-positive patients) will most likely develop active disease [12,13]. Latent infection occurs when the host's immune system contains the growth of the bacilli, preventing them from proliferating or causing tissue damage. This dormant (non-replicating) state is also thought to contribute to the need for prolonged therapy. Longer treatment duration, in turn, increase the risk of failure due to patient non-compliance, which can be triggered by severe and intolerable side effects of the drugs, the high cost of treatment, and the extended period during which patients remain contagious [12,14]. Vilcheze and co-workers suggested that most of the available antituberculosis therapies were only effective against metabolically active *Mycobacterium* and did not display the same potency against metabolically inactive clusters [15]. Hence, one of the solutions to this problem is to find active compounds that are effective not only against active *Mycobacterium* but also against the non-replicating ones [14].

In this study, we specifically looked for marine-fungal compounds that had been tested against non-replicating (dormant) mycobacteria. Surprisingly, we found only five metabolites that had been evaluated for activity against dormant *Mycobacterium*, and those five did show activity (Figure 6). This highlights a major opportunity in which many marine-fungal metabolites active against replicating *M. tuberculosis* have yet to be tested against dormant bacteria.

2.5. Antimycobacterials from Marine-Derived Fungi

The majority of the MF antimycobacterials were derived from *Aspergillus* (Figure 7), comprising polyketides as the most dominant compounds, followed by alkaloids and peptides and then steroids and terpenoids. The polyketides were also widely distributed in *Penicillium*, *Coniothyrium*, *Gliomastix*, *Fusarium*, *Sporendonema*, and *Ascochyta*, showing the abundance of polyketides in fungal metabolites. We found that the antimycobacterial compounds present in *Arthrinium*, *Tolypocladium*, *Trichoderma*, and *Talaromyces* were predom-

inantly alkaloids and peptides. However, terpenoids and steroids with antimycobacterial properties were only identified in *Gliomastix* and *Diaporthe*, as well as *Aspergillus*.

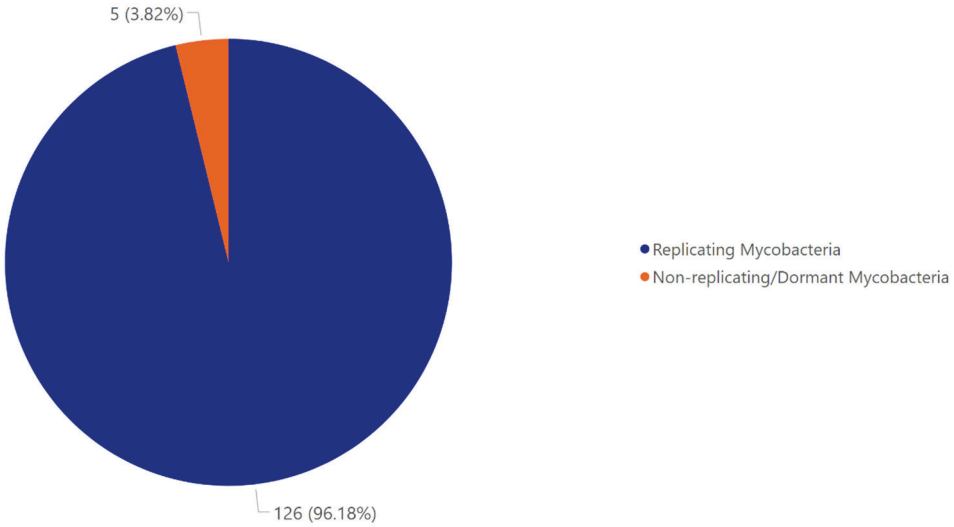

Figure 6. Antimycobacterial MF NPs against replicating and non-replicating *Mycobacterium*.

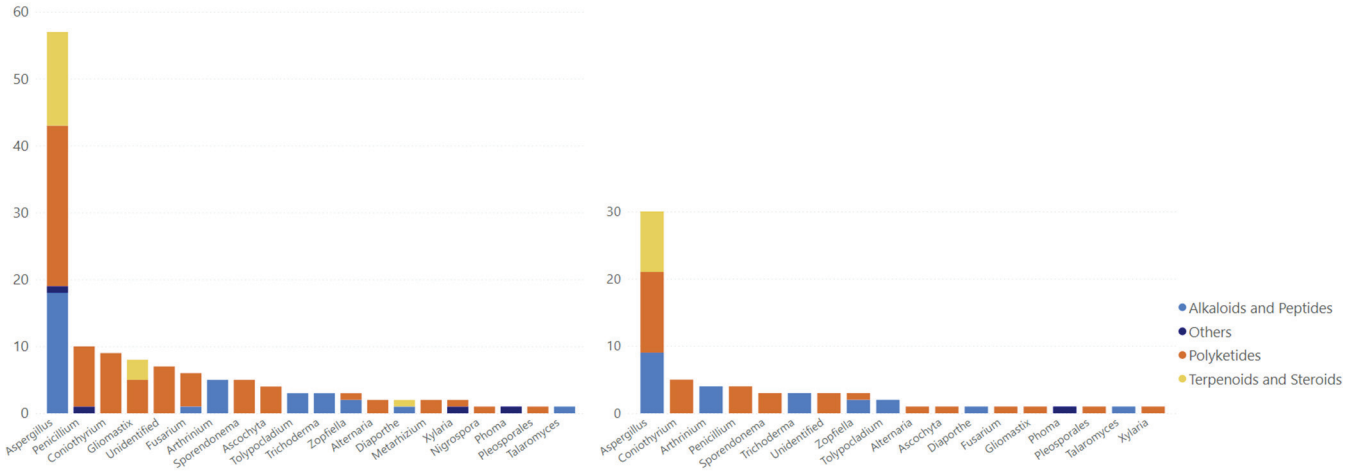

Figure 7. Compound distribution per producing genus: all compounds (**left**); novel compounds only (**right**).

There was a significant disparity in the number of compounds isolated from *Aspergillus* compared to other genera. *Aspergillus* yielded almost 60 antimycobacterial metabolites, whereas other genera produced fewer than 10 antimycobacterial compounds each. However, those compounds from the *Aspergillus* genus were derived from 20 *Aspergillus* species, yielding approximately 5–6 compounds per species, while other genera, such as *Fusarium* and *Penicillium*, consisted of five species each. Some of the genera only consisted of two species, such as *Gliomastix*, *Nigrospora*, and *Zopfiella*, and the rest only consisted of one species each. *Aspergillus* was found to be the most abundant genus in both marine and terrestrial environments and contributed most bioactive secondary metabolites, followed by *Penicillium*, making them the most potential sources for bioactive metabolite exploration, including novel compounds [16–19].

We attempted to plot the distribution of fungi from marine sources to determine the prevalence of fungal genera capable of producing antimycobacterial metabolites (Figure 8). Marine sediment contributed the greatest number of MF species with antimycobacterial

metabolites, followed by mangroves, marine sponges, and marine algae. Fewer MF were obtained from sea fan, coral, marine anemone, and ascidian. *Aspergillus* producing antimycobacterial metabolites was mainly found in marine sediments, mangroves, and sponges. Some of the lesser-studied genera capable of producing novel antimycobacterial compounds were apparently endophytic fungi, such as *Coniothyrium* (derived from marine alga), *Trichoderma* (from marine sponge), *Talaromyces* (from mangrove), *Phoma* (from marine sponge), and *Tolypocladium* (from marine alga). Other promising but underexplored genera capable of producing novel compounds with antimycobacterial activity were derived from marine sediments, including *Arthrinium*, *Pleosporales*, *Sporendonema*, and *Zopfiella*.

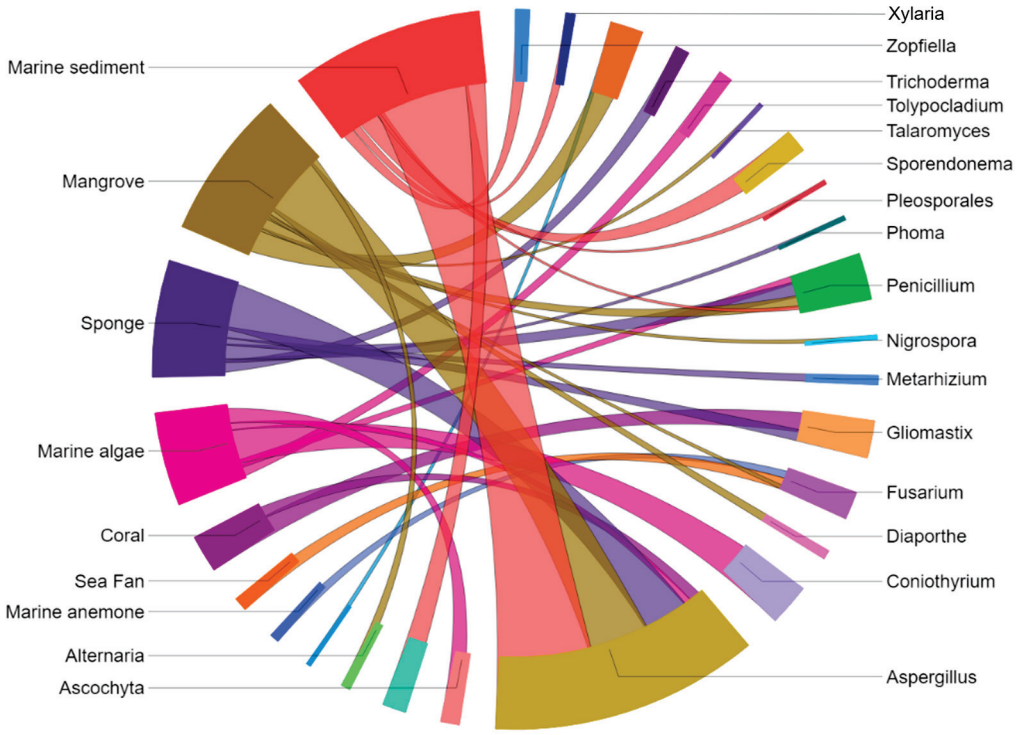

Figure 8. Fungal genera distribution in marine sources.

In the following sub-sections, we describe in detail the activity of each compound, summarized in Tables 1–4. To ease the categorization of the antimycobacterial activity, we recalculated any MIC or IC_{50} value from μg/mL into μM. We classified the antimycobacterial activity into strong, moderate, and weak activity based on the MIC or IC_{50} values. According to Cos and colleagues, anti-infectives from natural products can be categorized as "active" if the IC_{50} value is below 25 μM for pure compounds. Also, according to Elsebai, an inhibition zone of more than >15 mm from a 20 μg/disc of compound was considered to have considerable activity. Hence, we categorized compounds with $IC_{50} \leq 6.25$ μM or inhibition zone > 15 mm as having strong activity, 6.25 μM < $IC_{50} \leq 25$ μM or 10 mm < inhibition zone ≤ 15 mm as having moderate activity, and >25 μM or inhibition zone ≤ 10 mm as having weak activity. If the compound activity was stated by the MIC, then compounds with MIC ≤ 12.5 μM had strong activity, 12.5 μM < MIC ≤ 50 μM had moderate activity, and MIC > 50 μM had weak activity [20].

2.5.1. Polyketides

Two polyketides, alterporriol S (**1**), a novel anthranoid dimer of the alterporriol type featuring a distinctive linkage between C-10 and C-2′, and a previously identified anthraquinone derivative, (+)-a*S*-alterporriol C (**2**), were obtained from the fungus *Alternaria*

sp. SK11, which was collected from the mangrove *Excoecaria agallocha* (Shankou, Guangxi Province, China). Compound **2** displayed strong inhibitory activity against *M. tuberculosis* protein tyrosine phosphatase B (MptpB), a critical virulence factor released by *M. tuberculosis* to circumvent the host's immune response, with an IC_{50} value of 8.70 μM. Meanwhile, compound **1** showed weak inhibitory activity against MptpB, with an IC_{50} value of 64.70 μM [21]. Compound **2** (IC_{50} 8.7 μM) adopted a classical C-10–C-10′ biaryl linkage that locked the two anthraquinone halves into an almost coplanar atropoisomeric scaffold compared with the twisted C-10–C-2′ link in compound **1** (IC_{50} 64.7 μM). The rigidity of compound **2** likely lowered the entropic penalty of binding and enlarged the contiguous π-surface, allowing stronger π-stacking with the hydrophobic P-loop clamp of MptpB and producing a seven-fold potency gain. The coplanar geometry simultaneously positioned an extra quinone carbonyl and a C-11 methoxy-ester to project toward the Lys164/Arg166 oxyanion region adjacent to the catalytic Asp165, creating a bidentate hydrogen-bond/phosphate-mimic network that compound **1**, with its twisted axis, could not achieve efficiently [21–23].

An investigation of the marine alga-derived fungus *Ascochyta salicorniae* isolated from the North Sea, Germany, led to the isolation of new epimeric compounds (ascolactones A (**3**) and B (**4**)), along with other known compounds (hyalopyrone (**5**), ascochitine (**6**), and ascochital (**7**)) [24]. All compounds were tested against various phosphatases, including MptpB. However, only compound **6** exhibited moderate inhibition activity, with an IC_{50} of 11.5 μM, while compounds **4**, **5**, and **7** exhibited weak activities, with IC_{50} values of 95, 87.8, and 61.2 μM, respectively. Compound **3** showed no inhibitory activity. This suggested that the configuration at C-1 of compounds **3** and **4** (*R* or *S* configuration) was crucial for binding and affecting the activity (Figure 9). Within the 8-hydroxynaphthalenone series, the potency increased in the order hyalopyrone (**5**) < ascochital (**7**) < ascochitine (**6**), suggesting a positive contribution of the para-hydroxy-prenyl sidechain present only in **6** [24]. Compound **6** was the most potent member of this set (compounds **3**-**7**). Structurally, it was the only analogue that displayed an ortho-carboxylate flanked by two phenolic hydroxyls on a rigid chromone ring and retained two short, branched alkyl substituents. Together, these features likely match the polar Lys164/Arg166 oxyanion site and the adjacent Phe161/Tyr125 hydrophobic patch identified in multiple MptpB crystal structures, respectively [23,25]. Hyalopyrone (**5**) lacked carboxylate and a second phenol, hence giving it fewer hydrogen-bond donors/acceptors. Ascochital (**7**) preserved the dyad but lost one alkyl chain and planarity because of a saturated side arm. The ascolactones A (**3**) and B (**4**) introduced a spiro-lactone that distorted the phenol/acid alignment and, for epimer A (**3**), pointed the carbonyl lactone away from the catalytic Asp165, probably correlating with the sharp loss of activity. However, these geometric arguments remain hypotheses until corroborated by co-crystallography, docking with proper validation, or site-directed mutagenesis.

Two novel dimeric naphtho-ɣ-pyrones, 8′-*O*-demethylnigerone (**8**) and 8′-*O*-demethylisonigerone (**9**), and a known analogue, rubrofusarin B (**10**) (Figure 9), were isolated from the fungal strain *Aspergillus carbonarius* WZ-4-11, obtained from marine sediment collected at Weizhou Island, Guangxi Province, China. Those compounds exhibited relatively moderate antimycobacterial activity against *M. tuberculosis* H37Rv, with MICs of 43 μM (**8** and **10**) and 21.5 μM (**9**) [26].

A chemical investigation of deep-sea-derived fungus *Aspergillus fischeri* FS452 led to the discovery of six new polypropionate derivatives with a unique long hydrophobic chain, fiscpropionates A–F (**11**–**16**) (Figure 9). Compounds **11**–**14** demonstrated strong to moderate inhibitory activity against MptpB, with IC_{50} values of 5.1, 12, 4.0, and 11 μM, respectively, while compounds **15** and **16** were inactive. Further kinetic experiments revealed that the inhibitory

mechanism was noncompetitive. Interestingly, different activities between compounds **11**–**14** and **16** might have been derived from the different hydrophobicity and hydrophilicity of the opposing terminal functional groups of **11**–**14**. Compounds **11**–**14** possessed polar carboxyl and alkyl chains (C-12 to C-18) at the opposing terminal, while compound **16** was only substituted by the hydrophilic functional group at C-11. Furthermore, compound **14** was more active than **15**, which suggested the significance of the E configuration of the Δ^6 double bond [27]. The potency in the fiscpropionate series likely tracked with the preservation of a tripartite pharmacophore: (1) an E-configured α,β-unsaturated carbonyl flanked by a β-OH; (2) a terminal carboxylate or imide; and (3) a linear, methyl-branched aliphatic chain [27]. Fiscpropionate C (**13**) (IC_{50} 4 μM) was most active likely because of its acyclic backbone, allowing for the optimal alignment of the enone/β-OH while keeping the required acid tail [23,25]. Fiscpropionate A (**11**) (IC_{50} 5.1 μM) was slightly less potent yet still benefited most likely from the intact conjugated β-hydroxy-ketone, whereas fiscpropionate B (**12**) (IC_{50} 12 μM) lost activity after the reduction of this motif, and fiscpropionate D (**14**) (IC_{50} 11 μM) suffered from the weaker, less acidic imide handle. We speculate that the inactive fiscpropionates E (**15**) and F (**16**) abolish key hydrogen-bonding vectors and over-alkylate the chain (or append a bulky aryl), further reducing binding by preventing proper insertion and electrostatic engagement, thus failing to inhibit the phosphatase.

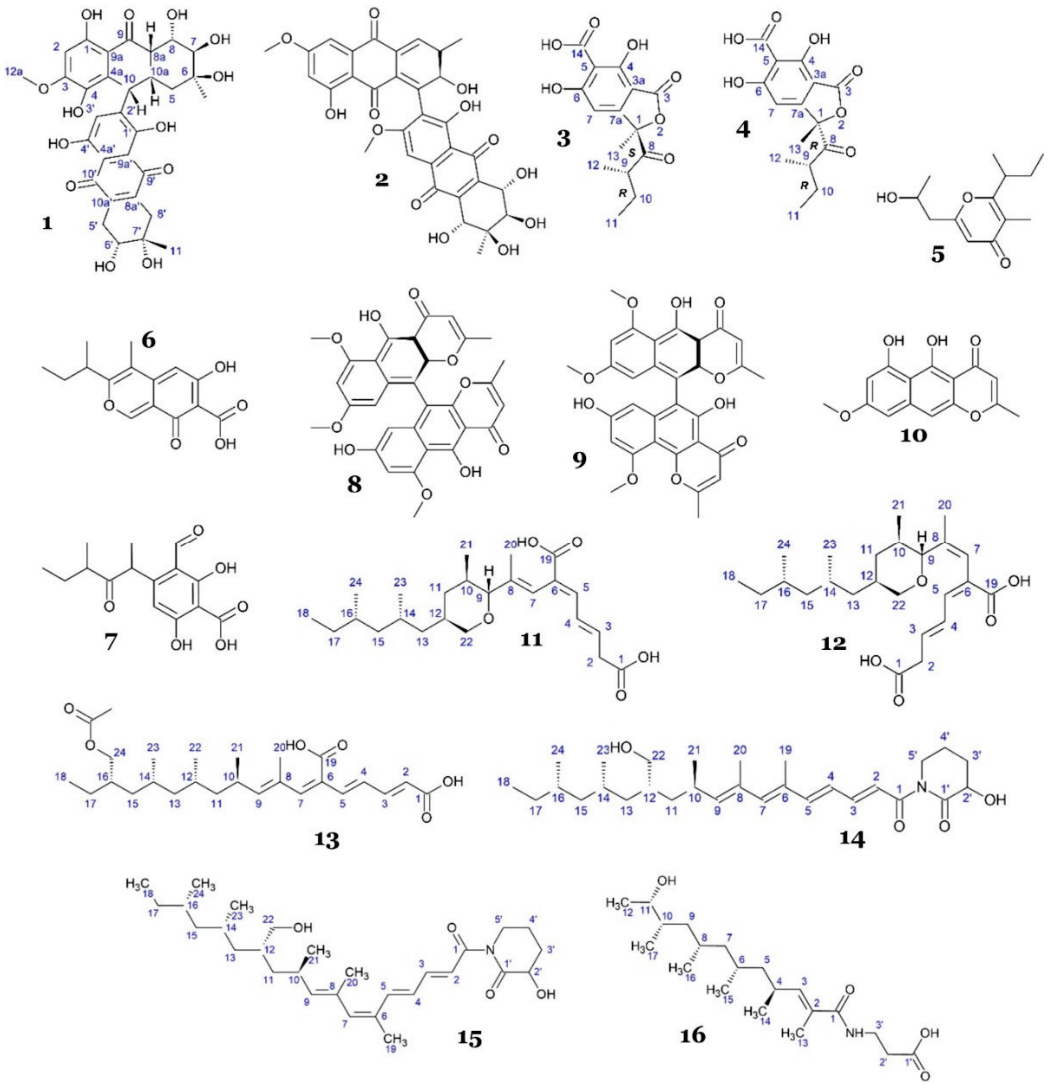

Figure 9. Chemical structures of compounds **1**–**16**.

Song and colleagues reported two compounds, emodin (**17**) and trypacidin (**18**) (Figure 10), discovered from *Aspergillus fumigatus* MF029 isolated from the marine sponge *Hymeniacidon perlevis*, obtained from the Bohai Sea, China. Both compounds demonstrated strong inhibition against *Mycobacterium bovis* BCG, with an MIC value of 1.25 μg/mL (4.6 and 3.63 μM, respectively) [28]. A separate study on **17** as an antimycobacterial revealed that its mechanism of action is targeting the G-quadruplex structure of mycobacterial genetic material. The molecule binds and thermally stabilizes G4 DNA motifs in the *mosR* (redox-stress regulator) and *ndhA* (NADH dehydrogenase) genes of *M. tuberculosis*, which suppresses their transcription and slows bacillary growth [29].

A new tetrahydroxanthone dimer, 5-*epi*-asperdichrome (**19**) (Figure 10), was discovered from *Aspergillus versicolor* HDN1009, isolated from soil around a mangrove area in Guangzhou, China. Compound **19** showed weak inhibitory activity against *Mycobacterium phlei*, with an MIC of 200 μM [30].

Solid rice fermentation of sponge-derived *Aspergillus niger* LS24 led to the discovery of three novel and one known 4-hydroxy-α-pyrones, nipyrones A–C (**20**–**22**) and germicidin C (**23**) (Figure 10), respectively. All compounds demonstrated weak antimycobacterial activity against *M. tuberculosis*, with MICs for **20**, **21**, and **23** of 128 μg/mL (570.66 μM, 537.093 μM, and 702.486 μM, respectively) and **22** of 64 μg/mL (251.652 μM) [31].

Prenylterphenyllin J (**24**) (Figure 10), a prenylated *p-terphenyl* isolated from the mangrove endophytic fungus *Aspergillus candidus* LDJ-5, showed weak antimycobacterial activity against *M. phlei*, with an IC_{50} of 45 μg/mL (99.88 μM). The fungus was obtained from the root of *Rhizophora apiculata* Blume collected from Sanya Bailu Park of Hainan Province, China [32].

A racemic of known dinaphthalenone derivatives, (±)-asperlone A (**25**), (±)-asperlone B (**26**), and (–)-mitorubrin (**27**) (Figure 10), were isolated from the mangrove-derived fungus *Aspergillus* sp. 16-5c. The fungal strain was obtained from leaves of the mangrove *Sonneratia apetala*, collected in Hainan Island, China. The compounds were tested against MptpB and demonstrated strong inhibitory activity, with IC_{50} values of 4.24, 4.32, and 3.99 μM, respectively [33]. Compounds **25**–**27** shared a rigid, nearly coplanar 1,4-diketone core flanked by phenolic or β-hydroxy groups. This carbonyl–phenol dyad is consistent with the dianionic pharmacophore required to engage the Lys164/Arg166 oxyanion pocket of MptpB, and the extended π-surface could plausibly interact with the hydrophobic Phe161–Tyr125 wall characteristic of the enzyme's unusually wide active site [23,34,35]. All three compounds inhibited MptpB in the low-micromolar range, while peripheral variations such as a prenyl side chain (**27**) or methoxy substitution (**25**,**26**) appeared to fine-tune lipophilicity rather than alter the core binding motif [33].

Kamiya and colleagues re-discovered viomellein (**28**) and xanthomegnin (**29**) (Figure 10) from a culture of the *Aspergillus* sp. isolated from marine sponge obtained from Sabang Island, Indonesia [36]. The compounds exhibited antimycobacterial activity against *M. smegmatis* and *M. bovis* BCG in both active and dormant states. Dormant *Mycobacterium* is a state where the cells are metabolically inactive; it has slower replication and phenotypically increased resistance to current antituberculosis treatments [37]. Compound **28** demonstrated stronger activity against *M. bovis* BCG (with MICs of 6.25 μg/mL (11.15 μM) for aerobic and 1.56 μg/mL (2.78 μM) for hypoxic conditions) than against *M. smegmatis* (with MICs of 25 μg/mL (44.6 μM) for aerobic and 50 μg/mL (89.20 μM) for hypoxic conditions), while compound **29** showed the opposite, with an MIC against *M. smegmatis* for both aerobic and hypoxic conditions of 12.5 μg/mL (21.76 μM) and MICs against *M. bovis* BCG for aerobic conditions of 25 μg/mL (43.52 μM) and hypoxic conditions of 50 μg/mL (87.03 μM). The authors suggested that the different tendencies in

the antimycobacterial activity from **28** and **29** against the tested *Mycobacterium* strains may derive from the hydroxyl group at C-9, which makes **28** more active against *M. bovis* BCG than *M. smegmatis*, compared with **29**. Interestingly, compound **28** also exhibited more potent activity against dormant *M. bovis* BCG compared with the control, isoniazid (MIC > 100 μg/mL) [36].

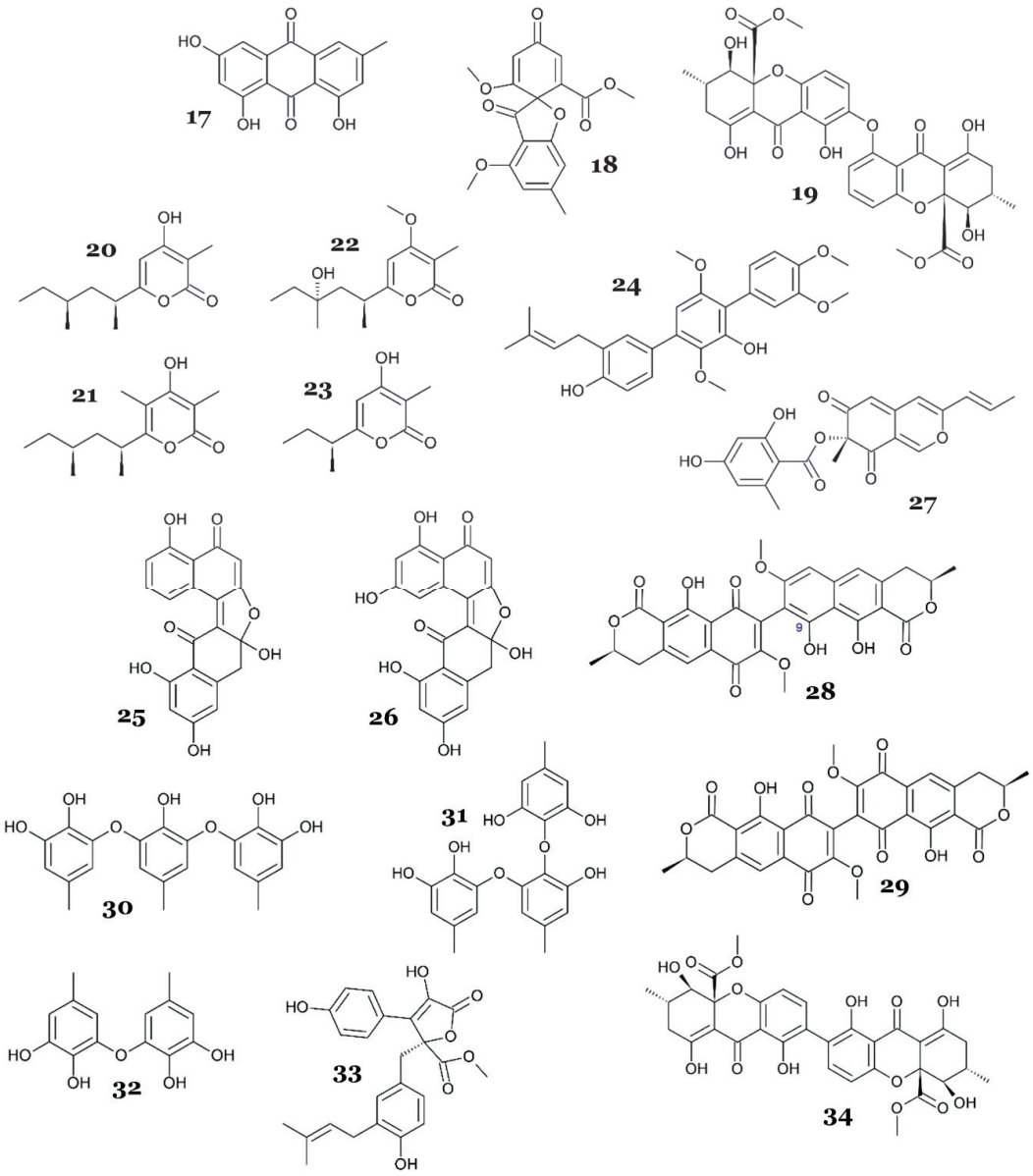

Figure 10. Chemical structures of compounds **17**–**34**.

Two new tris-pyrogallol ethers, sydowiol A (**30**) and C (**31**) (Figure 10), and the known bis-pyrogallol ether, violaceol I (**32**), were discovered from the marine-derived fungus *Aspergillus sydowii* MF357, which was isolated from marine sediment in the East China Sea. Compounds **30** and **31** showed weak inhibitory activity against MptpA, another virulence factor secreted by *M. tuberculosis* that is responsible for tuberculosis pathogenicity by inhibiting phagosome–lysosome fusion [38], with IC_{50} values of 14 μg/mL (36.42 μM) and 24 μg/mL (62.44 μM), respectively, while **32** was inactive. Interestingly, an in vitro assay against *M. tuberculosis* H37Rv (in the same study) showed that compounds **30** and **31** were inactive, while compound **32** was weakly active, with an MIC of 25 μg/mL (95.33 μM). These results suggest that

compounds **30** and **31** do not directly inhibit mycobacterial cells but rather neutralize the effect of MptpA, leading to enhanced host immune response and reduced viable bacteria. Although **32** may not demonstrate any alteration in the survival of mycobacterial cells post-infection of the macrophage, instead, it can directly inhibit mycobacterial cell growth [39]. The inhibition of MptpA likely improves when the scaffold can present three coplanar pyrogallol phenolates. Sydowiol A (**30**), with para/para ether bridges, retained full coplanarity and inhibited the phosphatase at IC_{50} = 14 μg/mL (36 μM). Shifting one bridge to an ortho position in sydowiol C (**31**) twisted the central ring, misaligned one phenolate, and reduced activity to IC_{50} = 24 μg/mL (62 μM), while both compounds showed only weak whole-cell activity (MIC > 50 μg/mL) against *M. bovis* BCG and *M. tuberculosis* H37Rv [39]. Violaceol I (**32**) contained only two pyrogallol units and was inactive against MptpA but displayed modest antibacterial activity (MIC = 25 μg/mL) that was attributed to non-specific oxidative stress. Although a co-crystal was lacking, molecular models based on the MptpA NMR structure (PDB 2LUO) suggested that three well-oriented phenolates were needed to satisfy the Lys21/Arg24 oxyanion site, whereas compounds offering only two donors formed sub-optimal contacts [40]. Hence, we speculate that the enzymatic potency correlated with the ability to deliver a coplanar, tri-dentate phenolate array, whereas whole-cell efficacy was governed by size and polarity rather than precise active-site binding.

A known compound, butyrolactone I (**33**) (Figure 10), was re-discovered from *Aspergillus terreus* SCSIO 41008, a marine-derived fungal isolated from sponge *Callyspongia* sp. obtained from Xuwen County, Guangdong, China. The compound exhibited strong, non-competitive inhibitory activity against MptpB, with an IC_{50} value of 5.11 μM [41]. Butyrolactone I (**33**) possessed a rigid, nearly coplanar γ-butyrolactone–aryl core bearing two conjugated carbonyls and flanking resorcinol OH groups. This carbonyl–phenol dyad is consistent with the dianionic pharmacophore that engages the Lys164/Arg166 oxyanion pocket of MptpB, and its extended π-surface could plausibly interact with the Phe161–Tyr125 hydrophobic wall seen in the crystal structure (PDB 2OZ5) [23,35]. The fused lactone rigidifies the aromatic array, lowering the entropic cost of binding, while the prenyl side chain may occupy part of the shallow lipophilic groove adjacent to Leu199. Together, these features rationalize the low-micromolar potency of butyrolactone I (IC_{50} = 5.11 μM) and mirror the design logic observed for other planar, phenolate-rich inhibitors such as (±)-asperlones (**25**–**26**) and (+)-a*S*-alterporriol C (**2**) [23].

A chemical investigation of the fermentation of marine sponge-derived *Aspergillus* sp. SCSIO XWS03F03 on a solid rice medium led to the isolation of secalonic acid D (**34**) (Figure 10). The bioactivity assay of **34** revealed that it demonstrated strong antimycobacterial activity against *M. tuberculosis*, with an IC_{50} of 1.26 μM [42].

Elsebai and colleagues reported nine compounds with antimycobacterial activity from *Coniothyrium cereale*, isolated from the marine alga *Enteromorpha* sp. collected from Fehmarn, the Baltic Sea. Five compounds were new phenalenone derivatives—(*Z*)-coniosclerodinol (**35**), (15*S*, 17*S*)-(–)-sclerodinol (**36**), conioscleroderolide (**37**), coniosclerodione (**38**), and coniolactone (**39**)—while the rest were known compounds, namely, (–)-7,8-dihydro-3,6-dihydroxy-1,7,7,8-tetramethyl-5*H*-furo-[2′,3′:5,6]naphtho[1,8-bc]furan-5-one (**40**), (–)-scleroderolide (**41**), (–)-sclerodione (**42**), and (–)-trypethelone (**43**) (Figure 11). Those compounds exhibited antimycobacterial activity against *M. phlei*, with the inhibition zone in the range of 10 – 22 mm at a concentration of 20 μg/disc [43,44].

New fusarielins, fusarielin M (**44**) and N (**45**), along with a known fusarielin, fusarielin G (**46**), were isolated from the marine-derived fungus *Fusarium graminearum* SYSU-MS5127, isolated from sea anemone obtained from Laishizhou Island, Shenzhen City, Guangdong Province, China. Those compounds were tested against MptpB, MptpA, and human protein

tyrosine phosphatase 1B (PTP1B). Compound **44** demonstrated strong MptpB inhibitory activity, with an IC_{50} value of 1.05 μM. It also inhibited MptpA (IC_{50} = 23.78 μM) and PTP1B (IC_{50} = 15.74 μM), which indicated high specificity for MptpB over MptpA and PTP1B. Compound **45** showed no measurable inhibition against MptpB (IC_{50} > 40 μM), which suggested that the hydroxyl group at C-3 fusarielin (Figure 11) possessed essential activity as an MptpB inhibitor. Moreover, compound **46** showed less potency as an MptpB inhibitor (IC_{50} = 23.75 μM) compared with **44**, which indicated that MptpB inhibition was hampered by the decalin's moiety epoxy bond group (Figure 11). An investigation of the cellular activity of **44** revealed that **44** restored the MAPK signaling pathway, which was affected by MptpB. Furthermore, an increased concentration of **44** significantly reduced the mycobacterial growth inside the macrophage without altering macrophage viability, which excluded the possibility of cytotoxicity effects of high concentrations of **44** against mycobacterial cells. An in silico study showed that **44** resided inside the MptpB active site, connected by a hydrogen bond from the carboxylate group of **44** with the side chain of Asp165, a residue in the phosphate-binding loop (P-loop). Asp165 was reported as a unique feature of MptpB [45], which may explain the selectivity of **44** as an MptpB inhibitor [46]. Docking into the 2OZ5 crystal structure predicted that its free C-3 β-OH could hydrogen-bond to the catalytic Asp165, while the nearly planar decalin–polyene backbone may extend along the Phe161/Tyr125 hydrophobic wall [23]. O-methylation of the hydroxyl (**45**) or epoxidation of the decalin core (**46**) reduced activity, supporting a working model in which (i) an unhindered C-3 phenolic donor, (ii) a rigid conjugated polyene that fits the shallow lipophilic groove, and (iii) limited steric bulk around the phenol are key for high affinity. Direct co-crystal or kinetic data with MptpA and human PTPs are still lacking, so the exact binding pose remains to be confirmed.

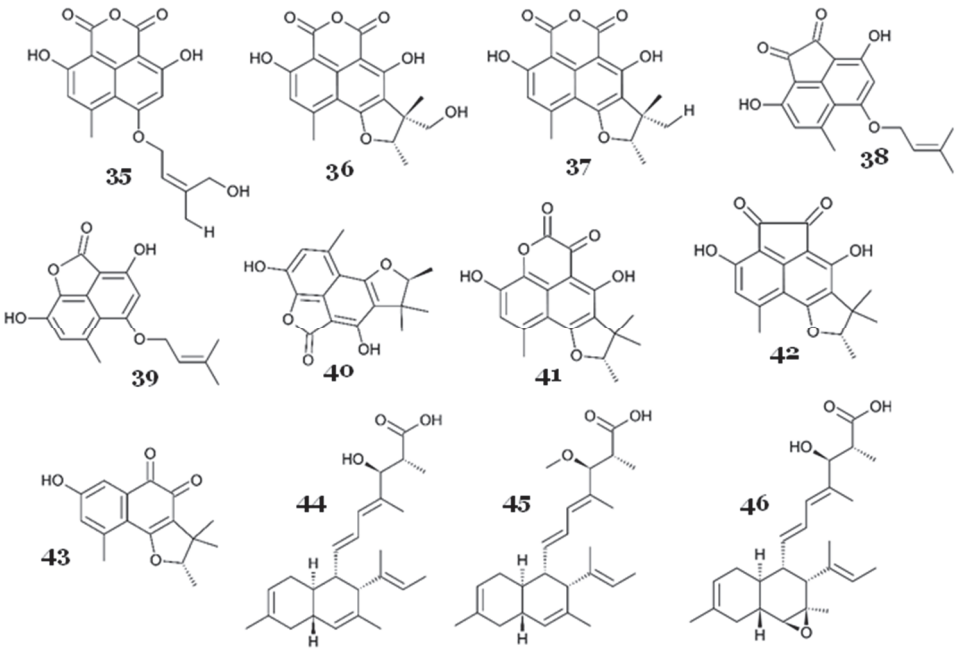

Figure 11. Chemical structures of compounds **35**–**46**.

Three compounds, 9α-hydroxyhalorosellinia (**47**), nigrosporin B (**48**), and anhydrofusarubin (**49**) (Figure 12), were re-discovered from marine-derived *Fusarium* spp. PSU-F14 and PSU-F135, isolated from gorgonian sea fan (*Annella* sp.) collected near Koh Hin Ran Pet, Suratthani Province, Thailand. Those compounds exhibited moderate antimy-

cobacterial activity against *M. tuberculosis* H37Ra, with MIC values of 39, 41, and 47 μM, respectively [47].

An investigation of the extract of *Metarhizium anisopliae* mxh-99, isolated from marine sponge from Naozhou Island, China, led to the isolation of isochaetochromin B_2 (**50**) and ustilaginoidin D (**51**) (Figure 12). Both compounds demonstrated weak antimycobacterial activity against *M. phlei*, with an MIC value of 50 μg/mL (91.15 and 91.49 μM, respectively) [48].

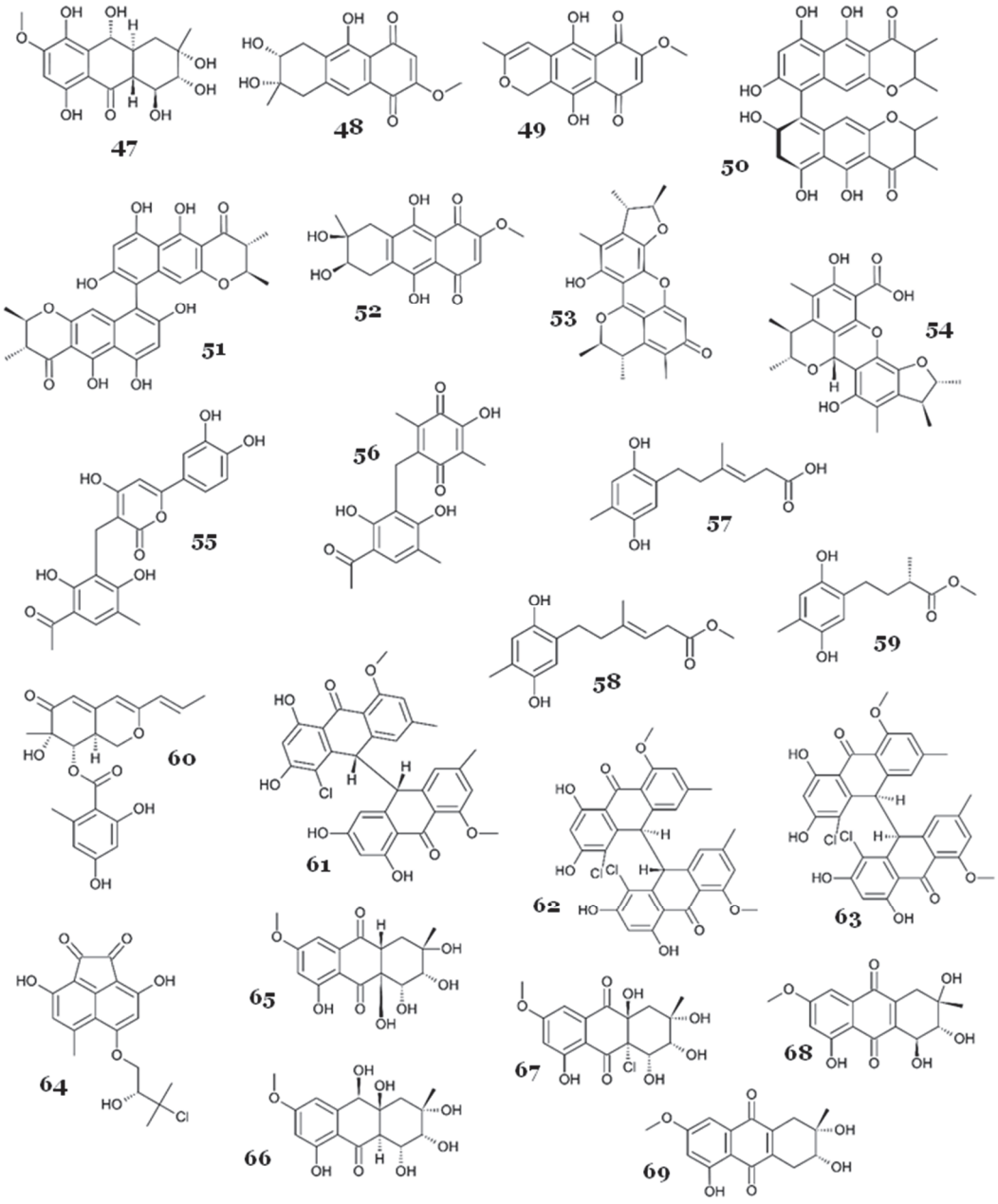

Figure 12. Chemical structures of compounds **47**–**69**.

4-deoxybostrycin (**52**) and its deoxy-derivative, **48**, were isolated from the endophytic fungus *Nigrospora* sp., which was obtained from the decayed wood of mangrove *Kandelia candel* (L.) Druce, collected from Mai Po, Hong Kong. The compounds were tested against various *M.* strains, both sensitive and resistant to antituberculosis agents (drug-resistant). Compound **52** was moderately active against *M. bovis* BCG, *M. tuberculosis* H37Rv, the clinical MDR *M. tuberculosis* strain K2903531 (resistant to SM, INH, RF, and ETH), the clinical MDR *M.*

tuberculosis strain 0907961 (resistant to SM and ETH), the clinical drug-resistant *M. tuberculosis* strain K0903557 (resistant to INH), and clinical drug-sensitive *M. tuberculosis*, with MIC values of 39, 15, <5, 10, 30, and 10 μg/mL, respectively (121.76, 46.83, 15.61, 31.22, 93.67, and 31.22 μM, respectively), while **48** was also moderately active against *M. bovis* BCG, *M. tuberculosis* H37Rv, the clinical MDR *M. tuberculosis* strain K2903531 (resistant to SM, INH, RF, and ETH), the clinical MDR *M. tuberculosis* strain 0907961 (resistant to SM and ETH), and the clinical drug-resistant *M. tuberculosis* strain K0903557 (resistant to INH), with MIC values of 15, 20, 30, 20, and 30 μg/mL, respectively (49.30, 65.73, 98.59, 65.73, and 98.59 μM, respectively) [49].

An endophytic fungus, *Penicillium citrinum* WK-P9, isolated from the marine sponge *Suberea* sp., produced two known citrinin derivatives, penicitrinone A (**53**) and penicitrinol J (**54**) (Figure 12). Compounds **53** and **54** exhibited weak antimycobacterial properties against *M. smegmatis* ATCC607, with an MIC value of 32 μg/mL (84.11 and 75.04 μM, respectively) [50].

Two new peniphenones, peniphenone B (**55**) and C (**56**) (Figure 12), with MptpB inhibitory activity were discovered from *Penicillium dipodomyicola* HN4-3A. The fungal strain was isolated from the stem of *Acanthus ilicifolius* obtained from the South China Sea, Hainan Province, China. Compounds **55** and **56** exhibited strong inhibitory properties against MptpB in vitro, with IC_{50} values of 0.16 and 1.37 μM, respectively [51]. Compound **55** was 9-fold more potent than its oxidized analogue **56**. A plausible explanation is that **55** retains three phenolic OH groups (one on the lower resorcinol ring and an ortho-dihydroxyl (catechol) pair on the upper ring) and an ether oxygen, in which these four hetero-atoms provide multiple hydrogen-bond donors/acceptors that could engage the polar residues lining the MptpB active site, while the fully aromatic, conjugated scaffold supplies an extended π-surface for hydrophobic or π-stacking contacts with residues such as Tyr125 and Phe161 that flank the shallow binding cleft [34,35]. In compound **56**, oxidation of the upper catechol to a para-benzoquinone replaced two hydroxyl donors with carbonyl groups and left only a single phenol available for deprotonation; hence, concomitant electron withdrawal was expected to lower the basicity of the remaining OH and central benzophenone carbonyl, cumulatively weakening potential hydrogen-bond and electrostatic interactions [51]. Because the overall backbone and substitution pattern remained similar, the loss of potency in compound **56** can be reasonably attributed to the reduced number and strength of polar contacts rather than to major conformational effects.

An Antarctica-associated fungi, *Penicillium* sp. HDN151272, isolated from unidentified sponge, produced three new polyketides, ketidocillinones A–C (**57**–**59**). All compounds were tested against *M. phlei*, with only **58** and **59** exhibiting antimycobacterial activity, with MIC values of 3.13 and 6.25 μg/mL, respectively (11.84 and 26.23 μM, respectively). Compound **57** did not show inhibition activity against *M. phlei*, which indicated the importance of the methoxy group of compounds **58** and **59** (Figure 12) for the antimycobacterial activity [52].

A mangrove-associated fungus, *Penicillium pinophilum* SCAU037, produced a known hydrogenated azaphilone, Sch725680 (**60**), which exhibited moderate antimycobacterial activity against *M. smegmatis*, with an MIC value of 23.5 μM [53].

Further chemical investigation of a marine alga-derived *Penicillium roseopurpureum* KP1-135C extract led to the isolation of three halogenated bianthrones, neobulgarones D–F (**61**–**63**), and their antibacterial activities were investigated. The study reported that only the *cis* isomers, compounds **61** and **63** (Figure 12), exhibited weak antimycobacterial activity against *M. tuberculosis* H37Ra ATCC 25177, with IC_{50} values of 46.1 and 31.1 μM, respectively. The *trans* isomer, **62**, however, did not show antimycobacterial activity but exhibited moderate inhibition against methicillin-resistant *Staphylococcus aureus*, which indicated that the *cis-trans* configuration of neobulgarones may affect the selectivity of antibacterial–antimycobacterial activity [54].

A marine sediment-derived *Pleosporales* sp. HDN1811400 produced a new phenalenone derivative, peniciphenalenin G (**64**), and two known analogues, **36** and **38**, which exhibited antimycobacterial activity against *M. phlei*, with MIC values of 50, 25, and 25 μM, respectively [55].

New anthraquinone derivatives, auxarthrols D (**65**), F (**66**), and G (**67**), along with two known analogues, 4-dehydroxyaltersolanol A (**68**) and altersolanol B (**69**) (Figure 12), were isolated from *Sporendonema casei* HDN16-802, which was obtained from marine sediment from Liaoning Province, China. All compounds exhibited antimycobacterial activity against *M. phlei*, with MIC values in the range of 25–200 μM. However, only **69** exhibited inhibitory activity against *M. tuberculosis*, with an MIC value of 20 μM [56].

Marine-derived fungus *Zopfiella marina* produced a new salicylaldehyde derivative, 2-hydroxy-6-((1E,3E)-7-hydroxyundeca-1,3dienyl)benzaldehyde (**70**) (Figure 13), with weak antimycobacterial activity against *M. tuberculosis* H37Ra, with an MIC value of 25 μg/mL (86.69 μM) [57].

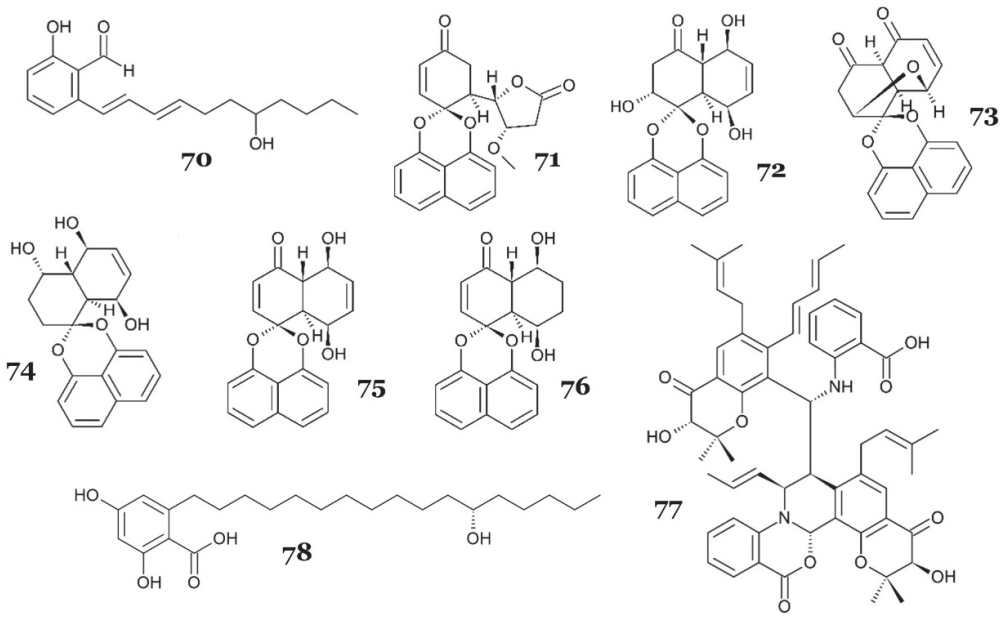

Figure 13. Chemical structures of compounds **70**–**78**.

Bunyapaiboonsri and colleagues reported an unidentified mangrove-associated fungus BCC 25093, which produced two new palmarumycins, palmarumycins P1 (**71**) and P3 (**72**) (Figure 13), along with two known palmarumycins, palmarumycins CP3 (**73**) and CR1 (**74**), and two known decaspirones, decaspirones A (**75**) and C (**76**), with potential antimycobacterial activity. The strongest activity was shown by **71** and **75**, with an IC_{50} value of 1.56 μg/mL (4.23 and 4.64 μM, respectively), followed by **73** and **76** (IC_{50} = 3.13 μg/mL or 9.36 and 9.25 μM, respectively) and **72** and **74** (IC_{50} = 12.5 μg/mL or 35.28 and 36.51 μM, respectively) [58].

Another unidentified, novel, marine-derived fungus strain 110162 in the Eurotiomycetes class was reported to produce a racemic of prenylated polyketide dimer, oxazinin A (**77**), with a pentacyclic structure formed with an unusual combination of benzoxazine, isoquinoline, and a pyran ring (Figure 13). Compound **77** also exhibited a strong antimycobacterial activity against *M. tuberculosis*, with an IC_{50} value of 2.9 μM [59].

Penixylarin C (**78**), a novel alkyl aromatic compound (Figure 13), was isolated from a mangrove-associated fungus *Xylaria* sp. HDN13-249. It exhibited a strong antimycobacterial activity against *M. phlei*, with an MIC value of 6.25 μM [60].

Table 1. Polyketide NPs with antimycobacterial activity from MF.

No.	Metabolites [Novelties at the Time of Isolation]	Producing Strains	Marine Sources	Fermentation Media and Method	Tested Against Mycobacterium Strain/Mycobacterial Enzyme	Potency	Mechanism of Action	Ref.
1	alterporriol S [N] [a]	*Alternaria* sp. SK1	Root of mangrove *Excoecaria agallocha*	Potato glucose liquid medium, static condition, 26 °C, 4 weeks	Mycobacterial Enzyme MptpB	IC_{50} = 64.7 μM	Inhibit virulence factor MptpB	[21]
2	(+)-a*S*-alterporriol C [K] [b]					IC_{50} = 8.7 μM		
3	ascolactone A [N]	*Ascochyta salicorniae*	Marine alga *Ulva* sp.	Solid medium (biomalt extract 2%, agar 1.5%, ASW * 80%), static condition, room temp., 52 days	Mycobacterial Enzyme MptpB	NA **	-	[24]
4	ascolactone B [N]					IC_{50} = 95 μM	Inhibit virulence factor MptpB	
5	hyalopyrone [K]					IC_{50} = 87.8 μM		
6	ascochitine [K]					IC_{50} = 11.5 μM		
7	ascochital [K]					IC_{50} = 61.2 μM		
8	8′-*O*-demethylnigerone [N]	*Aspergillus carbonarius* WZ-4-11	Marine sediment	Liquid medium (glucose 2%, peptone 0.5%, malt extract 0.3%, yeast extract 0.3%, sea water pH 7.0), static condition, 24 °C, 30 days	*M. tuberculosis* H37Rv	IC_{50} = 43 μM	NR ***	[26]
9	8′-*O*-demethylisonigerone [N]					IC_{50} = 21.5 μM		
10	rubrofusarin B [K]					IC_{50} = 43 μM		
11	fiscpropionate A [N]	*Aspergillus fisheri* FS452	Marine sediment	Solid medium (rice 250 g, 400 mL H_2O, natural sea salt 0.3%), static condition, room temp., 30 days	Mycobacterial Enzyme MptpB	IC_{50} = 5.1 μM	Inhibit virulence factor MptpB	[27]
12	fiscpropionate B [N]					IC_{50} = 12 μM		
13	fiscpropionate C [N]					IC_{50} = 4 μM		
14	fiscpropionate D [N]					IC_{50} = 11 μM		
15	fiscpropionate E [N]					NA	-	
16	fiscpropionate F [N]					NA	-	
17	emodin [K]	*Aspergillus fumigatus* MF029	Marine sponge *H. perleve*	Solid medium (160 g rice, 200 mL H_2O), static condition, 28 °C, 30 days	*M. bovis* BCG	IC_{50} = 1.25 μg/mL (4.6 μM)	Bind and thermally stabilize G4 DNA motifs in the *mosR* (redox-stress regulator) and *ndhA* (NADH dehydroge-nase) genes of *M. tuberculosis*	[28,29]
18	trypacidin [K]					IC_{50} = 1.25 μg/mL (3.63 μM)	NR	

Table 1. *Cont.*

No.	Metabolites [Novelties at the Time of Isolation]	Producing Strains	Marine Sources	Fermentation Media and Method	Tested Against Mycobacterium Strain/Mycobacterial Enzyme	Potency	Mechanism of Action	Ref.
19	5-*epi*-asperdichrome [N]	*Aspergillus versicolor* HDN1009	Soil around mangrove	Liquid medium (maltose 2%, mannitol 2%, glucose 1%, monosodium glutamate 1%, $MgSO_4.7H_2O$ 0.03%, KH_2PO_4 0.05%, yeast extract 0.3%, corn steep liquor 0.1%, ASW), static condition, 28 °C, 14 days	*M. phlei*	MIC = 200 μM	NR	[30]
20	nipyrone A [N]	*Aspergillus niger* LS24	Marine sponge *Haliclona* sp.	Solid medium (100 g rice, 160 mL H_2O), static condition, 28 °C, 30 days	*M. tuberculosis* H37Rv	MIC = 128 μg/mL (570.66 μM)	NR	[31]
21	nipyrone B [N]					MIC = 128 μg/mL (537.093 μM)		
22	nipyrone C [N]					MIC = 64 μg/mL (251.652 μM)		
23	germicidin C [K]					MIC = 128 μg/mL (702.486 μM)		
24	prenylterphenyllin J [K]	*Aspergillus candidus* LDJ-5	Root of mangrove *Rhizophora apiculata* Blume	Liquid medium (mannitol 2%, monosodium glutamate 1%, maltose 3%, yeast extract 0.3%, glucose 1%, corn steep liquor 0.1%, magnesium sulfate heptahydrate 0.03%, monopotassium phosphate 0.05%, H_2O), static condition, 28 °C, 30 days	*M. phlei*	MIC = 45 μg/mL (99.88 μM)	NR	[32]
25	(±)-asperlone A [K]	*Aspergillus* sp. 16-5c	Leaves of mangrove *Sonneratia apetala*	Liquid medium (glucose 1.5%, sea salt 0.3% in potato infusion), static condition, 28 °C, 30 days	Mycobacterial Enzyme MptpB	IC_{50} = 4.24 μM	Inhibit virulence factor MptpB	[33]
26	(±)-asperlone B [K]					IC_{50} = 4.32 μM		
27	(–)-mitorubrin [K]					IC_{50} = 3.99 μM		

Table 1. *Cont.*

No.	Metabolites [Novelties at the Time of Isolation]	Producing Strains	Marine Sources	Fermentation Media and Method	Tested Against Mycobacterium Strain/Mycobacterial Enzyme	Potency	Mechanism of Action	Ref.
28	viomellein [K]	*Aspergillus* sp. 02E28_2-2	Unidentified marine sponge	Solid medium (250 g unpolished rice, 500 ASW), static condition, 30 °C, 14 days	*M. smegmatis* mc^2155	MIC aerobic = 25 μg/mL (44.6 μM); hypoxic = 50 μg/mL (89.20 μM)	NR	[36]
					M. bovis BCG	MIC aerobic = 6.25 μg/mL (11.15 μM); hypoxic = 1.56 μg/mL (2.78 μM)		
29	xanthomegnin [K]				*M. smegmatis* mc^2155	MIC aerobic = 12.5 μg/mL (21.76 μM); hypoxic = 12.5 μg/mL (21.76 μM)		
					M. bovis BCG	MIC aerobic = 25 μg/mL (43.52 μM); hypoxic = 50 μg/mL (87.03 μM)		
30	sydowiol A [N]	*Aspergillus sydowii* MF357	Marine sediment	Solid medium (130 g rice, 80 mL ASW), static condition, 25 °C, 20 days	Mycobacterial Enzyme MptpA	IC_{50} = 14 μg/mL (36.42 μM)	Inhibit virulence factor MptpA	[39]
					M. bovis BCG	NA	-	
					M. tuberculosis H37Rv	NA	-	
31	sydowiol C [N]				Mycobacterial Enzyme MptpA	IC_{50} = 24 μg/mL (62.44 μM)	Inhibit virulence factor MptpA	
					M. bovis BCG	MIC = 100 μg/mL (260.16 μM)	NR	
					M. tuberculosis H37Rv	NA	-	
32	violaceol I [K]				Mycobacterial Enzyme MptpA	NA	-	
					M. bovis BCG	NA	-	
					M. tuberculosis H37Rv	MIC = 25 μg/mL (95.33 μM)	NR	

Table 1. *Cont.*

No.	Metabolites [Novelties at the Time of Isolation]	Producing Strains	Marine Sources	Fermentation Media and Method	Tested Against Mycobacterium Strain/Mycobacterial Enzyme	Potency	Mechanism of Action	Ref.
33	butyrolactone I [K]	*Aspergillus terreus* SCSIO 41008	Marine sponge *Callyspongia* sp.	Liquid medium (potato 20%, peptone 0.5%, mannitol 2%, maltose 2%, glucose 2%, monosodium glutamate 0.5%, yeast extract 0.3%, sea salt 2%) in fermenter (28 °C, 135 rpm, 12 L/min aseptic air, 3 Mpa for 7 days)	Mycobacterial Enzyme MptpB	IC_{50} = 5.11 μM	Inhibit virulence factor MptpB	[41]
34	secalonic acid D [K]	*Aspergillus* sp. SCSIO XWS03F03	Unidentified marine sponge	Solid medium (200 g rice, 2 g sea salt, 200 mL H_2O, supplemented with NaCl 1%), static condition, 25 °C, 45 days	*M. tuberculosis*	IC_{50} = 1.26 μM	NR	[42]
35	(Z)-coniosclerodinol [N]	*Coniothyrium cereale*	Marine alga *Enteromorpha* sp.	Solid BMS medium, static condition, room temp., 40 days	*M. phlei*	ZI = 16 mm	NR	[43,44]
36	(15*S*, 17*S*)-(–)-sclerodinol [N]					ZI = 20 mm		
37	coniosclerodinol [N]					ZI = 10 mm		
38	coniosclerodione [N]					ZI = 12 mm		
39	coniolactone [N]					ZI = 22 mm		
40	(–)-7,8-dihydro-3,6-dihydroxy-1,7,7,8-tetramethyl-5*H*-furo-[2′,3′:5,6]naphtho[1,8-bc]furan-5-one [K]					ZI = 12 mm		
41	(–)-scleroderolide [K]					ZI = 14 mm		
42	(–)-sclerodione [K]					ZI = 10 mm		
43	(–)-trypethelone [K]					ZI = 18 mm		
44	fusarielin M [N]				Mycobacterial Enzyme MptpB	IC_{50} = 1.05 μM	Inhibit virulence factor MptpB	[46]
					Mycobacterial Enzyme MptpA	IC_{50} = 23.78 μM	Inhibit virulence factor MptpA	
45	fusarielin N [N]				Mycobacterial Enzyme MptpB	NA	-	
					Mycobacterial Enzyme MptpA	NA	-	
46	fusarielin G [K]				Mycobacterial Enzyme MptpB	IC_{50} = 23.75 μM	Inhibit virulence factor MptpB	
					Mycobacterial Enzyme MptpA	NA	-	

Table 1. *Cont.*

No.	Metabolites [Novelties at the Time of Isolation]	Producing Strains	Marine Sources	Fermentation Media and Method	Tested Against Mycobacterium Strain/Mycobacterial Enzyme	Potency	Mechanism of Action	Ref.
47	9α-hydroxyhalorosellinia [K]				*M. tuberculosis* H37Ra	MIC = 39 μM		
					M. bovis BCG	NA		
					M. tuberculosis H37Rv	NA		
					Clinical MDR *M. tuberculosis* strain (K2903531, resistant to SM, INH, RFP, and EMB)	NA		
					Clinical MDR *M. tuberculosis* strain (0907961, resistant to SM and EMB)	NA		
					Clinical drug-resistant *M. tuberculosis* strain (K0903557, resistant to INH)	NA		
48	nigrosporin B [K]	*Fusarium* spp. PSU-F15	Marine gorgonian sea fan *Annella* sp.	Liquid medium (potato dextrose broth), static condition, room temp., 28 days	*M. tuberculosis* H37Ra	MIC = 41 μM	NR	[47,49]
					M. bovis BCG	MIC = 15 μg/mL (49.30 μM)		
					M. tuberculosis H37Rv	MIC = 20 (65.73 μM) μg/mL		
					Clinical MDR *M. tuberculosis* strain (K2903531, resistant to SM, INH, RFP, and EMB)	MIC = 30 (98.59 μM) μg/mL		
					Clinical MDR *M. tuberculosis* strain (0907961, resistant to SM and EMB)	MIC = 20 (65.73 μM) μg/mL		
					Clinical drug-resistant *M. tuberculosis* strain (K0903557, resistant to INH)	MIC = 30 (98.59 μM) μg/mL		
49	anhydrofusarubin [K]				*M. tuberculosis* H37Ra	MIC = 87 μM		
					M. bovis BCG	NA		
					M. tuberculosis H37Rv	NA		
					Clinical MDR *M. tuberculosis* strain (K2903531, resistant to SM, INH, RFP, and EMB)	NA		
					Clinical MDR *M. tuberculosis* strain (0907961, resistant to SM and EMB)	NA		
					Clinical drug-resistant *M. tuberculosis* strain (K0903557, resistant to INH)	NA		

Table 1. *Cont.*

No.	Metabolites [Novelties at the Time of Isolation]	Producing Strains	Marine Sources	Fermentation Media and Method	Tested Against Mycobacterium Strain/Mycobacterial Enzyme	Potency	Mechanism of Action	Ref.
50	isochaetochromin B_2 [K]	*Metarhizium anisopliae* mxh-99	Unidentified marine sponge	Liquid medium (mannitol 2%, maltose 2%, glucose 1%, monosodium glutamate 1%, KH_2PO_4 0.05%, $MgSO_4.7H_2O$ 0.03%, yeast extract 0.3%, corn steep liquor 0.1%, ASW pH 6.5), agitated condition (165 rpm), 28 °C, 8 days	*M. phlei*	MIC = 50 μg/mL (91.15 μM)	NR	[48]
51	ustilaginoidin D [K]					MIC = 50 μg/mL (91.49 μM)		
52	4-deoxybostrycin [K]	*Nigrospora* sp.	Unidentified sea anemone	Fermentation from *Nigrospora* sp. was not explained in detail	*M. bovis* BCG	MIC = 39 μg/mL (121.76 μM)	NR	[49]
					M. tuberculosis H37Rv	MIC = 15 μg/mL (46.83 μM)		
					Clinical MDR *M. tuberculosis* strain K2903531 (resistant to SM, INH, RF, and ETH)	MIC = < 5 μg/mL (< 15.61 μM)		
					Clinical MDR *M. tuberculosis* strain 0907961 (resistant to SM and ETH)	MIC = 10 μg/mL (31.22 μM)		
					Clinical drug-resistant *M. tuberculosis* strain K0903557 (resistant to INH)	MIC = 30 μg/mL (93.67 μM)		
					Clinical drug-sensitive *M. tuberculosis*	MIC = 10 μg/mL (31.22 μM)		
53	penicitrinone A [K]	*Penicillium citrinum* WK-P9	Marine sponge *Suberea* sp.	Liquid medium (malt extract broth), static condition, 24 °C, 12 days	*M. smegmatis* ATCC 607	MIC = 32 μg/mL (84.11 μM)	NR	[50]
54	penicitrinol J [K]					MIC = 32 μg/mL (75.04 μM)		
55	peniphenone B [N]	*Penicillium dipodomyicola* HN4-3A	Stem of mangrove *Acanthus ilicifolius*	Liquid medium (20 g glucose, 2 g sea salt in 1 L of potato infusion), static condition, 25–30 °C, 30 days	Mycobacterial Enzyme MptpB	IC_{50} = 0.16 μM	Inhibit virulence factor MptpB	[51]
56	peniphenone C [N]					IC_{50} = 1.37 μM		

Table 1. *Cont.*

No.	Metabolites [Novelties at the Time of Isolation]	Producing Strains	Marine Sources	Fermentation Media and Method	Tested Against Mycobacterium Strain/Mycobacterial Enzyme	Potency	Mechanism of Action	Ref.
57	ketidocillinone A [N]	*Penicillium* sp. HDN151272	Unidentified marine sponge	Liquid medium ((glucose 1%, maltose 2%, mannitol 2%, monosodium glutamate 1%, KH_2PO_4 0.05%, $MgSO_4.7H_2O$ 0.03%, corn steep liquor 0.1%, yeast extract 0.3% in addition to natural sea water pH 6.5), agitated condition, 28 °C, 9 days	*M. phlei*	NA	NR	[52]
58	ketidocillinone B [N]					MIC = 3.13 μg/mL (11.84 μM)		
59	ketidocillinone C [N]					MIC = 6.25 μg/mL (26.23 μM)		
60	Sch725680 [K]	*Penicillium pinophilum* SCAU037	Roots of mangrove *Rhizophora stylosa*	Liquid medium (yeast extract 0.3%, malt extract 0.3%, peptone 0.5%, glucose 2%, sorbitol 2%, sea salt 3%), static condition, 28 °C, 30 days	*M. smegmatis* ATCC 607	23.5 μM	NR	[53]
61	neobulgarone D [K]	*Penicillium roseopurpureum* KP1-13	Brown alga *Petalonia fascia*	Liquid medium (malt extract broth 2%), agitated condition at 150 rpm, room temp., 14 days	*M. tuberculosis* H37Ra ATCC 25177	IC_{50} = 46.1 μM	NR	[54]
62	neobulgarone E [K]					NA		
63	neobulgarone F [K]					IC_{50} = 31.1 μM		
64	peniciphenalenin G [N]	*Pleosporales* sp. HDN1811400	Marine sediment	Liquid medium (yeast extract 0.3%, malt extract 0.3%, peptone 0.5%, glucose 2% dissolved in naturally collected seawater), static condition, 28 °C, 35 days	*M. phlei*	MIC = 50 μM	NR	[55]
65	auxarthrol D [N]	*Sporendonema casei* HDN16-802	Marine sediment	Solid medium (53 g oatmeal, 125 mL natural seawater), static condition, room temp., 30 days	*M. phlei*	MIC = 25 μM	NR	[56]
					M. tuberculosis	NA		
66	auxarthrol F [N]				*M. phlei*	MIC = 200 μM		
					M. tuberculosis	NA		
67	auxarthrol G [N]				*M. phlei*	MIC = 50 μM		
					M. tuberculosis	NA		
68	4-dehydroxyaltersolanol A [K]				*M. phlei*	MIC = 25 μM		
					M. tuberculosis	NA		
69	altersolanol B [K]				*M. phlei*	MIC = 25 μM		
					M. tuberculosis	MIC = 20 μM		

Table 1. *Cont.*

No.	Metabolites [Novelties at the Time of Isolation]	Producing Strains	Marine Sources	Fermentation Media and Method	Tested Against Mycobacterium Strain/Mycobacterial Enzyme	Potency	Mechanism of Action	Ref.
70	2-hydroxy-6-((1E,3E)-7-hydroxyundeca-1,3dienyl)benzaldehyde [N]	*Zopfiella marina*	Marine sediment	Liquid medium (glucose 4%, yeast extract 0.5%, $MgSO_4.7H_2O$ 0.1%, KH_2PO_4 0.1% in distilled water), static condition, 25 °C, 35 days	*M. tuberculosis* H37Ra	MIC = 25 μg/mL (86.69 μM)	NR	[57]
71	palmarumycin P1 [N]	Unidentified marine-derived fungus BCC 250093	Unidentified mangrove wood	Liquid medium (potato dextrose broth), agitated condition at 200 rpm, 25 °C, 20 days	*M. tuberculosis* H37Ra	MIC = 1.56 μg/mL (4.23 μM)	NR	[58]
72	palmarumycin P3 [N]					MIC = 12.5 μg/mL (35.28 μM)		
73	palmarumycin CP3 [K]					MIC = 1.56 μg/mL (4.64 μM)		
74	palmarumycin CR1 [K]					MIC = 3.13 μg/mL (9.36 μM)		
75	decaspirone A [K]					MIC = 3.13 μg/mL (9.25 μM)		
76	decaspirone C [K]					MIC = 12.5 μg/mL (36.51 μM)		
77	oxazinin A [N]	*Xylaria* sp. HDN13-249	Root of mangrove *Sonneratia caseolaris*	Solid medium (soluble starch 4%, yeast extract 0.1%, $MgSO_4$ 0.3%, monosodium glutamate 0.2%, sucrose 4%, KH_2PO_4 0.05%, maltose 3%, bean flour 0.05%, peptone 0.2%, agar powder 2.5%, seawater), 28 °C, 30 days	*M. phlei*	MIC = 6.25 μM	NR	[59]
78	penixylarin C [N]	*Xylaria* sp. HDN13-249	Root of mangrove *Sonneratia caseolaris*	Solid medium (soluble starch 4%, yeast extract 0.1%, $MgSO_4$ 0.3%, monosodium glutamate 0.2%, sucrose 4%, KH_2PO_4 0.05%, maltose 3%, bean flour 0.05%, peptone 0.2%, agar powder 2.5%, seawater), 28 °C, 30 days	*M. phlei*	MIC = 6.25 μM	NR	[60]

* ASW = artificial sea water; ** NA = not active; *** NR = mechanism of action not reported; [a] N = novel compound; [b] K = known compound.

2.5.2. Peptides and Alkaloids

A collection of novel 4-hydroxy-2-pyridone alkaloids, designated as arthpyrones F-I (**79**–**82**), along with a previously identified compound, apiosporamide (**83**) (Figure 14), were isolated from the deep-sea fungus *Arthrinium* sp. UJNMF008, which was obtained from the South China Sea. Compound **83** strongly inhibited *M. smegmatis*, with an IC_{50} of 2.20 μM, and **79**, **81**, and **82** exhibited moderate to weak antimycobacterial activity, with IC_{50} values in the range of 11.4–35.3 μM, while **80** showed no activity up to 50 μM. Compared with **79**, compound **80** showed a significant loss of activity against *M. smegmatis*, indicating that the hydroxyl at C-20 may be responsible for the activity [61].

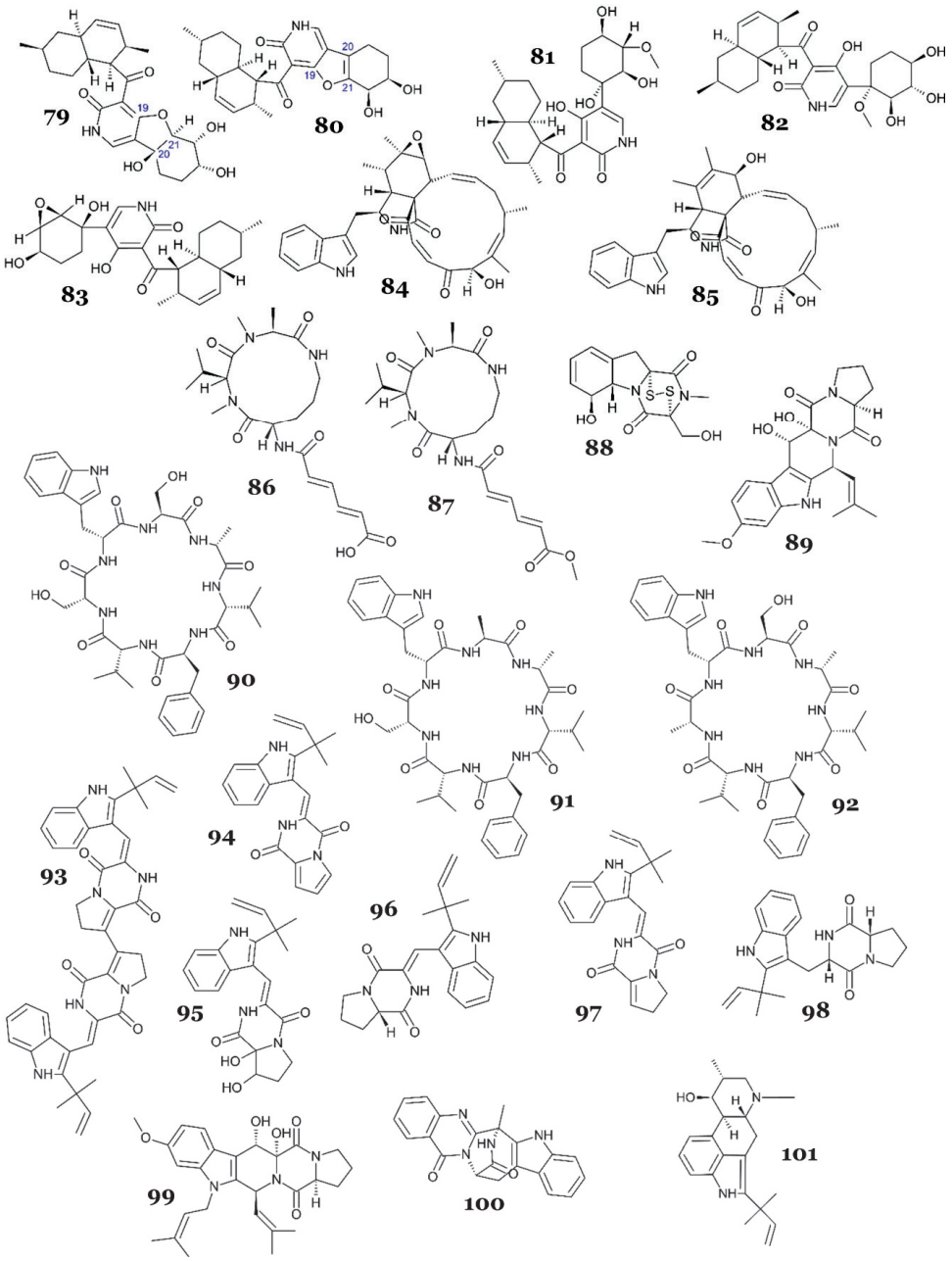

Figure 14. Chemical structures of compounds **79**–**101**.

Two indole alkaloids, chaetoglobosins A (**84**) and B (**85**) (Figure 14), were re-discovered from the marine alga-derived *Aspergillus fumigatus* AF3-093A collected from the North

Atlantic. They displayed antimycobacterial activity against *M. tuberculosis*, with IC_{50} values of 5 and 22 μM, respectively [62].

A chemical investigation of the ethyl acetate extract of marine sponge-derived fungus *Aspergillus insulicola* HDN151418 led to the discovery of two new aspochracin-type cyclic tripeptides, sclerotiotides M (**86**) and N (**87**) (Figure 14). Cyclic peptides, crucial metabolites found abundantly in various marine organisms [63–68], often feature a distinctive macrocyclic ring and a polyketide side chain in the structure of aspochracin-type cyclic tripeptides. These macrocyclic rings commonly comprise a 12-membered ring (consisting of Ala-Val-Orn) or a 13-membered ring (comprising Ala-Val-Lys). To date, only 15 variants of aspochracin-type cyclic tripeptides have been isolated from their natural origins. A bioactivity assay showed that **86** and **87** exhibited strong to moderate antimycobacterial activity, with MIC values of 3.13 and 12.5 μM, respectively [69].

Two diketopiperazine alkaloids with antimycobacterial activity, gliotoxin (**88**) and 12,13-dihydroxy-fumitremorgin C (**89**) (Figure 14), were obtained from the marine-derived *Aspergillus* sp. SCSIO Ind09F01. The fungus was isolated from deep-sea marine sediments (4530 m below sea level) collected from the Indian Ocean. Compounds **88** and **89** demonstrated strong antimycobacterial activity against *M. tuberculosis* H37Ra, with MIC_{50} values of <0.03 and 2.41 μM, respectively. Another compound with a tetracyclic triterpenoid structure, helvolic acid (**116**), also exhibited antimycobacterial properties (this will be described later) [70].

Three new cycloheptapeptides, asperversiamides A–C (**90**–**92**) (Figure 14), were successfully discovered from *Aspergillus versicolor* CHNSCLM-0063, isolated from the gorgonian coral *Rumphella aggregata* in South China. Based on the antimycobacterial assay against *M. marinum* and *M. tuberculosis*, all compounds exhibited moderate to weak activity against *M. marinum*, with MICs of 23.4, 81.2, and 87.5 μM, respectively, while only **91** exhibited weak antitubercular activity, with an MIC of 100 μM [71].

Six diketopiperazines were isolated from marine-derived fungus *Aspergillus versicolor* MF030, four of which were new, brevianamides S (**93**), T (**94**), U (**95**), and V (**96**), while the other two were known, brevianamide K (**97**) and deoxybrevianamide E (**98**) (Figure 14). The fungal strain was obtained from marine sediment (60 m below sea level) in the Bohai Sea, northeastern coast of China. All compounds were tested against a panel of microbes, including *M. bovis* BCG. All compounds displayed antimycobacterial activity, with MICs of 6.25, 50, 25, 100, 50, and 100 μg/mL, respectively (9.02, 144.76, 65.54, 286.18, 143.92, and 284.54 μM, respectively). Interestingly, all compounds showed selectivity toward *M. bovis* BCG (no activity against other tested microorganisms up to 100 μg/mL), with compound **93** being the most active against *M. bovis* BCG. This discovery highlights the noteworthy selectivity of dimeric diketopiperazine toward *M. bovis* BCG [72].

Aspergillus fumigatus MF071, isolated from marine sediment (60 m below sea level) in the Bohai Sea, China, produced alkaloids fumitremorgin B (**99**), fumiquinazoline J (**100**), and 9-deacetylfumigaclavine C (**101**) (Figure 14), along with terpenoid helvolic acid (**116**), with weak antimycobacterial activity against *M. smegmatis*, with an MIC value of 100 μg/mL (208.52, 280.60, 308.20, and 175.84 μM, respectively) [73].

Two novel isoprenylisoindole alkaloids, diaporisoindoles A (**102**) and B (**103**), were discovered from mangrove-associated fungus *Diaporthe* sp. SYSU-HQ3. Those compounds were the first reported isoprenylisoindole alkaloids with a rare 1,4-benzodioxan moiety. They were tested against MptpB and it was shown that only **102** exhibited potent MptpB inhibitor activity, with an IC_{50} of 4.2 μM, while no inhibitory activity was observed from **103** up to 50 μM. Compounds **102** and **103** differed in the C-8 configuration, 8*S* or 8*R* (Figure 15), which indicated that the 8*S* configuration at C-8 is more beneficial as an MptpB

inhibitor. Neither compound showed inhibitory activity against PTP1B up to 200 μM, which showed high selectivity toward MptpB. The kinetic analysis of **102** revealed that it acted as an uncompetitive inhibitor against MptpB. Compound **102** inhibited MptpB with strong activity, whereas its 8 *R* epimer **103** showed only weak activity at 50 μM. Since C-8 defines the relative orientation between the isoindolinone carbonyl, the neighbouring phenolic OH, and the tertiary amine, it is reasonable to propose that the 8 *S* stereochemistry enables these hetero-atoms to face the Lys164/Arg166/Asp165 oxyanion region, whereas the 8 *R* epimer directs them away and may introduce steric interference from the prenyl group. Although this hypothesis fits the observed potency gap, direct structural data are not yet available; hence, further docking or co-crystallography will be required to validate the binding pose. Another terpenoid metabolite, tenellone C (**128**) (which will be described later), also exhibited inhibition against MptpB [74].

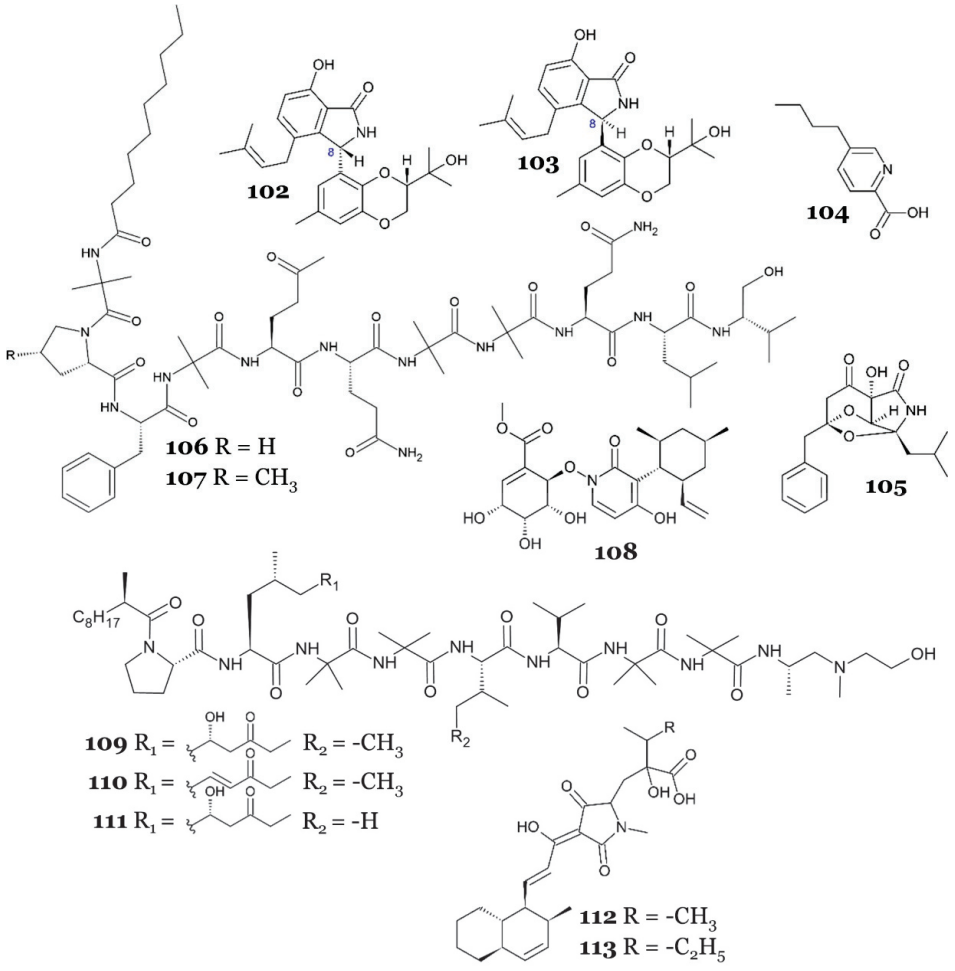

Figure 15. Chemical structures of compounds **102**–**113**.

A chemical investigation of the ethyl acetate extract of *Fusarium* sp. DZ-27, isolated from *Kandelia cande* (L.) Druce bark, led to the isolation of fusaric acid (**104**). The compound displayed inhibition activity against several mycobacterial strains, including *M. bovis* BCG, *M. tuberculosis* H37Rv, clinical multidrug-resistant *M. tuberculosis* (strain 18019, resistant to SM, INH, RF, and ETH), and clinical multidrug-resistant *M. tuberculosis* (strain 17016, resistant to SM, INH, and ETH), with MIC values of 1.8, 1.8, 30, and 30 μg/mL, respectively (10.04, 10.04, 167.40, and 167.40 μM, respectively) [75].

A unique alkaloid, talaramide A (**105**), was isolated from the mangrove endophytic fungus *Talaromyces* sp. HZ-YX1. The fungus strain was obtained from healthy leaves of the mangrove *Kandelia obovata*. The compound displayed antimycobacterial activity by inhibiting the mycobacterial protein kinase G (PknG), a thioredoxin-fold-containing eukaryotic-like serine/threonine protein kinase that acts as a virulence factor of *M. tuberculosis* responsible for the inhibition of phagolysosomal fusion [76], with an IC_{50} value of 55 μM [77].

Two novel lipopeptaibols, tolypocaibols A (**106**) and B (**107**), along with the known mixed nonribosomal peptide synthetase (NRPS)–polyketide–shikimate and natural product maximiscin (**108**) (Figure 15), were derived from marine-derived *Tolypocladium* sp. The fungus was isolated from the marine alga *Spongomorpha arcta*, collected from the shores at Green's Point, L' Etete, NB, Canada. All compounds were tested against a panel of microorganisms, including *M. smegmatis* and *M. tuberculosis*, and showed antimycobacterial activity, with an MIC of 80 μM against *M. smegmatis* (for compounds **106** and **107**; however, compound **108** was inactive). Antitubercular activity was also observed for all compounds, with MIC values of 20, 40, and 250 μM, respectively [78].

Three novel aminolipopeptides, identified as trichoderins A (**109**), A1 (**110**), and B (**111**), were discovered from *Trichoderma* sp., a fungus derived from marine sponge, showcasing antimycobacterial properties effective against both active and dormant bacilli. Compounds **109** and **111** contained the unsual amino acid 2-amino-6-hydroxy-4-methyl-8-oxodecanoic acid (AHMOD) while **110** had 2-amino-4-methy1-8-oxodec-6-enoic acid (AMOD) (Figure 15), which may have affected the antimycobacterial activity of **109**, **110**, and **111**. Those compounds displayed potent antimycobacterial activity against *M. smegmatis*, *M. bovis* BCG, and *M. tuberculosis* in aerobic and hypoxic (dormant state) conditions, with an MIC in the range of 0.02–2 μg/mL. Compounds **109** and **111** exhibited more potent activity (up to 16-fold) against all tested *Mycobacterium* compared with **110**, especially against *M. tuberculosis*. MICs for aerobic and hypoxic conditions for **109** and **111** were 0.12 and 0.13 μg/mL, respectively (103 and 113 nM, respectively), while the MIC for aerobic and hypoxic conditions for **110** was 2.00 μg/mL (1.75 μM) [79]. A further study was conducted to elucidate the possible mechanism of action of **109** by using **109**-resistant clones of *M. smegmatis* mc^2155. Gene identification on the resistant clones revealed that the target region of **109** contained *atpB*, *atpE*, *atpF*, *atpH*, and parts of *atpA* genes, which are known to express components related to mycobacterial ATP synthesis. This suggested that **109** inhibits mycobacterial cells by inhibiting the mycobacterial ATP synthesis. The prediction was confirmed by using transformants of *M. smegmatis* (over-expressed in the regions of *atpB*, *atpE*, *atpF*, and *atpH*), which exhibited resistance in the presence of **109** for up to 0.4 μg/mL, and by measuring the ATP content of *M. bovis* BCG, which showed a reduction of ATP content (80% reduction) in the concentration of 0.1 μg/mL. Trichoderins (**109**–**111**) not only showed activity against dormant mycobacteria but were found to inhibit ATP synthase, hence draining the ATP of non-replicating cells, a mechanism similar to the TB drug bedaquiline [80].

Two novel pyrrolidinone derivatives, zopfiellamides A (**112**) and B (**113**), were discovered from the facultative marine *Zopfiella latipes*, which was obtained from marine sediment in the Indian Ocean. They demonstrated antimycobacterial activity against *M. phlei*, with an MIC in the range of 2–10 μg/mL (4.35–22.44 μM), with **112** being five times more potent than **113** [81].

Table 2. Alkaloid and peptide NPs with antimycobacterial activity from MF.

No.	Metabolites [Novelties at the Time of Isolation]	Producing Strains	Marine Sources	Fermentation Media and Method	Tested Against Mycobacterium Strain/Mycobacterial Enzyme	Potency	Mechanism of Action	Ref.
79	arthpyrone F [N] [a]	*Arthrinium* sp. UJNMF008	Marine sediment	Solid medium (80 g commercial rice, 0.4 g yeast extract, 0.4 g glucose, 120 mL water with 3% sea salt), static condition, 28 °C, 30 days	*M. smegmatis*	IC_{50} = 11.4 μM	NR ***	[61]
80	arthpyrone G [N]					NA **		
81	arthpyrone H [N]					IC_{50} = 19.4 μM		
82	arthpyrone I [N]					IC_{50} = 35.3 μM		
83	apiosporamide [K] [b]					IC_{50} = 2.20 μM		
84	chaetoglobosin A [N]	*Aspergillus fumigatus* AF3-093A	Marine alga *Fucus vesiculosus*	Liquid medium (malt extract broth 2%), agitated condition at 150 rpm, room temp., 14 days	*M. tuberculosis* H37Ra	MIC = 47 μM	NR	[62]
85	chaetoglobosin B [N]					MIC = 95 μM		
86	sclerotiotide M [N]	*Aspergillus insulicola* HDN151418	Unidentified marine sponge	Liquid medium (potato dextrose broth), static condition, 28 °C, 30 days	*M. phlei*	MIC = 3.13 μM	NR	[69]
87	sclerotiotide N [N]					MIC = 12.5 μM		
88	gliotoxin [K]	*Aspergillus* sp. SCSIO Ind09F01	Marine sediment	Liquid medium (mannitol 2%, maltose 2%, glucose 1%, corn steep liquor 0.1%, monosodium glutamate 1%, KH_2PO_4 0.05%, $MgSO_4.7H_2O$ 0.03%, yeast extract 0.3%, sea salt 1.5%, pH 7.4), agitated condition at 172 rpm, 27 °C, 15 days	*M. tuberculosis* H37Ra	MIC = <0.03 μM	NR	[70]
89	12,13-dihydroxy-fumitremorgin C [K]					MIC = 2.41 μM		
90	asperversiamide A [N]	*Aspergillus versicolor CHNSCLM*-0063	Marine gorgonian coral *Rumphella aggregate*	Solid medium (50 g rice, 50 mL sea water), static condition, room temp., 50 days	*M. marinum*	MIC = 23.4 μM	NR	[71]
					M. tuberculosis	NA		
91	asperversiamide B [N]				*M. marinum*	MIC = 81.2 μM		
					M. tuberculosis	MIC = 100 μM		
92	asperversiamide C [N]				*M. marinum*	MIC = 87.5 μM		
					M. tuberculosis	NA		

Table 2. *Cont.*

No.	Metabolites [Novelties at the Time of Isolation]	Producing Strains	Marine Sources	Fermentation Media and Method	Tested Against Mycobacterium Strain/Mycobacterial Enzyme	Potency	Mechanism of Action	Ref.
93	brevianamide S [N]	*Aspergillus versicolor* MF030	Marine sediment	Solid medium (100 g rice, 3.25 g soya bean powder, 30 mL ASW * 3.5%), static condition, 28 °C, 19 days	*M. bovis* BCG	MIC = 6.25 μg/mL (9.02 μM)	NR	[72]
94	brevianamide T [N]					MIC = 50 μg/mL (144.76 μM)		
95	brevianamide U [N]					MIC = 25 μg/mL (65.54 μM)		
96	brevianamide V [N]					MIC = 100 μg/mL (286.18 μM)		
97	brevianamide K [K]					MIC = 50 μg/mL (143.92 μM)		
98	deoxybrevianamide E [K]					MIC = 100 μg/mL (284.54 μM)		
99	fumitremorgin B [K]	*Aspergillus fumigatus* MF071	Marine sediment	Solid medium (160 g rice, 240 mL distilled water), static condition, 28 °C, 30 days	*M. smegmatis*	MIC = 100 μg/mL (208.52 μM)	NR	[73]
100	fumiquinazoline J [K]					MIC = 100 μg/mL (280.60μM)		
101	9-deacetylfumigaclavine C [K]					MIC = 100 μg/mL (308.20 μM)		
102	diaporisoindole A [N]	*Diaporthe* sp. SYSU-HQ3	Branches of mangrove *Excoecaria agallocha*	Solid medium (50 g rice, 50 mL saline water 0.3%), static condition, room temp., 28 days	Mycobacterial Enzyme MptpB	IC_{50} = 4.2 μM	Inhibit virulence factor MptpB	[74]
103	diaporisoindole B [N]					NA	-	

Table 2. *Cont.*

No.	Metabolites [Novelties at the Time of Isolation]	Producing Strains	Marine Sources	Fermentation Media and Method	Tested Against Mycobacterium Strain/Mycobacterial Enzyme	Potency	Mechanism of Action	Ref.
104	fusaric acid [K]	*Fusarium* sp. DZ-27	Bark of *Kandelia cande* (L.)	Liquid medium (glucose 1%, pepton 0.2 %, yeast extract 0.1%, NaCl 0.3%), static condition, 28 °C, 30 days	*M. bovis* BCG	MIC = 1.8 μg/mL (10.04 μM)	NR	[75]
					M. tuberculosis H37Rv	MIC = 1.8 μg/mL (10.04 μM)		
					Clinical multidrug-resistant *M. tuberculosis* (strain 18019, resistant to SM, INH, RF, and ETH)	MIC = 30 μg/mL (167.40 μM)		
					Clinical multidrug-resistant *M. tuberculosis* (strain 17016, resistant to SM, INH, and ETH)	MIC = 30 μg/mL (167.40 μM)		
105	talaramide A [N]	*Talaromyces* sp. HZ-YX1	Leaves of mangrove *Kandelia obovata*	Solid medium (50 g rice, 1.5 g artificial sea salts, 50 mL distilled H_2O), static condition, room temp., 28 days	Mycobacterial Enzyme PknG	IC_{50} = 55 μM	Inhibit virulence factor PknG	[77]
106	tolypocaibol A [N]	*Tolypocladium* sp.	Marine alga *Spongomorpha arcta*	Liquid medium (potato dextrose broth 1.2%), agitated condition at 150 rpm, room temp., 14 days	*M. smegmatis* ATCC 70084	MIC = 80 μM	NR	[78]
					M. tuberculosis H37Ra	MIC = 20μM		
107	tolypocaibol B [N]				*M. smegmatis* ATCC 70084	MIC = 80 μM		
					M. tuberculosis H37Ra	MIC = 40 μM		
108	maximiscin [K]				*M. smegmatis* ATCC 70084	NA		
					M. tuberculosis H37Ra	MIC = 250 μM		

Table 2. *Cont.*

No.	Metabolites [Novelties at the Time of Isolation]	Producing Strains	Marine Sources	Fermentation Media and Method	Tested Against Mycobacterium Strain/Mycobacterial Enzyme	Potency	Mechanism of Action	Ref.
109	trichoderin A [N]	*Trichoderma* sp.	Unidentified marine sponge	Solid medium (2.3 kg rice, 4.5 L ASW), static condition, 30 °C, 14 days	*M. smegmatis*	MIC = 0.1 µg/mL (85.95 nM)	Inhibit the mycobacterial F_1F_0-ATP–synthase	[79]
					M. bovis BCG	MIC = 0.02 µg/mL (17.19 nM)		
					M. tuberculosis	MIC = 0.12 µg/mL (103.14 nM)		
110	trichoderin A1 [N]				*M. smegmatis*	MIC = 1.56 µg/mL (1.36 µM)		
					M. bovis BCG	MIC = 0.16 µg/mL (139.68 nM)		
					M. tuberculosis	MIC = 2 µg/mL (1.75 µM)		
111	trichoderin B [N]				*M. smegmatis*	MIC = 0.63 µg/mL (548.06 nM)		
					M. bovis BCG	MIC = 0.02 µg/mL (17.40 nM)		
					M. tuberculosis	MIC = 0.13 µg/mL (113.09 nM)		
112	zopfiellamide A [N]	Zopfiella latipes	Marine sediment	Liquid medium (glucose 0.5%, yeast extract 0.1%, peptone from soybean 0.1%, pH 7) in fermentor with aeration rate 3 L/min, 120 rpm, 22 °C, 11 days	*M. phlei*	MIC = 2–10 µg/mL (4.35–22.44 µM)	NR	[81]
113	zopfiellamide B [N]					MIC = 2–10 µg/mL (4.35–22.44 µM)		

* ASW = artificial sea water; ** NA = not active; *** NR = mechanism of action not reported; [a] N = novel compound; [b] K = known compound.

2.5.3. Terpenoids and Steroids

Asperterpenoid A (**114**), a novel sesterterpenoid with a 5/7/(3)6/5 pentacyclic system (Figure 16), was isolated from the marine-derived fungus *Aspergillus* sp. 16-5c, which was obtained from the mangrove *Sonneratia apetala* collected from the South China Sea. This compound displayed a potent MptpB inhibitor with an IC_{50} of 2.2 μM [82]. In another study, Huang J H and colleagues uncovered a gene cluster comprised of three genes through genome exploration, which was demonstrated to be accountable for the synthesis of asperterpenoid A. The experimental reassembly in *Aspergillus oryzae* NSAR1 unveiled that the terpene synthase AstC functions akin to PvPS, producing preasperterpenoid A. Following this, the P450 AstB-mediated four-step oxidation reactions transformed preasperterpenoid A into the potent MptpB inhibitor **114**, along with a minor byproduct, asperterpenoid B (**115**). The same study also showed that **114** and **115** acted as noncompetitive inhibitors against MptpB, with IC_{50} values of 3.34 and 5.67 μM, respectively, and *K*i values of 2.12 and 2.20 μM, respectively [83]. Asperterpenoids A and B are rigid 5/7/(3)6/5 pentacyclic sesterterpenoids; each bears a carboxylic acid at C-19 and a β-hydroxyl group at C-21, the two polar handles most likely involved in binding to MptpB. Although no co-crystal or docking study is available, the acid/β-OH pair is reminiscent of the multidentate acidic motifs seen in other potent MptpB ligands, suggesting that it may interact with the Lys164/Arg166 oxyanion pocket and/or Asp165, while the bulky terpene cage could fill the hydrophobic groove defined by Phe161 and Tyr125. The modest loss of activity in B may arise from subtle conformational or electronic changes introduced by the epoxide rather than from the addition of a new carbonyl. Further structural data would be required to confirm this binding model [82].

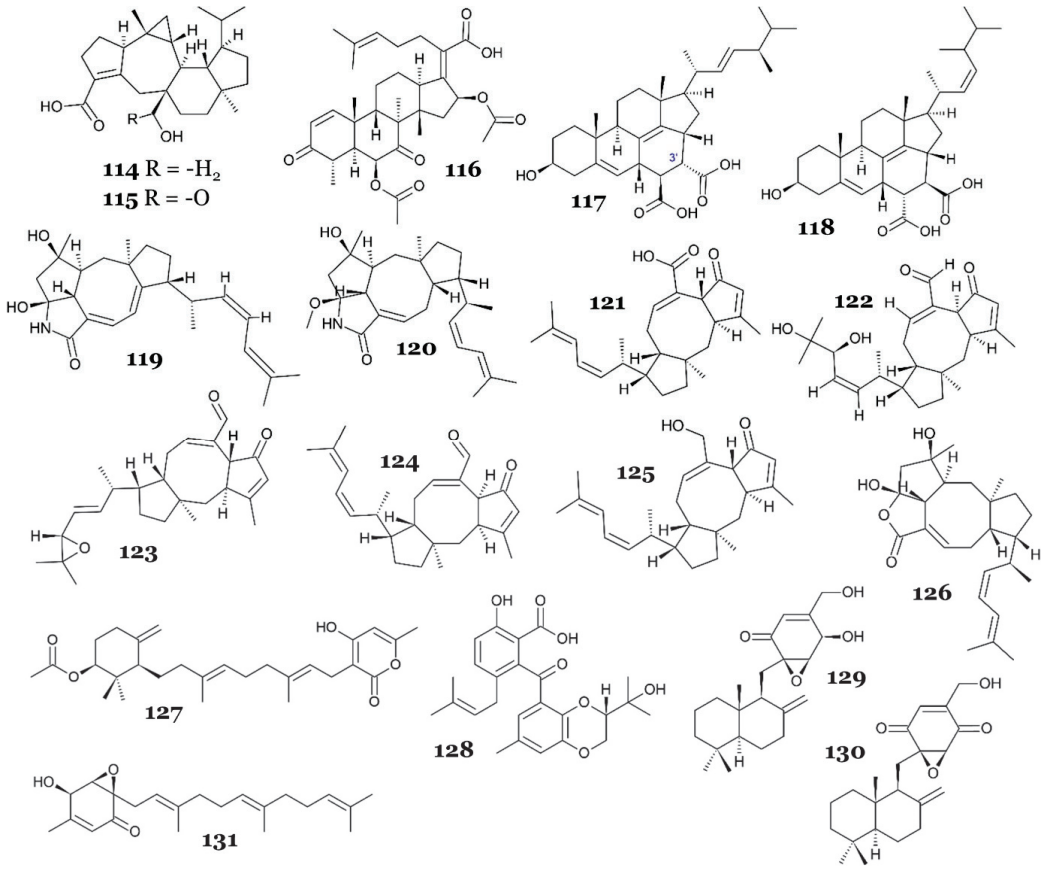

Figure 16. Chemical structures of compounds **114**–**131**.

A C-21 steroid, helvolic acid (**116**), was isolated from the marine-derived *Aspergillus* sp. SCSIO Ind09F01, along with **88** and **89**. It exhibited potent antimycobacterial activity against *M. tuberculosis* H37Ra, with an MIC_{50} of 0.894 μM [70].

A chemical investigation of marine-derived *Aspergillus* sp. DM2 ethyl acetate extract led to the discovery of two novel, natural Diels–Alder additive steroids, ergosterdiacids A (**117**) and B (**118**) (Figure 16), with a 6/6/6/6/5 pentacyclic system. An antimycobacterial assay against MptpB showed that **117** and **118** displayed moderate inhibition, with IC_{50} values of 15.1 and 30.1 μM, respectively. According to the docking results, **117** and **118**, alongside oleanolic acid, bound within the active pocket of MptpB, were characterized by amino acid residues of Arg210, Arg63, Arg59, Met206, Phe161, Lle207, Lle203, Phe211, and Glu60. Notably, both compounds displayed interactions between their carboxyl groups and the alkaline amino acids (Arg59, Arg63, Arg210) within the binding pocket, which was reminiscent of (oxalylamino-methylene)–thiophene sulfonamide (OMTS), a potent MptpB inhibitor with an IC_{50} of 440 nM. Specifically, **117** formed four hydrogen bonds in its docking mode: two between the carbonyl carbon of C-3′ and the guanidyl of Arg 210 and Arg63 and two with Arg 63 and Arg59, while **118** exhibited a similar interaction pattern involving the carbonyl carbon of C-3′ and the guanidyl of Arg63 and Arg210. These hydrogen bonds played a pivotal role in stabilizing the protein–ligand complex. Furthermore, the predicted Ki values for **117** and **118** were 267.3 and 34.05 nM, respectively. An in-depth analysis of the structural characteristics of the isolated compounds and OMTS indicated that the carboxyl groups may serve as key functional groups contributing to the inhibitory effects against MptpB [16].

Rai and colleagues discovered 11 new ophiobolin-type sesterterpenoids from mangrove-associated Aspergillus sp. ZJ-68, in which five of them exhibited antimycobacterial properties, asperophiobolins B (**119**), D (**120**), E (**121**), H (**122**), and I (**123**), along with 12 known analogues, three of which, ophiobolin G (**124**), 21-deoxo-21-hydroxy-6-epi-ophiobolin G (**125**), and ophiobolin P (**126**) (Figure 16), also displayed antimycobacterial activity. The assay was conducted against MptpB and revealed that the IC_{50} values of those compounds were in the range of 19–42 μM [84]. Across this ophiobolin/asperophiobolin series, all molecules shared a cavernous 5-8-5 tricyclic cage and a long isoprenyl tail that could fill the hydrophobic Phe161-Leu199 tunnel of MptpB, but provided at most two donors, typically arranged as one dominant lactam/γ-lactone dyad to engage the Lys164/Arg166/Asp165 polar patch, giving uniform, mid-micromolar potencies (IC_{50} = 19–42 μM) [84].

A chemical investigation of an ethyl acetate extract of rice fermentation from the marine-derived *Aspergillus* sp. WHUF03110 led to the isolation of sartopyrone A (**127**). The fungal strain was obtained from the mangrove soil sediment from Yalong Bay, Sanya, Hainan, China. Compound **127** demonstrated moderate activity against *M. smegmatis* ATCC 607, with an MIC of 8 μg/mL (17.52 μM) [85].

A meroterpenoid, tenellone C (**128**), was also isolated from the fungus *Diaporthe* sp. SYSU-HQ3, along with **102** and **103**. Compound **128** was found to be the precursor to **102** and **103**, which could be produced after consecutive reactions of the reduction, nucleophilic addition, and dehydration of **128**. Unlike **102**, compound **128**'s inhibiting property was shown to be a competitive inhibitor against MptpB, with an IC_{50} value of 5.2 μM. However, it had the same selectivity as **102** against MptpB over PtpB [74].

Macrophorin A (**129**), 4′-oxomacrophorin (**130**), and 7-deacetoxyyanuthone A (**131**) were isolated from an ethyl acetate extract of a rice medium of *Gliomastix* sp. obtained from the sponge *Phakellia fusca* Thiele collected in the Yongxing Island of Xisha. Those compounds displayed antimycobacterial activity against *M. tuberculosis* with IC_{50} values of 22.1, 2.44, and 17.5 μM, respectively [86].

Table 3. Terpenoid and steroid NPs with antimycobacterial activity from MF.

No.	Metabolites [Novelties at the Time of Isolation]	Producing Strains	Marine Sources	Fermentation Media and Method	Tested Against Mycobacterium Strain/Mycobacterial Enzyme	Potency	Mechanism of Action	Ref.
114	asperterpenoid A [N] [a]	*Aspergillus* sp. 16-5c	Mangrove *Sonneratia apetala*	Solid medium (100 g rice, 20 mL 3% sea salt liquid), static condition, 25 °C, 28 days	Mycobacterial Enzyme MptpB	IC_{50} = 3.34 μM *Ki* = 2.12 μM	Inhibit virulence factor MptpB	[82, 83]
115	asperterpenoid B [N]					IC_{50} = 5.67 μM *Ki* = 2.20 μM		
116	helvolic acid [K] [b]	*Aspergillus* sp. SCSIO Ind09F01	Marine sediment	Liquid medium (mannitol 2%, maltose 2%, glucose 1%, corn steep liquor 0.1%, monosodium glutamate 1%, KH_2PO_4 0.05%, $MgSO_4.7H_2O$ 0.03%, yeast extract 0.3%, sea salt 1.5%, pH 7.4), agitated condition at 172 rpm, 27 °C, 15 days	*M. tuberculosis* H37Ra	MIC_{50} = 0.894 μM	NR *	[70]
117	ergosterdiacid A [N]	*Aspergillus* sp. DM2	Mangrove *Aegiceras corniculatum*	Solid medium (50 g corn niblet, 0.86 g yeast extract, 2.37 g ammonium tartrate, 0.17 g $MgSO_4$, 0.25 g KH_2PO_4, 0.4 g sea salt, 20 mL distilled water), static condition, 28 °C, 20 days	Mycobacterial Enzyme MptpB	IC_{50} = 15.1 μM *Ki* = 267.3 nM	Inhibit virulence factor MptpB	[16]
118	ergosterdiacid B [N]					IC_{50} = 30.1 μM *Ki* = 34.05 nM		
119	asperophiobolin B [N]	*Aspergillus* sp. ZJ-68	Leaves of mangrove *Kandelia candel*	Solid medium (50 g rice, 50 mL 0.3% saline water), static condition, 25 °C, 28 days	Mycobacterial Enzyme MptpB	IC_{50} = 39 μM	Inhibit virulence factor MptpB	[84]
120	asperophiobolin D [N]					IC_{50} = 42 μM		
121	asperophiobolin E [N]					IC_{50} = 28 μM		
122	asperophiobolin H [N]					IC_{50} = 19 μM		
123	asperophiobolin I [N]					IC_{50} = 35 μM		
124	ophiobolin G [K]					IC_{50} = 24 μM		
125	21-deoxo-21-hydroxy-6-epi-ophiobolin G [K]					IC_{50} = 37 μM		
126	ophiobolin P [K]					IC_{50} = 36 μM		

Table 3. *Cont.*

No.	Metabolites [Novelties at the Time of Isolation]	Producing Strains	Marine Sources	Fermentation Media and Method	Tested Against Mycobacterium Strain/Mycobacterial Enzyme	Potency	Mechanism of Action	Ref.
127	sartopyrone A [K]	Aspergillus sp. WHUF03110	Marine sediment	Solid medium (200 g rice, 200 mL distilled water), static condition, 26 °C, 30 days	*M. smegmatis* ATCC 607	MIC = 8 μg/mL (17.52 μM)	NR	[85]
128	tenellone C [K]	*Diaporthe* sp. SYSU-HQ3	Branches of mangrove *Excoecaria agallocha*	Solid medium (50 g rice, 50 mL saline water 0.3%), static condition, room temp., 28 days	Mycobacterial Enzyme MptpB	IC_{50} = 5.2 μM	Inhibit virulence factor MptpB	[74]
129	macrophorin A [K]	*Gliomastix* sp.	Marine sponge *Phakellia fusca*	Solid medium (200 g rice, 2.5 g sea salt, 200 mL distilled water), static condition, 26 °C, 40 days	*M. tuberculosis*	IC_{50} = 22.1 μM	NR	[86]
130	4′-oxomacrophorin [K]					IC_{50} = 2.44 μM		
131	7-deacetoxyyanuthone A [K]					IC_{50} = 17.5 μM		

* NR = mechanism of action not reported; [a] N = novel compound; [b] K = known compound.

2.5.4. Other Compounds

One novel compound, gliomastin C (**132**), and four known hydroquinone derivatives, methylhydroquinone (**133**), acremonin A (**134**), prenylhydroquinone (**135**), and F-11334A1 (**136**) (Figure 17), were isolated from marine-derived *Gliomastix* sp. The fungus was obtained from the hard coral *Stylophora* sp. (from the Red Sea, Egypt). The compounds displayed antimycobacterial activity against the *M. tuberculosis* strain H37Rv with MICs of 12.5, 12.5, 25, 12.5, and 25 μM, respectively [87].

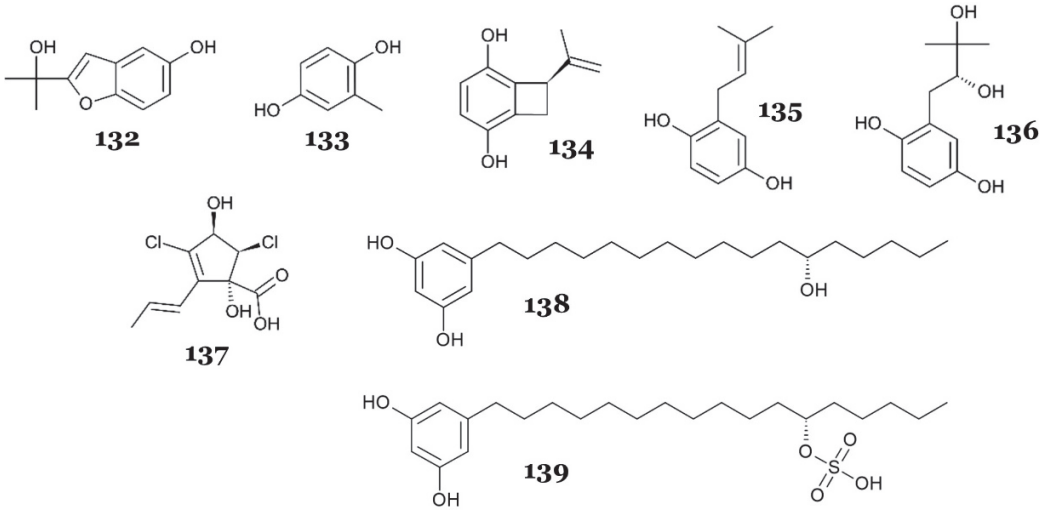

Figure 17. Chemical structures of compounds **132**–**139**.

A novel halogenated metabolite, cryptophomic acid (**137**) (Figure 17), was discovered from marine-derived *Phoma* sp. 135, which was obtained from the sponge *Ectyplasia perox*, collected in Dominica, Lauro Club Reef. It exhibited moderate antimycobacterial activity against *M. phlei*, with an MIC of 16 μM [88].

Two alkyl aromatics, 1,3-dihydroxy-5-(12-hydroxyheptadecyl)benzene (**138**) and 1,3-dihydroxy-5-(12-sulfoxyheptadecyl)benzene (**139**), were isolated from *Xylaria* sp. HDN13-249, along with **77**. The same study also revealed that the yields of those compounds were increased when *Xylaria* sp. HDN13-249 was co-cultivated with the deep-sea fungus *Penicillium crustocum* PRB-2. Compounds **138** and **139** showed antimycobacterial activity against *M. phlei*, with MICs of 25 and 12.5 μM, respectively [60].

Table 4. Other NPs with antimycobacterial activity from MF.

No.	Metabolites [Novelties at the Time of Isolation]	Producing Strains	Marine Sources	Fermentation Media and Method	Tested Against Mycobacterium Strain/Mycobacterial Enzyme	Potency	Mechanism of Action	Ref.
132	gliomastin C [N] [a]	*Gliomastix* sp.	Marine coral *Stylophora* sp.	Solid medium (100 g rice, 110 mL water), static condition, 25 °C, 30 days	*M. tuberculosis* H37Rv	MIC = 12.5 μM	NR *	[87]
133	methylhydroquinone [K] [b]					MIC = 12.5 μM		
134	acremonin A [K]					MIC = 25 μM		
135	prenylhydroquinone [K]					MIC = 12.5 μM		
136	F-11334A1 [K]					MIC = 25 μM		
137	cryptophomic acid [N]	*Phoma* sp. 135	Marine sponge *Ectyplasia perox*	Solid medium (biomalt agar medium 1.5%), static condition, room temp.	*M. phlei*	MIC = 16 μM	NR	[88]
138	1,3-dihydroxy-5-(12-hydroxyheptadecyl)benzene [K]	*Xylaria* sp. HDN13-249	Root of mangrove *Sonneratia caseolaris*	Solid medium (soluble starch 4%, yeast extract 0.1%, $MgSO_4$ 0.3%, monosodium glutamate 0.2%, sucrose 4%, KH_2PO_4 0.05%, maltose 3%, bean flour 0.05%, peptone 0.2%, agar powder 2.5%, seawater), 28 °C, 30 days	*M. phlei*	MIC = 25 μM	NR	[60]
139	1,3-dihydroxy-5-(12-sulfoxyheptadecyl)benzene [K]					MIC = 12.5 μM		

* NR = mechanism of action not reported; [a] N = novel compound; [b] K = known compound.

3. Perspectives and Outlooks

3.1. The Opportunity of Exploring Antimycobacterials from Marine-Derived Fungi

Most of the isolated fungi came from marine sediments, followed by mangrove, marine sponge, and marine algae, with a lesser amount isolated from marine corals, sea fan, ascidian, and marine anemone. This dominance could be attributed to the rich organic matter and unique ecological conditions in sediments, which provide a favorable environment for the growth and metabolic diversification of fungi [89,90]. Mangroves were characterized by their nutrient-rich, brackish waters, and hence can serve as fertile ground for diverse fungal communities [91–93]. From this review, it can be seen that marine sponges represent a crucial source of fungi capable of producing bioactive metabolites due to their symbiotic relationships with microorganisms [94].

In contrast, marine sources such as algae, corals, sea fans, ascidians, and marine anemones were not well explored in previous studies. This disparity likely reflects a combination of biological and methodological factors, such as their structural and ecological characteristics, or they might have been less extensively sampled in prior studies. While these sources contribute a smaller proportion of fungal isolates, they represent a largely untapped fungal genus that could yield novel compounds, such as compounds **3**, **4**, **35**–**39**, **44**–**45**, **77**, **84**–**85**, **90**–**92**, **132**, **106**, and **107**. This suggests that expanding sampling efforts in corals, sea fans, ascidians, and marine anemones could lead to the discovery of new fungal genera or metabolites.

Our review revealed that *Aspergillus* is the most prevalent species in both marine and terrestrial habitats and produced the most antimycobacterial metabolites, followed by *Penicillium*, making them the most promising sources for the investigation of bioactive metabolites, including potent and novel antimycobacterial agents (compounds **11**, **13**, **55**, **56**, **86**, **114**, and **115**) [16–19]. However, some less-studied genera, such as *Phoma, Pleosporales, Arthrinium*, *Coniothyrium*, *Talaromyces, Trichoderma*, *Tolycopladium*, and *Zopfiella*, also hold great potential for yielding novel, potent antimycobacterial compounds. For example, *Trichoderma* sp. isolated from unidentified sponge produced novel compounds **109**–**111** that exhibited activity against various *Mycobacterium* strains, not only against the active phenotype but also against the dormant one [79]. *Arthrinium* sp. UJNMF008 produced novel compounds **79**–**82** and known compound **83** with potent activity against *M. smegmatis* [61]. *Zopfiella latipes* from marine sediments produced novel compounds **112**–**113** with potent activity against *M. phlei* [81]. This suggests that exploring antimycobacterials from marine *Aspergillus* and *Penicillium* might be a promising approach due to their abundance in marine environments and ability to produce a variety of active metabolites, but with the possible disadvantage of there being a higher risk of rediscovering known metabolites, or worse, previously reported antimycobacterials. Nonetheless, their lesser discovery was not without reason: their abundance in the environment is, in fact, quite low. Therefore, when attempting to isolate fungi from marine sources, it is recommended to use a larger number of marine samples as one of the strategies to increase the likelihood of isolating fungi from specific genera [19].

Finding novel compounds is somewhat crucial in the fight against tuberculosis due to the increased number of drug-resistant strains. Novel compounds may offer alternative mechanisms of action that could potentially overcome existing drug resistance by offering new mechanisms of action. Additionally, novel drugs are hoped to reduce treatment duration and side effects, which could enhance patient compliance and treatment outcomes [95,96]. Since the rediscovery of known compounds remains a significant challenge in the journey of drug discovery from marine resources, integrating dereplication strategies early in the discovery process, such as advanced spectrometric methods, chemoinformatic tools, and genome mining approaches, might help identify previously unknown metabolites [97–99]. For example, the use of molecular networking through platforms like GNPS

(Global Natural Products Social Molecular Networking) can rapidly dereplicate known compounds, which can save time and resources [100,101]. In addition, combinatorial biosynthesis approaches that combine genetic elements from different fungal species could also diversify the metabolite pool and overcome the limitations of rediscovery [102,103]. Moreover, advances in fermentation optimization and bioprocess engineering, such as the use of co-cultivation strategies, can enhance the metabolic output of marine fungi [104,105].

The research of antituberculosis utilizes not only the *M. tuberculosis* strain but also non-tuberculosis strains such as *M. smegmatis*, *M. bovis* BCG, *M. phlei*, and *M. marinum*. The *M. tuberculosis* strain is a slow-organism and pathogenic organism; hence, research using *M. tuberculosis* must be done in a facility with high safety measures, such as biosafety level 3 (BSL 3), which is not easily available and accessible in most countries [106–108]. In addition, research using *M. tuberculosis* requires a long time for practical experiments [106–108]. Therefore, most researchers use alternative models with low pathogenicity and rapid growth to investigate antituberculosis activity, but still show comparable susceptibility to *M. tuberculosis*, especially in the screening phase. A study on *M. tuberculosis* genome analysis revealed that about 2800 of 4000 protein-coding genes have comparable equivalents in *M. smegmatis* and *M. bovis* BCG, with >50% similarity in the amino acid composition, suggesting that *M. smegmatis* and *M. bovis* BCG may show comparative susceptibility to *M. tuberculosis* and can be used as a model in the antituberculosis screening process [107]. A successful story of using a non-tuberculosis strain in antituberculosis discovery is the study of bedaquiline, a novel anti-TB drug that acts as a mycobacterial ATP synthase inhibitor that was initially investigated against *M. smegmatis* [109]. Also, the activity spectrum against various *Mycobacterium* strains, such as *M. tuberculosis*, *M. smegmatis*, and *M. bovis* BCG, highlights the utility of surrogate models in early-stage drug discovery. This is particularly relevant for initial screening due to the biosafety and logistical challenges associated with *M. tuberculosis* studies. However, before claiming to be antituberculosis to treat *M. tuberculosis* infection, any potential antimycobacterial hits or leads from screening using *M. smegmatis* or other non-tuberculosis strains must be investigated against *M. tuberculosis* strains eventually.

As described previously, the need to find sterilizing agents (anti-dormant) that are effective in eradicating tubercles in aerobic and dormant states to shorten the therapy remains critical in antituberculosis discovery [14,36,79,80]. Current TB therapies are time-consuming and ineffective against latent infections, often leading to relapse and contributing to the global disease burden [110–113]. This review revealed another critical gap in antituberculosis discovery, which is the limited focus on anti-dormancy activity. Dormant *Mycobacterium* populations are key contributors to prolonged tuberculosis therapy, as they exhibit a state of metabolic inactivity that can render them resistant to most conventional antibiotics targeting active bacterial processes [36,79,80]. We found that only 5 out of 131 MF antimycobacterials were tested against non-replicating or dormant phenotypes. This review showed the scarcity of exploring MF NPs and anti-dormancy. To our knowledge, in the last five years, only one study on anti-dormancy from marine-derived fungi has been reported, which is the activity of the ethyl-acetate extract of marine-derived *Aspergillus ostianus* and *Aspergillus flavus* fermentation products against hypoxic-induced dormant *M. smegmatis* [114]. These findings encourage the investigation of MF NPs (previously identified as active against replicating mycobacteria) for their efficacy against dormant *Mycobacterium*.

3.2. Mechanisms of Action of Antimycobacterials

Marine-derived fungi's natural products target a remarkably broad spectrum of mycobacterial biochemical pathways, illustrating the power of diverse scaffolds to hit both

classical and unconventional targets. A number of isolated metabolites disable mycobacterial virulence factors: for instance, polyketide-derived inhibitors of the secreted protein tyrosine phosphatases MptpB and MptpA can impair the pathogen's ability to modulate host immune responses. For example, compounds **25**–**27** exemplify this by potently inhibiting MptpB through a distinctive pharmacophore (a rigid 1,4-diketone core flanked by phenolic or β-hydroxy groups) that mimics the phosphate dianion and fits into the enzyme's wide active site. Other metabolites act on entirely different targets. Compound **105**, a unique alkaloid from *Talaromyces*, inhibits the eukaryotic-like serine/threonine kinase PknG, thereby potentially preventing *M. tuberculosis* from blocking phagosome–lysosome fusion. Likewise, *Trichoderma*-derived aminolipopeptides trichoderins A/A1 (**109**, **110**) and B (**111**) bind the mycobacterial ATP synthase, collapsing ATP generation in non-replicating bacilli in a mechanism analogous to the TB drug bedaquiline. The anthraquinone emodin (**17**) and related planar polyketides offer yet another strategy by intercalating into guanine-rich DNA to stabilize G-quadruplex structures in vital genes (e.g., *mosR* and *ndhA*), thereby suppressing gene expression and slowing growth. This breadth of targets, from central metabolism to DNA topology and virulence signaling, highlights the unique therapeutic promise of marine fungal metabolites in tackling TB from multiple angles. An illustration of the mechanism of action is shown in Figure 18.

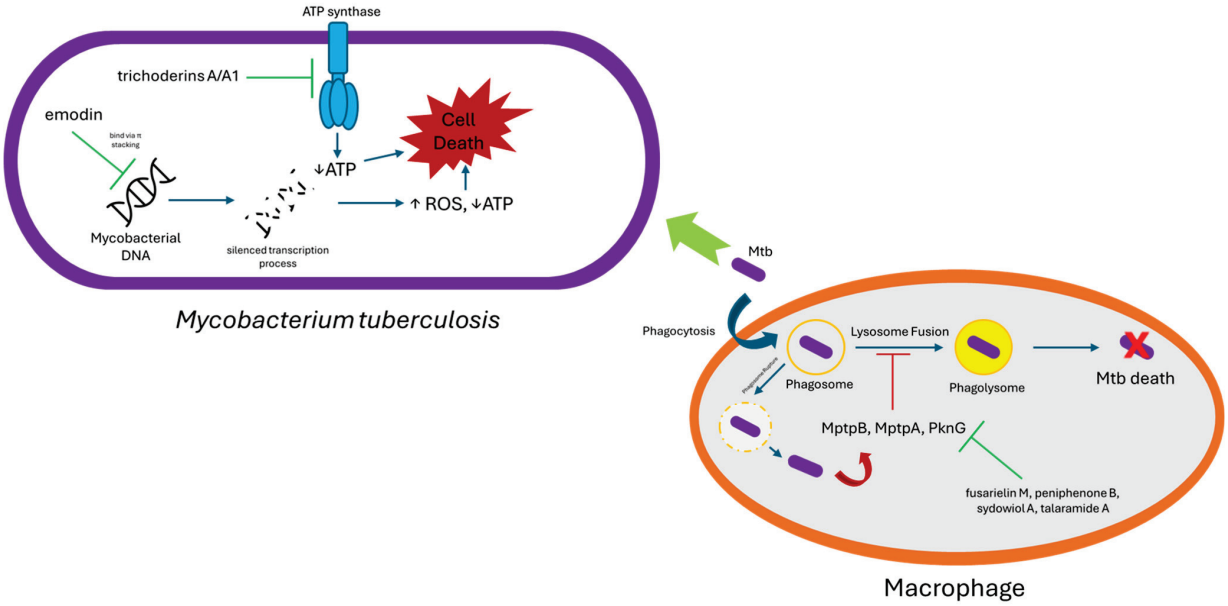

Figure 18. The mechanism of action of several metabolites by inhibiting different targets from *Mycobacterium tuberculosis*.

3.3. Challenges Posed by Mycotoxins

One of the main challenges with drug exploration from fungi, including in marine and terrestrial environments, is their frequent co-classification as mycotoxins or potent cytotoxins. Some of the compounds reported in this article, including those with potent antimycobacterial activity, were reported as mycotoxins and posed significant toxicities to mammals.

Gliotoxin (**88**) was found to provoke pronounced immunosuppression and lymphocyte apoptosis in mammals, illustrating how potent antimycobacterial efficacy can coexist with unacceptable host toxicity [115]. Secalonic acid D (**34**), while active against *M. tuberculosis*, is simultaneously a teratogenic mycotoxin that induces fetal malformations in rodent models [116]. Helvolic acid (**116**) exerts broad cytotoxic effects on human cancer cell lines and shows limited tolerability in murine in vivo studies [117]. Viomellein (**28**) was reported

as a nephrotoxic historically linked to animal mycotoxicoses in contaminated grain, and its structural congener, xanthomegnin (**29**), is both nephrotoxic and mutagenic [118,119]. Tremorgenic indole-diterpenes such as fumitremorgin B (**99**) were found to trigger sustained convulsions, DNA damage in human lymphocytes, and even lethality in mice [120]. Actin-binding cytochalasins including chaetoglobosins A (**84**) and B (**85**) disrupt microfilament polymerization and exhibit potent cytotoxicity toward mammalian cells [121]. Other compounds such as **18**, **104**, **119**, and **124** were found to exhibit cytotoxicity against human cells, neurotoxicity, and immunotoxicity [115,117,122].

Many of the most potent antimycobacterial metabolites isolated from marine fungi carry well-documented liabilities that range from immunosuppression and teratogenicity to nephro- and neurotoxicity in mammalian systems. Their shared propensity for off-target damage suggests a fundamental paradox of fungal natural-product discovery in which structural motifs that confer high antimycobacterial potency often coincide with chemical features that drive host toxicity. Therefore, recognizing these dualities is critical, as it informs the decision of whether a scaffold should be deprioritized, re-engineered, or delivered in a way that limits systemic exposure.

3.4. Anticipating and Mitigating Toxicity in Marine-Derived Fungal Antimycobacterial Discovery

Marine-derived fungi metabolites provide a rich but risk-laden reservoir for antimycobacterial lead discovery. Because many potent hits harbor mycotoxin-associated toxicophores, an effective discovery pipeline must anticipate liabilities as early as dereplication and then deploy a suite of chemical, biosynthetic, pharmacological, and formulation-based tactics to widen the therapeutic window.

High-resolution LC-MS/MS datasets of an extract can be visualized in GNPS molecular networks or matched in silico to curate the fungal metabolites, hence allowing for the rapid flagging of hazardous chemotypes such as mycotoxins before laborious purification begins [123]. This strategy is also useful as a dereplication tool to avoid re-isolating known fungal metabolites or compounds with previously reported bioactivities [124]. Hence, by overlaying feature-based molecular networking (FBMN) with the public GNPS spectral libraries and in-house mycotoxin databases, investigators can rank network nodes by novelty scores, triage sub-clusters that match hazardous scaffolds, and channel purification resources toward molecular families lacking confident annotations [125]. The FBMN workflow also incorporates quantitative ion-intensity data, enabling the early estimation of compound abundance and signaling when a low-level but novel node may not justify extensive scale-up [125]. Complementary mass-defect filtering and mass-shift searches further sharpen dereplication by excluding spectra that fall within characteristic mass windows of regulated mycotoxins [126,127].

Targeted delivery and formulation-based dose-sparing also offer a complementary route to toxicity mitigation by physically shielding reactive fungal metabolites from off-target tissues and restricting drug exposure to the primary site of infection. Liposomal encapsulation is a clinically validated paradigm that is best exemplified by liposomal amphotericin B, whose reformulation can cut nephro- and infusion-related toxicity relative to the parent macrolide while preserving antifungal potency [128,129]. Similar nanocarrier principles are now being translated to tuberculosis, such as polymeric, lipid, and PLGA nanoparticles that consistently lower the effective doses of rifampicin, isoniazid, and bedaquiline in animal models, thereby reducing systemic adverse effects without compromising bactericidal activity [130,131]. Proof-of-concept for mycotoxins has emerged with magnetic nanoparticle conjugates of gliotoxin, which showed attenuated cytotoxicity in mammalian cells yet retained intracellular antimicrobial activity, demonstrating that

nano-shielding can tame even highly reactive species [132,133]. Hence, by applying these orthogonal yet synergistic approaches, researchers can systematically convert hazardous marine-fungal mycotoxins into selective and clinically relevant antitubercular leads.

4. Conclusions

Marine-derived fungi (MF) are potential sources of natural products (NPs) with antimycobacterial activity, contributing to a diverse array of metabolites classified into polyketides, alkaloids, peptides, terpenoids, and miscellaneous compounds. Of the 139 identified metabolites, 131 exhibited antimycobacterial activity, with 25 compounds demonstrating strong activity and 50% classified as novel compounds. *Aspergillus* remains the most dominant and productive genus for antimycobacterial compound; however, the utilization of dereplication strategies is necessary to prevent the rediscovery of known antimycobacterials from *Aspergillus*. In addition, focusing on underexplored fungal genera such as *Arthrinium*, *Coniothyrium*, *Zopfiella*, *Trichoderma*, and *Tolypocladium* and targeting marine sources like mangroves, marine sediments, sponges, and algae offer promising avenues for MF antimycobacterial compounds. Nonetheless, the less extensive studies on algae, corals, sea fans, ascidians, and marine anemones suggest that these sources might be a promising source for obtaining novel and unique fungal genera capable of producing bioactive compounds with antimycobacterial activity. Recurrent structural motifs can be discerned, pointing to privileged scaffolds for antimycobacterial activity. For example, several conjugated polyketide frameworks (featuring α,β-unsaturated carbonyls adjacent to hydroxyls) consistently appear in potent isolates, as do planar polyphenolic scaffolds capable of multivalent interactions (e.g., the tri-phenolate arrangement in pyrogallol ethers) and lipophilic cyclic peptides with amphipathic profiles. These pharmacophores underpin interactions with diverse targets, from enzyme active sites to bacterial membranes and DNA, and thus represent valuable starting points for medicinal chemistry optimization. Our SAR analysis across different compound series highlights that even subtle modifications (e.g., the stereochemistry of a double bond or the presence of a specific functional group) can dramatically influence antimycobacterial potency, offering clues for designing analogues with improved efficacy and reduced toxicity. We showed that marine fungal metabolites can inhibit targets and pathways not addressed by current TB drugs, such as virulence factors like MptpB, MptpA, and PknG, and essential bacterial machinery like ATP synthase and DNA topology, thereby opening avenues to overcome existing drug resistance. Compounds acting on such novel targets could retain activity against drug-resistant *M. tuberculosis* strains and even bypass common resistance mechanisms, since their modes of action differ fundamentally from those of first-line agents. Only a small fraction of MF antimycobacterial has been investigated against the dormant phenotype, highlighting a critical gap in current research. These findings underscore the potential of MF as a valuable resource for TB drug discovery, including in addressing drug resistance and dormancy-related challenges.

Author Contributions: Conceptualization, M.A. (Muhammad Azhari), N.M. and E.J.; investigation, M.A. (Muhammad Azhari), M.S., M.A. (Masayoshi Arai) and E.J.; resources, M.A. (Muhammad Azhari) and N.M.; data curation, M.A. (Muhammad Azhari) and N.M.; writing—original draft preparation, M.A. (Muhammad Azhari) and N.M.; writing—review and editing, M.A. (Muhammad Azhari), N.M. and M.S.; visualization, M.A. (Muhammad Azhari) and E.J.; supervision, M.S., M.A. (Masayoshi Arai) and E.J. All authors have read and agreed to the published version of the manuscript.

Funding: Elin Julianti thanks the ITB Research, Community Service and Innovation Program (PPMI) 2022 (no. 16A/IT1.C10/SK-KP/2022); Fundamental Research 2023, The Ministry of Education, Culture, Research, and Technology of the Republic of Indonesia (no. 110/E5/PG.02.00.PL/2023); and the ITB Research Program 2024 (no. 1250/IT1.C10/TA/2024) for supporting the research on bioactive

compounds from marine-derived fungi in the Laboratory of Microbiology and Bioprocess, School of Pharmacy, ITB.

Acknowledgments: Muhammad Azhari acknowledges the Indonesia Endowment Fund for Education Agency (LPDP) (no. 202207213210477) for supporting his PhD study for which this article was written. Muhammad Azhari and Elin Julianti also thank the Nishimura International Scholarship Foundation (NISF) for supporting the antituberculosis and anticancer research training at Osaka University.

Conflicts of Interest: The authors declare that they have no competing financial interests or personal relationships that could have appeared to influence the work reported in this paper.

References

1. Barberis, I.; Bragazzi, N.L.; Galluzzo, L.; Martini, M. The History of Tuberculosis: From the First Historical Records to the Isolation of Koch's Bacillus. *J. Prev. Med. Hyg.* **2017**, *58*, E9.
2. World Health Organization. *WHO Consolidated Guidelines on Tuberculosis*; WHO: Geneva, Switzerland, 2022.
3. Lai, P.-C.; Low, C.-T.; Tse, W.-S.C.; Tsui, C.-K.; Lee, H.; Hui, P.-K. Risk of Tuberculosis in High-Rise and High Density Dwellings: An Exploratory Spatial Analysis. *Environ. Pollut.* **2013**, *183*, 40–45. [CrossRef] [PubMed]
4. Hunter, R.L. The Pathogenesis of Tuberculosis: The Early Infiltrate of Post-Primary (Adult Pulmonary) Tuberculosis: A Distinct Disease Entity. *Front. Immunol.* **2018**, *9*, 2108. [CrossRef]
5. Rahlwes, K.C.; Dias, B.R.S.; Campos, P.C.; Alvarez-Arguedas, S.; Shiloh, M.U. Pathogenicity and Virulence of *Mycobacterium tuberculosis*. *Virulence* **2023**, *14*, 2150449. [CrossRef] [PubMed]
6. Smith, I. *Mycobacterium Tuberculosis* Pathogenesis and Molecular Determinants of Virulence. *Clin. Microbiol. Rev.* **2003**, *16*, 463–496. [CrossRef]
7. Sigwart, J.D.; Blasiak, R.; Jaspars, M.; Jouffray, J.-B.; Tasdemir, D. Unlocking the Potential of Marine Biodiscovery. *Nat. Prod. Rep.* **2021**, *38*, 1235–1242. [CrossRef]
8. Carroll, A.R.; Copp, B.R.; Davis, R.A.; Keyzers, R.A.; Prinsep, M.R. Marine Natural Products. *Nat. Prod. Rep.* **2021**, *38*, 362–413. [CrossRef] [PubMed]
9. Cox, R.J.; Skellam, E.; Williams, K. Biosynthesis of Fungal Polyketides. In *Physiology and Genetics*; Springer International Publishing: Cham, Switzerland, 2018; pp. 385–412.
10. Harwani, D.; Barupal, S.; Begani, J.; Lakhani, J. Genetic Diversity of Polyketide Synthases and Nonribosomal Peptide Synthetases in Fungi. In *New and Future Developments in Microbial Biotechnology and Bioengineering*; Elsevier: Amsterdam, The Netherlands, 2020; pp. 11–21.
11. Rodrigues, A.G. Secondary Metabolism and Antimicrobial Metabolites of Aspergillus. In *New and Future Developments in Microbial Biotechnology and Bioengineering*; Elsevier: Amsterdam, The Netherlands, 2016; pp. 81–93.
12. Connolly, L.E.; Edelstein, P.H.; Ramakrishnan, L. Why Is Long-Term Therapy Required to Cure Tuberculosis? *PLoS Med.* **2007**, *4*, e120. [CrossRef]
13. Sholeye, A.R.; Williams, A.A.; Loots, D.T.; Tutu van Furth, A.M.; van der Kuip, M.; Mason, S. Tuberculous Granuloma: Emerging Insights From Proteomics and Metabolomics. *Front. Neurol.* **2022**, *13*, 804838. [CrossRef]
14. Arai, M.; Kamiya, K.; Pruksakorn, P.; Sumii, Y.; Kotoku, N.; Joubert, J.-P.; Moodley, P.; Han, C.; Shin, D.; Kobayashi, M. Anti-Dormant Mycobacterial Activity and Target Analysis of Nybomycin Produced by a Marine-Derived *Streptomyces* Sp. *Bioorg. Med. Chem.* **2015**, *23*, 3534–3541. [CrossRef]
15. Vilchèze, C. Mycobacterial Cell Wall: A Source of Successful Targets for Old and New Drugs. *Appl. Sci.* **2020**, *10*, 2278. [CrossRef]
16. Liu, Z.; Dong, Z.; Qiu, P.; Wang, Q.; Yan, J.; Lu, Y.; Wasu, P.; Hong, K.; She, Z. Two New Bioactive Steroids from a Mangrove-Derived Fungus *Aspergillus* Sp. *Steroids* **2018**, *140*, 32–38. [CrossRef] [PubMed]
17. Lee, J.W.; Lee, W.; Perera, R.H.; Lim, Y.W. Long-Term Investigation of Marine-Derived *Aspergillus* Diversity in the Republic of Korea. *Mycobiology* **2023**, *51*, 436–444. [CrossRef]
18. Gonçalves, M.F.M.; Esteves, A.C.; Alves, A. Marine Fungi: Opportunities and Challenges. *Encyclopedia* **2022**, *2*, 559–577. [CrossRef]
19. Imhoff, J. Natural Products from Marine Fungi—Still an Underrepresented Resource. *Mar. Drugs* **2016**, *14*, 19. [CrossRef] [PubMed]
20. Cos, P.; Vlietinck, A.J.; Berghe, D.V.; Maes, L. Anti-Infective Potential of Natural Products: How to Develop a Stronger In Vitro 'Proof-of-Concept'. *J. Ethnopharmacol.* **2006**, *106*, 290–302. [CrossRef]
21. Xia, G.; Li, J.; Li, H.; Long, Y.; Lin, S.; Lu, Y.; He, L.; Lin, Y.; Liu, L.; She, Z. Alterporriol-Type Dimers from the Mangrove Endophytic Fungus, Alternaria Sp. (SK11), and Their MptpB Inhibitions. *Mar. Drugs* **2014**, *12*, 2953–2969. [CrossRef]

22. Fan, L.; Wu, X.; Jin, C.; Li, F.; Xiong, S.; Dong, Y. MptpB Promotes Mycobacteria Survival by Inhibiting the Expression of Inflammatory Mediators and Cell Apoptosis in Macrophages. *Front. Cell Infect. Microbiol.* **2018**, *8*, 171. [CrossRef]
23. Vickers, C.F.; Silva, A.P.G.; Chakraborty, A.; Fernandez, P.; Kurepina, N.; Saville, C.; Naranjo, Y.; Pons, M.; Schnettger, L.S.; Gutierrez, M.G.; et al. Structure-Based Design of MptpB Inhibitors That Reduce Multidrug-Resistant *Mycobacterium Tuberculosis* Survival and Infection Burden in Vivo. *J. Med. Chem.* **2018**, *61*, 8337–8352. [CrossRef]
24. Seibert, S.F.; Eguereva, E.; Krick, A.; Kehraus, S.; Voloshina, E.; Raabe, G.; Fleischhauer, J.; Leistner, E.; Wiese, M.; Prinz, H.; et al. Polyketides from the Marine-Derived Fungus *Ascochyta Salicorniae* and Their Potential to Inhibit Protein Phosphatases. *Org. Biomol. Chem.* **2006**, *4*, 2233–2240. [CrossRef]
25. Zhou, B.; He, Y.; Zhang, X.; Xu, J.; Luo, Y.; Wang, Y.; Franzblau, S.G.; Yang, Z.; Chan, R.J.; Liu, Y.; et al. Targeting Mycobacterium Protein Tyrosine Phosphatase B for Antituberculosis Agents. *Proc. Natl. Acad. Sci. USA* **2010**, *107*, 4573–4578. [CrossRef] [PubMed]
26. Zhang, Y.; Ling, S.; Fang, Y.; Zhu, T.; Gu, Q.; Zhu, W. Isolation, Structure Elucidation, and Antimycobacterial Properties of Dimeric Naphtho-γ-pyrones from the Marine-Derived Fungus *Aspergillus carbonarius*. *Chem. Biodivers.* **2008**, *5*, 93–100. [CrossRef] [PubMed]
27. Liu, Z.; Wang, Q.; Li, S.; Cui, H.; Sun, Z.; Chen, D.; Lu, Y.; Liu, H.; Zhang, W. Polypropionate Derivatives with *Mycobacterium Tuberculosis* Protein Tyrosine Phosphatase B Inhibitory Activities from the Deep-Sea-Derived Fungus *Aspergillus Fischeri* FS452. *J. Nat. Prod.* **2019**, *82*, 3440–3449. [CrossRef] [PubMed]
28. Song, Z.; Liu, Y.; Gao, J.; Hu, J.; He, H.; Dai, S.; Wang, L.; Dai, H.; Zhang, L.; Song, F. Antitubercular Metabolites from the Marine-Derived Fungus Strain *Aspergillus Fumigatus* MF029. *Nat. Prod. Res.* **2021**, *35*, 2647–2654. [CrossRef]
29. Dey, A.; Anand, K.; Singh, A.; Prasad, R.; Barthwal, R. Binding-Induced Thermal Stabilization of MosR and NdhA G-Quadruplex Comprising Genes by Emodin Leads to Downregulation and Growth Inhibition in Mtb: Potential as Anti-Tuberculosis Drug. *Results Chem.* **2023**, *6*, 101114. [CrossRef]
30. Yu, G.; Wu, G.; Sun, Z.; Zhang, X.; Che, Q.; Gu, Q.; Zhu, T.; Li, D.; Zhang, G. Cytotoxic Tetrahydroxanthone Dimers from the Mangrove-Associated Fungus Aspergillus Versicolor HDN1009. *Mar. Drugs* **2018**, *16*, 335. [CrossRef]
31. Ding, L.; Ren, L.; Li, S.; Song, J.; Han, Z.; He, S.; Xu, S. Production of New Antibacterial 4-Hydroxy-α-Pyrones by a Marine Fungus *Aspergillus Niger.* Cultivated in Solid Medium. *Mar. Drugs* **2019**, *17*, 344. [CrossRef]
32. Zhou, G.; Chen, X.; Zhang, X.; Che, Q.; Zhang, G.; Zhu, T.; Gu, Q.; Li, D. Prenylated *p* -Terphenyls from a Mangrove Endophytic Fungus, *Aspergillus Candidus* LDJ-5. *J. Nat. Prod.* **2020**, *83*, 8–13. [CrossRef]
33. Xiao, Z.; Lin, S.; Tan, C.; Lu, Y.; He, L.; Huang, X.; She, Z. Asperlones A and B, Dinaphthalenone Derivatives from a Mangrove Endophytic Fungus Aspergillus Sp. 16-5C. *Mar. Drugs* **2015**, *13*, 366–378. [CrossRef]
34. Beresford, N.; Patel, S.; Armstrong, J.; Szöor, B.; Fordham-Skelton, A.P.; Tabernero, L. MptpB, a Virulence Factor from *Mycobacterium Tuberculosis*, Exhibits Triple-Specificity Phosphatase Activity. *Biochem. J.* **2007**, *406*, 13–18. [CrossRef]
35. Mascarello, A.; Mori, M.; Chiaradia-Delatorre, L.D.; Menegatti, A.C.O.; Monache, F.D.; Ferrari, F.; Yunes, R.A.; Nunes, R.J.; Terenzi, H.; Botta, B.; et al. Discovery of Mycobacterium Tuberculosis Protein Tyrosine Phosphatase B (PtpB) Inhibitors from Natural Products. *PLoS ONE* **2013**, *8*, e77081. [CrossRef] [PubMed]
36. Kamiya, K.; Arai, M.; Setiawan, A.; Kobayashi, M. Anti-Dormant Mycobacterial Activity of Viomellein and Xanthomegnin, Naphthoquinone Dimers Produced by Marine-Derived *Aspergillus* Sp. *Nat. Prod. Commun.* **2017**, *12*, 1934578X1701200. [CrossRef]
37. Gupta, V.K.; Kumar, M.M.; Singh, D.; Bisht, D.; Sharma, S. Drug Targets in Dormant *Mycobacterium Tuberculosis*: Can the Conquest Against Tuberculosis Become a Reality? *Infect. Dis.* **2018**, *50*, 81–94. [CrossRef] [PubMed]
38. Kovermann, M.; Stefan, A.; Palazzetti, C.; Immler, F.; Dal Piaz, F.; Bernardi, L.; Cimone, V.; Bellone, M.L.; Hochkoeppler, A. The *Mycobacterium Tuberculosis* Protein Tyrosine Phosphatase MptpA Features a PH Dependent Activity Overlapping the Bacterium Sensitivity to Acidic Conditions. *Biochimie* **2023**, *213*, 66–81. [CrossRef] [PubMed]
39. Liu, X.; Song, F.; Ma, L.; Chen, C.; Xiao, X.; Ren, B.; Liu, X.; Dai, H.; Piggott, A.M.; Av-Gay, Y.; et al. Sydowiols A–C: *Mycobacterium Tuberculosis* Protein Tyrosine Phosphatase Inhibitors from an East China Sea Marine-Derived Fungus, *Aspergillus sydowii*. *Tetrahedron Lett.* **2013**, *54*, 6081–6083. [CrossRef]
40. Stehle, T.; Sreeramulu, S.; Löhr, F.; Richter, C.; Saxena, K.; Jonker, H.R.A.; Schwalbe, H. The Apo-Structure of the Low Molecular Weight Protein-Tyrosine Phosphatase A (MptpA) from Mycobacterium Tuberculosis Allows for Better Target-Specific Drug Development. *J. Biol. Chem.* **2012**, *287*, 34569–34582. [CrossRef]
41. Luo, X.-W.; Lin, Y.; Lu, Y.-J.; Zhou, X.-F.; Liu, Y.-H. Peptides and Polyketides Isolated from the Marine Sponge-Derived Fungus Aspergillus Terreus SCSIO 41008. *Chin. J. Nat. Med.* **2019**, *17*, 149–154. [CrossRef]
42. Wang, Y.; Lin, X.-P.; Ju, Z.-R.; Liao, X.-J.; Huang, X.-J.; Zhang, C.; Zhao, B.-X.; Xu, S.-H. Aspergchromones A and B, Two New Polyketides from the Marine Sponge-Associated Fungus *Aspergillus* Sp. SCSIO XWS03F03. *J. Asian Nat. Prod. Res.* **2017**, *19*, 684–690. [CrossRef]

43. Elsebai, M.F.; Kehraus, S.; Lindequist, U.; Sasse, F.; Shaaban, S.; Gütschow, M.; Josten, M.; Sahl, H.-G.; König, G.M. Antimicrobial Phenalenone Derivatives from the Marine-Derived Fungus *Coniothyrium cereale*. *Org. Biomol. Chem.* **2011**, *9*, 802–808. [CrossRef]
44. Elsebai, M.F.; Natesan, L.; Kehraus, S.; Mohamed, I.E.; Schnakenburg, G.; Sasse, F.; Shaaban, S.; Gütschow, M.; König, G.M. HLE-Inhibitory Alkaloids with a Polyketide Skeleton from the Marine-Derived Fungus *Coniothyrium cereale*. *J. Nat. Prod.* **2011**, *74*, 2282–2285. [CrossRef]
45. Grundner, C.; Perrin, D.; Hooft van Huijsduijnen, R.; Swinnen, D.; Gonzalez, J.; Gee, C.L.; Wells, T.N.; Alber, T. Structural Basis for Selective Inhibition of *Mycobacterium tuberculosis* Protein Tyrosine Phosphatase PtpB. *Structure* **2007**, *15*, 499–509. [CrossRef] [PubMed]
46. Chen, D.; Liu, L.; Lu, Y.; Chen, S. Identification of Fusarielin M as a Novel Inhibitor of *Mycobacterium Tuberculosis* Protein Tyrosine Phosphatase B (MptpB). *Bioorg Chem.* **2021**, *106*, 104495. [CrossRef] [PubMed]
47. Trisuwan, K.; Khamthong, N.; Rukachaisirikul, V.; Phongpaichit, S.; Preedanon, S.; Sakayaroj, J. Anthraquinone, Cyclopentanone, and Naphthoquinone Derivatives from the Sea Fan-Derived Fungi *Fusarium* Spp. PSU-F14 and PSU-F135. *J. Nat. Prod.* **2010**, *73*, 1507–1511. [CrossRef]
48. Kong, X.; Ma, X.; Xie, Y.; Cai, S.; Zhu, T.; Gu, Q.; Li, D. Aromatic Polyketides from a Sponge-Derived Fungus *Metarhizium Anisopliae* Mxh-99 and Their Antitubercular Activities. *Arch. Pharm. Res.* **2013**, *36*, 739–744. [CrossRef] [PubMed]
49. Wang, C.; Wang, J.; Huang, Y.; Chen, H.; Li, Y.; Zhong, L.; Chen, Y.; Chen, S.; Wang, J.; Kang, J.; et al. Anti-Mycobacterial Activity of Marine Fungus-Derived 4-Deoxybostrycin and Nigrosporin. *Molecules* **2013**, *18*, 1728–1740. [CrossRef]
50. Sabdaningsih, A.; Liu, Y.; Mettal, U.; Heep, J.; Riyanti; Wang, L.; Cristianawati, O.; Nuryadi, H.; Triandala Sibero, M.; Marner, M.; et al. A New Citrinin Derivative from the Indonesian Marine Sponge-Associated Fungus Penicillium Citrinum. *Mar. Drugs* **2020**, *18*, 227. [CrossRef]
51. Li, H.; Jiang, J.; Liu, Z.; Lin, S.; Xia, G.; Xia, X.; Ding, B.; He, L.; Lu, Y.; She, Z. Peniphenones A–D from the Mangrove Fungus *Penicillium Dipodomyicola* HN4-3A as Inhibitors of *Mycobacterium tuberculosis* Phosphatase MptpB. *J. Nat. Prod.* **2014**, *77*, 800–806. [CrossRef]
52. Shah, M.; Sun, C.; Sun, Z.; Zhang, G.; Che, Q.; Gu, Q.; Zhu, T.; Li, D. Antibacterial Polyketides from Antarctica Sponge-Derived Fungus *Penicillium* Sp. HDN151272. *Mar. Drugs* **2020**, *18*, 71. [CrossRef]
53. He, F.; Li, X.; Yu, J.-H.; Zhang, X.; Nong, X.; Chen, G.; Zhu, K.; Wang, Y.-Y.; Bao, J.; Zhang, H. Secondary Metabolites from the Mangrove Sediment-Derived Fungus *Penicillium Pinophilum* SCAU037. *Fitoterapia* **2019**, *136*, 104177. [CrossRef]
54. Morehouse, N.J.; Flewelling, A.J.; Johnson, J.A.; Gray, C.A. Halogenated Bianthrones from *Penicillium Roseopurpureum*: A Fungal Endophyte of the Marine Alga *Petalonia fascia*. *Nat. Prod. Commun.* **2020**, *15*, 1934578X2090140. [CrossRef]
55. Han, Y.; Sun, C.; Li, C.; Zhang, G.; Zhu, T.; Li, D.; Che, Q. Antibacterial Phenalenone Derivatives from Marine-Derived Fungus *Pleosporales* Sp. HDN1811400. *Tetrahedron Lett.* **2021**, *68*, 152938. [CrossRef]
56. Ge, X.; Sun, C.; Feng, Y.; Wang, L.; Peng, J.; Che, Q.; Gu, Q.; Zhu, T.; Li, D.; Zhang, G. Anthraquinone Derivatives from a Marine-Derived Fungus *Sporendonema Casei* HDN16-802. *Mar. Drugs* **2019**, *17*, 334. [CrossRef] [PubMed]
57. Chokpaiboon, S.; Unagul, P.; Nithithanasilp, S.; Komwijit, S.; Somyong, W.; Ratiarpakul, T.; Isaka, M.; Bunyapaiboonsri, T. Salicylaldehyde and Dihydroisobenzofuran Derivatives from the Marine Fungus *Zopfiella marina*. *Nat. Prod. Res.* **2018**, *32*, 149–153. [CrossRef]
58. Bunyapaiboonsri, T.; Yoiprommarat, S.; Nopgason, R.; Intereya, K.; Suvannakad, R.; Sakayaroj, J. Palmarumycins from the Mangrove Fungus BCC 25093. *Tetrahedron* **2015**, *71*, 5572–5578. [CrossRef]
59. Lin, Z.; Koch, M.; Abdel Aziz, M.H.; Galindo-Murillo, R.; Tianero, M.D.; Cheatham, T.E.; Barrows, L.R.; Reilly, C.A.; Schmidt, E.W. Oxazinin A, a Pseudodimeric Natural Product of Mixed Biosynthetic Origin from a Filamentous Fungus. *Org. Lett.* **2014**, *16*, 4774–4777. [CrossRef]
60. Yu, G.; Sun, Z.; Peng, J.; Zhu, M.; Che, Q.; Zhang, G.; Zhu, T.; Gu, Q.; Li, D. Secondary Metabolites Produced by Combined Culture of *Penicillium crustosum* and a *Xylaria* Sp. *J. Nat. Prod.* **2019**, *82*, 2013–2017. [CrossRef]
61. Bao, J.; Zhai, H.; Zhu, K.; Yu, J.-H.; Zhang, Y.; Wang, Y.; Jiang, C.-S.; Zhang, X.; Zhang, Y.; Zhang, H. Bioactive Pyridone Alkaloids from a Deep-Sea-Derived Fungus *Arthrinium* Sp. UJNMF0008. *Mar. Drugs* **2018**, *16*, 174. [CrossRef]
62. Flewelling, A.J.; Bishop, A.L.; Johnson, J.A.; Gray, C.A. Polyketides from an Endophytic *Aspergillus Fumigatus* Isolate Inhibit the Growth of *Mycobacterium Tuberculosis* and MRSA. *Nat. Prod. Commun.* **2015**, *10*, 1934578X1501001. [CrossRef]
63. Zheng, J.; Xu, Z.; Wang, Y.; Hong, K.; Liu, P.; Zhu, W. Cyclic Tripeptides from the Halotolerant Fungus *Aspergillus Sclerotiorum* PT06-1. *J. Nat. Prod.* **2010**, *73*, 1133–1137. [CrossRef]
64. Vellé, A.; Cebollada, A.; Macías, R.; Iglesias, M.; Gil-Moles, M.; Sanz Miguel, P.J. From Imidazole toward Imidazolium Salts and N-Heterocyclic Carbene Ligands: Electronic and Geometrical Redistribution. *ACS Omega* **2017**, *2*, 1392–1399. [CrossRef]

65. Wu, Y.; Liao, H.; Liu, L.-Y.; Sun, F.; Chen, H.-F.; Jiao, W.-H.; Zhu, H.-R.; Yang, F.; Huang, G.; Zeng, D.-Q.; et al. Phakefustatins A–C: Kynurenine-Bearing Cycloheptapeptides as RXRα Modulators from the Marine Sponge *Phakellia fusca*. *Org. Lett.* **2020**, *22*, 6703–6708. [CrossRef] [PubMed]
66. Xu, W.-J.; Liao, X.-J.; Xu, S.-H.; Diao, J.-Z.; Du, B.; Zhou, X.-L.; Pan, S.-S. Isolation, Structure Determination, and Synthesis of Galaxamide, A Rare Cytotoxic Cyclic Pentapeptide from a Marine Algae *Galaxaura filamentosa*. *Org. Lett.* **2008**, *10*, 4569–4572. [CrossRef] [PubMed]
67. Teta, R.; Marteinsson, V.T.; Longeon, A.; Klonowski, A.M.; Groben, R.; Bourguet-Kondracki, M.-L.; Costantino, V.; Mangoni, A. Thermoactinoamide A, an Antibiotic Lipophilic Cyclopeptide from the Icelandic Thermophilic Bacterium *Thermoactinomyces vulgaris*. *J. Nat. Prod.* **2017**, *80*, 2530–2535. [CrossRef]
68. Skehan, P.; Storeng, R.; Scudiero, D.; Monks, A.; McMahon, J.; Vistica, D.; Warren, J.T.; Bokesch, H.; Kenney, S.; Boyd, M.R. New Colorimetric Cytotoxicity Assay for Anticancer-Drug Screening. *JNCI J. Natl. Cancer Inst.* **1990**, *82*, 1107–1112. [CrossRef]
69. Sun, C.; Zhang, Z.; Ren, Z.; Yu, L.; Zhou, H.; Han, Y.; Shah, M.; Che, Q.; Zhang, G.; Li, D.; et al. Antibacterial Cyclic Tripeptides from Antarctica-Sponge-Derived Fungus *Aspergillus Insulicola* HDN151418. *Mar. Drugs* **2020**, *18*, 532. [CrossRef]
70. Luo, X.; Zhou, X.; Lin, X.; Qin, X.; Zhang, T.; Wang, J.; Tu, Z.; Yang, B.; Liao, S.; Tian, Y.; et al. Antituberculosis Compounds from a Deep-Sea-Derived Fungus *Aspergillus* Sp. SCSIO Ind09F01. *Nat. Prod. Res.* **2017**, *31*, 1958–1962. [CrossRef] [PubMed]
71. Hou, X.-M.; Liang, T.-M.; Guo, Z.-Y.; Wang, C.-Y.; Shao, C.-L. Discovery, Absolute Assignments, and Total Synthesis of Asperversiamides A–C and Their Potent Activity Against *Mycobacterium marinum*. *Chem. Commun.* **2019**, *55*, 1104–1107. [CrossRef]
72. Song, F.; Liu, X.; Guo, H.; Ren, B.; Chen, C.; Piggott, A.M.; Yu, K.; Gao, H.; Wang, Q.; Liu, M.; et al. Brevianamides with Antitubercular Potential from a Marine-Derived Isolate of *Aspergillus versicolor*. *Org. Lett.* **2012**, *14*, 4770–4773. [CrossRef]
73. Han, J.; Liu, M.; Jenkins, I.D.; Liu, X.; Zhang, L.; Quinn, R.J.; Feng, Y. Genome-Inspired Chemical Exploration of Marine Fungus *Aspergillus Fumigatus* MF071. *Mar. Drugs* **2020**, *18*, 352. [CrossRef]
74. Cui, H.; Lin, Y.; Luo, M.; Lu, Y.; Huang, X.; She, Z. Diaporisoindoles A–C: Three Isoprenylisoindole Alkaloid Derivatives from the Mangrove Endophytic Fungus *Diaporthe* Sp. SYSU-HQ3. *Org. Lett.* **2017**, *19*, 5621–5624. [CrossRef]
75. Pan, J.-H.; Chen, Y.; Huang, Y.-H.; Tao, Y.-W.; Wang, J.; Li, Y.; Peng, Y.; Dong, T.; Lai, X.-M.; Lin, Y.-C. Antimycobacterial Activity of Fusaric Acid From a Mangrove Endophyte and Its Metal Complexes. *Arch. Pharm. Res.* **2011**, *34*, 1177–1181. [CrossRef] [PubMed]
76. Khan, M.Z.; Bhaskar, A.; Upadhyay, S.; Kumari, P.; Rajmani, R.S.; Jain, P.; Singh, A.; Kumar, D.; Bhavesh, N.S.; Nandicoori, V.K. Protein Kinase G Confers Survival Advantage to *Mycobacterium Tuberculosis* during Latency-Like Conditions. *J. Biol. Chem.* **2017**, *292*, 16093–16108. [CrossRef]
77. Chen, S.; He, L.; Chen, D.; Cai, R.; Long, Y.; Lu, Y.; She, Z. Talaramide A, an Unusual Alkaloid From The Mangrove Endophytic Fungus *Talaromyces* Sp. (HZ-YX1) as an Inhibitor of Mycobacterial PknG. *New J. Chem.* **2017**, *41*, 4273–4276. [CrossRef]
78. Morehouse, N.J.; Flewelling, A.J.; Liu, D.Y.; Cavanagh, H.; Linington, R.G.; Johnson, J.A.; Gray, C.A. Tolypocaibols: Antibacterial Lipopeptaibols from a *Tolypocladium* Sp. Endophyte of the Marine Macroalga *Spongomorpha arcta*. *J. Nat. Prod.* **2023**, *86*, 1529–1535. [CrossRef] [PubMed]
79. Pruksakorn, P.; Arai, M.; Kotoku, N.; Vilchèze, C.; Baughn, A.D.; Moodley, P.; Jacobs, W.R.; Kobayashi, M. Trichoderins, Novel Aminolipopeptides from a Marine Sponge-Derived Trichoderma Sp., Are Active Against Dormant Mycobacteria. *Bioorg. Med. Chem. Lett.* **2010**, *20*, 3658–3663. [CrossRef]
80. Pruksakorn, P.; Arai, M.; Liu, L.; Moodley, P.; Jacobs, W.R., Jr.; Kobayashi, M. Action-Mechanism of Trichoderin A, an Anti-Dormant Mycobacterial Aminolipopeptide from Marine Sponge-Derived *Trichoderma* Sp. *Biol. Pharm. Bull.* **2011**, *34*, 1287–1290. [CrossRef]
81. Daferner, M.; Anke, T.; Sterner, O. Zopfiellamides A and B, Antimicrobial Pyrrolidinone Derivatives from the Marine Fungus *Zopfiella latipes*. *Tetrahedron* **2002**, *58*, 7781–7784. [CrossRef]
82. Huang, X.; Huang, H.; Li, H.; Sun, X.; Huang, H.; Lu, Y.; Lin, Y.; Long, Y.; She, Z. Asperterpenoid A, a New Sesterterpenoid as an Inhibitor of *Mycobacterium Tuberculosi* s Protein Tyrosine Phosphatase B from the Culture of *Aspergillus* Sp. 16-5c. *Org. Lett.* **2013**, *15*, 721–723. [CrossRef]
83. Huang, J.-H.; Lv, J.-M.; Wang, Q.-Z.; Zou, J.; Lu, Y.-J.; Wang, Q.-L.; Chen, D.-N.; Yao, X.-S.; Gao, H.; Hu, D. Biosynthesis of an Anti-Tuberculosis Sesterterpenoid Asperterpenoid A. *Org. Biomol. Chem.* **2019**, *17*, 248–251. [CrossRef]
84. Cai, R.; Jiang, H.; Mo, Y.; Guo, H.; Li, C.; Long, Y.; Zang, Z.; She, Z. Ophiobolin-Type Sesterterpenoids from the Mangrove Endophytic Fungus *Aspergillus* Sp. ZJ-68. *J. Nat. Prod.* **2019**, *82*, 2268–2278. [CrossRef]
85. Lv, H.; Wang, K.; Xue, Y.; Chen, J.; Su, H.; Zhang, J.; Wu, Y.; Jia, J.; Bi, H.; Wang, H.; et al. Three New Metabolites From the Marine-Derived Fungus *Aspergillus* Sp. WHUF03110. *Nat. Prod. Commun.* **2021**, *16*, 1934578X2110550. [CrossRef]
86. He, W.-J.; Zhou, X.-J.; Qin, X.-C.; Mai, Y.-X.; Lin, X.-P.; Liao, S.-R.; Yang, B.; Zhang, T.; Tu, Z.-C.; Wang, J.-F.; et al. Quinone/Hydroquinone Meroterpenoids with Antitubercular and Cytotoxic Activities Produced by the Sponge-Derived Fungus *Gliomastix* Sp. ZSDS1-F7. *Nat. Prod. Res.* **2017**, *31*, 604–609. [CrossRef]

87. Elnaggar, M.S.; Ebrahim, W.; Mándi, A.; Kurtán, T.; Müller, W.E.G.; Kalscheuer, R.; Singab, A.; Lin, W.; Liu, Z.; Proksch, P. Hydroquinone Derivatives from the Marine-Derived Fungus *Gliomastix* Sp. *RSC Adv.* **2017**, *7*, 30640–30649. [CrossRef]
88. Elsebai, M.F.; Ghabbour, H.A.; Legrave, N.; Fontaine-Vive, F.; Mehiri, M. New Bioactive Chlorinated Cyclopentene Derivatives from the Marine-Derived Fungus *Phoma* Sp. *Med. Chem. Res.* **2018**, *27*, 1885–1892. [CrossRef]
89. Amend, A.; Burgaud, G.; Cunliffe, M.; Edgcomb, V.P.; Ettinger, C.L.; Gutiérrez, M.H.; Heitman, J.; Hom, E.F.Y.; Ianiri, G.; Jones, A.C.; et al. Fungi in the Marine Environment: Open Questions and Unsolved Problems. *mBio* **2019**, *10*, 01189-18. [CrossRef]
90. Sen, K.; Sen, B.; Wang, G. Diversity, Abundance, and Ecological Roles of Planktonic Fungi in Marine Environments. *J. Fungi* **2022**, *8*, 491. [CrossRef]
91. Akram, H.; Hussain, S.; Mazumdar, P.; Chua, K.O.; Butt, T.E.; Harikrishna, J.A. Mangrove Health: A Review of Functions, Threats, and Challenges Associated with Mangrove Management Practices. *Forests* **2023**, *14*, 1698. [CrossRef]
92. Augusthy, S.; Nizam, A.; Kumar, A. The Diversity, Drivers, Consequences and Management of Plant Invasions in the Mangrove Ecosystems. *Sci. Total Environ.* **2024**, *945*, 173851. [CrossRef]
93. Thatoi, H.; Behera, B.C.; Mishra, R.R. Ecological Role and Biotechnological Potential of Mangrove Fungi: A Review. *Mycology* **2013**, *4*, 54–71. [CrossRef]
94. Kushveer, J.S.; Rashmi, M.; Sarma, V.V. Bioactive Compounds from Marine-Derived Fungi and Their Potential Applications. In *Fungi Bio-Prospects in Sustainable Agriculture, Environment and Nano-Technology*; Elsevier: Amsterdam, The Netherlands, 2021; pp. 91–173.
95. Lienhardt, C.; Raviglione, M.; Spigelman, M.; Hafner, R.; Jaramillo, E.; Hoelscher, M.; Zumla, A.; Gheuens, J. New Drugs for the Treatment of Tuberculosis: Needs, Challenges, Promise, and Prospects for the Future. *J. Infect. Dis.* **2012**, *205*, S241–S249. [CrossRef]
96. Motta, I.; Boeree, M.; Chesov, D.; Dheda, K.; Günther, G.; Horsburgh, C.R.; Kherabi, Y.; Lange, C.; Lienhardt, C.; McIlleron, H.M.; et al. Recent Advances in the Treatment of Tuberculosis. *Clin. Microbiol. Infect.* **2024**, *30*, 1107–1114. [CrossRef] [PubMed]
97. Albarano, L.; Esposito, R.; Ruocco, N.; Costantini, M. Genome Mining as New Challenge in Natural Products Discovery. *Mar. Drugs* **2020**, *18*, 199. [CrossRef] [PubMed]
98. Gaudêncio, S.P.; Pereira, F. Dereplication: Racing to Speed up the Natural Products Discovery Process. *Nat. Prod. Rep.* **2015**, *32*, 779–810. [CrossRef]
99. Tawfike, A.F.; Viegelmann, C.; Edrada-Ebel, R. Metabolomics and Dereplication Strategies in Natural Products. In *Metabolomics Tools for Natural Product Discovery: Methods and Protocols*; Springer: New York, NY, USA, 2013; pp. 227–244.
100. Qin, G.-F.; Zhang, X.; Zhu, F.; Huo, Z.-Q.; Yao, Q.-Q.; Feng, Q.; Liu, Z.; Zhang, G.-M.; Yao, J.-C.; Liang, H.-B. MS/MS-Based Molecular Networking: An Efficient Approach for Natural Products Dereplication. *Molecules* **2022**, *28*, 157. [CrossRef] [PubMed]
101. Wang, M.; Carver, J.J.; Phelan, V.V.; Sanchez, L.M.; Garg, N.; Peng, Y.; Nguyen, D.D.; Watrous, J.; Kapono, C.A.; Luzzatto-Knaan, T.; et al. Sharing and Community Curation of Mass Spectrometry Data with Global Natural Products Social Molecular Networking. *Nat. Biotechnol.* **2016**, *34*, 828–837. [CrossRef]
102. Jiang, C.; Lv, G.; Tu, Y.; Cheng, X.; Duan, Y.; Zeng, B.; He, B. Applications of CRISPR/Cas9 in the Synthesis of Secondary Metabolites in Filamentous Fungi. *Front. Microbiol.* **2021**, *12*, 638096. [CrossRef]
103. Skellam, E.; Rajendran, S.; Li, L. Combinatorial Biosynthesis for the Engineering of Novel Fungal Natural Products. *Commun. Chem.* **2024**, *7*, 89. [CrossRef]
104. Naseema Rasheed, R.; Pourbakhtiar, A.; Mehdizadeh Allaf, M.; Baharlooeian, M.; Rafiei, N.; Alishah Aratboni, H.; Morones-Ramirez, J.R.; Winck, F.V. Microalgal Co-Cultivation-Recent Methods, Trends in Omic-Studies, Applications, and Future Challenges. *Front. Bioeng. Biotechnol.* **2023**, *11*, 1193424. [CrossRef]
105. Oppong-Danquah, E.; Blümel, M.; Scarpato, S.; Mangoni, A.; Tasdemir, D. Induction of Isochromanones by Co-Cultivation of the Marine Fungus Cosmospora Sp. and the Phytopathogen Magnaporthe Oryzae. *Int. J. Mol. Sci.* **2022**, *23*, 782. [CrossRef]
106. Mtafya, B.; Musisi, E.; Qwaray, P.; Sichone, E.; Walbaum, N.; Ntinginya, N.E.; Gillespie, S.H.; Sabiiti, W. Quantifying Viable M. Tuberculosis Safely Obviating the Need for High Containment Facilities. *Methods Mol. Biol.* **2024**, *2833*, 145–152.
107. Gordon, S.V.; Parish, T. Microbe Profile: Mycobacterium Tuberculosis: Humanity's Deadly Microbial Foe. *Microbiology* **2018**, *164*, 437–439. [CrossRef] [PubMed]
108. Baker, J.J.; Johnson, B.K.; Abramovitch, R.B. Slow Growth of *Mycobacterium tuberculosis* at Acidic pH Is Regulated by *PhoPR* and Host-associated Carbon Sources. *Mol. Microbiol.* **2014**, *94*, 56–69. [CrossRef] [PubMed]
109. Andries, K.; Verhasselt, P.; Guillemont, J.; Göhlmann, H.W.H.; Neefs, J.-M.; Winkler, H.; Van Gestel, J.; Timmerman, P.; Zhu, M.; Lee, E.; et al. A Diarylquinoline Drug Active on the ATP Synthase of *Mycobacterium tuberculosis*. *Science* **2005**, *307*, 223–227. [CrossRef]
110. Dutta, N.K.; Karakousis, P.C. Latent Tuberculosis Infection: Myths, Models, and Molecular Mechanisms. *Microbiol. Mol. Biol. Rev.* **2014**, *78*, 343–371. [CrossRef]
111. Magombedze, G.; Dowdy, D.; Mulder, N. Latent Tuberculosis: Models, Computational Efforts and the Pathogen's Regulatory Mechanisms during Dormancy. *Front. Bioeng. Biotechnol.* **2013**, *1*, 1–15. [CrossRef] [PubMed]

112. Ahmad, S. Pathogenesis, Immunology, and Diagnosis of Latent *Mycobacterium Tuberculosis* Infection. *Clin. Dev. Immunol.* **2011**, *2011*, 814943. [CrossRef]
113. Lin, P.L.; Flynn, J.L. Understanding Latent Tuberculosis: A Moving Target. *J. Immunol.* **2010**, *185*, 15–22. [CrossRef]
114. Azhari, M.; Litanjuasari, A.P.; Singgih, M.; Arai, M.; Handayani, D.; Artasasta, M.A.; Julianti, E. Activity of Ethyl Acetate Extracts of Marine-Derived Fungi against Active and Hypoxia-Induced Dormant Mycobacterium. *J. Pharm. Pharmacogn. Res.* **2025**, *13*, 16–26. [CrossRef]
115. Pahl, H.L.; Krauss, B.; Schulze-Osthoff, K.; Decker, T.; Traenckner, E.B.; Vogt, M.; Myers, C.; Parks, T.; Warring, P.; Mühlbacher, A.; et al. The Immunosuppressive Fungal Metabolite Gliotoxin Specifically Inhibits Transcription Factor NF-KappaB. *J. Exp. Med.* **1996**, *183*, 1829–1840. [CrossRef]
116. Mayura, K.; Wallace Hayes, A.; Berndt, W.O. Teratogenicity of Secalonic Acid d in Rats. *Toxicology* **1982**, *25*, 311–322. [CrossRef]
117. Xiao, J.-H.; Zhang, Y.; Liang, G.-Y.; Liu, R.-M.; Li, X.-G.; Zhang, L.-T.; Chen, D.-X.; Zhong, J.-J. Synergistic Antitumor Efficacy of Antibacterial Helvolic Acid from *Cordyceps Taii* and Cyclophosphamide in a Tumor Mouse Model. *Exp. Biol. Med.* **2017**, *242*, 214–222. [CrossRef] [PubMed]
118. Hald, B.; Christensen, D.H.; Krogh, P. Natural Occurrence of the Mycotoxin Viomellein in Barley and the Associated Quinone-Producing Penicillia. *Appl. Env. Microbiol.* **1983**, *46*, 1311–1317. [CrossRef] [PubMed]
119. Gupta, A.K.; Ahmad, I.; Borst, I.; Summerbell, R.C. Detection of Xanthomegnin in Epidermal Materials Infected with Trichophyton Rubrum. *J. Investig. Dermatol.* **2000**, *115*, 901–905. [CrossRef] [PubMed]
120. Sabater-Vilar, M.; Nijmeijer, S.; Fink-Gremmels, J. Genotoxicity Assessment of Five Tremorgenic Mycotoxins (Fumitremorgen B, Paxilline, Penitrem A, Verruculogen, and Verrucosidin) Produced by Molds Isolated from Fermented Meats. *J. Food Prot.* **2003**, *66*, 2123–2129. [CrossRef]
121. Lambert, C.; Schmidt, K.; Karger, M.; Stadler, M.; Stradal, T.E.B.; Rottner, K. Cytochalasans and Their Impact on Actin Filament Remodeling. *Biomolecules* **2023**, *13*, 1247. [CrossRef]
122. Gauthier, T.; Wang, X.; Sifuentes Dos Santos, J.; Fysikopoulos, A.; Tadrist, S.; Canlet, C.; Artigot, M.P.; Loiseau, N.; Oswald, I.P.; Puel, O. Trypacidin, a Spore-Borne Toxin from Aspergillus Fumigatus, Is Cytotoxic to Lung Cells. *PLoS ONE* **2012**, *7*, e29906. [CrossRef]
123. Villanueva-Silva, R.; Velez, P.; Riquelme, M.; Fajardo-Hernández, C.A.; Martínez-Cárdenas, A.; Arista-Romero, A.; Wan, B.; Ma, R.; Qader, M.; Franzblau, S.G.; et al. Chemical Diversity and Antimicrobial Potential of Cultivable Fungi from Deep-Sea Sediments of the Gulf of Mexico. *Molecules* **2021**, *26*, 7328. [CrossRef]
124. Chen, M.; Hao, B.-C.; Zhu, X.-H.; Zhang, L.-K.; Zheng, Y.-Y.; Zhou, X.-J.; Schäberle, T.F.; Shen, L.; Wang, C.-Y.; Liu, Y. Molecular Networking Reveals Indole Diterpenoids from the Marine-Derived Fungus Penicillium Sp. N4-3. *Mar. Life Sci. Technol.* **2025**, *7*, 302–312. [CrossRef]
125. Nothias, L.-F.; Petras, D.; Schmid, R.; Dührkop, K.; Rainer, J.; Sarvepalli, A.; Protsyuk, I.; Ernst, M.; Tsugawa, H.; Fleischauer, M.; et al. Feature-Based Molecular Networking in the GNPS Analysis Environment. *Nat. Methods* **2020**, *17*, 905–908. [CrossRef]
126. Paguigan, N.D.; El-Elimat, T.; Kao, D.; Raja, H.A.; Pearce, C.J.; Oberlies, N.H. Enhanced Dereplication of Fungal Cultures via Use of Mass Defect Filtering. *J. Antibiot.* **2017**, *70*, 553–561. [CrossRef]
127. Gao, Y.; Wang, Y.; Chung, H.; Chen, K.; Shen, T.; Hsu, C. Molecular Networking as a Dereplication Strategy for Monitoring Metabolites of Natural Product Treated Cancer Cells. *Rapid Commun. Mass Spectrom.* **2020**, *34*, e8549. [CrossRef] [PubMed]
128. Roberts, J.; Bingham, J.; McLaren, A.C.; McLemore, R. Liposomal Formulation Decreases Toxicity of Amphotericin B In Vitro and In Vivo. *Clin. Orthop. Relat. Res.* **2015**, *473*, 2262–2269. [CrossRef] [PubMed]
129. Faustino, C.; Pinheiro, L. Lipid Systems for the Delivery of Amphotericin B in Antifungal Therapy. *Pharmaceutics* **2020**, *12*, 29. [CrossRef] [PubMed]
130. Kumar, M.; Virmani, T.; Kumar, G.; Deshmukh, R.; Sharma, A.; Duarte, S.; Brandão, P.; Fonte, P. Nanocarriers in Tuberculosis Treatment: Challenges and Delivery Strategies. *Pharmaceuticals* **2023**, *16*, 1360. [CrossRef]
131. Shao, L.; Shen, S.; Liu, H. Recent Advances in PLGA Micro/Nanoparticle Delivery Systems as Novel Therapeutic Approach for Drug-Resistant Tuberculosis. *Front. Bioeng. Biotechnol.* **2022**, *10*, 941077. [CrossRef]
132. Comas, L.; Polo, E.; Domingo, M.; Hernández, Y.; Arias, M.; Esteban, P.; Martínez-Lostao, L.; Pardo, J.; Martínez de la Fuente, J.; Gálvez, E. Intracellular Delivery of Biologically-Active Fungal Metabolite Gliotoxin Using Magnetic Nanoparticles. *Materials* **2019**, *12*, 1092. [CrossRef]
133. Ye, W.; Liu, T.; Zhang, W.; Zhang, W. The Toxic Mechanism of Gliotoxins and Biosynthetic Strategies for Toxicity Prevention. *Int. J. Mol. Sci.* **2021**, *22*, 13510. [CrossRef]

Disclaimer/Publisher's Note: The statements, opinions and data contained in all publications are solely those of the individual author(s) and contributor(s) and not of MDPI and/or the editor(s). MDPI and/or the editor(s) disclaim responsibility for any injury to people or property resulting from any ideas, methods, instructions or products referred to in the content.

marine drugs

MDPI

Review

Marine Fungi Bioactives with Anti-Inflammatory, Antithrombotic and Antioxidant Health-Promoting Properties Against Inflammation-Related Chronic Diseases

Maria-Aliki Papikinou [1], Konstantinos Pavlidis [1], Paschalis Cholidis [1], Dimitrios Kranas [1], Theodora Adamantidi [1], Chryssa Anastasiadou [2] and Alexandros Tsoupras [1,*]

[1] Hephaestus Laboratory, School of Chemistry, Faculty of Sciences, Democritus University of Thrace, Kavala University Campus, St. Lucas, 65404 Kavala, Greece; mapapik@chem.duth.gr (M.-A.P.); kopavlm@chem.duth.gr (K.P.); paoholi@chem.duth.gr (P.C.); dikrana@chem.duth.gr (D.K.); theadam@chem.duth.gr (T.A.)

[2] Fisheries Research Institute, Nea Peramos, 64007 Kavala, Greece; anastasiadou@inale.gr

* Correspondence: atsoupras@chem.duth.gr

Abstract: Fungi play a fundamental role in the marine environment, being promising producers of bioactive molecules in the pharmacological and industrial fields, which have demonstrated potential health benefits against cardiovascular and other chronic diseases. This review pertains to the analysis of the lipid compositions across various species of marine fungi and their constantly discovered substances, as well as their anti-inflammatory, antioxidant, and antithrombotic effects. The health-promoting aspects of these microorganisms will be explored, through the investigation of several mechanisms of action and interference of their bioactives in biochemical pathways. Despite exceptional results in this field, the potential of marine microorganisms remains largely unexplored due to the limited number of specialists in marine microbiology and mycology, a relatively recent science with significant contributions and potential in biodiversity and biotechnology.

Keywords: marine fungi; anti-inflammatory; antioxidant; antithrombotic; PUFA; terpenes; alkaloids; lipid bioactives; chronic diseases

1. Introduction

Marine ecosystems are a valuable resource for humans, as they offer numerous direct and indirect benefits to the ecosystem. They play fundamental roles in the control of atmospheric gases, regulation of climate, and biogeochemical cycles of several elements; they provide raw materials and nourishment and are also important for many recreational and cultural activities [1]. The sea is home to a rich biotic community that includes animals, plants, and algae but also many microorganisms like bacteria, protozoa, and fungi. While there is a certain degree of knowledge about the macroscopic world, only during the last decade has a wider focus on the microscopic world for the pharmaceutical and life sciences been achieved. In terms of diversity, seas and oceans represent an almost 'inexhaustible' source of microorganisms still unknown and, among these, fungi have received relatively less attention until recently [2].

The first studies referring to marine fungi date back to the mid-19th century, when two new species—*Phaeosphaeria typharum* and *Halotthia posidoniae*—were discovered and isolated from the submerged portions of *Typha* sp. and from the rhizomes of *Posidonia oceanica* [3,4]. In the following years, marine mycological research did not exhibit progress, which explains the research on marine fungi for about 150 years, except for a few sporadic reports. This was due to technical difficulties linked to the collection of samples and the widespread belief that aquatic fungi constituted a marginal aspect, and thus, their presence was occasional and associated with terrestrial contamination phenomena. Only in

the second half of the 20th century did some researchers begin to study these organisms systematically and based on the first promising results, a progressively growing number of mycologists focused on sea substrates, leading to the birth of "marine mycology".

Although in recent years it has been realized that fungi are an essential component of marine ecosystems, having fundamental roles in many processes, ranging from the maintenance of water fertility to the control and regulation of phytoplankton communities. Understanding the biodiversity and ecology of marine fungi, particularly in relation to other living organisms in their ecosystem, is still being studied to assess their benefits to human health and well-being. In addition, these fungi are considered important subjects of research due to their biotechnological potential and practical applications.

Estimates of the global number of fungal species currently present on our planet are quite variable and indicate a range from 2 to over 11 million species. To date, there have been 156,286 species formally described, and among these, only a percentage equal to 1.2% are associated with marine environments (1947 species) [5,6]. Based on the estimates recorded and the information available, it is quite evident that knowledge relating to fungal biodiversity, and especially the marine one, is still quite scarce. In support of this statement, it must be taken into account that new taxonomic entities are attributed practically every time research is undertaken and completed in new marine habitats [7,8].

Based on what has previously been reported and the fact that new species and molecules are continually discovered, research in this area appears extremely promising and could lead to the discovery of several useful compounds, potentially providing solutions to diseases caused by emerging pathogens or those resistant to various synthetic drugs. In the cardiovascular (CV) field related to diseases, occurrences, events, and conditions, there is a series of resources that have identified elements and compounds, which are thoroughly tested as potential treatment mechanisms for CV conditions and diseases caused by chronic inflammation [9].

The primary and secondary metabolites that have been identified from marine fungi include peptides, polyketides, alkaloids, and terpenoids. Many of these identified marine metabolites are bioactive against bacteria, viruses, fungi, protozoa, and tumor cell lines and are currently being studied from the perspective of new pharmaceutical formulations [10,11]. The first marketed product derived from a marine fungus was cephalosporin C, which was isolated from *Cephalosporium acremonium* (now *Acremonium chrysogenum*). Cephalosporin C, is an important antibiotic belonging to the β-lactam family, which blocks synthesis of the bacterial wall and has broad-spectrum bactericidal action [12]. Many other molecules with antibiotic activity, were also described in subsequent years.

This review aims to depict the lipid composition of different species of marine fungi, as well as the presence of significant bioactives, such as terpenes, polyketides, and phenols. Additionally, extensive reference is made to the health-promoting effects related to cardiovascular diseases from bioactives extracted from marine fungi. Lastly, emphasis is also given to the health-promoting effects of marine fungi extracts associated with other pestering diseases and disorders, such as diabetesand cancer.

2. Lipid Composition of Marine Fungi

Marine fungi are unique producers of diverse lipids, mainly including constituents like fatty acids, sterols, and other bioactives. Their lipid compositions vary significantly across species and habitats and often display structural adaptations capable of providing them with the ability to survive under extreme marine conditions (e.g., low temperatures, varying pressure, and high salinity). Commonly, marine fungi lipids are high in polyunsaturated fatty acids (PUFAs), including n-3 and n-6 fatty acids, which promote membrane fluidity and protection against environmental stresses while also being high in sterols and other lipophilic compounds that contribute to cell structure stability and support specific metabolic functions. Cellular functions including hormone synthesis, energy generation, and fat storage, in fact, depend heavily on lipid metabolism [13].

Recently, the importance of marine-fungi-derived lipids has also been highlighted for their association with several chronic diseases, as many of these lipids exhibit antioxidant, antimicrobial, anti-inflammatory, antithrombotic, and even anticancer properties. Globally, chronic diseases are a leading source of morbidity and mortality, and interactions between genetic, epigenetic, and environmental variables are present in many disorders. The utilization of substances like lipids in regulating gene expression and providing the individual with diverse health properties is a growing trend thanks to recent developments [14].

Inflammation-related diseases are one of the most common pathologies nowadays [15]. Inflammation is the body's natural and vital reaction to signals from pathogenic infections or tissue injury. It is crucial for both reestablishing homeostasis and responding to danger signaling deriving from tissue damage. Cardiovascular disorders, autoimmune diseases, and cancer are among the numerous illnesses that have dysregulated inflammatory responses [15,16]. Apoptosis and phagocytosis, for instance, are important processes in resolution events actively carried out by lipids. Therefore, a significant reorganization of lipid metabolic pathways and energy programs occurs throughout the development of pro- and anti-inflammatory processes, which play a key role in the various phagocytic cell polarization states.

Moreover, several lipid bioactives found in marine fungi have excellent responses against specific thrombo-inflammatory signaling and, thus, against several chronic disorders associated to such manifestations, such as lipid vitamins, like vitamin D and A and their vitaminoids and carotenoids; unsaturated fatty acids (UFAs), like omega-3 polyunsaturated fatty acids; amphiphilic polar lipids, including phospholipids and glycolipids, baring the UFAs within their structures; and alkaloids, terpenes, terpenoids, etc. [17].

Because of their unique profiles and bioactivities, marine fungi and their lipid bioactives are great resources for biotechnological applications. Current research especially focuses on extracting and characterizing these lipids for their potential use in pharmaceutical, nutraceuticals, and cosmeceuticals. However, there remains a need for further exploration of the lipid compositions of lesser-studied marine fungi species in order to better understand their potential contributions to health and industry [18].

As aforementioned, marine fungi contain a variety of bioactive compounds derived from lipids that are beneficial for human health, including terpenes, polyketides, and sterols. Lipids, defined by their hydrophobic characteristics, encompass an extensive array of molecules, each with unique properties and functions necessary for any organism. Their synthesis begins with acetyl-CoA, which is transformed into lipids through several biochemical pathways [19]. In marine fungi, the total lipid content was estimated in the species *Clonostachys rosea* 7.9–31.1% of dry weight (DW). In the following subsections, the fatty-acid-, polar-lipid-, neutral-lipid-, and lipid-derived bioactives' compositions are thoroughly discussed on the basis of a corresponding literature review.

2.1. Fatty Acid Composition of Marine Fungi

Fatty acids, which have a carboxylic acid group, and a long chain of aliphatic hydrocarbons are energy sources and biofunctional components in cell membranes. Their biological action affects the metabolism, functionality, and reactivity of cells and tissues to hormones and other signals [20]. They are separated into the following three categories: polyunsaturated fatty acids (PUFAs), monosaturated fatty acids (MUFAs), and saturated fatty acids (SFAs). Marine fungi are rich in SFAs; in particular, several species have been found to have abundant levels of palmitic acid (C16:0) (12.0–78.12% of total fatty acids) and stearic acid (C18:0) (1.34–35.77% of total fatty acids). More specifically, high values of SFAs were observed in the species *P. puberulum* and *Anamorphic fungi* (89.34–90.39%), while in *V. tenerum* it was found that only SFAs existed.

Compared to SFAs and PUFAs, MUFAs (8.38–19.57%) were the lowest subclass of fatty acids, and oleic acid (18:1) was the most prevalent in this group (7.87–56.73%). Furthermore, PUFAs were reported in one study; however, the compositions of the n-3 fatty acids eicosapentaenoic acid (EPA) and docosahexaenoic acid (DHA), well-known for their

functions in CV health, were not retrieved. Thus, PUFAs account for 24.19–55.30% of the total fatty acids in these two marine fungi species that were examined in this research. Additional fatty acids that belong under the PUFA class are α-linoleic acid (18:3 n-6) and linoleic acid (18:2 n-6), which are estimated to be between 0.0 and 9.42% and 17.19 and 57.90%, respectively. An overview of the fatty acids detected in several marine fungi is presented in Table 1.

Table 1. Compositions of fatty acids (%) to the total fatty acids of different marine fungi species.

(% of Total FAs)	16:00	18:00	18:1	18:2	18:3	SFAs	MUFAs	PUFAs	TL% [1] (DW)	References
A. caelatus	15.12–15.44	6.98–9.12	15.62–25.38	49.47–54.11	2.79–5.29	-	-	-	-	[21]
E. cladophorae	15.24–16.70	7.96–19.06	17.76–18.94	40.59–50.17	3.53–4.91	26.06–36.26	18.41–19.57	44.40–55.30	-	[22]
A. flavus	13.60–16.34	8.97–12.67	31.04–40.60	29.32–39.20	0.13–1.55	-	-	-	-	[21]
A. fumigatus	17.78–19.18	5.07–7.67	19.93–28.35	45.40–54.00	ND [1]	-	-	-	-	[21]
P. islandicum	21.70–40.13	1.34–2.84	12.34–56.73	57.90		23.04–42.97	-	-	-	[23]
Z. maritima	24.92–30.36	17.09–35.77	7.87–14.27	17.19–31.83	6.48–9.42	43.62–67.12	8.38–15.18	24.19–40.91	-	[22]
A. nomius	18.23–19.87	5.40–6.78	28.34–34.84	35.86–42.84	0–0.90	-	-	-	-	[21]
A. ochraceus	19.28–21.12	6.79–8.43	32.06–34.56	36.34–38.32	0–1.25	-	-	-	-	[21]
A. parasiticus	15.64–16.44	9.90–15.30	15.14–27.90	40.26–51.52	0.71–4.33	-	-	-	-	[21]
P. puberulum	69.18	20.16	10.65	-		89.34	10.65	-	-	[23]
C. rosea	12.0–25.0	4.0–12.0	39.0–77.0	-		-	-	-	7.9–31.1	[24]
V. tenerum	78.18	21.81	-	-		99.99	-	-	-	[23]
Anamorphic fungi (*Agonomycetes*)	33.54–79.12	9.94–11.27	-	-		33.54–90.39	-	-	-	[23]

[1] ND stands for "not defined"; TL stands for "total lipids".

2.2. Polar Lipid Composition of Marine Fungi

As opposed to fatty acids, polar lipids (PLs) are characterized by their amphiphilicity, which originates from the existence of both polar and non-polar groups in the structure of the molecule. Specifically, PLs consist of a polar head (phosphate groups, carbohydrates, choline, etc.) and hydrophobic tails, most commonly fatty acids. They are divided into phospholipids and glycolipids. Phospholipids contain a polar phosphate group, and they can be further divided into glycerophospholipids, which are composed of a glycerol backbone, and sphingolipids, which contain a sphingosine molecule as a backbone. On the other hand, glycolipids are a group of polar lipids characterized by the existence of bonds with carbohydrates, and they are further divided into sphingoglycolipids and glyceroglycolipids (galactolipids and sulfolipids). PLs implement important biological processes in the cell [20], while marine PLs have also shown important anti-inflammatory and antithrombotic potential against CVDs and other associated inflammation-related disorders [17,25].

PLs can be found as the main components in cell membranes due to their amphiphilic character, which provides them with the opportunity to form cell bilayers. PL concentrations were measured to range from 4.0 to 32.0 mg/g of DW in several marine fungal strains. Furthermore, 2.0–6.0% and 6.0–18.0% of total lipids, respectively, were made up of glycolipids and phospholipids. Phosphatidylcholines (PCs), a class of phospholipids that includes choline as a headgroup, was estimated for 78.0% of PLs, while other classes of phospholipids, like phosphatidylethanolamine (PE) and phosphatidylinositol (PI), had lower values (6.0% and 0–1.0%, respectively). This study discovered that the values of betaine dodecyl glycerol-3-phosphorylcholine phospholipids were comparable to PE. The polar lipid contents of several marine fungi are presented in Table 2.

Table 2. Composition of polar and neutral lipid bioactives from strains of marine fungi.

Polar lipids (mg/g DW)	4.0–32.0
Phospholipids (% of TLs)	6.0–18.0
Glycolipids (% of TLs)	2.0–6.0
PC (% of PLs)	78.0
Betaine-DGTS (% of PLs)	6.0
PE (% of PLs)	6.0
PI (% of PLs)	0–1.0
References	[24,26]
TAGS (% of TLs)	77.0–91.0
FAMEs (mg/g DW)	0.1–3
References	[24,26]
Sterols (μg/g DW)	10–600
Ergosterol (% of sterols)	85.0
Dehydrostellasterol (% of sterols)	-
References	[26]

2.3. Neutral Lipid Composition of Marine Fungi

Neutral lipids are responsible for the energy storage of the cell, and they consist of triacylglycerols (TAGs), diacylglycerols (DAGs), and wax esters. TAGs are composed of a glycerol molecule connected through an ester bond with three fatty acids. Fatty acid methyl esters (FAMEs), which are produced by trans-esterifying fats with methanol, were reported for 0.1–3.0 mg/g of DW marine fungi, whereas the composition of TAGS was estimated to account for 77.0–91.0% of total lipids (TLs), as shown in Table 2.

2.4. Lipid-Derived Bioactives of Marine Fungi

Many studies have shown through identification methods and qualitative analysis the presence of terpenes in marine fungi. Terpenes represent a broad category of natural hydrocarbons that function as secondary metabolites, while terpenoids are their oxygenated derivatives that belong to the lipids class. A terpenoid's biosynthesis is initiated by acetyl-CoA and mevalonic acid's interaction and involves the assembly of five-carbon isoprene units (C_5H_8), usually arranged in a head-to-tail manner; however, alternative construction methods can also be used, incorporating various levels of ring formations, functional groups, oxidation, and unsaturation. Consequently, there exists a wide array of structural classes, and new skeletal forms are continually being identified [27]. Terpenes, moreover, are capable of creating complex structures through several cyclization, backbone assembly and tailoring processes. Although the biological action of many of these compounds has not yet been fully understood, it is known that they act as precursors for a plethora of bioactives, such as steroids, sterols, retinol (vitamin A), and carotenoids. Thus, terpenes take part in the production of significant metabolites, which display defense-related activities against pathogens [28].

It is also important to mention that apart from classic lipid bioactives, like UFAs, MUFAs, PUFAs, PL, lipid vitamins, terpenes, and terpenoids [17], many other bioactives can also be traced in respectable amounts in marine fungi, either more lipophilic ones like sterols or more amphiphilic ones like quinones and phenols. The structures of the most representative bioactives of these classes detected in marine fungi are shown in Figure 1, while the most important terpenes and terpenoids are analyzed in Table 3.

Sterols, as a subgroup of steroids, consist of a tetracyclic cyclopentanoperhydrophenanthrene structure, and their biological function is to maintain and adjust different parameters of the cell membranes, like fluidity, rigidity, and permeability. Marine fungal strains that were dry weighed (DW) contained 10–600 μg/g of sterols, with ergosterol being the most prevalent sterol which, when combined with dehydrostellasterol, comprised 85.0% of sterols. Quinones are composed of hexacarbon cyclic dione with two double bonds. These lipophilic redox compounds act as electron transporters in different biological processes

and take part in cell respiration. Lastly, phenols consist of an hydroxyl group (-OH) connected to a carbon atom that is, in turn, part of an aromatic ring. Pigmentation and the reduction in free radicals are some of the features exhibited by phenols.

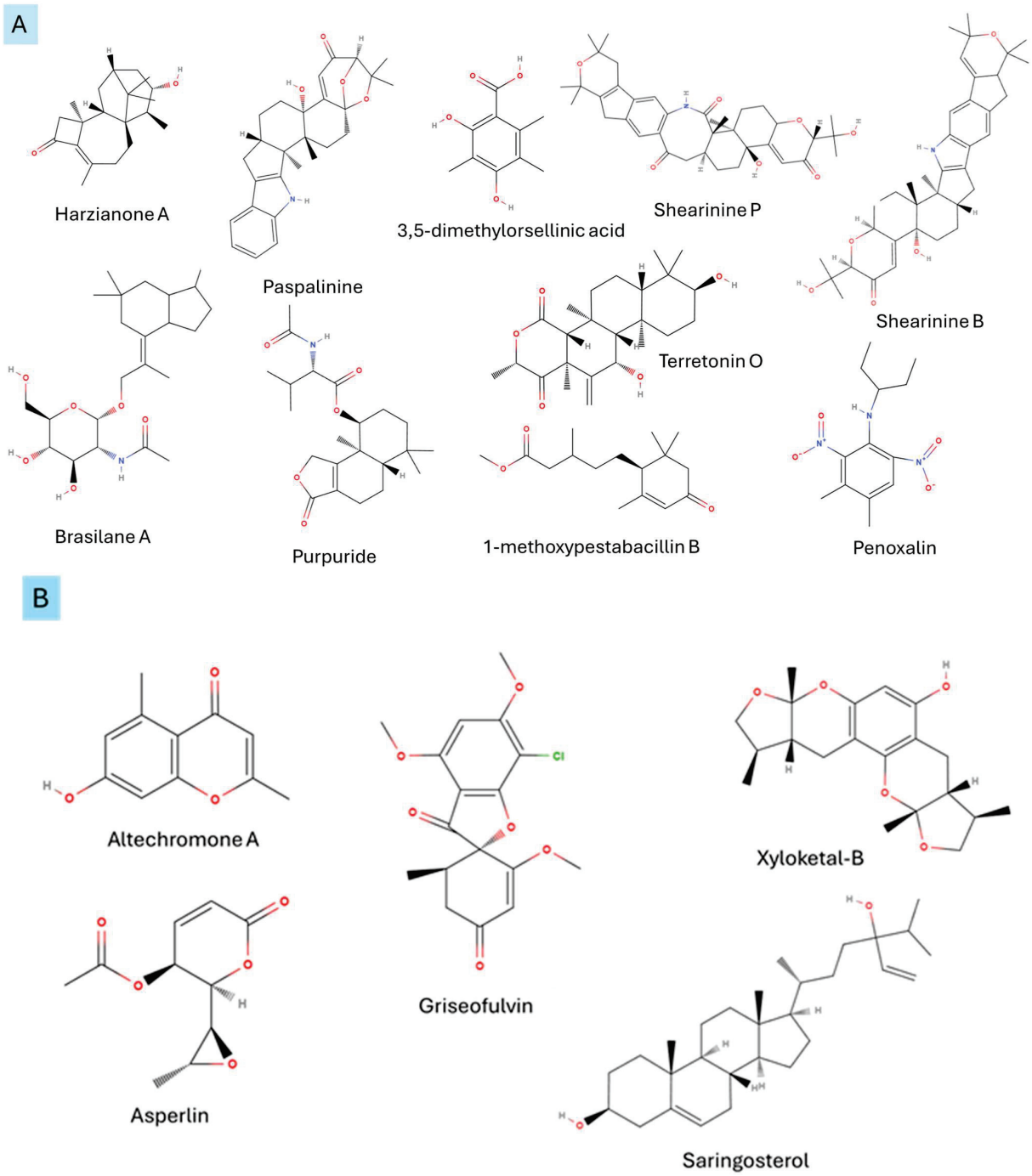

Figure 1. Structures of the most representative terpenoids and polyketides (**A**) and other bioactives with cardioprotective properties (**B**) present in marine fungi (structures were obtained from Molview.org).

Apart from the functions of all of these bioactive molecules in the cell, the vast majority display health-promoting effects on human health. For example, PLs have shown antithrombotic activity by inhibiting the biosynthesis of the platelet-activating factor (PAF) [29]. Additionally, phenols are known for their antioxidant activity and their anti-aging and anti-inflammatory action.

Table 3. Novel and well-known terpenoids and polyketides extracted from various strains of marine fungus (2019–2024) (structures were loaded from the free databases PubChem, ChemSpider, and Molview).

	Species	Compounds	Structures *	References
Monoterpenes	*Penicillium* sp. SCSIO 41691	1-methyl-12a,12b-epoxyarisugacin M 1-methyl-4a,12b-epoxyarisugacin M 2,3-dihydroxy-3,4a-epoxy-12a-dehydroxyisoterreulactone A 2-hydroxy-12a-dehydroxyisoterreulactone A 3′-demethoxyterritrems B′ 4a-hydroxyarisugacin P 1-epi-arisugacin H	- - - - - - -	[30]
	Diaporthe sp. SYSU-MS4722	diaporterpene A–C	-	[31]
Sesquiterpenes	*Penicillium* sp. OPR23-FS02	purpuride	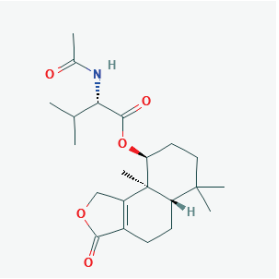	[32]
	Trichoderma lixii R22	brasilane A	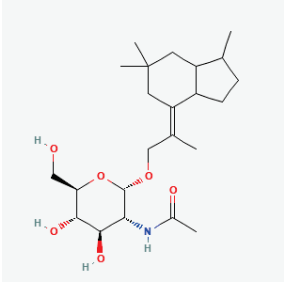	[33]

Table 3. *Cont.*

Species	Compounds	Structures *	References
Trichoderma hamatum Z36-7	5-hydroxyepicyclonerodiol oxide	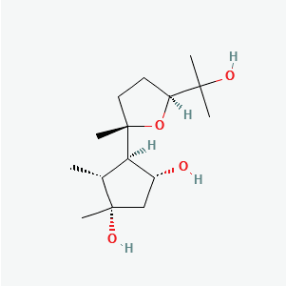	[34]
	4-hydroxyepicyclonerodiol oxide	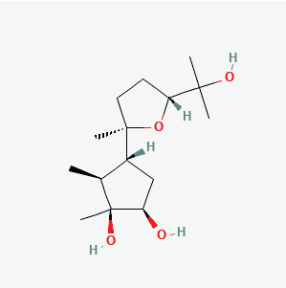	
	trichodermol chlorohydrin	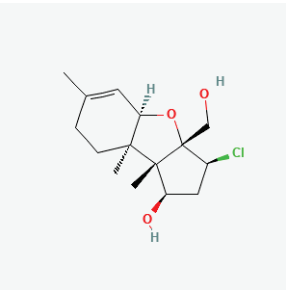	

Table 3. *Cont.*

	Species	Compounds	Structures *	References
	Diaporthe sp. SCSIO 41011	1-methoxypestabacillin B	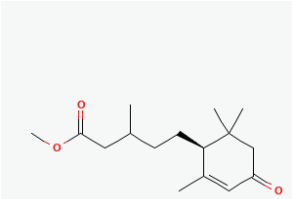	[35]
		11-Nor-8,9*R*-drimanediol	-	
Diterpenes	*Penicillium* sp. OPR23-FS02	penioxalicin	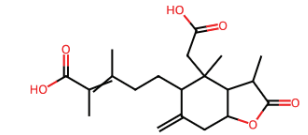	[32]
	Trichoderma lixii R22	harzianone A	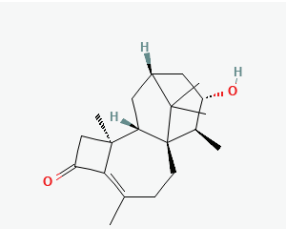	[33]

Table 3. *Cont.*

Species	Compounds	Structures *	References
Penicillium sp. KFD28	7-hydroxypaxilline-13-ene	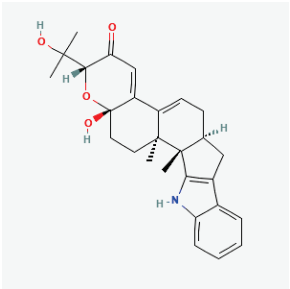	[36]
	paspalinine	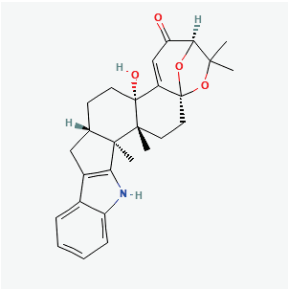	
	paspaline B	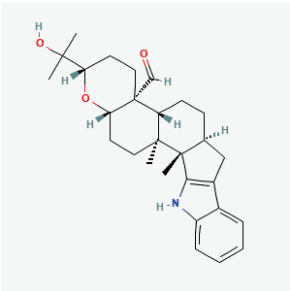	

Table 3. *Cont.*

Species	Compounds	Structures *	References
	pyrapaxilline	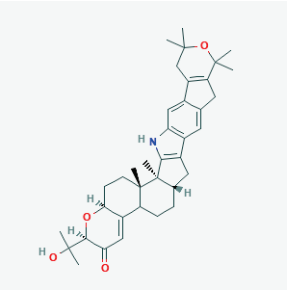	
	shearinine B	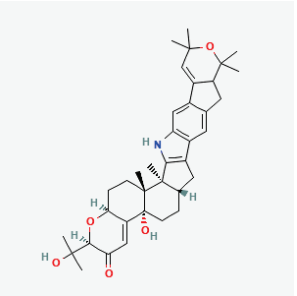	[36]
	shearinine P	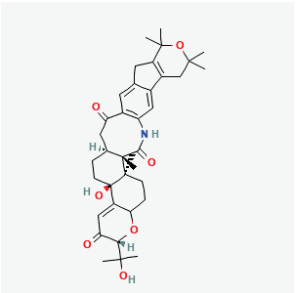	

Table 3. *Cont.*

Species	Compounds	Structures *	References
	3-deoxo-4b-deoxypaxilline	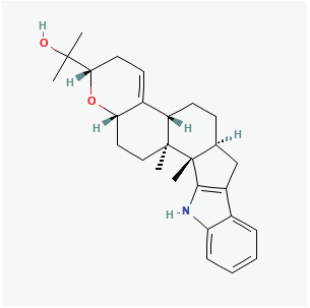	[36]
Peroneutypa sp. M16	solanapyrones	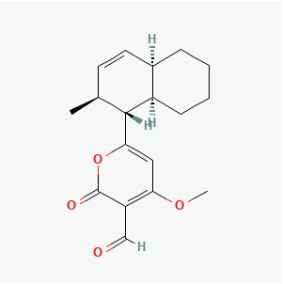	[37]

i.e.,

Table 3. *Cont.*

	Species	Compounds	Structures *	References
	Aspergillus sp. CSYZ-1	3,5-dimethylorsellinic acid	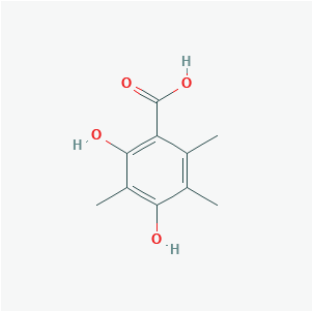	[38]
Meroterpenes	*Penicillium* sp. A18	penimeroterpenoids A–C	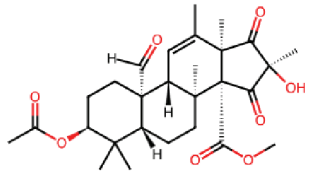 penimeroterpenoid 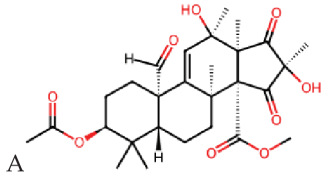 A penimeroterpenoid 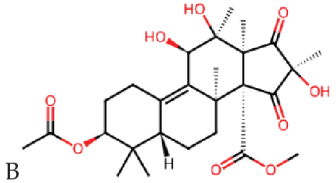 B penimeroterpenoid C	[39]

Table 3. *Cont.*

Species	Compounds	Structures *	References
Diaporthe sp. SCSIO 41011	chrodrimanins A/B/E/F/G/H	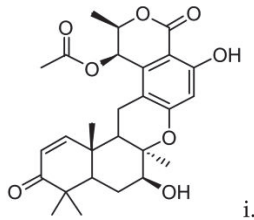 i.e.,	[35]
Stemphylium sp. FJJ006	tricycloalterfurenes E–G	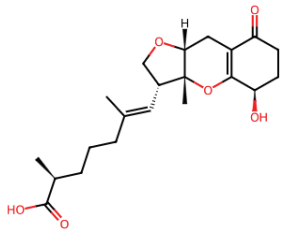 tricycloalterfurene E 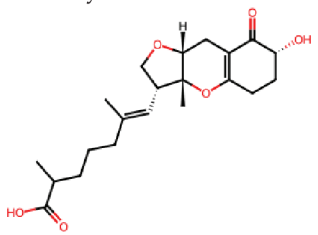 tricycloalterfurene F 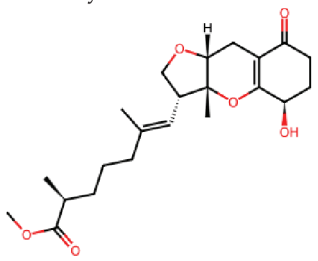 tricycloalterfurene G	[40]

Table 3. *Cont.*

Species	Compounds	Structures *	References
Aspergillus terreus GZU-31-1.	aspermeroterpene A–C	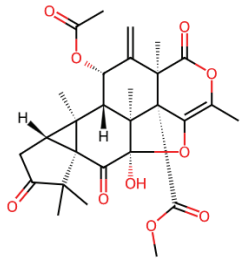 aspermeroterpene A 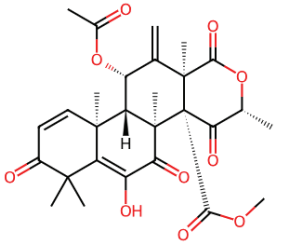 aspermeroterpene B 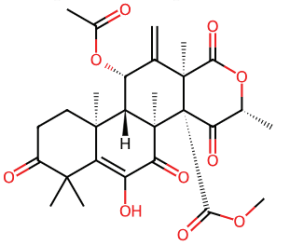 aspermeroterpene B	[41]

Table 3. *Cont.*

Species	Compounds	Structures *	References
	furanasperterpenes A and B	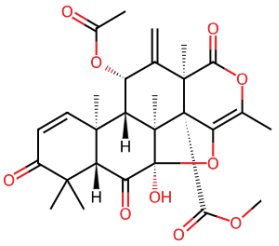 furanasperterpene A 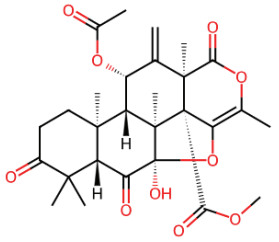 furanasperterpene B	[42]
	11-acetoxy-terretonin E	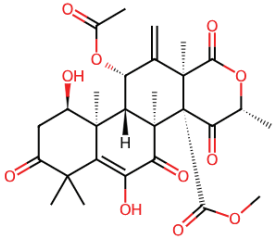	

Table 3. *Cont.*

Species	Compounds	Structures *	References
Aspergillus terreus LGO13	terretonin O	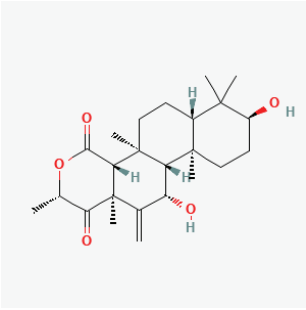	[43]
Penicillium bilaiae MA-267 and *Penicillium chermesinum* EN-480	chermebilaenes A and B	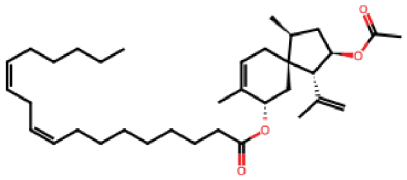 chermebilaene A 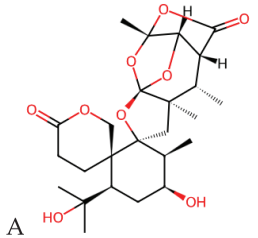 chermebilaene B	[44]

Table 3. *Cont.*

Species	Compounds	Structures *	References
Aspergillus sp. ZYH026	asperaustins A–C	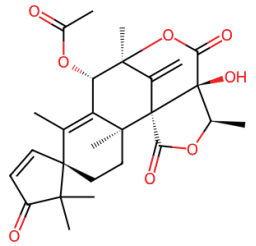 asperaustin 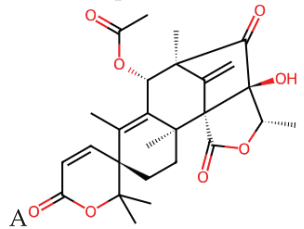 A asperaustin 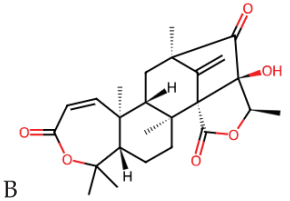 B asperaustin C	[45]

Table 3. *Cont.*

	Species	Compounds	Structures *	References
Polyketides	*Penicillium* sp. OPR23-FS02	*trans*-3,4-dihydro-3,4,8-trihydroxynaphthalen-1(2*H*)-one	-	[32]
		chloromonilinic acid B	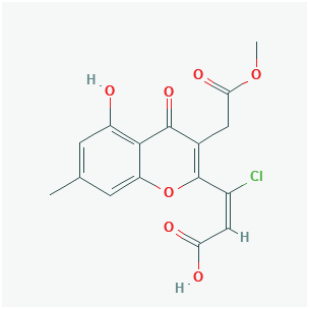	
		chrysophanol	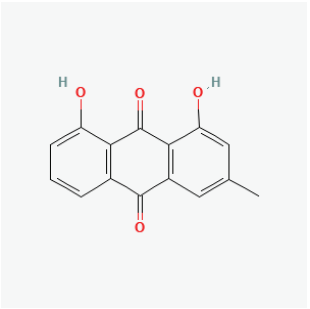	
		emodin	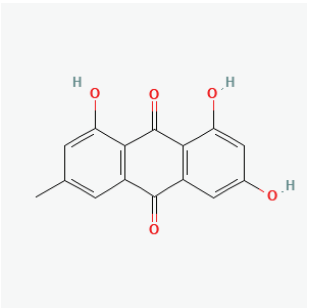	

Table 3. *Cont.*

Species	Compounds	Structures *	References
	ω-hydroxyemodin (citreorosein)	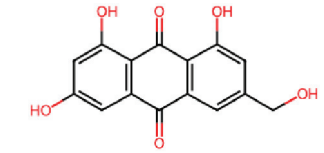	
	questin	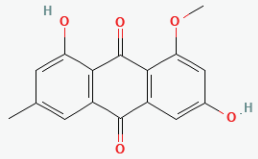	
	endocrocin	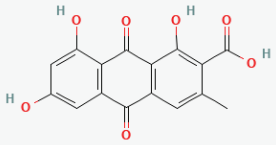	[32]
	ergochrome F	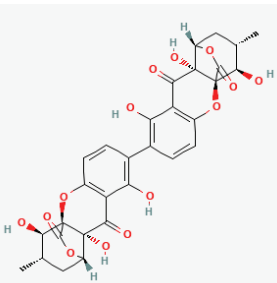	

Table 3. *Cont.*

Species	Compounds	Structures *	References
Diaporthe sp. SYSU-MS4722	acropyrone	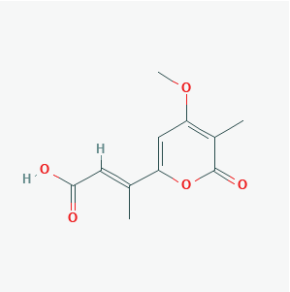	[31]
	nectriapyrone	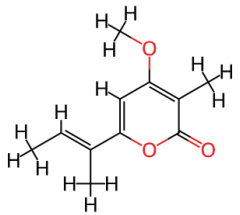	
	monodictyphenone	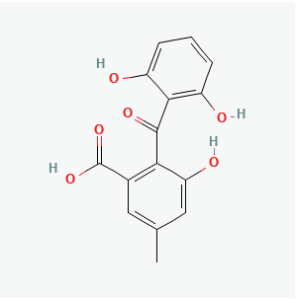	
	2,2′,6′-trihydroxy-4-methyl-6-methoxy-acyl-diphenylmethanone	-	
	pestacin	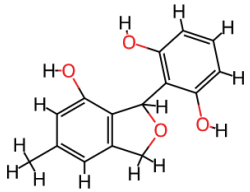	

Table 3. *Cont.*

Species	Compounds	Structures *	References
	3-(2,6-dihydroxyphenyl)-4-hydroxy-6-methyl-isobenzofuran-1(3*H*)-one	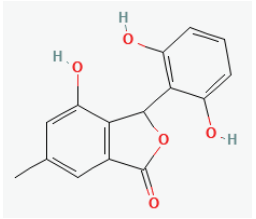	
	3,4-dihydro-6,8-dihydroxy-3-methylisocoumarin	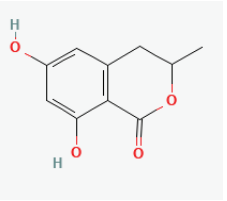	
	2,5-dimethyl-7-hydroxychromone	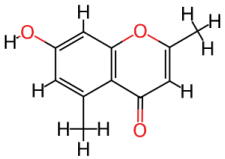	[31]
	4-hydroxyphenethyl-2-(4-hydroxyphenyl) acetate	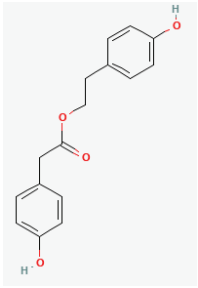	

Table 3. *Cont.*

	Species	Compounds	Structures *	References
Anthraquinones	*Aspergillus unguis* 158SC-067 and *A. Flocculosus* 01NT-1.1.5	averantin	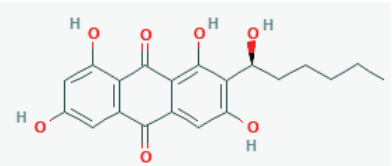	[46]
		7-chloroaverantin	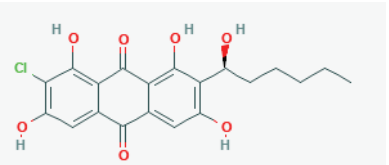	
		1′-*O*-methylaverantin	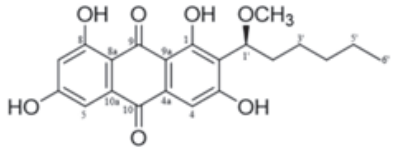	
Bianthraquinones	*Stemphylium* sp. FJJ006	alterporriol Z1–Z3	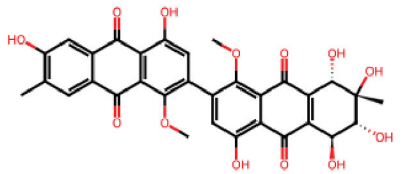 alterporriol Z1 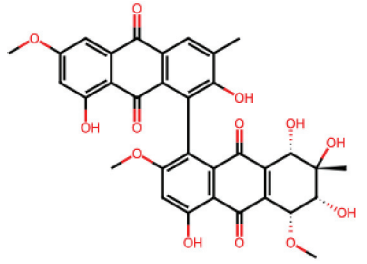 alterporriol Z3	[40]

Table 3. *Cont.*

	Species	Compounds	Structures *	References
Phenols	*Aspergillus unguis* 158SC-067/*A. Flocculosus* 01NT-1.1.5	grifolin B	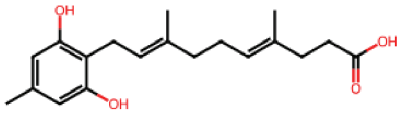	[46]
		12-hydroxyhomovalencic acid	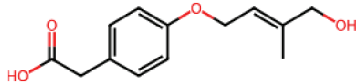	

* Structures were obtained from Molview.org., PubChem, and ChemSpider.

3. Marine Fungi Bioactives with Numerous Health-Promoting Properties Against Cardiovascular Diseases

Cardiovascular diseases (CVDs) are among the most impactful illnesses globally. The available therapeutic options have several side effects, including hypotension, bradycardia, arrhythmia, and alteration in different ion concentrations. Recently, bioactive compounds from natural sources, including plants, microorganisms, and marine organisms, have gained plenty of interest. Marine sources serve as reservoirs for new bioactive metabolites with various pharmacological activities. Marine-derived compounds, especially those from marine fungi, such as n-3 acid ethyl esters, xyloketal B, asperlin, and saringosterol, showed promising results in several CVDs. More specifically, Sajaroketide A, altechromone A, and griseofulvin, three bioactive polyketides isolated from the marine-derived fungal strains KMM4718 and KMM4747 from the sea urchin *Scaphechinus mirabilis*, showed significant cardioprotective effects in an in vitro model of infectious myocarditis, with H9c2 cardiomyocytes co-cultured with Staphylococcus aureus [47]. The structures of the most representative compounds and substances detected in the reported marine fungi are shown in Table 4. Studies, interventions, and clinical trials on the benefits of bioactive extracts derived from marine fungi against cardiovascular diseases are summarized in Table 5, while an overview of the cardioprotective benefits and several other health-promoting properties of marine fungi and their bioactives are depicted in Figure 2.

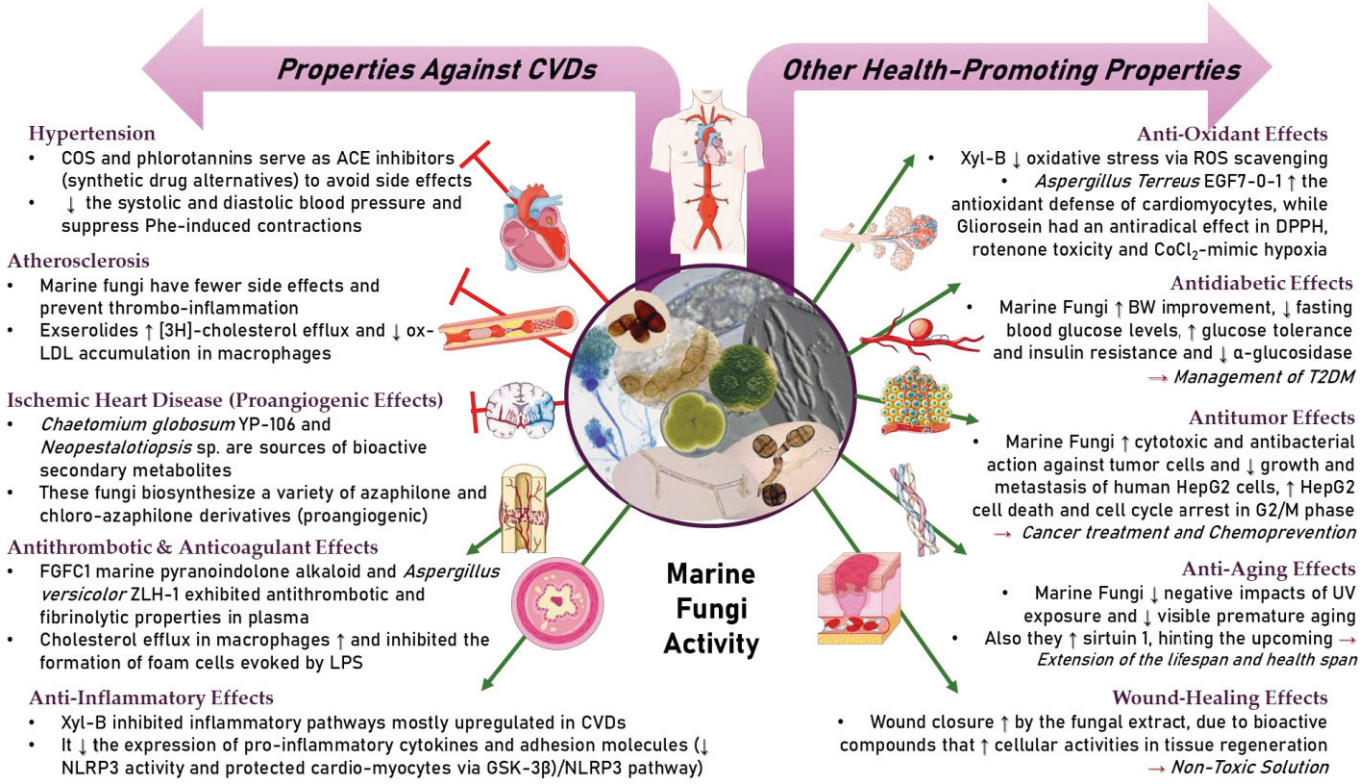

Figure 2. A summary of the cardioprotective benefits and other health-promoting properties of marine fungi and their bioactives.

3.1. Marine Fungi Extracts Against Hypertension

Among all cardiovascular diseases (CVDs), hypertension is one of the most serious concerns. It is the leading cause of stroke, ischemic heart disease, dementia, chronic kidney disease, and other CVDs. [48]. Age-standardized prevalence data from 2019 showed that 32% of women and 34% of men aged 30 to 79 had hypertension globally [49]. Numerous natural compounds found in marine species, such as bioactive molecules, chitooligosaccharide derivatives (COS), and phlorotannins, have the potential to serve as angiotensin-converting enzyme (ACE) inhibitors and have been developed into nutraceutical medicinal com-

pounds, which are used to treat hypertension [50,51]. Emphasis is given to natural marine ACE inhibitors as alternatives to synthetic drugs to avoid several serious side effects, as they hold significant potential to become newly emerging therapeutic options for the treatment of hypertension [52]. Xyloketal-B (Xyl-B), a natural pentacyclic fungal marine product, was examined for whether it exerted an antihypertensive effect in a hypertensive rat model, and the corresponding mechanisms were explored. The systolic and diastolic blood pressures in two-kidney, two-clip (2K2C) renovascular hypertensive rats decreased after being supplied with 20 $mgkg^{-1}d^{-1}$ Xyl-B for 12 weeks. Moreover, pretreatment with Xyl-B (20 μmol/L) notably suppressed phenylephrine (Phe)-induced contractions in thoracic aortic rings, which were both endothelium-denuded and endothelium-intact, suggesting that both endothelial-dependent and endothelial-independent mechanisms are responsible for the vasorelaxant effect of the drug [53].

3.2. Marine Fungi Extracts Against Atherosclerosis

The formation of arterial thrombosis is mostly caused by platelet adhesion under high shear stress, which arises in stenotic atherosclerotic arteries [54]. Atherosclerosis is a chronic, inflammatory, and progressive CVD that is induced by persistent damage to blood vessels resulting from hyperlipidemia and, specifically, elevated low-density lipoprotein (LDL) cholesterol [55]. Compounds derived from marine sources have been beneficial against atherosclerosis. These substances are more effective and have fewer side effects than synthetic ones intending to cure atherosclerosis [56]. PAF is a potent lipid mediator that plays a crucial role in inflammation by activating platelets and repurchasing neutrophils in the process of atherosclerosis, as it operates via the PAF/PAF receptor (PAF-R) pathways. Many medications with marine origins have been studied for their ability to prevent thrombo-inflammation in CVDs. Exserolides increase [3H]-cholesterol efflux and decrease oxidized-LDL (ox-LDL) accumulation in RAW264.7 macrophages via the LXRα-ABCA1 and PPARα pathways, as well as total cholesterol (TC) and triglycerides (TGs) in HepG2 cells and CD36 protein uptake in macrophages [57].

3.3. Marine Fungi Extracts Against Ischemic Heart Disease (IHD) and Proangiogenic Effects

Ischemic heart disease (IHD) is caused by insufficient coronary artery blood flow to the heart. The primary mechanism underlying IHD is endothelial dysfunction. Of all CVDs, it is deemed as the primary cause of morbidity and mortality worldwide [58]. In 2019, a report stated that 197 million cases of this disease existed and that it was responsible for 9.14 million deaths worldwide [59]. Marine-derived drugs are better than synthetic ones in treating IHD because of their beneficial action and better results. Three new alkaloids and nine known analogues were extracted from the marine-derived fungus *Penicillium expansum* Y32 and to compounds **4–6**, likely comprising fumiquinazolines or communesins, namely, fumiquinazoline Q (4), cottoquinazoline A (5), and prelapatin B (6), and compounds **8–12**, namely, protuboxepin E (8), protuboxepin A (9), protuboxepin B (10), chaetoglobosin C (11), and penochalasin E (12), were recognized as the principal compounds exhibiting this vasculogenic activity. These compounds could represent a promising therapeutic option for conditions characterized by angiogenesis insufficiency, such as IHD, where the heart muscle's blood supply is restricted [60]. Studies show that a new deep-sea fungus from the Yap Trench, called *Chaetomium globosum* YP-106 and *Neopestalotiopsis* sp. HN-1-6, has been identified as a possible source of bioactive secondary metabolites with significant implications for CV health applications. These fungi have the ability to biosynthesize a variety of azaphilone and chloro-azaphilone derivatives, which have been demonstrated to possess pro-angiogenic effects in a dose-dependent manner using the zebrafish model [61,62].

3.4. Antithrombotic and Anticoagulant Effects of Marine Fungi Extracts

Marine compounds derived from marine fungi may also have antithrombotic and anticoagulant activities. CVDs account for around 20 million deaths worldwide each year,

and thrombosis may enhance acute myocardial infarction, IHD, valvular heart disease, peripheral vascular disease, and other CVDs. Studies show that isaridin E concentration-dependently suppressed adenosine diphosphate (ADP)-induced mouse platelet activation, a crucial step in the development of arterial thrombosis and platelet hyperactivity in CVDs associated with an elevated risk of thrombosis. An internal agonist called ADP induced the aggregation, which is essential for physiological hemostasis. While it had no effect on aggregation induced by collagen or thrombin, it was found that isaridin E specifically decreased adenosine triphosphate (ATP) release, platelet activation, and ADP-induced platelet aggregation in a concentration-dependent manner. This finding suggested that isaridin E's antiplatelet and antithrombotic activities may be attributed to its inhibitory effects on ADP-induced platelet activation and secretion. Safe marine isaridin E, had potent antiplatelet and antithrombotic properties without appreciably altering coagulation parameters, bleeding time, or platelet numbers [63].

The active ingredient fungi fibrinolytic compound **1** (FGFC) 1, a marine pyranoindolone alkaloid small molecule compound, which was extracted from the marine fungal culture *Stachybotrys longispora* FG216, showed antithrombotic, anti-inflammatory, antioxidant, and fibrinolytic properties [64]. The fibrinolytic activity of FGFC1 in plasma, which interfered with the release of fibrinopeptide B to influence protofibril lateral aggregation and raised the vulnerability of clots to fibrinolysis by changing its shape, was demonstrated. It was discovered that FGFC1 can facilitate the FITC-fibrin dissolution in vitro, which is mediated by plasminogen and the single-chain urokinase-type plasminogen activator (scu-PA) [65]. Fibrinolytic enzymes play a crucial role in the management of conditions linked to thrombosis. Aspergillus versicolor ZLH-1, a marine-derived fungus, moreover, yielded versiase, a novel bifunctional fibrinolytic enzyme. Versiase's anticoagulant activity was evaluated in vitro by timing the clotting of mouse blood. Versiase's thrombolytic and anticoagulant potencies, as well as its efficient and quick ability to dissolve blood clots, are made possible by its special bifunctional fibrinolytic mechanism. Furthermore, versiase's low hemolysis rate and minimal effect on human umbilical vein endothelial cell (HUVEC) proliferation led to the conclusion that it is safe for use. Future research will reveal versiase's thrombolysis and anticoagulant mechanisms, which will open up new avenues in the treatment of thrombosis [66]. Further, from *Aspergillus versicolor* LZD4403, fungus asperlin was isolated, which was then examined for its potential anti-atherosclerotic properties both in vitro and in vivo. Asperlin promoted cholesterol efflux in RAW264.7 macrophages and markedly inhibited the formation of foam cells evoked by lipopolysaccharides (LPS) but not by ox-LDL [67].

3.5. Antioxidant Effects of Marine Fungi Extracts

With a range of therapeutic qualities, most notably anticancer and antioxidant activities, marine fungi have become an important and mainly unexplored resource for drug discovery. Recent studies have been conducted, regarding the biological activity of bioactive natural chemicals from fungi against different cancer cell lines and dangerous bacteria. Notably, there are various ways in which a fungal extract with antibacterial and anticancer activities could be useful. *Aspergillus fumigatus* WA7S6, a marine fungus that was found on a sea sponge, seemed to have a variety of potential uses in medicine, in addition to having strong antibacterial and antioxidant properties, and its potential anticancer properties were investigated as well. It was discovered that methyl ester, dehydromevalonic lactone, 9-tetradecynoic acid, and 11-hexadecynoic acid were important compounds with antioxidant action. These results highlight *Aspergillus fumigatus* WA7S6′s diverse therapeutic potential and its applications in the creation of antibacterial, antioxidant, and anticancer drugs. Cancer is a huge global disease burden. Every year, tens of millions of people worldwide are diagnosed with cancer, and more than half of them die as a result of it. The great biodiversity of the marine environment has increasingly piqued the interest of experts, especially in the field of drug discovery. The marine fungus Aspergillus fumigatus WA7S6 has been selected among a group of fungi isolated from marine sponges, as it exhibits a

pronounced antimicrobial activity toward a group of pathogenic microbes. The fungus was identified genetically by amplification and analysis of its 18srRNA gene. The fungus' crude extract was obtained by cultivation of the fungus on rice media. The crude extract was tested for antibacterial activity against a variety of pathogenic microorganisms. The results demonstrated a pronounced antimicrobial action against *P. aeruginosa*, *S. aureus*, *A. niger*, and *Candida albicans*. Furthermore, we tested the antioxidant potential of the Aspergillus fumigatus WA7S6 crude extract using the following three different methods: ATBS, DPPH, and lipid peroxidation assays. The results showed that the crude extract WA7S6 had an IC50 value of 21.35 μg/mL. The anticancer potential of the crude extract was also evaluated against cancer cell lines such as Hela, MCF, and WI-38. The chemical profiling of the fungus extract was identified via GC-mass and in silico molecular docking of the identified compounds on heme oxygenase as a stress protein included in cellular protection, antioxidant, and anti-inflammatory activities, suggesting that some compounds, such as 9-tetradecynoic acid, 11-hexadecynoic acid, methyl ester, and dehydromevalonic lactone, could be relevant for the antioxidant purposes of marine microbes, which can provide fresh approaches to combating oxidative stress and resistant infections, tackling urgent health issues [68,69]. One of the main causes of cardiovascular diseases is an unbalanced state between free radicals and antioxidants in the human body, which results in oxidative stress. One important step in the process of atherosclerotic plaque formation is the oxidative modification of LDL. Therefore, in the case these fungal metabolites possessed antioxidant properties, they would scavenge free radicals and reduce LDL oxidation and, thus, they may be protective against such a sequence of oxidative damage, leading to endothelial dysfunction and the formation of plaques.

According to a recent study, xyloketal B (Xyl-B) is a very potent compound. One of its main mechanisms is reducing oxidative stress, which is a major contributor to the establishment and progression of atherosclerosis and hypertension CVDs, through the scavenging of reactive oxygen species (ROS) and upregulation of the activities of their antioxidant enzymes. This decrease in oxidative stress not only protects the vascular endothelium but also improves overall vascular function [70]. Another study discovered that the *Aspergillus terreus* EGF7-0-1 compound might facilitate an antioxidant defense of cardiomyocytes. By reducing oxidative damage, the compound preserved its structural and functional integrity in myocardial cells, which is vital for preventing future progression of CVDs [71]. Gliorosein, a polyketide separated from a sponge-derived fungus, *Lopadostoma pouzarii*, showed a statistically significant anti-radical effect in the radical scavenging activity test of 2,2-diphenyl-1-picrylhydrazyl (DPPH), but was not particularly potent, due to differing free radical concentrations. Thus, gliorosein apart from DPPH radical-scavenging activity, also exhibited in vitro cardioprotective effects toward rotenone toxicity and $CoCl_2$-mimic hypoxia [72].

3.6. Anti-Inflammatory Effects of Marine Fungi Extracts

A widespread, nonspecific, and advantageous host response to a foreign challenge or tissue damage is inflammation. Although prolonged inflammation is considered undesirable, it can result in the loss of organ function, including warmth, discomfort, swelling, and redness. In recent decades, a notable increase in interest in marine fungi due to their exceptional anti-inflammatory qualities has been issued. These organisms are found in a variety of marine settings, such as coastal mangroves and deep-sea trenches. They produce a broad range of bioactive chemicals with great promise in the treatment of inflammatory diseases. Numerous new secondary metabolites from fungus living in or on algae, sediments, water, and corals have been reported to possess strong anti-inflammatory properties. Marine fungal compounds have drawn increasing attention due to their distinct method of action, making them of prime interest for the creation of anti-inflammatory medications. Various compounds are isolated from marine fungi, such as alkaloids, terpenoids, polyketides, and peptides. A large proportion of such secondary metabolites, is produced by the species of *Aspergillus* and *Penicillium* [73].

Xyl-B was observed to inhibit some of the main inflammatory pathways, which are mostly upregulated in CVDs. Xyl-B downregulated the expression of pro-inflammatory cytokines and adhesion molecules involved in endothelial dysfunction and atherogenesis. This agent, by suppressing these inflammatory responses, exhibited a preservative action on endothelial integrity and prevented the formation of atherosclerotic plaque [70]. The results for *Aspergillus terreus* EGF7-0-1 sheds light on NLRP3 inflammasome's activity in the protein complex, related to the inflammatory response. Activation of NLRP3 is linked to the production of inflammatory cytokines and, hence, is damaging to heart tissues. Aspergteroid G was able to downregulate such NLRP3 activity and, thus, formed a base to reduce inflammation and its harmful effects on the heart by protecting cardiomyocytes through the glycogen synthase kinase-3 beta (GSK-3β)/NLRP3 pathway [71].

Table 4. Structures of the compounds detected in the referenced marine fungi with a cardioprotective role.

Compounds	Structures *	References
(4) Fumiquinazoline Q	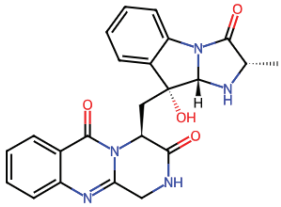	[60]
(5) Cottoquinazoline A	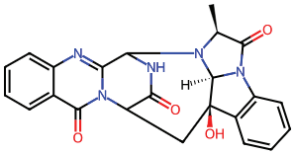	
(6) Prelapatin B	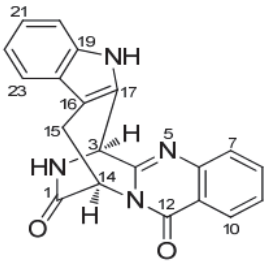	
(8) Protuboxepin E	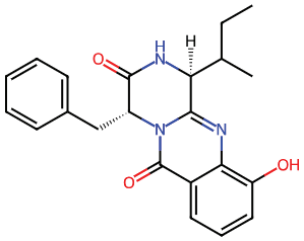	[60]
(9) Protuboxepin A	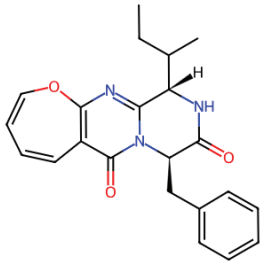	

Table 4. *Cont.*

Compounds	Structures *	References
(10) Protuboxepin B	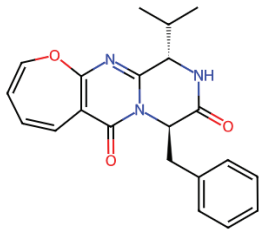	
(11) Chaetoglobosin C	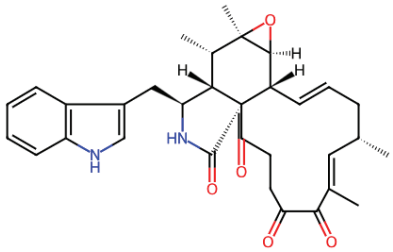	[60]
(12) Penochalasin E	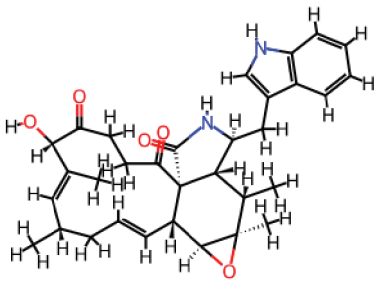	
Isaridin E	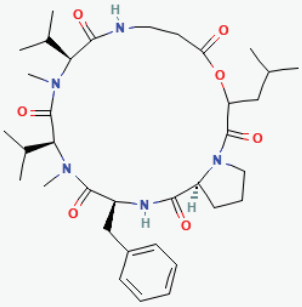	[63]
Methyl ester	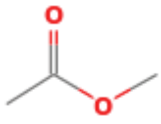	
Dehydromevalonic lactone	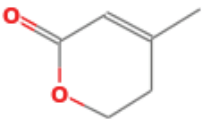	
9-Tetradecynoic acid	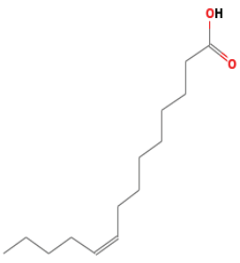	[69]

Table 4. *Cont.*

Compounds	Structures *	References
11-Hexadecynoic acid	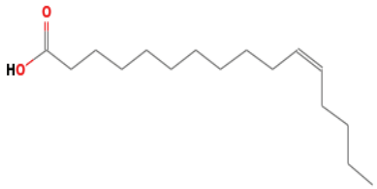	[69]
Asperlin	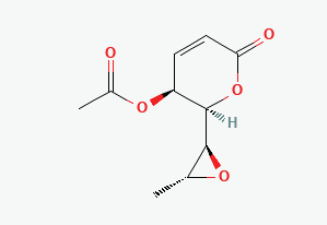	[67]
Aspergteroid G	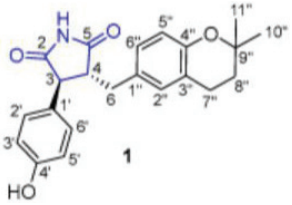	[71]

* Structures were obtained from Molview.org., PubChem, and ChemSpider.

Table 5. Studies, interventions, and clinical trials on the benefits of bioactive extracts derived from marine fungi against cardiovascular diseases.

Hypothesis–Intervention	Study Design/Parameters Examined	Main Findings	Structures	Specific Benefits/Other Benefits Observed—Mechanisms of Action(s)	Year	Ref.
Lopadostoma pouzarii strain 168CLC-57.3 was isolated from an unidentified marine sponge and cultured for low—molecular weight metabolite isolation	Fungal strain 168CLC-57.3 was isolated from a sponge at Cu Lao Cham, Vietnam. Assays tested DPPH, cell viability, and cardioprotective activities	The isolated compounds, namely, lopouazone A and B, showed weak cytotoxicity against PC-3 cells and H9c2 cardiomyocytes; gliorosein exhibited cardioprotective effects	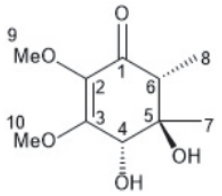 lopouazone A 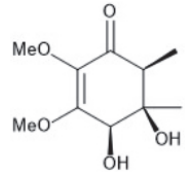 lopouazone B	Gliorosein's antiradical effect in the DPPH test was statistically significant but not highly potent and may not directly correlate with intracellular ROS action due to differing free radical concentrations	2022	[72]
Isolation of 11 polyketides from the natural complex of the sea-urchin-associated fungi *P. sajarovii* KMM 4718 and *A. protuberus* KMM 4747	The fungal complex, likely from the sea urchin *S. mirabilis* (Sea of Japan), includes co-cultured *P. sajarovii* and *A. protuberus*. Procedures involved DNA extraction, cultivation, urease inhibition assay, and antimicrobial activity tests	Compounds **1** and **2**, namely, sajaroketide A and sajaroketide B were analyzed; some showed cardioprotective effects against *S.-aureus*-induced myocarditis	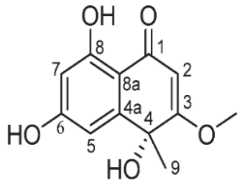 sajaroketide A 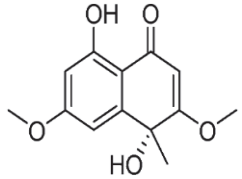 sajaroketide B	Altechromone A increased cell viability by up to 39.9%. Compounds **2**, **6**, and **11** showed no significant effect	2023	[47]

Table 5. *Cont.*

Hypothesis–Intervention	Study Design/Parameters Examined	Main Findings	Structures	Specific Benefits/Other Benefits Observed—Mechanisms of Action(s)	Year	Ref.
Analyzed XKB and rat Cyp3a2 interactions via homology modeling, molecular docking, and oral XKB's effects on hepatic Cyp3a	A rat Cyp3a2 homology model was created; XKB's effects were assessed using high-performance liquid chromatography (HPLC) and luminescence	XKB inhibited Cyp3a-mediated midazolam metabolism in rats, affecting hepatic Cyp3a activity and suggesting possible CYP3A4/Cyp3a2 interactions	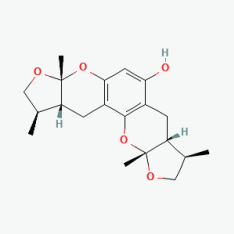 xyloketal B	XKB interacted with the rat Cyp3a2 model via hydrogen bonds. Oral XKB increased midazolam's area under the curve (AUC) and the maximum achieved concentration of a drug (C_{max}) while decreasing oral clearance (CL/F), showing similar inhibition to ketoconazole	2014	[70]
The FGFC1's effect on fibrin clot structure, lysis, and plasminogen activation using various assays was studied	FGFC1, isolated from *Stachybotrys longispora* FG216 with >98% purity, was extracted from fermentation samples using 2-butanone and ethyl acetate	FGFC1, a marine alkaloid, promoted fibrin dissolution in vitro and effectively treated pulmonary thrombosis in rats	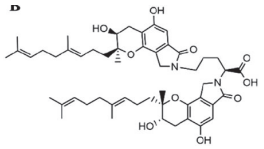 FGFC1	This study showed that FGFC1 had strong fibrinolytic activity in plasma by reducing clot aggregation and increasing lysis sensitivity. It provided a basis for future clinical research on FGFC1 in thrombotic diseases	2023	[65]
Versiase, a fibrinolytic enzyme from *Aspergillus versicolor*, showed anticoagulant potential	*Aspergillus versicolor* ZLH-1, isolated from *Callyspongia* sp., was cultured, and its fibrinolytic enzyme was tested for its activity and toxicity	Versiase's anticoagulant activity increased with concentration, exceeding 185 s at 100 μg/mL. It showed thrombolytic activity in vitro	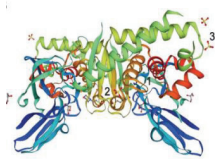 Versiase	Versiase effectively dissolved blood clots with thrombolytic and anticoagulant properties and was safe for use, showing low hemolysis and minimal impact on HUVEC proliferation	2022	[66]
Isaridin E effects on arterial thrombus and the PI3K/Akt pathway were studied in an appropriate mouse model	Mice were treated with isaridin E or clopidogrel before tail transection to measure bleeding time. Hematologic and coagulation parameters were assessed from blood samples after treatment	Isaridin E inhibited ADP-induced platelet activation and aggregation in a concentration-dependent manner, without affecting collagen or thrombin-induced aggregation	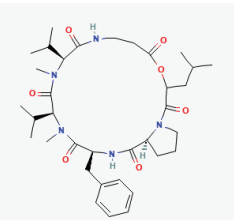 isaridin E	It is safe at 400 μM, with no significant effects on bleeding time or coagulation, making it a promising candidate for treating thrombotic diseases	2022	[63]

Table 5. *Cont.*

Hypothesis–Intervention	Study Design/Parameters Examined	Main Findings	Structures	Specific Benefits/Other Benefits Observed—Mechanisms of Action(s)	Year	Ref.
This study aimed to explore, *Setosphaeria*-sp.-derived exserolides (I, J, E, and F) to lower lipids by enhancing reverse cholesterol transport (RCT) in vitro	Procedure: Preparation of lipoproteins, cell viability assay, cholesterol efflux assay, determination of intracellular TC and TG levels, and immunoblotting and molecular docking	Exserolide J reduced ox-LDL accumulation and cholesterol efflux via LXRα-ABCA1 and PPARα pathways, decreased CD36 uptake in macrophages, and lowered total cholesterol (TC) and triglyceride contents (TG) in HepG2 cells. Exserolides I, J, and E enhanced PPARα levels; J showed the strongest LXRα interaction, while E had the weakest	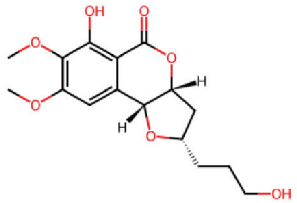 exserolide I 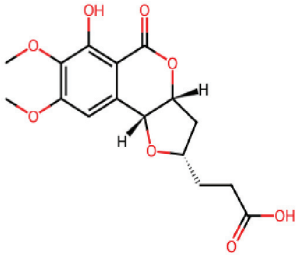 exserolide J 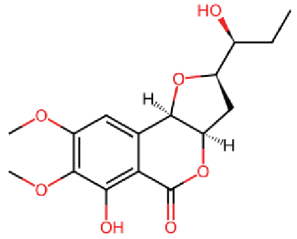 exserolide E 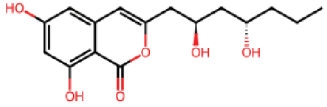 exserolide F	Hyperlipidemia, especially LDL cholesterol, is a key risk factor for atherosclerosis and cardiovascular diseases. Exserolides reduced ox-LDL accumulation and boosted [3H]-cholesterol efflux in RAW264.7 macrophages	2024	[57]

Table 5. *Cont.*

Hypothesis–Intervention	Study Design/Parameters Examined	Main Findings	Structures	Specific Benefits/Other Benefits Observed—Mechanisms of Action(s)	Year	Ref.
Searching for new drugs to combat CVDs is crucial. Penicillium expansum Y32, isolated from Indian Ocean seawater, may provide lead compounds	Key experiments included extraction, purification, zebrafish heart rate, vasculogenesis, and antiangiogenic vessel growth assays	Compounds **4**, **6**, **8**, and **10**, identified by spectroscopy and quantum electronic circular dichroism (ECD), reduced bradycardia and enhanced vasculogenesis in zebrafish, showing potential for cardiovascular disease	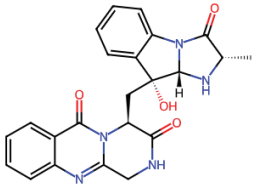 fumiquinazoline Q (4) 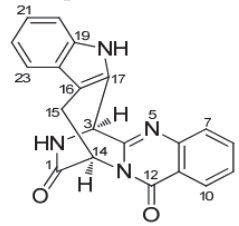 prelapatin B (6) 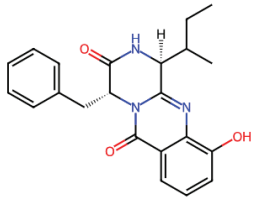 protuboxepin E (8) 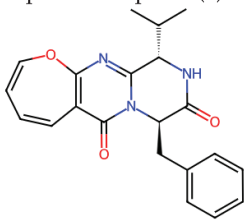 protuboxepin B (10)	Compounds **4**, **6**, **8**, and **10**, namely, fumiquinazoline Q, prelapatin B, protuboxepin E, and protuboxepin B, respectively, promoted vessel growth; others had limited or no activity	2015	[60]

Table 5. *Cont.*

Hypothesis–Intervention	Study Design/Parameters Examined	Main Findings	Structures	Specific Benefits/Other Benefits Observed—Mechanisms of Action(s)	Year	Ref.
In this search for proangiogenic metabolites, *Chaetomium globosum* YP-106 was isolated from hadal-zone seawater	*C. globosum* YP-106 was isolated from Yap Trench seawater, cultured in 50 flasks at 28 °C, and extracted after fermentation. Spectral data and pro-angiogenic activity were then assessed	Chaetoviridin L (1) and four analogues (2–5) were isolated from *Chaetomium globosum* YP-106 Compounds **1**, **2**, and **5**, namely, chaetoviridin L, chaetomugilin A, and chaephilone D, respectively promoted vascular growth in zebrafish models, while 3 and 4, namely, chaetoviridin E and chaetomugilin O, did not. Compounds **1**, **2**, and **5** are promising for CVD treatment	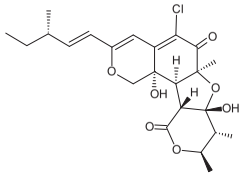 chaetoviridin L (1) 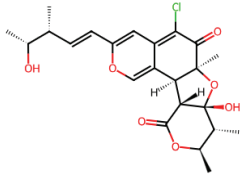 chaetomugilin A (2) 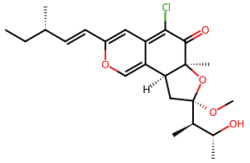 chaephilone D (5) 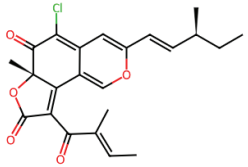 chaetoviridin E (3) 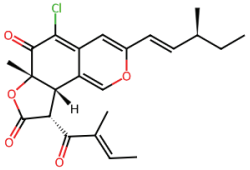 chaetomugilin O (4)	Azaphilones, from deep-sea fungi, may protect against photodamage and may display potential uses as food colorants and UV-proof products	2023	[61]

Table 5. *Cont.*

Hypothesis–Intervention	Study Design/Parameters Examined	Main Findings	Structures	Specific Benefits/Other Benefits Observed—Mechanisms of Action(s)	Year	Ref.
Four new compounds were isolated from Neopestalotiopsis sp. HN-1-6. Azaphilones (1–3, 5–7) were screened for proangiogenic activity in zebrafish	A fungal strain from Qinzhou was tested for cytotoxicity, antibacterial, and proangiogenic effects using Tg zebrafish embryos	From Neopestalotiopsis sp., three new azaphilones and one phenylpropanoid showed proangiogenic activity and no cytotoxicity	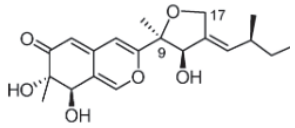 pestaphilone J 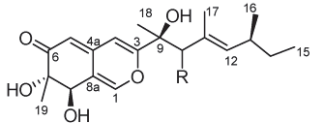 pestaphilone G 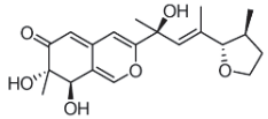 pestaphilone I	Compounds **3**, **5**, and **7**, namely, pestaphilones J, G and I, demonstrated remarkable proangiogenic activities	2024	[62]
Asperlin was isolated from *Aspergillus versicolor* LZD4403. Its anti-inflammatory and atheropreventive activities, were confirmed in high-fat diet (HFD)-fed ApoE−/− mice.	*Aspergillus versicolor* LZD4403 was isolated from a gorgonian and analyzed for anti-inflammatory and lipid effects	Asperlin enhanced cholesterol efflux via PPARγ-ABCA1/G1 and shifted macrophage polarization to M2, indicating potential in atherosclerosis prevention and treatment	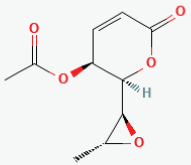 asperlin	Asperlin (1–10 μM) effectively suppressed LPS-induced foam cell formation, comparable to simvastatin, by shifting macrophage polarization from M1 to M2	2017	[67]

Table 5. *Cont.*

Hypothesis–Intervention	Study Design/Parameters Examined	Main Findings	Structures	Specific Benefits/Other Benefits Observed—Mechanisms of Action(s)	Year	Ref.
Xyl-B, isolated from *Xylaria* sp., was evaluated for hypertension effects using a 2-kidney, 2-clip rat model	Xyl-B, isolated and characterized by HPLC and 1D-nuclear magnetic resonance spectroscopy (D-NMR), was tested in 2K2C rats, with various vascular and cellular assays	This study showed that Xyl-B reduced blood pressure in 2K2C hypertensive rats and induced endothelium-dependent relaxation in aortic rings	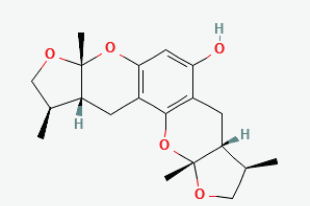 xyloketal B	A limitation of the study is the unverified nitric oxide-soluble guanylate cyclase-cyclic guanosine monophosphate (NO-sGC/cGMP) pathway and Ca^{2+} signaling mechanisms in vascular smooth muscle cells (VSMCs). Caution is needed in interpreting Xyl-B's antihypertensive effects	2018	[53]
Two new 4,5-disubstituted aspergteroids and four known 4,5-disubstituted analogs were isolated from a soft-coral-associated symbiotic and epiphytic fungus *Aspergillus terreus* EGF7-0-1	Strain EGF7-0-1 was isolated from soft coral in the South China Sea and identified as *Aspergillus terreu* Isolation, quantum chemical calculations, Western blot assays, were conducted	The results suggested that compound **1**, known as aspergteroid G, may reduce the inflammatory response and protect cardiomyocytes through GSK-3β/NLRP3 pathway	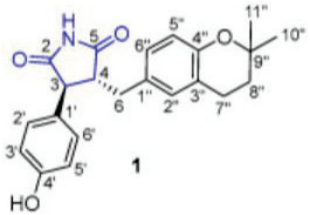 aspergteroid G	The expression of caspase-3 and Bax was regulated, the antiapoptotic gene Bcl-2 was upregulated, the antioxidant capacity of cells was improved, and apoptosis was inhibited	2023	[71]

Structures were obtained from Molview.org., PubChem, and ChemSpider.

4. Other Health-Promoting Properties of Marine Fungi Bioactives

Marine fungi bioactives have also shown numerous benefits against several inflammation- and oxidative-stress-related manifestations and chronic disorders. The structures of certain compounds contained in marine fungi associated with these diseases are summarized in Table 6 and studies and clinical trials in Table 7. The compounds mentioned in the clinical trials in Table 7, are depicted in Figure 3.

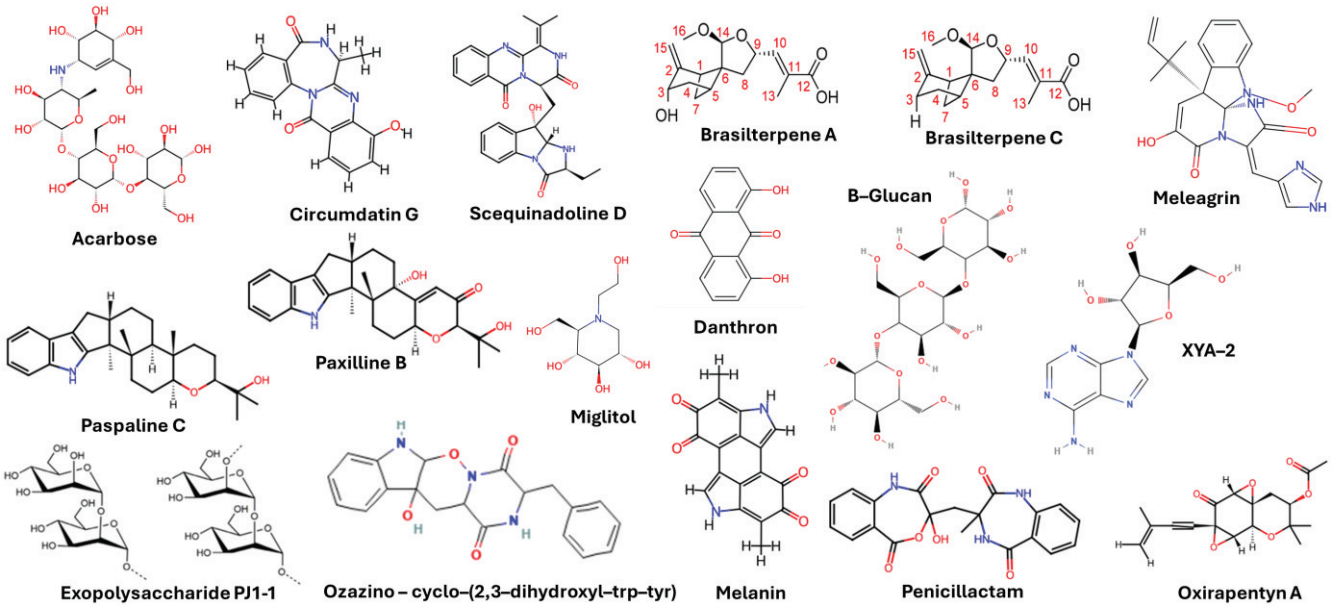

Figure 3. Marine-fungi-derived bioactive compounds and extracts used in the interventions and clinical trials presented in Table 7 and evaluated for their antidiabetic, anticancer, anti-aging, and wound-healing effects.

4.1. Antidiabetic Effects of Marine Fungi

Recent studies have pointed out that marine-derived fungi exhibit great promise in the development of antidiabetic agents. In this respect, single components isolated from such fungi showed promising in vitro and in vivo activities. Among the most important examples, is exopolysaccharide PJ1-1, an extract of a marine fungus that expressed a potent antidiabetic effect in a Type 2 diabetes mellitus (T2DM) mouse model. The T2DM model was induced in mice with a combination of a high-fat diet and a low dose of streptozotocin, mimicking human diabetes at an early stage. Administration of PJ1-1 resulted in significant improvements in body weight and reductions in the fasting blood glucose levels of the diabetic mice. Over the five-week course of treatment, PJ1-1 decreased the level of fasting blood glucose in a dose-dependent manner; at the highest dose, it decreased by 42.16%. Moreover, PJ1-1 improved glucose tolerance and insulin resistance, which implicated its potential against diabetes [74].

Another marine fungus that has been investigated is *Scedosporium apiospermum* F41-1 for its generation of fumiquinazoline alkaloids, compounds of interest showing insulin-sensitizing activities. These alkaloids have been screened for their ability to induce triglyceride accumulation in 3T3-L1 adipocytes, a cell model often used for studying fat storage and insulin sensitivity. The most important and effective fumiquinazolines, were scequinadolines A, B, D, and E. Among the isolated compounds, the most efficient was scequinadoline D (9) with a half maximal effective concentration (EC_{50}) value of 0.27 μM. It was shown that the compound works via the PPARγ pathway, which is one of the most crucial regulators of adipocyte differentiation and insulin sensitivity. Since scequinadoline D activated genes involved in adipogenesis and lipid metabolism, it enhanced sensitivity to insulin and, thus, is a potent candidate for T2DM treatment [75].

The marine-derived fungus *Aspergillus flavipes* HN4-13, isolated from coastal sediments, was found to produce a number of secondary metabolites, including three new butenolide derivatives, namely, flavipesolides A-C, in addition to other known compounds. These metabolites showed considerable antidiabetic activity, especially by the inhibition of α-glucosidase involved in carbohydrate breakdown into glucose. This work revealed that the identified α-glucosidase inhibitors, exhibited potency in different ranges. Compounds **4–6**, namely, 5-[(3,4-dihydro-2,2-dimethyl-2H-1-benzopyran-6-yl)methyl]-3-hydroxy4-(4-hydroxyphenyl)-2(5H) furanone (4), aspernolide (5), and emodin (6), as well as methyl dichloroasterrate (9), acted as non-competitive inhibitors of α-glucosidase, with inhibition constant (Ki) values of 0.43 and 2.8 μM, half maximal inhibitory concentration (IC_{50}) values of 19 and 90 μM, respectively. On the other hand, compounds **1–3**, known as flavipesolides A–C, geodin hydrate (8), monomethylosoic acid (10), and epicoccolide B (13) were mixed inhibitors, including both competitive and non-competitive inhibition mechanisms against α-glucosidase. The IC_{50} value of such mixed inhibitors ranged from 9.9 to 95 μM, showing more effective inhibition than well-known antidiabetic drugs like acarbose and 1-deoxynojirimycin, with IC_{50} values of 101 μM and 79 μM, correspondingly. The study pointed out that these compounds, especially butenolide derivatives, demonstrated prominent inhibitory activity against a-glucosidase and low cytotoxicity on the human colon cancer cell line of Caco-2. In view of this, it is an indication that the secondary metabolites from *Aspergillus flavipes* HN4-13 could be a promising leading compound in developing safe and effective antidiabetic drugs [76].

The marine-derived fungus *Paraconiothyrium brasiliense* HDN15-135, isolated from deep-sea sediments, exhibits remarkable antidiabetic potential through its production of unique sesquiterpenoid compounds called brasilterpenes. Out of the five brasilterpenes that were identified, (brasilterpenes A–E), brasilterpenes A and C revealed promising hypoglycemic activities. In an in vivo study with a diabetic zebrafish model, brasilterpenes A (1) and C (3) resulted in a significant decrease in the blood sugar levels of hyperglycemic zebrafish. These compounds exerted their actions by enhancing insulin sensitivity and suppressing gluconeogenesis, a major metabolic pathway by which glucose is synthesized from non-carbohydrate sources. This double action becomes of special relevance in the management of diabetes, since it can help to not only decrease glucose levels in the blood but also to enhance insulin responsiveness of the body, which is reportedly impaired in most diabetic conditions. Furthermore, it was determined that brasilterpene C (3) displayed potent hypoglycemic activity in comparison to the widely used antidiabetic drug rosiglitazone. This result, therefore, suggests brasilterpenes and, especially, brasilterpene C, as leading compounds with strong potential for the development of new antidiabetic therapies [77]. Other deep-sea fungal compounds, such as cladosporol C, tenellone F, ozazino-cyclo-(2,3-dihydroxyl-trp-tyr), penicillactam, and circumdatin G, were identified as inhibitors of α-amylase, α-glucosidase, pancreatic-lipoprotein lipase, hexokinase-II, and protein tyrosine phosphatase-1B, by delaying sugar absorption [78].

4.2. Antitumor Effects of Marine Fungi

Marine fungi are a valuable source of natural resources for the creation of anticancer medications due to their unusual structures and distinct functions. Cell cycle arrest is a potentially effective method of halting the growth of cancer cells, since cancer is characterized by an unchecked cell cycle and the uncontrolled proliferation of tumor cells. Therefore, studies have focused on marine compounds that may inhibit human cell proliferation and metastasis and may induce cell apoptosis and cell cycle arrest in the G2/M phase. A major focus of research is the strain *Penicillium* sp. OUCMDZ-1435, known for its contributions to food production, medicinal applications, and natural ecosystems.

Meleagrine, a bioactive substance derived from the fungus *Penicillium* sp. OUCMDZ-1435, has demonstrated strong cytotoxic action against a variety of tumor cells, suggesting that it may have antitumor properties. Meleagrine exhibited antibacterial action, making it a viable option for pharmaceutical research targeted at creating novel antibiotics. This

is particularly relevant considering the growing issue of antibiotic resistance. Meleagrin and oxaline have been shown in a study to successfully stop the growth and metastasis of human HepG2 cells, as well as to boost HepG2 cell death and cell cycle arrest in the G2/M phase [79]. Danthron, an hydroxy anthraquinone on the other hand, extracted from the fermentation broth of a marine fungal, is a novel inhibitor of angiogenesis, providing insight into its mode of action. This compound's antioxidant, antiangiogenic, and anticancer properties pointed to its potential application in cancer treatment and chemoprevention [80]. From the sponge-derived marine fungus *Lopadostoma pouzarii* strain 168CLC-57.3, the new polyketides lopouzanones A and B, as well as the new 1-*O*-acetyl and 2-*O*-acetyl derivatives of dendrodochol B, were isolated. Additionally, the identities of six known polyketides, were determined. All these substances exhibited low cytotoxicity toward PC-3 human prostate cancer cells and H9c2 normal rat cardiomyocytes [72]. A compound derived from a marine fungus, XYA-2, exhibited significant effects on various cellular processes in pancreatic cancer; in addition, it affected the transition of cancer cells during the cell cycle by increasing the apoptotic rate at higher concentrations [81]. Moreover, effective suppression of glioma cell migration, invasion, and proliferation was realized, while apoptosis induction was achieved by oxirapentyn A, which also crosses the blood–brain barrier, according to an in silico analysis [82].

Table 6. Structures of certain compounds contained in marine fungi associated with chronic disorders.

Compounds	Structures	References
Exopolysaccharide PJ1-1	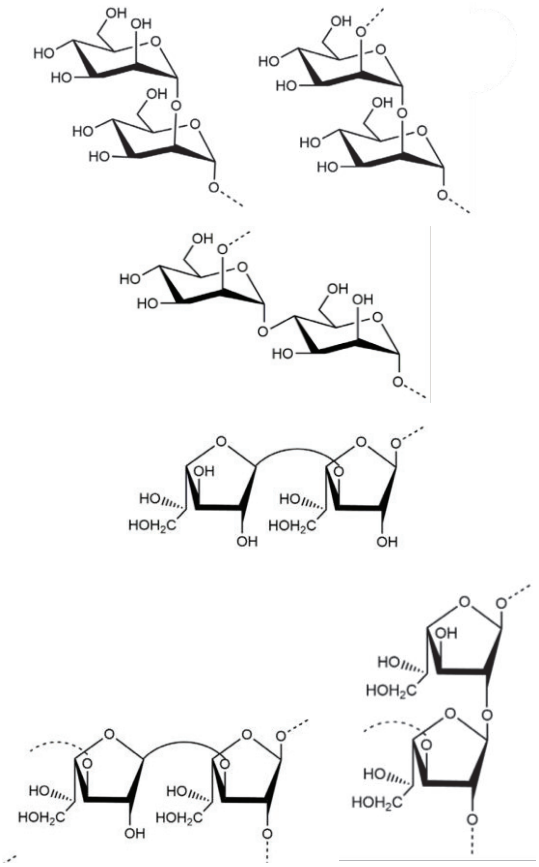 (possible structures of the main repeating disaccharides in PJ1-1)	[74]

Table 6. *Cont.*

Compounds	Structures	References
Scequinadoline A, B, D, and E (compounds 7–10—most important and effective fumiquinazolines)	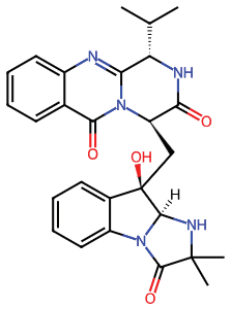 scequinadoline A 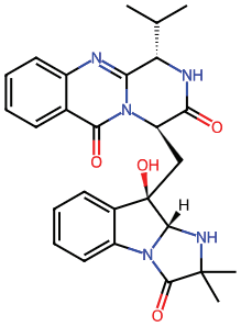 scequinadoline B 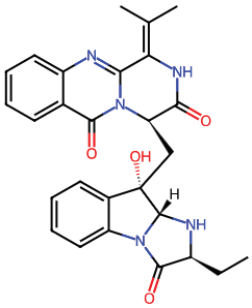 scequinadoline D 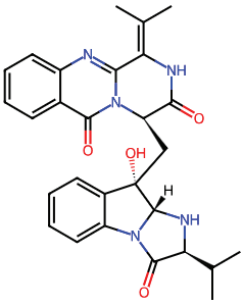 scequinadoline E	[75]

Table 6. *Cont.*

Compounds	Structures	References
Flavipesolides A–C	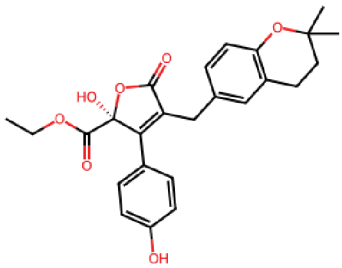 flavipesolide A 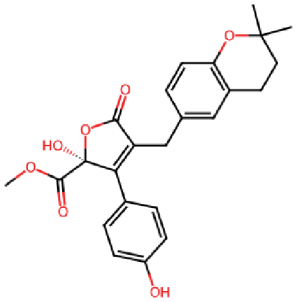 flavipesolide B 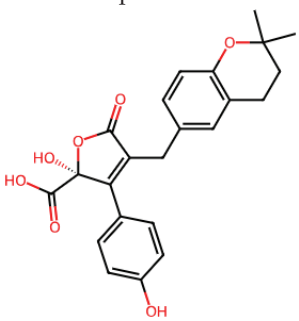 flavipesolide C	[76]
5-[(3,4-Dihydro-2,2-dimethyl-2*H*-1-benzopyran-6-yl) methyl]-3-hydroxy4-(4-hydroxyphenyl)-2(5*H*) furanone (compound **4**) and aspernolide (compound **5**)	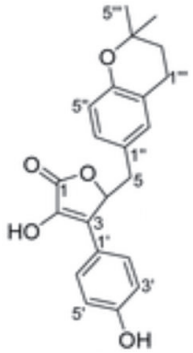 5-[(3,4-dihydro-2,2-dimethyl-2*H*-1-benzopyran-6-yl) methyl]-3-hydroxy4-(4-hydroxyphenyl)-2(5*H*) furanone (4) 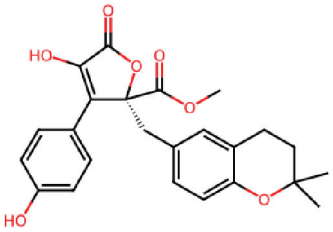 aspernolide A (5)	

Table 6. *Cont.*

Compounds	Structures	References
Emodin	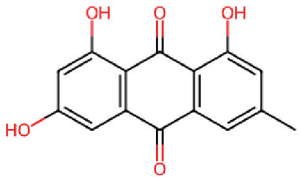	[76]
Geodin hydrate (8), methyl dichloroasterrate (9), and monomethylosoic acid (10)	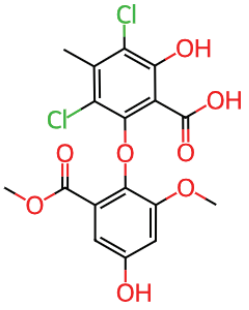 geodin hydrate (8) 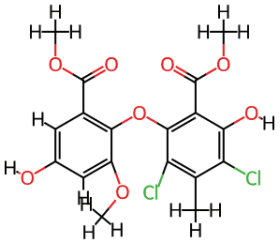 methyl dichloroasterrate (9) 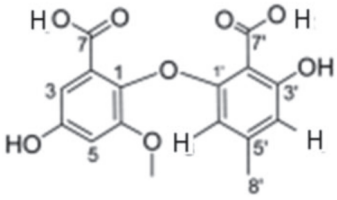 monomethylosoic acid (10)	
Epicoccolide B (13)	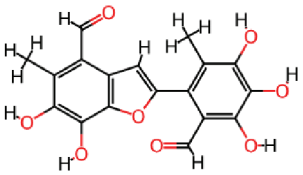	
Brasilterpenes A and C	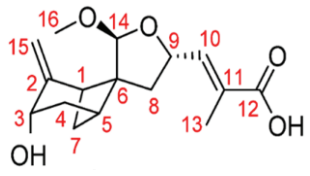 brasilterpene A (1) 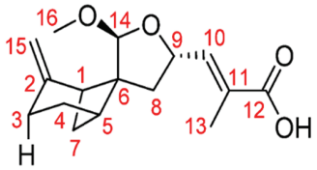 brasilterpene C (3)	[77]

Table 6. *Cont.*

Compounds	Structures	References
Cladosporol C	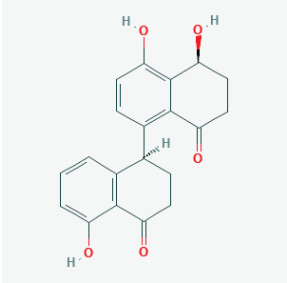	
Tenellone F	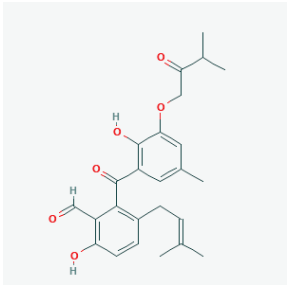	
Ozazino-cyclo-(2,3-dihydroxyl-trp-tyr)	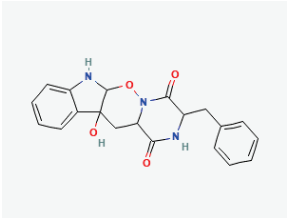	[78]
Penicillactam	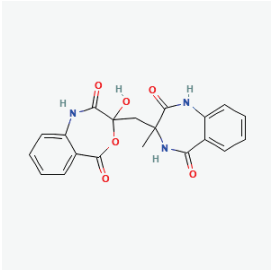	
Circumdatin G	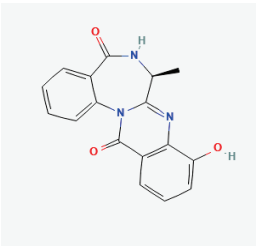	
Meleagrine	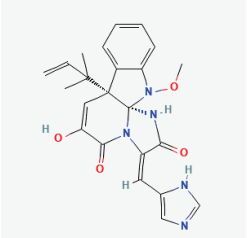	[79]

Table 6. *Cont.*

Compounds	Structures	References
Oxaline	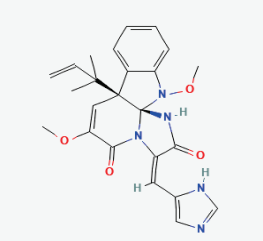	
Danthron	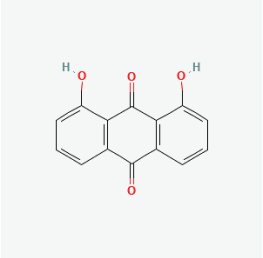	[80]
Lopouzanones A and B	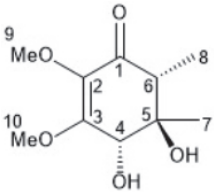 lopouazone A (1) 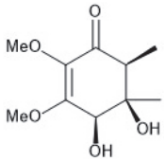 lopouazone B (2)	[72]
1.-.O-acetyl dendrodochol B	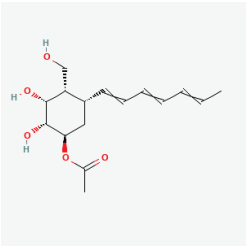	
Oxirapentyn A	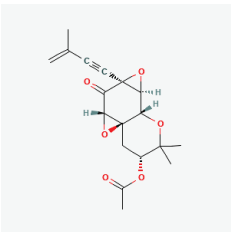	

Structures were obtained from Molview.org., PubChem, and ChemSpider.

4.3. Anti-Aging Effects of Marine Fungi

B-glucan is a naturally occurring polysaccharide, found in abundant quantities in the cell walls of several fungi, particularly marine yeast. It belongs to that rare category of compounds with immense anti-aging potential, so it is useful in skincare formulations.

B-glucan enhances the intrinsic mechanisms of skin repair, by increasing the retention of moisture and the synthesis of collagen—all vital processes for reducing visible signs of aging like wrinkles, fine lines, and loss of skin firmness. B-glucan extracted from marine yeast was studied with the UV-mutated strain of *Rhodotorula* sp. DAMB1, displaying respectable antioxidant actions. Antioxidants aid in neutralizing free radicals—the main cause of oxidative stress and precocious aging phenomena of skin cells. B-Glucan is, in fact, capable of preserving the youthful appearance of skin by reducing oxidative damage through its action. More importantly, β-glucan has been demonstrated to have excellent skin absorption abilities, which may boost collagen-stimulating activity. Collagen is an important protein that normally promotes skin elasticity and firmness but decreases because of aging. Application of β-glucan topically reestablished collagen levels, hence regenerating firmer and more elastic skin. It also provided protection from UV radiation, one of the comprehensive causes of skin aging, in addition to its anti-aging benefits. Application of β-glucan has been observed to reduce the negative impacts of exposure to UV radiation and to prevent visible premature aging based on environmental factors [83].

In general, this research articulated that *Scopalina hapalia* is a good source of naturally occurring anti-aging agents, since most of its bioactive compounds acted on core key mechanisms involved in the process. More studies are, therefore, recommended, in order to carry on with the isolation and characterization of such bioactive molecules for their potential therapeutic applications [84].

Wound-Healing Effects of Marine Fungi

The melanin purified from the halotolerant black yeast *Hortaea werneckii* AS1 was tested for its wound-healing potential using an in vitro scratch assay, a representative model for cell migration and proliferation events occurring during wound closure, against human skin fibroblast (HSF) cells. Observations indicated that the application of melanin did not have a negative impact on tissue regeneration of HSF cells at a dosage of 100 μg/mL. Noticeably, the scratch on HSF cells completely closed at 72 h of incubation regardless of the presence or absence of melanin, indicating that melanin did not hamper the natural process of wound healing of the cells. The known antioxidant and antibacterial activities of melanin should, moreover, account for the potential wound-healing properties of this pigment in cosmetic formulations. The results showed that wound healing was promoted by the fungal extract. This can be attributed to its bioactive compounds that stimulate cellular activities involved in tissue regeneration. The efficacy of the wound healing by the extract is related to its antioxidant and antimicrobial properties, which are projected not only against infection in a wound but also reduce oxidative stress, hence, further improving the healing process. Consequently, this work evidenced that although melanin from *H. werneckii* AS1 did not exert a direct effect on the acceleration of wound closure, it is non-toxic and did not impede the natural process of wound healing, a hypothesis that confirms and supports its candidacy for further exploration for wound-healing applications [85]. These findings open a new avenues in the exploration of this fungus regarding its potential in the development of new therapeutic pathways for better management of wound care.

Table 7. Studies, Interventions and Clinical trials of the anti-diabetic, anticancer, anti-aging and wound-healing effects of bioactive extracts derived from marine fungi.

Hypothesis–Intervention	Study Design/Parameters Examined	Main Findings	Specific Benefits/Other Benefits Observed–Mechanisms of Action(s)	Year of Study	References
α-Glucosidase and new inhibitors from *Aspergillus flavipes* HN4-13 are introduced	*Aspergillus flavipes* HN4-13 was isolated from Lianyungang sediment by fermentation and extraction assays	α-Glucosidase inhibitors like acarbose and miglitol treated diabetes but caused side effects	Natural products from *Aspergillus* fungi show anti-tobacco mosaic virus (TMV), DPPH scavenging, α-glucosidase inhibition, and antiviral activities	2016	[76]
This study isolated 3 new and 12 known fumiquinazoline alkaloids from *Scedosporium apiospermum* F41-1 and assessed their antidiabetic potential	*Scedosporium apiospermum* F41-1 was isolated from *Lobophytum crassum* in Hainan, China. Fermentation, extraction, 3T3-L1 differentiation, triglyceride assay, oil red O staining, qPCR, procedures were conducted	The results suggested that scequinadoline D (9) targeted adipocytes and could treat T2DM effectively	Fumiquinazolines and related alkaloids from *Scedosporium apiospermum* F41-1 showed antiviral activity against hepatitis C	2020	[75]
Sixteen indole diterpenoids, including five novel ones, were tested for their cytotoxic and antimicrobial activities	The strain produced a crude extract, which was purified and tested for antimicrobial activity using disk diffusion	Paspaline (C–D)- and paxilline (B–D)-type indole diterpenoids rarely exhibited antimicrobial activity but may have variable cytotoxic effects across different cancer cell lines	Five new and eleven known indole diterpenoids from *Penicillium brefeldianum* WZW-F-69 were observed, highlighting the potential of marine fungi in discovering novel bioactive compounds	2022	[64]
This manuscript presented danthron as a new angiogenesis inhibitor, with antiangiogenic, antitumor, and antioxidant properties	The cell culture included HUVECs treated with danthron or controls. Chick CAM assays and cell cycle analysis followed	Danthron, an hydroxy anthraquinone from a marine fungus, inhibited angiogenesis and tumor cell proliferation by inducing apoptosis	The link between danthron's antiangiogenic and antioxidant activities warranted further study, supporting its potential as an anticancer drug	2023	[80]
In this study, a homogeneous exopolysaccharide, PJ1-1, was obtained from *Penicillium janthinellum* N29′s fermented broth	C57BL/6 J mice were used; *P. janthinellum* N29 derived from *Acanthus ilicifolius*. Fermentation, composition, and analysis methods, as well as in vivo experiments and fasting insulin assays, were performed	PJ1-1 enhanced glucose metabolism, improved insulin efficiency, and lipid metabolism in T2DM mice, suggesting its potential as an antidiabetic agent	PJ1-1 improved lipid metabolism in T2DM mice by lowering TG, TC, LDL-C, and increasing high-density lipoprotein (HDL)-C	2023	[74]

Table 7. *Cont.*

Hypothesis–Intervention	Study Design/Parameters Examined	Main Findings	Specific Benefits/Other Benefits Observed–Mechanisms of Action(s)	Year of Study	References
Five bergamotane sesquiterpenoid derivatives, brasilterpenes, were isolated from *Paraconiothyrium brasiliense* HDN15-135	The fungus was isolated from Indian Ocean sediment. Procedures conducted were fermentation, NMR, glucose assays, toxicity evaluation, and hypoglycemic mechanism studies	Brasilterpenes A (1) and C (3) lowered blood glucose in hyperglycemic zebrafish by enhancing insulin sensitivity	The hypoglycemic activities of compounds **1** and **3** are linked to the S configuration at C-14. Compound **3**, with an hydroxyl group at C-3, is more active	2022	[77]
B-glucan methyl ester compounds were checked for their applications in the cosmetics field	Assays used for antioxidant, metal-chelating, reducing power, and antibacterial activities.B-glucan was applied in cosmetics and used for almond facial scrub preparation	B-glucan improved skin firmness, collagen production, and has antioxidant, antibacterial effects	Carboxymethylated β-glucan showed greater antibacterial activity against *S. aureus* than the original compound	2024	[83]
Structure-based virtual screening (SBVC) of various deep-sea fungi derived metabolites was performed	Retrieve and prepare protein/ligand structures, virtual screening, molecular docking, molecular dynamics (MD) simulations, residue interaction analysis, and binding free-energy determination, were performed	*Cladosporol C*, *tenellone F*, ozazino-cyclo-(2,3-dihydroxyl-trp-tyr), penicillactam, and circumdatin G were identified as potential inhibitors of key diabetes-related enzymes	Inhibiting α-amylase, α-glucosidase, and hexokinase II (HK-II) delayed sugar absorption, while protein tyrosine phosphatase-1B (PTP-1B) impaired insulin signaling	2023	[78]
Marine fungi are valuable for an antitumor drug development	Annexin FITC/PI assays were used for compound analysis and apoptosis detection L-tryptophan and L-histidine are key precursors in Meleagrin biosynthesis	Challenges in chemical synthesis of bioactive compounds led to the optimization of Meleagrin's fermentation The initial pH significantly affected the yield; pH 3.0 was optimal for a simpler composition and higher Meleagrin production	These compounds inhibited HepG2 cell proliferation and metastasis, induced apoptosis, and caused cell cycle arrest in G2/M phase	2023	[79]

Table 7. *Cont.*

Hypothesis–Intervention	Study Design/Parameters Examined	Main Findings	Specific Benefits/Other Benefits Observed–Mechanisms of Action(s)	Year of Study	References
The study attempted to examine the various valuable medical and environmental utilizations of this beneficial pigment	The purified melanin was evaluated for antioxidant activity, cytotoxicity, in vitro anticancer effects, wound healing, antimicrobial activity, and environmental impact	The pigment showed an antibacterial activity toward *S. aureus* and *A. hydrophila* It can further be applied as an antimicrobial agent against fatal pathogenic strains affecting the aquaculture industry	These findings showed that melanin at a concentration of 100 µg/mL did not influence cell migration	2022	[85]
The impact of XYA-2, a nitrogenated azaphilon previously reported from a deep-sea-derived fungus, on the progression of pancreatic cancer cells was evaluated	Procedures conducted: Cell cycle arrest assay, apoptosis assay, Western blot assay, wound-healing assay, and transwell migration assay	XYA-2 exhibited significant effects on various cellular processes in pancreatic cancer Furthermore, it influenced the transition of cancer cells during the cell cycle, leading to increased apoptosis at higher concentrations	The results from the wound-healing assay, underscored the concentration-dependent inhibitory effects of XYA-2 on the migratory capacity of MIA-PACA2 cells	2024	[81]
In this research on ascidian-derived fungi in the South China Sea, it was discovered that a culture extract of the fungus *Amphichorda felina* SYSU-MS7908 exhibited moderate cytotoxicity against U87-MG human glioma cells	Procedures included: X-ray crystallographic analysis, antiproliferative activity by MTT assay, prediction of blood–brain barrier permeation in silico, cell migration by wound-healing assay, cell invasion by transwell assay, and cell apoptosis assay by flow cytometry	In an anti-glioma assay, oxirapentyn A (7) effectively inhibited the proliferation, migration, and invasion of glioma cells and induced their apoptosis. Furthermore, an in silico analysis suggested that oxirapentyn A has the potential to penetrate the blood–brain barrier	These findings highlight the potential of oxirapentyn A as a candidate for the development of novel antiglioma drugs	2023	[82]

5. Materials and Methods

This systematic review was conducted using the Preferred Reporting Items for Systematic Reviews and Meta-Analyses (PRISMA). The Scopus and PubMed databases were used to search for relevant literature. The database search was conducted from April 1, 2024 to August 1, 2024. The keywords used were marine fungi AND lipids, lipid composition, bioactives, polar lipids, neutral lipids, terpenes, fatty acids, PUFAs, n-3 fatty acids, polyketides, alkaloids, peptides, phenols, cardiovascular health, cardioprotective, inflam-

mation, oxidative stress, thrombosis, hypertension, antidiabetic, antitumor, anticancer, antimicrobial, anti-aging, and wound healing.

The articles that were deemed related to the subject were screened according to the following criteria: (i) written in the English language; (ii) research articles; and (iii) published between 2015 and 2024. Firstly, the titles of the articles were considered, followed by the abstract along with the keywords, and then the text thoroughly. From the total number of articles examined, many of them did not meet the criteria and were excluded from this review. The time frame was adjusted further due to the research gap, especially in lipid composition and cardiovascular-promoting effects. For the theoretical part of this review, articles as well as other reviews were examined in a wider time frame of 2005–2024.

6. Conclusions

Natural marine products have demonstrated their adequacy against a wide array of diseases, with some possessing novel mechanisms of action and others being the strongest among their inhibitor classes. Innovations in several fields have overcome obstacles related to marine drug discovery and development. Advancements in several procedures, for example, sampling techniques and nanomole structure determination, as well as genome sequencing and mining, upgrade the effectiveness of exploring marine samples for novel therapeutics. Several advanced strategies end up being effective in defeating the supply problem, including total chemical synthesis and microbial fermentation, as well as molecular biology tools. Numerous compounds in different phases of development that effectively use those innovations, highlight natural marine products as the new wave of effective, adaptable, economically, and environmentally friendly drugs.

The marine environment creates a distressing condition, where inhabitants are forced to adapt so as to survive. A large portion of survivors is rich in secondary metabolites, which are restoratively useful. Among the marine organisms, numerous unrefined extracts, improved fractions, and compounds obtained, have exhibited fascinating potential medical advantages over the years. These effects are mediated by compounds from different chemical classes including polysaccharides, terpenoids, phenolic compounds, sterols, carotenoids, alkaloids, and fatty acids.

Owing to a diverse chemical ecology, marine flora are potential sources of bioactive compounds; however, they are the least explored. Regardless of the unprecedented potential for sourcing new prescriptions from natural marine products, very few compounds have actually been utilized for treatment.

Thus, endeavors should be made to develop marine functional compounds responsibly, since their consumption could result in a decrease in the occurrence and gravity of chronic diseases. In order to meet the growing need for a wide range of pharmaceuticals, marine sources hold great promise for providing potent, cheaper, and safer drug candidates toward solving several medical problems and deserve further extensive exploration. This review takes a bird's-eye view of marine anticancer compounds, both known and yet-to-be discovered, which may be answers to some of our current biological queries and provide novel, safe, and cost-effective solutions in the near future.

Author Contributions: Conceptualization, A.T.; methodology, A.T.; software, all authors; validation, A.T. and C.A.; investigation, all authors; data curation, all authors; writing—original draft preparation, M.-A.P., K.P., P.C., D.K. and A.T.; writing—review and editing, T.A., C.A. and A.T.; visualization, A.T.; supervision, A.T. All authors have read and agreed to the published version of the manuscript.

Funding: This research received no external funding.

Acknowledgments: The authors would like to thank the School of Chemistry, Faculty of Sciences of the Democritus University of Thrace and the Fisheries Research Institute at Kavala, Greece, for their continuous support.

Conflicts of Interest: The authors declare no conflicts of interest.

References

1. Nash, K.L.; van Putten, I.; Alexander, K.A.; Bettiol, S.; Cvitanovic, C.; Farmery, A.K.; Flies, E.J.; Ison, S.; Kelly, R.; Mackay, M.; et al. Oceans and Society: Feedbacks between Ocean and Human Health. *Rev. Fish Biol. Fish.* **2022**, *32*, 161–187. [CrossRef] [PubMed]
2. Sogin, M.L.; Morrison, H.G.; Huber, J.A.; Welch, D.M.; Huse, S.M.; Neal, P.R.; Arrieta, J.M.; Herndl, G.J. Microbial Diversity in the Deep Sea and the Underexplored "Rare Biosphere". *Proc. Natl. Acad. Sci. USA* **2006**, *103*, 12115–12120. [CrossRef] [PubMed]
3. Vargas-Gastélum, L.; Riquelme, M. The Mycobiota of the Deep Sea: What Omics Can Offer. *Life* **2020**, *10*, 292. [CrossRef] [PubMed]
4. Shin, H.J. Natural Products from Marine Fungi. *Mar. Drugs* **2020**, *18*, 230. [CrossRef] [PubMed]
5. Phukhamsakda, C.; Nilsson, R.H.; Bhunjun, C.S.; de Farias, A.R.G.; Sun, Y.-R.; Wijesinghe, S.N.; Raza, M.; Bao, D.-F.; Lu, L.; Tibpromma, S.; et al. The Numbers of Fungi: Contributions from Traditional Taxonomic Studies and Challenges of Metabarcoding. *Fungal Divers.* **2022**, *114*, 327–386. [CrossRef]
6. Jones, E.B.G.; Pang, K.-L.; Abdel-Wahab, M.A.; Scholz, B.; Hyde, K.D.; Boekhout, T.; Ebel, R.; Rateb, M.E.; Henderson, L.; Sakayaroj, J.; et al. An Online Resource for Marine Fungi. *Fungal Divers.* **2019**, *96*, 347–433. [CrossRef]
7. Poli, A.; Bovio, E.; Ranieri, L.; Varese, G.C.; Prigione, V. News from the Sea: A New Genus and Seven New Species in the Pleosporalean Families Roussoellaceae and Thyridariaceae. *Diversity* **2020**, *12*, 144. [CrossRef]
8. Nguyen, V.D.; Pham, T.T. *Penicillium vietnamense* sp. Nov., the First Novel Marine Fungi Species Described from Vietnam with a Unique Conidiophore Structure and Molecular Phylogeny of Penicillium Section Charlesia. *Mycobiology* **2022**, *50*, 155–165. [CrossRef]
9. Hasan, S.; Ansari, M.I.; Ahmad, A.; Mishra, M. Major Bioactive Metabolites from Marine Fungi: A Review. *Bioinformation* **2015**, *11*, 176–181. [CrossRef]
10. Uras, I.S.; Karsli, B.; Konuklugil, B.; Ocsoy, I.; Demirbas, A. Organic–Inorganic Nanocomposites of Aspergillus Terreus Extract and Its Compounds with Antimicrobial Properties. *Sustainability* **2023**, *15*, 4638. [CrossRef]
11. Deshmukh, S.K.; Prakash, V.; Ranjan, N. Marine Fungi: A Source of Potential Anticancer Compounds. *Front. Microbiol.* **2018**, *8*, 2536. [CrossRef] [PubMed]
12. Silber, J.; Kramer, A.; Labes, A.; Tasdemir, D. From Discovery to Production: Biotechnology of Marine Fungi for the Production of New Antibiotics. *Mar. Drugs* **2016**, *14*, 137. [CrossRef] [PubMed]
13. Song, R.; Hu, M.; Qin, X.; Qiu, L.; Wang, P.; Zhang, X.; Liu, R.; Wang, X. The Roles of Lipid Metabolism in the Pathogenesis of Chronic Diseases in the Elderly. *Nutrients* **2023**, *15*, 3433. [CrossRef] [PubMed]
14. González-Becerra, K.; Ramos-Lopez, O.; Barrón-Cabrera, E.; Riezu-Boj, J.I.; Milagro, F.I.; Martínez-López, E.; Martínez, J.A. Fatty Acids, Epigenetic Mechanisms and Chronic Diseases: A Systematic Review. *Lipids Health Dis.* **2019**, *18*, 178. [CrossRef] [PubMed]
15. Tsoupras, A.; Lordan, R.; Zabetakis, I. Inflammation, Not Cholesterol, Is a Cause of Chronic Disease. *Nutrients* **2018**, *10*, 604. [CrossRef]
16. Tsoupras, A.; Adamantidi, T.; Finos, M.A.; Philippopoulos, A.; Detopoulou, P.; Tsopoki, I.; Kynatidou, M.; Demopoulos, C.A. Re-Assessing the Role of Platelet Activating Factor and Its Inflammatory Signaling and Inhibitors in Cancer and Anti-Cancer Strategies. *Front. Biosci. Landmark Ed.* **2024**, *29*, 345. [CrossRef]
17. Tsoupras, A.; Davi, K.G. Bioactive Metabolites from Fungi with Anti-Inflammatory and Antithrombotic Properties: Current Status and Future Perspectives for Drug Development. In *Fungi Bioactive Metabolites: Integration of Pharmaceutical Applications*; Deshmukh, S.K., Takahashi, J.A., Saxena, S., Eds.; Springer Nature: Singapore, 2024; pp. 427–494, ISBN 978-981-9956-96-8.
18. Astudillo, A.M.; Balboa, M.A.; Balsinde, J. Compartmentalized Regulation of Lipid Signaling in Oxidative Stress and Inflammation: Plasmalogens, Oxidized Lipids and Ferroptosis as New Paradigms of Bioactive Lipid Research. *Prog. Lipid Res.* **2023**, *89*, 101207. [CrossRef]
19. Shi, L.; Tu, B.P. Acetyl-CoA and the Regulation of Metabolism: Mechanisms and Consequences. *Curr. Opin. Cell Biol.* **2015**, *33*, 125–131. [CrossRef]
20. Calder, P.C. Functional Roles of Fatty Acids and Their Effects on Human Health. *JPEN J. Parenter. Enteral Nutr.* **2015**, *39*, 18S–32S. [CrossRef]
21. Fraga, M.E.; Santana, D.M.N.; Gatti, M.J.; Direito, G.M.; Cavaglieri, L.R.; Rosa, C.A.R. Characterization of Aspergillus Species Based on Fatty Acid Profiles. *Mem. Inst. Oswaldo Cruz.* **2008**, *103*, 540–544. [CrossRef]
22. Abraúl, M.; Alves, A.; Hilário, S.; Melo, T.; Conde, T.; Domingues, M.R.; Rey, F. Evaluation of Lipid Extracts from the Marine Fungi Emericellopsis Cladophorae and Zalerion Maritima as a Source of Anti-Inflammatory, Antioxidant and Antibacterial Compounds. *Mar. Drugs* **2023**, *21*, 199. [CrossRef] [PubMed]
23. Khudyakova, Y.V.; Sobolevskaya, M.P.; Smetanina, O.F.; Slinkina, N.N.; Pivkin, M.V.; Moiseenko, O.P.; Kuznetsova, T.A. Fatty-Acid Composition of Certain Species of Marine Mycelial Fungi. *Chem. Nat. Compd.* **2009**, *45*, 18–20. [CrossRef]
24. Dias, A.C.D.S.; Ruiz, N.; Couzinet-Mossion, A.; Bertrand, S.; Duflos, M.; Pouchus, Y.-F.; Barnathan, G.; Nazih, H.; Wielgosz-Collin, G. The Marine-Derived Fungus Clonostachys Rosea, Source of a Rare Conjugated 4-Me-6E,8E-Hexadecadienoic Acid Reducing Viability of MCF-7 Breast Cancer Cells and Gene Expression of Lipogenic Enzymes. *Mar. Drugs* **2015**, *13*, 4934–4948. [CrossRef]
25. Tsoupras, A.; Brummell, C.; Kealy, C.; Vitkaitis, K.; Redfern, S.; Zabetakis, I. Cardio-Protective Properties and Health Benefits of Fish Lipid Bioactives; The Effects of Thermal Processing. *Mar. Drugs* **2022**, *20*, 187. [CrossRef]
26. Gutiérrez, M.; Vera, J.; Srain, B.; Quiñones, R.; Wörmer, L.; Hinrichs, K.; Pantoja-Gutiérrez, S. Biochemical Fingerprints of Marine Fungi: Implications for Trophic and Biogeochemical Studies. *Aquat. Microb. Ecol.* **2020**, *84*, 75–90. [CrossRef]

27. Mabou, F.D.; Yossa, I.B.N. TERPENES: Structural Classification and Biological Activities. *IOSR J. Pharm. Biol. Sci.* **2021**, *16*, 25–40.
28. Ninkuu, V.; Zhang, L.; Yan, J.; Fu, Z.; Yang, T.; Zeng, H. Biochemistry of Terpenes and Recent Advances in Plant Protection. *Int. J. Mol. Sci.* **2021**, *22*, 5710. [CrossRef]
29. Harishkumar, R.; Hans, S.; Stanton, J.E.; Grabrucker, A.M.; Lordan, R.; Zabetakis, I. Targeting the Platelet-Activating Factor Receptor (PAF-R): Antithrombotic and Anti-Atherosclerotic Nutrients. *Nutrients* **2022**, *14*, 4414. [CrossRef] [PubMed]
30. Tang, Y.-Q.; Liang, X.; Zou, Q.-H.; Cui, H.; Luo, L.-X.; Qi, S.-H. HPPO-Derived Meroterpenoids from the Marine-Derived Fungus *Penicillium* sp. SCSIO 41691. *J. Nat. Prod.* **2024**, *87*, 1209–1216. [CrossRef]
31. Zhai, G.; Chen, S.; Shen, H.; Guo, H.; Jiang, M.; Liu, L. Bioactive Monoterpenes and Polyketides from the Ascidian-Derived Fungus *Diaporthe* sp. SYSU-MS4722. *Mar. Drugs* **2022**, *20*, 553. [CrossRef]
32. Anh, D.H.; Tu, N.T.; Hanh, T.T.H.; Cuong, N.X.; Vien, L.T.; Ngan, N.T.T.; Ha, D.V.; Quang, T.H. Terpenes and Polyketides from the Marine-Derived Fungus *Penicillium* sp. OPR23-FS02 with Cytotoxic and Antimicrobial Effects. *Vietnam. J. Chem.* **2024**, *62*, 638–646. [CrossRef]
33. Li, C.-P.; Shi, Z.-Z.; Fang, S.-T.; Song, Y.-P.; Ji, N.-Y. Lipids and Terpenoids from the Deep-Sea Fungus Trichoderma Lixii R22 and Their Antagonism against Two Wheat Pathogens. *Molecules* **2023**, *28*, 6220. [CrossRef] [PubMed]
34. Ma, X.-Y.; Song, Y.-P.; Shi, Z.-Z.; Ji, N.-Y. Three Sesquiterpenes from the Marine-Alga-Epiphytic Fungus *Trichoderma Hamatum* Z36-7. *Phytochem. Lett.* **2021**, *43*, 98–102. [CrossRef]
35. Luo, X.-W.; Chen, C.-M.; Li, K.-L.; Lin, X.-P.; Gao, C.-H.; Zhou, X.-F.; Liu, Y.-H. Sesquiterpenoids and Meroterpenoids from a Mangrove Derived Fungus *Diaporthe* sp. SCSIO 41011. *Nat. Prod. Res.* **2021**, *35*, 282–288. [CrossRef]
36. Zhou, L.-M.; Kong, F.-D.; Fan, P.; Ma, Q.-Y.; Xie, Q.-Y.; Li, J.-H.; Zheng, H.-Z.; Zheng, Z.-H.; Yuan, J.-Z.; Dai, H.-F.; et al. Indole-Diterpenoids with Protein Tyrosine Phosphatase Inhibitory Activities from the Marine-Derived Fungus *Penicillium* sp. KFD28. *J. Nat. Prod.* **2019**, *82*, 2638–2644. [CrossRef]
37. de Amorim, M.R.; Barbosa, C.d.S.; Paz, T.A.; Ióca, L.P.; Nicácio, K.J.; de Oliveira, L.F.P.; Goulart, M.O.; Paulino, J.M.; da Cruz, M.O.; Ferreira, A.G.; et al. Polyketide- and Terpenoid-Derived Metabolites Produced by a Marine-Derived Fungus, *Peroneutypa* sp. *J. Nat. Prod.* **2023**, *86*, 1476–1486. [CrossRef]
38. Cen, S.; Jia, J.; Ge, Y.; Ma, Y.; Li, X.; Wei, J.; Bai, Y.; Wu, X.; Song, J.; Bi, H.; et al. A New Antibacterial 3,5-Dimethylorsellinic Acid-Based Meroterpene from the Marine Fungus *Aspergillus* sp. CSYZ-1. *Fitoterapia* **2021**, *152*, 104908. [CrossRef]
39. Ren, J.; Huo, R.; Liu, G.; Liu, L. New Andrastin-Type Meroterpenoids from the Marine-Derived Fungus *Penicillium* sp. *Mar. Drugs* **2021**, *19*, 189. [CrossRef]
40. Hwang, J.-Y.; Park, S.C.; Byun, W.S.; Oh, D.-C.; Lee, S.K.; Oh, K.-B.; Shin, J. Bioactive Bianthraquinones and Meroterpenoids from a Marine-Derived Stemphylium Sp. Fungus. *Mar. Drugs* **2020**, *18*, 436. [CrossRef]
41. Tang, Y.; Liu, Y.; Ruan, Q.; Zhao, M.; Zhao, Z.; Cui, H. Aspermeroterpenes A–C: Three Meroterpenoids from the Marine-Derived Fungus Aspergillus Terreus GZU-31-1. *Org. Lett.* **2020**, *22*, 1336–1339. [CrossRef]
42. Tang, Y.; Li, Y.; Zhao, M.; Ruan, Q.; Liu, Y.; Li, C.; Zhao, Z.; Cui, H. Furanasperterpenes A and B, Two Meroterpenoids with a Novel 6/6/6/6/5 Ring System from the Marine-Derived Fungus Aspergillus Terreus GZU-31-1. *Bioorganic Chem.* **2020**, *100*, 103968. [CrossRef] [PubMed]
43. Hamed, A.; Abdel-Razek, A.S.; Omran, D.A.; El-Metwally, M.M.; El-Hosari, D.G.; Frese, M.; Soliman, H.S.M.; Sewald, N.; Shaaban, M. Terretonin O: A New Meroterpenoid from Aspergillus Terreus. *Nat. Prod. Res.* **2020**, *34*, 965–974. [CrossRef] [PubMed]
44. Meng, L.-H.; Li, X.-M.; Li, H.-L.; Wang, B.-G. Chermebilaenes A and B, New Bioactive Meroterpenoids from Co-Cultures of Marine-Derived Isolates of Penicillium Bilaiae MA-267 and Penicillium Chermesinum EN-480. *Mar. Drugs* **2020**, *18*, 339. [CrossRef]
45. Wen, H.; Yang, X.; Liu, Q.; Li, S.; Li, Q.; Zang, Y.; Chen, C.; Wang, J.; Zhu, H.; Zhang, Y. Structurally Diverse Meroterpenoids from a Marine-Derived *Aspergillus* sp. Fungus. *J. Nat. Prod.* **2020**, *83*, 99–104. [CrossRef]
46. Anh, C.V.; Kang, J.S.; Choi, B.-K.; Lee, H.-S.; Heo, C.-S.; Shin, H.J. Polyketides and Meroterpenes from the Marine-Derived Fungi Aspergillus Unguis 158SC-067 and A. Flocculosus 01NT-1.1.5 and Their Cytotoxic and Antioxidant Activities. *Mar. Drugs* **2021**, *19*, 415. [CrossRef] [PubMed]
47. Leshchenko, E.V.; Berdyshev, D.V.; Yurchenko, E.A.; Antonov, A.S.; Borkunov, G.V.; Kirichuk, N.N.; Chausova, V.E.; Kalinovskiy, A.I.; Popov, R.S.; Khudyakova, Y.V.; et al. Bioactive Polyketides from the Natural Complex of the Sea Urchin-Associated Fungi Penicillium Sajarovii KMM 4718 and Aspergillus Protuberus KMM 4747. *Int. J. Mol. Sci.* **2023**, *24*, 16568. [CrossRef] [PubMed]
48. Xiang, Z.; Han, M.; Zhang, H. Erratum to: Nanomaterials Based Flexible Devices for Monitoring and Treatment of Cardiovascular Diseases (CVDs) (Nano Research, (2023), 16, 3, (3939-3955), 10.1007/S12274-022-4551-8). *Nano Res.* **2023**, *16*, 8051. [CrossRef]
49. Roth, G.A.; Mensah, G.A.; Johnson, C.O.; Addolorato, G.; Ammirati, E.; Baddour, L.M.; Barengo, N.C.; Beaton, A.Z.; Benjamin, E.J.; Benziger, C.P.; et al. Global Burden of Cardiovascular Diseases and Risk Factors, 1990–2019: Update from the GBD 2019 Study. *J. Am. Coll. Cardiol.* **2020**, *76*, 2982–3021. [CrossRef]
50. Badawy, M.A.E.M.D.; Naing, L.; Johar, S.; Ong, S.; Rahman, H.A.; Tengah, D.S.N.A.P.; Chong, C.L.; Tuah, N.A.A. Evaluation of Cardiovascular Diseases Risk Calculators for CVDs Prevention and Management: Scoping Review. *BMC Public Health* **2022**, *22*, 1742. [CrossRef]
51. Roth, G.A.; Mensah, G.A.; Fuster, V. The Global Burden of Cardiovascular Diseases and Risks: A Compass for Global Action. *J. Am. Coll. Cardiol.* **2020**, *76*, 2980–2981. [CrossRef]

52. Woodward, M. Cardiovascular Disease and the Female Disadvantage. *Int. J. Environ. Res. Public Health* **2019**, *16*, 1165. [CrossRef] [PubMed]
53. Zhao, L.; Li, J.; Huang, X.; Wang, G.; Lv, X.; Meng, W.; Chen, W.; Pang, J.; Lin, Y.; Sun, H.; et al. Xyloketal B Exerts Antihypertensive Effect in Renovascular Hypertensive Rats via the NO-sGC-cGMP Pathway and Calcium Signaling. *Acta Pharmacol. Sin.* **2018**, *39*, 875–884. [CrossRef] [PubMed]
54. Festa, M.; Sansone, C.; Brunet, C.; Crocetta, F.; Di Paola, L.; Lombardo, M.; Bruno, A.; Noonan, D.M.; Albini, A. Cardiovascular Active Peptides of Marine Origin with ACE Inhibitory Activities: Potential Role as Anti-Hypertensive Drugs and in Prevention of SARS-CoV-2 Infection. *Int. J. Mol. Sci.* **2020**, *21*, 8364. [CrossRef] [PubMed]
55. Soehnlein, O.; Libby, P. Targeting Inflammation in Atherosclerosis—From Experimental Insights to the Clinic. *Nat. Rev. Drug Discov.* **2021**, *20*, 589–610. [CrossRef] [PubMed]
56. Patil, N.P.; Le, V.; Sligar, A.D.; Mei, L.; Chavarria, D.; Yang, E.Y.; Baker, A.B. Algal Polysaccharides as Therapeutic Agents for Atherosclerosis. *Front. Cardiovasc. Med.* **2018**, *5*, 153. [CrossRef]
57. Zhang, Y.; Wang, X.; Liu, T.; Zhang, Z.-Y.; Song, W.-G.; Guo, S.-D. Exserolide J Ameliorates Lipid Accumulation in Vitro by Regulating Liver X Receptor Alpha and Peroxisome Proliferator-Activated Receptor Alpha Proteins. *Heliyon* **2024**, *10*, e31861. [CrossRef]
58. Khan, M.A.; Hashim, M.J.; Mustafa, H.; Baniyas, M.Y.; Al Suwaidi, S.K.B.M.; AlKatheeri, R.; Alblooshi, F.M.K.; Almatrooshi, M.E.A.H.; Alzaabi, M.E.H.; Al Darmaki, R.S.; et al. Global Epidemiology of Ischemic Heart Disease: Results from the Global Burden of Disease Study. *Cureus* **2020**, *12*, e9349. [CrossRef]
59. Wu, P.; Yu, S.; Wang, J.; Zou, S.; Yao, D.-S.; Xiaochen, Y. Global Burden, Trends, and Inequalities of Ischemic Heart Disease among Young Adults from 1990 to 2019: A Population-Based Study. *Front. Cardiovasc. Med.* **2023**, *10*, 1274663. [CrossRef]
60. Fan, Y.-Q.; Li, P.-H.; Chao, Y.-X.; Chen, H.; Du, N.; He, Q.-X.; Liu, K.-C. Alkaloids with Cardiovascular Effects from the Marine-Derived Fungus Penicillium Expansum Y32. *Mar. Drugs* **2015**, *13*, 6489–6504. [CrossRef]
61. Fan, Y.; Jiang, C.; Li, P.; Wang, C.; Chen, H. A New Chloro-Azaphilone Derivative with pro-Angiogenesis Activity from the Hadal Trench-Derived Fungus Chaetomium Globosum YP-106. *J. Oceanol. Limnol.* **2023**, *41*, 1145–1151. [CrossRef]
62. Feng, T.; Wu, R.; Wang, Y.; Wang, P.; Zhou, L.; Wang, C.; Kong, F. Proangiogenic Azaphilones from the Marine-Derived Fungus Neopestalotiopsis Sp. HN-1-6. *Mar. Drugs* **2024**, *22*, 241. [CrossRef] [PubMed]
63. Pan, N.; Li, Z.-C.; Li, Z.-H.; Chen, S.-H.; Jiang, M.-H.; Yang, H.-Y.; Liu, Y.-S.; Hu, R.; Zeng, Y.-W.; Dai, L.-H.; et al. Antiplatelet and Antithrombotic Effects of Isaridin E Isolated from the Marine-Derived Fungus via Downregulating the PI3K/Akt Signaling Pathway. *Mar. Drugs* **2022**, *20*, 23. [CrossRef] [PubMed]
64. Lin, W.; Li, H.; Wu, Z.; Su, J.; Zhang, Z.; Yang, L.; Deng, X.; Xu, Q. Paspalines C–D and Paxillines B–D: New Indole Diterpenoids from Penicillium Brefeldianum WZW-F-69. *Mar. Drugs* **2022**, *20*, 684. [CrossRef]
65. Gao, C.; Bao, B.; Bao, C.; Wu, W. Fungi Fibrinolytic Compound 1 Plays a Core Role in Modulating Fibrinolysis, Altering Plasma Clot Structure, and Promoting Susceptibility to Lysis. *Pharmaceutics* **2023**, *15*, 2320. [CrossRef]
66. Zhao, L.; Lin, X.; Fu, J.; Zhang, J.; Tang, W.; He, Z. A Novel Bi-Functional Fibrinolytic Enzyme with Anticoagulant and Thrombolytic Activities from a Marine-Derived Fungus Aspergillus Versicolor ZLH-1. *Mar. Drugs* **2022**, *20*, 356. [CrossRef]
67. Zhou, Y.; Chen, R.; Liu, D.; Wu, C.; Guo, P.; Lin, W. Asperlin Inhibits LPS-Evoked Foam Cell Formation and Prevents Atherosclerosis in ApoE−/− Mice. *Mar. Drugs* **2017**, *15*, 358. [CrossRef]
68. Alharbi, N.K.; Azeez, Z.F.; Alhussain, H.M.; Shahlol, A.M.A.; Albureikan, M.O.I.; Elsehrawy, M.G.; Aloraini, G.S.; El-Nablaway, M.; Khatrawi, E.M.; Ghareeb, A. Tapping the Biosynthetic Potential of Marine Bacillus Licheniformis LHG166, a Prolific Sulphated Exopolysaccharide Producer: Structural Insights, Bio-Prospecting Its Antioxidant, Antifungal, Antibacterial and Anti-Biofilm Potency as a Novel Anti-Infective Lead. *Front. Microbiol.* **2024**, *15*, 1385493. [CrossRef]
69. Hassan, M.G.; Elmezain, W.A.; Baraka, D.M.; AboElmaaty, S.A.; Elhassanein, A.; Ibrahim, R.M.; Hamed, A.A. Anti-Cancer and Anti-Oxidant Bioactive Metabolites from Aspergillus Fumigatus WA7S6 Isolated from Marine Sources: In Vitro and In Silico Studies. *Microorganisms* **2024**, *12*, 127. [CrossRef]
70. Su, J.; Chang, C.; Xiang, Q.; Zhou, Z.-W.; Luo, R.; Yang, L.; He, Z.-X.; Yang, H.; Li, J.; Bei, Y.; et al. Xyloketal B, a Marine Compound, Acts on a Network of Molecular Proteins and Regulates The Activity and Expression of Rat Cytochrome P450 3a: A Bioinformatic and Animal Study. *Drug Des. Devel. Ther.* **2014**, *8*, 2555–2602. [CrossRef]
71. Fan, H.; Wang, L.; Zhang, Z.-K.; Wu, P.-P.; He, Y.-P.; Chen, L.-Y.; Wang, Q.; Zhang, C.-X. Bioactive Aspergteroids G-J from Soft-Coral-Associated Symbiotic and Epiphytic Fungus Aspergillus Terreus EGF7-0-1. *Bioengineering* **2023**, *10*, 805. [CrossRef]
72. Trinh, P.T.H.; Yurchenko, A.N.; Khmel, O.O.; Dieu, T.V.T.; Ngoc, N.T.D.; Girich, E.V.; Menshov, A.S.; Kim, N.Y.; Chingizova, E.A.; Van, T.T.T.; et al. Cytoprotective Polyketides from Sponge-Derived Fungus Lopadostoma Pouzarii. *Molecules* **2022**, *27*, 7650. [CrossRef] [PubMed]
73. Gao, C.; Tang, S.; Zhang, H.; Zhang, H.; Zhang, T.; Bao, B.; Zhu, Y.; Wu, W. A Novel Marine Pyran-Isoindolone Compound Enhances Fibrin Lysis Mediated by Single-Chain Urokinase-Type Plasminogen Activator. *Mar. Drugs* **2022**, *20*, 495. [CrossRef]
74. Shao, Z.; Tian, Y.; Liu, S.; Chu, X.; Mao, W. Anti-Diabetic Activity of a Novel Exopolysaccharide Produced by the Mangrove Endophytic Fungus Penicillium Janthinellum N29. *Mar. Drugs* **2023**, *21*, 270. [CrossRef] [PubMed]
75. Li, C.-J.; Chen, P.-N.; Li, H.-J.; Mahmud, T.; Wu, D.-L.; Xu, J.; Lan, W.-J. Potential Antidiabetic Fumiquinazoline Alkaloids from the Marine-Derived Fungus Scedosporium Apiospermum F41-1. *J. Nat. Prod.* **2020**, *83*, 1082–1091. [CrossRef] [PubMed]

76. Wang, C.; Guo, L.; Hao, J.; Wang, L.; Zhu, W. α-Glucosidase Inhibitors from the Marine-Derived Fungus Aspergillus Flavipes HN4-13. *J. Nat. Prod.* **2016**, *79*, 2977–2981. [CrossRef]
77. Wang, W.; Shi, Y.; Liu, Y.; Zhang, Y.; Wu, J.; Zhang, G.; Che, Q.; Zhu, T.; Li, M.; Li, D. Brasilterpenes A–E, Bergamotane Sesquiterpenoid Derivatives with Hypoglycemic Activity from the Deep Sea-Derived Fungus Paraconiothyrium Brasiliense HDN15-135. *Mar. Drugs* **2022**, *20*, 338. [CrossRef]
78. Alanzi, A.R.; Parvez, M.K.; Alqahtani, M.J.; Al-Dosari, M.S. Deep-Sea Fungal Metabolites as Potential Inhibitors of Glucose-Regulatory Enzymes: In Silico Structure–Activity Analysis. *Saudi Pharm. J.* **2023**, *31*, 101776. [CrossRef]
79. He, X.; Jin, Y.; Kong, F.; Yang, L.; Zhu, M.; Wang, Y. Discovery, Antitumor Activity, and Fermentation Optimization of Roquefortines from *Penicillium* sp. OUCMDZ-1435. *Molecules* **2023**, *28*, 3180. [CrossRef]
80. Vidal, I.; Torres-Vargas, J.A.; Sánchez, J.M.; Trigal, M.; García-Caballero, M.; Medina, M.Á.; Quesada, A.R. Danthron, an Anthraquinone Isolated from a Marine Fungus, Is a New Inhibitor of Angiogenesis Exhibiting Interesting Antitumor and Antioxidant Properties. *Antioxidants* **2023**, *12*, 1101. [CrossRef]
81. Guan, X.; Li, Y.; Guan, X.; Fan, L.; Ying, J. XYA-2: A Marine-Derived Compound Targeting Apoptosis and Multiple Signaling Pathways in Pancreatic Cancer. *PeerJ* **2024**, *12*, e16805. [CrossRef]
82. Jiang, M.; Wu, Q.; Guo, H.; Lu, X.; Chen, S.; Liu, L.; Chen, S. Shikimate-Derived Meroterpenoids from the Ascidian-Derived Fungus Amphichorda Felina SYSU-MS7908 and Their Anti-Glioma Activity. *J. Nat. Prod.* **2023**, *86*, 2651–2660. [CrossRef] [PubMed]
83. Sarkar, A.; Philip, A.M.; Thakker, D.P.; Bhaskara Rao, K.V. Extraction and Characterization of Beta-Glucan Methyl Esters Derived from UV-Mutated Marine Yeast and Their Applications in Cosmetics. *Thalassas* **2024**, *40*, 721–733. [CrossRef]
84. Said Hassane, C.; Fouillaud, M.; Le Goff, G.; Sklirou, A.D.; Boyer, J.B.; Trougakos, I.P.; Jerabek, M.; Bignon, J.; de Voogd, N.J.; Ouazzani, J.; et al. Microorganisms Associated with the Marine Sponge Scopalina Hapalia: A Reservoir of Bioactive Molecules to Slow Down the Aging Process. *Microorganisms* **2020**, *8*, 1262. [CrossRef]
85. Elsayis, A.; Hassan, S.W.M.; Ghanem, K.M.; Khairy, H. Suggested Sustainable Medical and Environmental Uses of Melanin Pigment from Halotolerant Black Yeast Hortaea Werneckii AS1. *Front. Microbiol.* **2022**, *13*, 871394. [CrossRef] [PubMed]

Disclaimer/Publisher's Note: The statements, opinions and data contained in all publications are solely those of the individual author(s) and contributor(s) and not of MDPI and/or the editor(s). MDPI and/or the editor(s) disclaim responsibility for any injury to people or property resulting from any ideas, methods, instructions or products referred to in the content.

MDPI AG
Grosspeteranlage 5
4052 Basel
Switzerland
Tel.: +41 61 683 77 34

Marine Drugs Editorial Office
E-mail: marinedrugs@mdpi.com
www.mdpi.com/journal/marinedrugs

Disclaimer/Publisher's Note: The title and front matter of this reprint are at the discretion of the Guest Editor. The publisher is not responsible for their content or any associated concerns. The statements, opinions and data contained in all individual articles are solely those of the individual Editor and contributors and not of MDPI. MDPI disclaims responsibility for any injury to people or property resulting from any ideas, methods, instructions or products referred to in the content.

Academic Open
Access Publishing

mdpi.com

ISBN 978-3-7258-4948-2